FLUORESCENCE CORRELATION SPECTROSCOPIC STUDY OF THE PHOTOPHYSICAL BEHAVIOR OF QUANTUM DOTS AND DIFFUSION BEHAVIOR OF SOME DYES IN COMPLEX ENVIRONMENTS

A Thesis

Submitted for the Degree of

DOCTOR OF PHILOSOPHY

by

Satyajit Patra

School of Chemistry

University of Hyderabad

Hyderabad 500 046

INDIA

November 2014

Dedicated

To

My Parents

“The true sign of intelligence is not knowledge but imagination.”

Albert Einstein

“To succeed in your mission, you must have single-minded devotion to your goal.”

A. P. J. Abdul Kalam

CONTENTS

Chapter 2. Materials, Instrumentation and Methods

Chapter 3. Modulation of Photophysical Properties of Mercaptopropionic Acid Capped CdTe Quantum Dots upon Exposure to Light

Chapter 4. Effect of Capping Agent and Medium on Light-Induced Variation of the Luminescence Properties of CdTe Quantum Dots

STATEMENT

I hereby declare that the matter embodied in the thesis entitled "***Fluorescence Correlation Spectroscopic Study of the Photophysical behavior of Quantum Dots and Diffusion Behavior of Some Dyes in Complex Environments***" is the result of investigations carried out by me in the School of Chemistry, University of Hyderabad, India under the supervision of **Prof. Anunay Samanta**.

In keeping with the general practice of reporting scientific investigations, the acknowledgements have been made wherever the work described is based on the findings of other investigators. Any omission or error that might have crept in is regretted.

November 2014 **Satyajit Patra**

SCHOOL OF CHEMISTRY

UNIVERSITY OF HYDERABAD

HYDERABAD-500 046, INDIA

Phone: +91-40-2313 4813 (O)
+91-40-2313 0715 (R)
Fax: +91-40-2301 1594
Email: assc@uohyd.ernet.in
anunay.samanta@gmail.com

Prof. Anunay Samanta

CERTIFICATE

Certified that the work embodied in the thesis entitled **"*Fluorescence Correlation Spectroscopic Study of the Photophysical behavior of Quantum Dots and Diffusion Behavior of Some Dyes in Complex Environments*"** has been carried out by **Mr. Satyajit Patra** under my supervision and the same has not been submitted elsewhere for any degree.

Anunay Samanta
(Thesis Supervisor)

Dean
School of Chemistry
University of Hyderabad

Acknowledgement

It gives me immense pleasure and satisfaction to express my sincere gratitude to Prof. Anunay Samanta, my research supervisor, for his constant cooperation, encouragement and kind guidance. He has been quite helpful to me in both academic and personal fronts.

I would like to thank the former and present Dean(s), School of Chemistry, for their constant support, inspiration and for the available facilities. I am extremely appreciative individually to all the faculty members of the school for their help, cooperation and encouragement at various stages. I thank Mr. Durga Prasad for Transmission Electron Microscope (TEM) measurements at Centre for Nanotechnology, University of Hyderabad. I am also grateful to all my former teachers for their help and encouragements.

Financial assistance from DST and CSIR, New Delhi is greatly acknowledged. Special thanks are due to International Travel Support scheme of DST and University Purse Grant to UOH by DST for providing me the financial assistance for attending International Symposium on Methods and Applications of Fluorescence (MAF 13), Genoa, Italy during September, 2013.

I value my association with my former lab-mates: Ravi, Dinesh, Santhosh, Uday, Tanmay, Sanghamitra and Praveen from whom I have learned many valuable aspects of research. I am extremely thankful to Ravi, Dinesh and Santhosh for their help in learning instruments. I acknowledge my present colleagues Soumya, Ashok, Chandrasekhar, Navendu, Shalini, Sudipta (Jamba) and Sneha for maintaining the friendly and cooperative atmosphere in the lab. I am really lucky to have them as my lab-mates. I would also like to thank my project students Jerrin, Jyoti and Jamba who helped me in my research projects and with whom I had spent a wonderful time. I am extremely thankful to Ashok and Chandrasekhar for the useful discussions. I offer my heartiest thanks to Dinesh da and Navendu for their help not only helping me in academically but also otherwise.

I thank all the non-teaching staff of the school of chemistry for their time-to-time cooperation. They had all been quite helpful. I am thankful to all my colleagues in the school of chemistry for helping me with various things.

I would like to express my sincere thanks to all my big brothers; Utpal, Pradip, Ghana, Pati, Ghanta, Tapta, Sandip, Arindam, Tanmay and Palash. A special thanks to Pati da for cooking such delicious food.

I am really lucky for my close association with "the bindaas gang" of HCU which includes Rishi da, Dinesh Da, Santanu da, Paromita di, Raja, Anup da, Nayan da, Maity da, Mona, Raju, Tanmay da, Sugata, Rudra, Suman (Ghosh), Koushik, Navendu, Jamba, Suman (dana), Subha. I will cherish each and every moments I have spent with them throughout my life. I am also thankful to Hari, Gupta, Sudalay, Balaswamy, Suresh, Sanatan, Tridip, Brijesh, Sanjeeb, Ramu, Srinivas, Arun, Tulika, Supratim, Pramithi, Arpita, Debparna, Olivia, Kallol, Dipta and many others.

I am also grateful for the valuable friendship of Sourin, Jayanta, Krishnendu, Somnath, Koushik, Deabanjan, Subhashis, Jaytara, Deba, Apurba, Anup, Arup, Amit, Trilochan, Rajnish, Kaustav, Anish, Sandipan, Anubendu, Kanak, Partha with whom I have spent a lot of memorable moments. I might not forget my childhood buddies. I

sincerely thank Rebati, Santanu, Chinmoy (Piku), Soumen (Jolu), Atanu (Rintu), Animesh (Biltu), Mukta. I am really lucky to have them in my life.

Without my parents' and sister's relentless support and love I would have not reached at this stage. I owe everything to them. I would like to thank all my relatives for their close association with me. I am blessed with two very special people in my life my sweetest niece, Ritu and nephew, Suraj, without them life would have been so color-less.

When she is reading this she might be thinking how come I have forgotten her. It's very difficult to forget you Mousumi (my fiancée). You are so special to me. The amount of patience and love you have kept for me, I just can't believe.

Satyajit

List of Publications

1. "Fluorescence Quenching of CdS Quantum Dots by 4-Azetidinyl-7-Nitrobenz-2-Oxa-1,3-Diazole: A Mechanistic Study." K. Santhosh, **S. Patra**, S. Soumya, D. C. Khara and A. Samanta, ***ChemPhysChem***, 12 **(2011)**, 2735-2741.
2. "Diffusion of Organic Dyes in Bovine Serum Albumin Solution Studied by Fluorescence Correlation Spectroscopy." **S. Patra**, K. Santhosh, A. Pabbathi and A. Samanta, ***RSC Advances***, 2 **(2012)**, 6079-6086.
3. "Microheterogeneity of Some Imidazolium Ionic Liquids As Revealed by Fluorescence Correlation Spectroscopy and Lifetime Studies." **S. Patra** and A. Samanta, **J. Phys. Chem. B**, 116 **(2012)**, 12275-12283.
4. "Structural Transformation of Bovine Serum Albumin Induced by Dimethyl Sulfoxide and Probed by Fluorescence Correlation Spectroscopy and Additional Methods." A. Pabbathi, **S. Patra** and A. Samanta, ***ChemPhysChem***, 14 **(2013)**, 2441-2449.
5. "A Fluorescence Correlation Spectroscopy, Steady-State, and Time-Resolved Fluorescence Study of Modulation of Photophysical Properties of Mercaptopropionic Acid Capped CdTe Quantum Dots upon Exposure to Light." **S. Patra** and A. Samanta, ***J. Phys. Chem. C***, 117 **(2013)**, 23313-23321.
6. "Effect of Capping Agent and Medium on Light-Induced variation of the Luminescence Properties of CdTe Quantum Dots: A Study Based on Fluorescence Correlation Spectroscopy, Steady-State and Time-Resolved Fluorescence Techniques." **S. Patra** and A. Samanta, ***J. Phys. Chem. C***, 118 **(2014)**, 18187-18196.
7. "Effect of ZnS Shell on the Photostability and Photoactivation of the CdTe Quantum Dots." **S. Patra**, S. Seth and A. Samanta **(manuscript under preparation)**.

Conference Presentations

Oral Presentations

1. "An FCS, Steady State and Time Resolved Fluorescence Study of Modulation of the Photophysical Properties of Mercaptopropionic Acid Capped CdTe Quantum Dots Upon Irradiation with Light", **International Conference on Methods and Applications of Fluorescence (MAF 13)**, Genoa, Italy, September 8th-11th, **2013**.
2. "Effect of Light Irradiation on the Fluorescence Behavior of the Quantum Dots: An FCS, Steady State and Time Resolved Fluorescence Study", **Chemfest-2012**, **10th Annual In-House Symposium of the School of Chemistry**, University of Hyderabad, February 21st-22nd, **2014.**

Poster Presentations

1. "Diffusion of Organic Dyes in Bovine Serum Albumin solution Studied by Fluorescence Correlation Spectroscopy", **International Symposium on Recent Trends in Spectroscopy and Dynamics of Chemical Systems**, University of Hyderabad, December 7th-8th, **2011**.
2. "Microheterogeneity of Some Imidazolium Ionic Liquids As Revealed by Fluorescence Correlation Spectroscopy and Lifetime Studies", **National Fluorescence Workshop FCS-2012**, SINP and IICB, Kolkata, December 3rd-7th, **2012**.
3. "A Fluorescence Correlation Spectroscopy, Steady-State, and Time-Resolved Fluorescence Study of Modulation of Photophysical Properties of Mercaptopropionic Acid Capped CdTe Quantum Dots upon Exposure to Light", **Trombay Symposium on Radiation and Photochemistry (TSRP),** Bhaba Atomic Research Centre (BARC), Mumbai, January, 6th-9th, **2014**. **(Best Poster Presentation Award)**

CHAPTER 1

Introduction

This chapter gives an overview of the basic principles of fluorescence correlation spectroscopy; a single molecule technique, based on temporal fluctuation of the fluorescence intensity. Some applications of this technique in exploring various dynamic processes responsible for fluorescence fluctuation are also presented. This chapter introduces the quantum dots (QDs), discusses their surface stabilization, solubility, optical properties, multiple exciton generation, single particle photoblinking behavior, and applications in various fields. Structures of the proteins and fluorescence-based techniques for probing its microenvironment are presented. A brief discussion on room temperature ionic liquids highlighting their key properties and applications in various fields is provided. Finally, the motivation of this thesis and a brief outline of its chapterwise-contents are provided.

1.1. Fluorescence correlation spectroscopy (FCS) technique :

1.1.1. Fundamentals:

1.1.1.1. Principles of FCS:

Fluorescence correlation spectroscopy (FCS) is an advanced technique based on fluctuations of the fluorescence intensity originating from some dynamic processes. [1-6] In order to obtain a fluorescence fluctuation, it is important to have a single molecule or very few molecules in the detection volume. For a large number of molecules in the detection volume one will always see almost the same average number of molecules and hence, no effective fluorescence fluctuation. In order to achieve a single molecule in the detection volume one needs a very small detection volume and a very dilute solution. The smallest detection volume can be obtained at the focal spot of the excitation light and its size can be approximated from Abbe's law (Equation 1.1)

$$d = \frac{\lambda}{2NA} \qquad (1.1)$$

Where NA is the numerical aperture of the lens and is defined as NA = n sinθ, n is the refractive index of the sample solution and θ is the half angle of the maximum cone of light that can enter or exit the lens. The detection volume or the observation volume is ~ 1 fL. For a nanomolar (nM) concentration of a solution the average number of molecules in this observation volume is $N = 6.023 \times 10^{23} \times 10^{-9} \times 10^{-15} = 0.6$ as the molecules will randomly

diffuse in and out of the observation volume. Diffusion is a random process and for any random discrete event, the number of fluorophores in a volume is described by Poisson distribution (Equation 1.2)[4,7]

$$P(n,N) = \frac{N^n}{n!} e^{-N} \qquad (1.2)$$

Here, P(n,N) is the probability of finding n molecules in the observation volume when the average number of molecules present in the observation volume is N. According to Equation 1.2, for N = 0.6, there is 55% probability that the observation volume does not contain any fluorophore, 33% probability that it contains one fluorophore and 10% probability that the observation volume contains two fluorophores (Scheme 1.1).

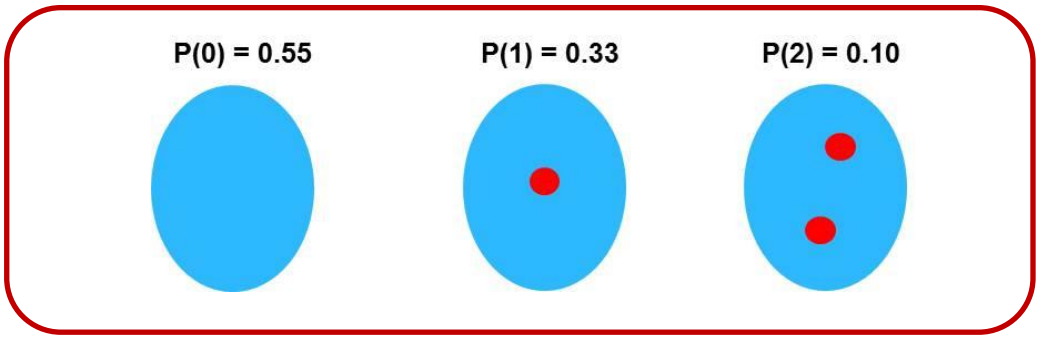

Scheme 1.1. Probability of occupancy in the observation volume (1 fL) for a 1 nM solution of fluorophore obtained from Poisson distribution, N = 0.6.

This fluctuation of the number of molecules in the observation volume will result in fluctuation of the fluorescence intensity. If the diffusion is slow then the molecules will move slowly and as a result fluctuation of the number of molecules and fluorescence intensity will be slow. Fluctuation of fluorescence intensity will be rapid in case of fast diffusion. In case of FCS these fluctuations can be quantified in their strength and duration by temporally autocorrelating the recorded fluorescence intensity fluctuations. This autocorrelation, a mathematical procedure gave the technique its name. Autocorrelation analysis determines the self-similarity of a time series of fluorescence signal and contains the dynamic information of molecular processes responsible for fluorescence fluctuation.

FCS was introduced by Madge, Elson and Webb in 1972 to study the diffusion and chemical dynamics of DNA-drug intercalation.[1] However, the early FCS measurements suffered from low signal to noise ratio due to large number of molecules in the detection

volume, unstable laser source, low detection efficiency and insufficient background suppression. By early 1990s a number of technical advancements such as confocal microscopy (limits the detection volume to focal volume), stable lasers, highly efficient single photon avalanche photodiodes, commercially available instruments made FCS a very popular and practical technique.[8-11] FCS is now widely used to study the translational diffusion of the fluorescent probes in microheterogeneous media like gel, polymer matrix, cell, biological membranes, lipid vesicles, protein solution, ionic liquids and ligand macromolecule binding, intersystem crossing, conformational dynamics of macromolecules, excited state reactions, to name a few.[5,7,12-36]

1.1.1.2. Theory of FCS:

In an FCS experiment, autocorrelation analysis on the fluctuation of fluorescence intensity is performed to generate an autocorrelation function which contains information on all dynamic processes leading to fluctuations in the fluorescence intensity. Scheme 1.2 shows the diffusion of the fluorophore through the observation volume and fluorescence intensity fluctuation. Autocorrelation function is defined as the product of the fluorescence intensity fluctuation at time t, $\delta F(t)$ and the intensity fluctuation at time $t+\tau$, $\delta F(t+\tau)$ and averaged it over a large number of measurements. The autocorrelation function normalized by the square of average fluorescence intensity ($\langle F(t) \rangle$) is given by the following Equation[3,4,6]

$$G(\tau) = \frac{\langle \delta F(t) \delta F(t+\tau) \rangle}{\langle F(t) \rangle^2} \qquad (1.3)$$

$G(\tau)$ gives the probability of finding a fluorescence photon at time $t+\tau$, provided that there is already a photon detection event at time t. FCS measures the degree of self-similarity of a fluorescence time series signal with itself at different time lags (τ). The decay of the autocorrelation function gives the duration of the fluctuation.

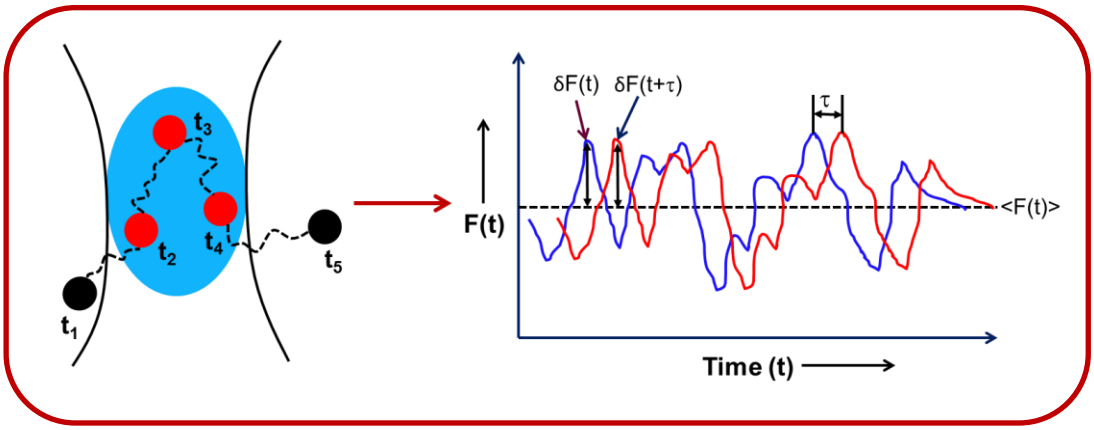

Scheme 1.2. Diffusion of a fluorophore through the observation volume and corresponding fluorescence intensity fluctuation with time (blue curve). Red curve represents time-shifted replica of the blue curve.

The emission of the single fluorophore in the focal spot is recorded photon by photon. For a stable excitation source the fluorescence fluctuations, [δF(t) and δF(t+τ)] are simply the deviations from the temporal average of the fluorescence intensity(<F(t)>).

$$\delta F(t) = F(t) - \langle F(t)\rangle \text{ and } \delta F(t+\tau) = F(t+\tau) - \langle F(t)\rangle \quad (1.4)$$

Here, $$\langle F(t)\rangle = \frac{1}{T}\int_0^T F(t)dt \quad (1.5)$$

Fluorescence collected from the observation volume may be written as[3,4,6]

$$F(t) = \kappa \int I_{ex}(r)\cdot S(r)\cdot \sigma.Q.C(r,t)\cdot dV \quad (1.6)$$

Where, κ is the overall detection efficiency of the FCS set up, $I_{ex}(r)$ is the spatial distribution of excitation light with maximum amplitude I_0, S(r) defines the optical transfer function of the objective pinhole combination and determines the spatial collection efficiency of a confocal FCS set up, σ and Q are the absorption cross section and quantum yield of the fluorophore respectively and C(r,t) is the concentration of the fluorophore in the detection volume.

Equation 1.6 looks complex and it can be simplified by convoluting spatial distribution of excitation light (I_{ex}/I_0) and spatial collection efficiency function (S(r)) into a single spatial

distribution function W(r), which determines the spatial distribution of the emitted light and is approximated by three-dimensional Gaussian as given in Equation (1.7) and defines the observation volume (Scheme 1.3).[3,6]

$$W(r) = \frac{I_{ex}}{I_0}.S(r) = e^{-\frac{2(x^2+y^2)}{r_0^2}}.e^{-\frac{2z^2}{z_0^2}} \qquad (1.7)$$

r_0 and z_0 are the lateral and axial radius at which the intensity decays to$1/e^2$.

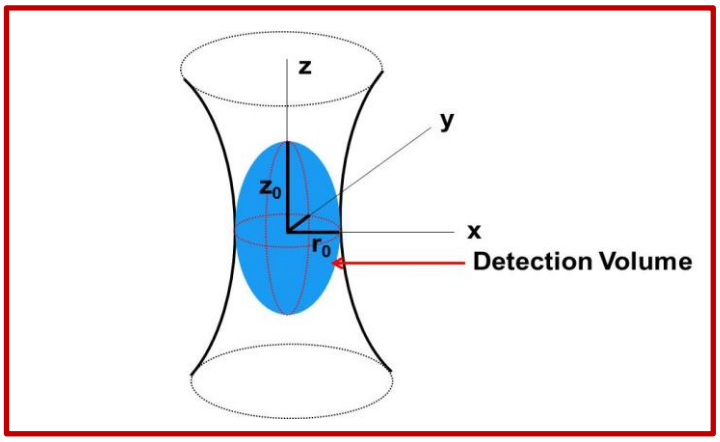

Scheme 1.3. Ellipsoidal observation volume defined by objective and pinhole combination in a confocal microscope set up.

κ, σ, Q of Equation 1.6 can be multiplied with the excitation intensity amplitude (I_0) to give a parameter, which determines the number of photons detected per molecule per second called brightness: $\eta_0 = I_0.\ \kappa.\ \sigma.\ Q$. Now for a stable excitation source the fluctuations of the fluorescence intensity can be written as,

$$\delta F(t) = \int W(r) \cdot \delta(\eta.C(r,t)) \cdot dV \qquad (1.8)$$

Substituting the Equation (1.8) to Equation (1.3) yields:

$$G(\tau) = \frac{\iint W(r)W(r')\langle\delta(\eta.C(r,t))\delta(\eta.C(r',t+\tau))\rangle dVdV'}{\left(\int W(r)\langle\eta.C(r,t)\rangle dV\right)^2} \qquad (1.9)$$

It is possible now to separate the fluctuation terms

$$\delta(\eta.C(r,t)) = C\delta\eta + \eta\delta C \tag{1.10}$$

Assuming that the fluctuation of fluorescence occurs only due to change in concentration of the molecule in the observation volume and the molecule's fluorescence properties remain constant in the observation volume, $\delta\eta = 0$ and Equation 1.9 can be rewritten as

$$G(\tau) = \frac{\iint W(r)W(r')\langle \delta C(r,0)\delta C(r',\tau)\rangle dVdV'}{\left(\langle C\rangle \int W(r)dV\right)^2} \tag{1.11}$$

In Equation (1.11) t is replaced by 0. Here delay time τ is always relative to a data point of some earlier time and hence τ is relevant. Considering molecules are undergoing free 3-dimensional diffusion in the solution with diffusion coefficient D, the concentration autocorrelation term can be calculated as,[3,37]

$$\langle \delta C(r,0)\delta C(r',\tau)\rangle = \langle C\rangle \frac{1}{(4\pi D\tau)^{-\frac{3}{2}}} e^{-\frac{(r-r')^2}{4D\tau}} \tag{1.12}$$

Inserting Equation (1.12) into Equation (1.11) and some complex mathematical calculations yield autocorrelation function for 3-dimensional diffusion as[4,6]

$$G(\tau) = \frac{1}{V_{eff}\langle C\rangle} \frac{1}{\left(1+\frac{\tau}{\tau_D}\right)\left(1+\left(\frac{r_0}{z_0}\right)^2 \frac{\tau}{\tau_D}\right)^{\frac{1}{2}}} \tag{1.13}$$

So, $G(\tau) = G(0)\, D(\tau)$

$$G(0) = \frac{1}{V_{eff}\langle C\rangle} = \frac{1}{\langle N\rangle} \quad \text{and} \quad D(\tau) = \frac{1}{\left(1+\frac{\tau}{\tau_D}\right)\left(1+\left(\frac{r_0}{z_0}\right)^2 \frac{\tau}{\tau_D}\right)^{\frac{1}{2}}} \tag{1.14}$$

G(0) is the amplitude of the correlation at τ=0, <N> is the average number of fluorophore in the observation volume and D(τ) is the portion of the correlation function containing the

diffusion coefficient (D). D can be obtained from the decay of the correlation function (τ_D) by using the following Equation

$$D = \frac{r_0^{\,2}}{4\tau_D} \tag{1.15}$$

where r_0 is the lateral radius of the observation volume (Scheme 1.3) and τ_D is the diffusion time of the fluorophore.

While derivation of autocorrelation function in the previous section it was assumed that fluorescence fluctuation is only occurring due to diffusion which changes the particle concentration in the observation volume. However, this is not the case always. Fluorophore may undergo reversible fluorescence on and off transition during its stay in the observation volume. The most common reason for such fluctuation is the transition of the dye molecule to the first excited triplet state. As this transition is forbidden by quantum mechanics, the fluorophore needs a comparably longer relaxation time to the ground state. During this time the fluorophore will appear dark and interrupts otherwise continuous fluorescence of the molecules during its stay in the observation volume. These fluctuations due to intersystem crossing appear at much faster time scale than the diffusion. In that case total correlation function can be written as[4-6,18]

$$G_{total}(\tau) = G_{diffusion}(\tau) G_{triplet}(\tau) \tag{1.16}$$

Correlation function for triplet blinking can be expressed as

$$G_{triplet}(\tau) = 1 + \frac{T}{1-T}\exp\left(-\frac{\tau}{\tau_t}\right) \tag{1.17}$$

Where T is the average fraction of molecules in the triplet state and τ_t is the triplet state relaxation time. So, the total correlation function is

$$G_{total}(\tau) = \left(1 + \frac{T}{1-T}\exp\left(-\frac{\tau}{\tau_t}\right)\right)\frac{1}{N}\left(1+\frac{\tau}{\tau_D}\right)^{-1}\left(1+\frac{\tau}{\kappa^2\tau_D}\right)^{-\frac{1}{2}} \tag{1.18}$$

Equation 1.17 can be generalized to any fast Photophysical process that results in fast reversible transition between bright (B) and dark state (D) of a fluorophore.

$$B \underset{k_b}{\overset{k_d}{\rightleftharpoons}} D \qquad (1.19)$$

Now, the expression for τ_t and T can be obtained as[6]

$$\tau_t = \frac{1}{k_d + k_b} \quad \text{and} \quad T = \frac{k_d}{k_b + k_d} \qquad (1.20)$$

Here τ_t is dark state relaxation time and T is the fraction of the molecules in the dark state. Scheme 1.4 represents a typical correlation curve containing contribution from both diffusion and triplet blinking.

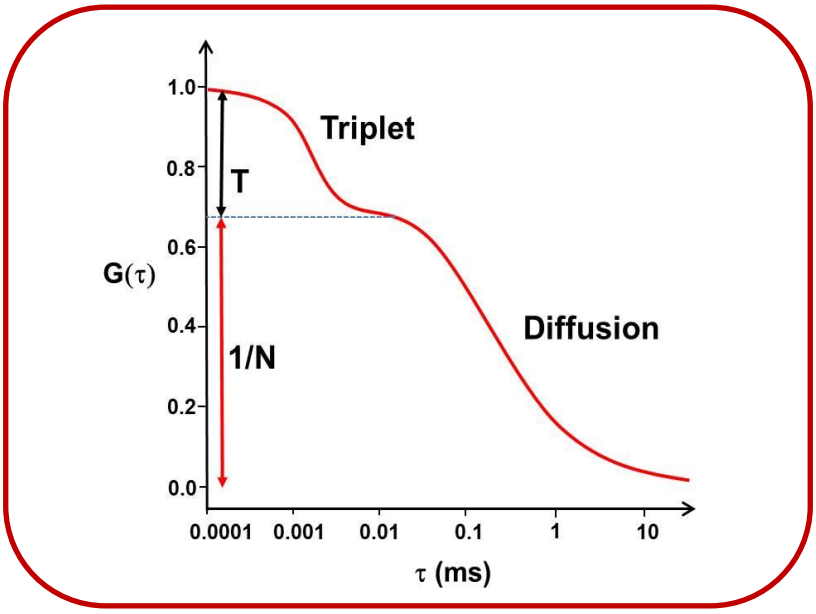

Scheme 1.4. A typical correlation curve showing both diffusion and triplet dynamics as defined by Equation 1.18.

1.1.1.3. Instrumental setup for FCS measurements:

1.1.1.3.1. Autocorrelation-based setup:

As stated previously FCS requires a very small detection volume of ~1 fL. This is achieved by a fluorescence confocal microscope set up. Confocal FCS set up for autocorrelation is illustrated schematically in Scheme 1.5. The output of the laser source is guided into a microscope objective lens through a dichroic mirror and then focused on the

sample. Fluorescence is collected by the same objective and passed through the dichroic mirror and emission filter and spatially filtered by focusing onto a pinhole to cut the out of focus light. This limits the detection volume to only the focal point of the objective lens. Finally the light is focused onto an avalanche photodiode with single photon sensitivity. A dedicated correlation board is used to correlate the fluorescence fluctuations to generate the autocorrelation function for a range of delay times τ.

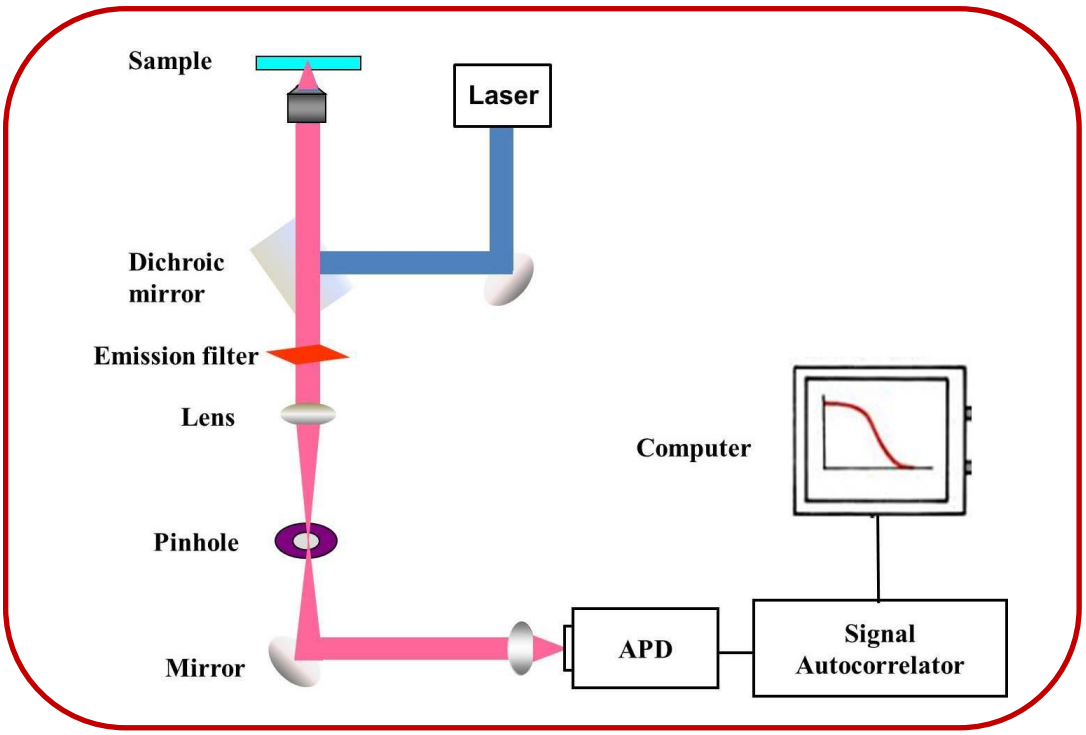

Scheme 1.5. Schematic diagram of FCS set up for autocorrelation.

1.1.1.3.2. Cross-correlation based setup:

In case of autocorrelation, signal is compared with itself at different delay times τ to measure the self-similarity. This is a common practice in electronics for decade to correlate two different signals and thus to measure the similarity between them (crosstalk). Modern FCS set up consists of two detectors to cross-correlate the fluorescence signal from the two detectors (Scheme 1.6). This removes the unwanted artifacts introduced by the detectors such as afterpulsing of an avalanche photodiode or intensity fluctuation of the illumination source and provides much higher detection specificity.[6,37]

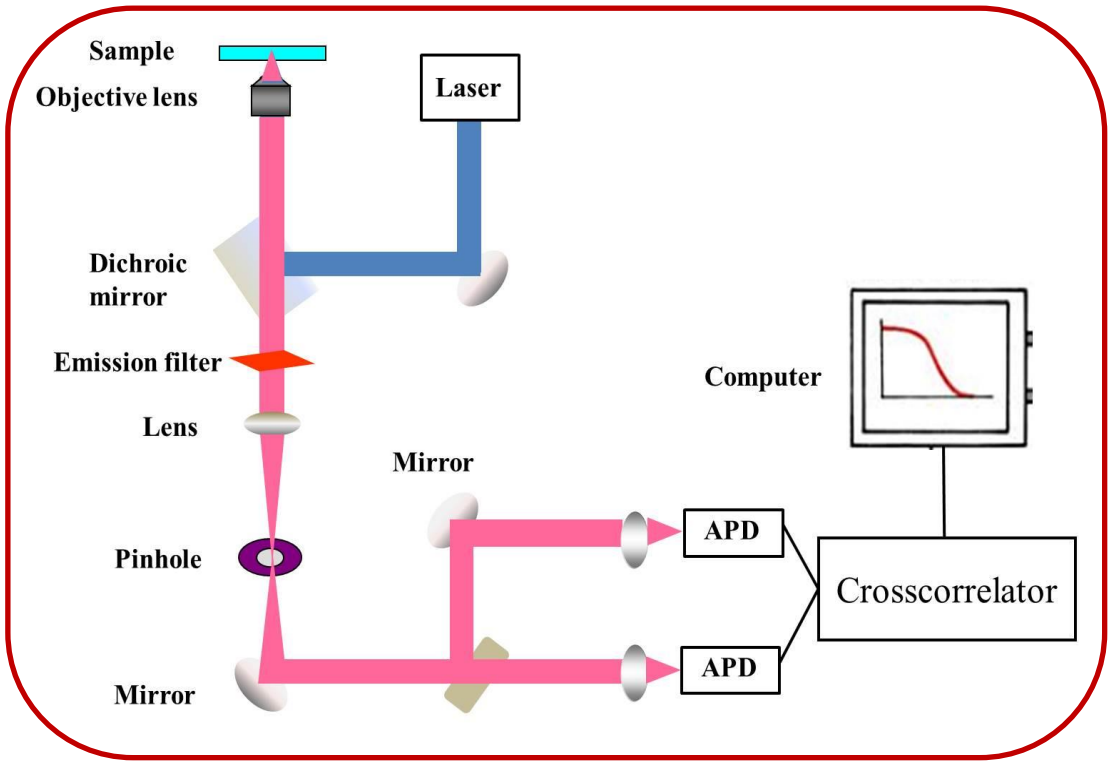

Scheme 1.6. Modern FCS set up which cross-correlate the fluorescence signal by using two detectors.

1.1.2. Applications of FCS:

1.1.2.1. Measurement of concentration and aggregation:

In dilute solutions (nM) used in the FCS experiments, the nominal concentration may be much greater than the actual concentration of the fluorophore solution present in the sample chamber. This is due to the adsorption of the molecules on the cover slip surface (prominent for most of the protein molecules due to their surface charges) which is largely unnoticed in case of concentrated solution. To determine exact binding constant between a ligand and a receptor it is important to have knowledge of the local concentrations. Since the amplitude of the correlation function at $\tau = 0$ i.e. G(0) is equal to the inverse of the number of molecules N in the observation volume (V_{eff}), FCS is an ideal technique to determine the local concentration of the fluorophore.[34,38] It is also possible to study molecular aggregation by monitoring the change in the G(0) value.[39,40]

1.1.2.2. Study of diffusion behavior of fluorophores:

1.1.2.2.1. Effect of size and molecular interaction:

Determination of the diffusion coefficient of the molecule in a medium is one of the most common applications of an FCS measurement. Equation (1.13) gives the expression of the correlation function for 3-dimensional diffusion. Diffusion coefficient of a molecule (assume spherical) in solution is related to its size by Stokes-Einstein equation,

$$D = \frac{kT}{6\pi\eta R} \tag{1.21}$$

where, k is the Boltzmann's constant, T is the temperature, η is viscosity of the solvent and R is the hydrodynamic radius of the molecule in solution. So, the size of the molecule in solution can be measured by FCS. Any changes in R will affect the diffusion time and hence the decay of the correlation function with time. Hence, it is in principle possible to monitor any process such as binding interaction between two molecules, protein folding and unfolding transitions, and chemical reactions, which leads to a change in the diffusion coefficient of the fluorophore.[41-48] Let us consider a fluorescent ligand A binds to a large host molecule, a protein B which is nonfluorescent to form a fluorescent complex AB. This can be represented by Equation 1.22

$$A + B \underset{k_{diss}}{\overset{k_{ass}}{\rightleftharpoons}} AB \tag{1.22}$$

Where, k_{ass} and k_{diss} are the association and dissociation rate constant respectively. At the start of the reaction only A is present and as the reaction proceeds concentration of AB increases until chemical equilibrium is reached. Now size of A and AB are drastically different and so, their diffusion coefficients also will be different. So, two diffusing species will be present during the course of the reaction. Let us consider D_f and D_b are the diffusion coefficients of A and AB, respectively. For a solution containing two diffusing species Equation 1.13 can be modified as

$$G(\tau) = \frac{1}{N}\left[(1-\alpha)D_f(\tau) + \alpha D_b(\tau)\right] \tag{1.23}$$

Here α is fraction of A bound to B and form AB. $D_f(\tau)$ and $D_b(\tau)$ are the diffusion parts of the correlation function with diffusion coefficients D_f and D_b. N is the total number of free and bound fluorophores in the detection volume. α can be expressed as

$$\alpha = \frac{K[AB]}{1+K[AB]} \qquad (1.24)$$

Here $K=k_{ass}/k_{diss}$ is the binding constant and can be determined from the plot of α vs [AB]. It is important to note that the two components diffusion term will only appear in the correlation function if the association and dissociation dynamics are longer than the diffusion time of the molecule in the observation volume.[27,49] If the association and dissociation dynamics is much faster than the diffusion time then the correlation function can be expressed with 1-component diffusion term with average diffusion coefficient containing contribution from both free and bound fluorescent probe.[27,49,50] This will be discussed in details in chapter 6. However, to observe a significant change in the diffusion coefficient mass ratio of the bound and free fluorophore must be at least 10 because of cube root dependent of diffusion coefficient with molecular weight. So, a 2-fold increase in molecular weight decreases the diffusion coefficient by $2^{1/3}$=1.26 fold only.

1.1.2.2.2. Probing of the microenvironment of the complex medium:

Diffusion of the fluorophore is strongly depends on its surrounding environment and hence it can sense the local environment of a microheterogeneous medium it experiences. Lipid vesicles are simplified model system of cell membrane and so, their structure and dynamics are of special interest in cell biology. FCS is ideally suited for this work.[18,21,23,26,51] It was possible to identify the multiphase state of a giant unilamellar lipid vesicle by studying the diffusion of the fluorescent probes in it using FCS.[23] This technique has been successfully employed to characterize the microscopic structural details of various complex medium e.g. polymer matrices, gels, micelle, protein solution etc.[52] Recently some groups have applied FCS to highlight the structural heterogeneity of the room temperature ionic liquids.[28,53-56] This will be discussed in details in chapter 7. One of the most important applications of FCS is to understand the diffusion behavior of the biologically relevant molecule in intracellular medium. It is necessary to distinguish between diffusion, active transport, anomalous diffusion or even convection to understand the function of the biological processes in detail.[34]

Comprehension of the underlying transport mechanism will help to understand the signal transduction or metabolic regulatory pathways. However, selections of the dyes are very crucial here. The selected dyes should neither interfere with the monitored mechanism nor introduce their own dynamics. As for example highly lipophilic dyes like rhodamine and cyanine tend to attach with intracellular membrane and deviates severely from free diffusion in the cytosol.[34]

1.1.2.3. Monitoring the fast fluctuations:

Diffusion related fluorescence fluctuation appear at a longer time scale. A fluorophore can also undergo fluorescence fluctuation during its stay in the observation volume. This fluctuation appears at a much faster time scale than the diffusion and is expressed by the correlation function given in Equation 1.17. From the analysis of the correlation function it is possible to obtain the dynamics of the processes responsible for the fast fluorescence fluctuation of a fluorophore.[6] The most common process for such fluorescence fluctuation is the transition of the fluorophore from singlet to triplet sate, known as intersystem crossing (ISC). This triplet state blinking will appear at a shorter time scale of an autocorrelation curve defined by Equation 1.18 (Scheme 1.4). ISC depends on excitation intensity and presence of oxygen or heavy atoms in the surrounding environment of the fluorophore.[25] Photoisomerization of the fluorophores also leads to fluctuation if the brightness of both the isomers is not same or one of the isomers is nonfluorescent. Trans-cis photoisomerization of cyanine dyes were investigated using FCS technique.[24,57] Like ISC, photoisomerzation also occurs in μs time scale. Family of the green fluorescent protein (GFP) used to exhibit pH induced fluctuation of the fluorescence intensity. The chromophore of this class of proteins upon protonation exhibits a shift in the absorption spectrum and thus becomes non excitable at a given wavelength and appears dark. This protonation dynamics has been monitored using FCS.[58]

One of the extensive uses of FCS is the study of conformational fluctuation of biomolecules.[29,31,59-64] In such kind of application the biomolecule of interest is labelled with a fluorophore and this fluorophore gets quenched when it comes within the close proximity of the quencher already present in the biomolecule. Conformational fluctuation will lead to fluorescence fluctuation as this motion will sometimes bring the fluorophore close to

quencher and sometimes away from quencher. Thus, by monitoring the fluorescence fluctuation one can get the conformational dynamics of the biomolecule being studied. This conformational dynamics can also be studied by using Foster resonance energy transfer (FRET) by dual labelling of the biomolecule at suitable locations using proper donor-acceptor pair.[65,66]

1.2. Quantum dots:

1.2.1. Fundamentals:

Quantum dots (QDs) are nanocrystalline semiconductor materials typically of size ~1-10 nm.[67] QDs are receiving a great deal of attention in recent years because of their interesting size dependent optical and electronic properties.[68-71] QDs were discovered in a glass matrix by Alexei Ekimov and in colloidal solutions by Louis E. Brus in 1980's.[72,73] The term "quantum dot" was coined by Mark Reed.[70] The size dependent optical and electronic properties of the QDs arises due to three dimensional quantum confinement of the exciton (bound electron-hole pair), produced during photoexcitation of QDs.[67,68,74] This quantum confinement occurs in QDs when the size of the QDs becomes comparable to or smaller than the exciton Bohr radius (most probable distance between electron and hole). Electronic states of the QDs become discrete due to this quantum confinement effect. Scheme 1.7 shows the density of states of the semiconductors with increasing dimensionality of the confinement. QDs display discrete electronic transitions reminiscent of isolated atoms or molecules and also exhibit useful properties of the bulk crystal.[67] Therefore QDs act as a linker between small molecules and bulk crystals.

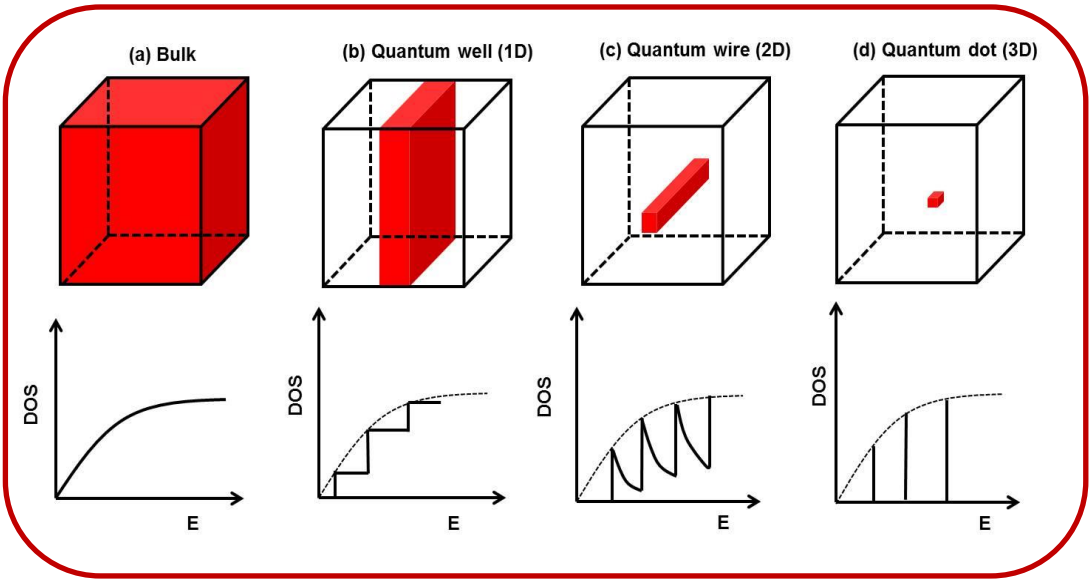

Scheme 1.7. Density of states (DOS) of (a) bulk semiconductor, (b) quantum well (confined in 1D), (c) quantum wire (confined in 2D) and (d) quantum dots (confined in 3D).

Scheme 1.8 shows the electronic energy levels of a semiconductor in transition from molecule to nanocrystal to bulk crystal. Bulk crystalline semiconductors impart a large density of electronic states and as a consequence valence band (VB) and conduction band (CB) become continuous with a fixed energy separation of E_g (bulk) between them. Whereas the energy levels of nano crystalline materials are discrete in nature and the energy gap between VB and CB varies with the size of nano particles. Treating the QD as a spherical well with infinite potential barrier, the energy of the lowest exciton band which is a bound pair of 1S electron in the conduction band (CB) and 1S hole in the valence band (VB), is given by the following equation.[68,69,75]

$$E_g(QD) = E_g(Bulk) + \frac{\hbar^2\pi^2}{2R^2m_e^*} + \frac{\hbar^2\pi^2}{2R^2m_h^*} - \frac{1.8e^2}{4\pi\varepsilon_0\varepsilon R} \qquad (1.25)$$

where E_g is the bulk band gap energy of the QD, R is the radius of the QD, m_e^* and m_h^* are the effective mass of electron and hole. The second and third term represent the confinement energies of the electron in the conduction band and the hole in the valence band, respectively. The final term explains the Coulomb attraction between electron and hole. The intense fluorescence of quantum dots is due to electron and hole recombination produced on electronic excitation. QDs have several advantages over conventional organic fluorophores, like high molar extinction coefficient, broad absorption spectra and narrow emission spectra

(multiple QDs can be excited at a single wavelength and narrow emission profile will allow easy spectral separation), long fluorescence lifetime, multiple exciton generation, high photothermal stability etc.[67,76,77] QDs are generally binary compounds formed by the combination of groups II-VI, III-V and IV-VI atoms.[78] For example CdSe, CdTe belong to II-VI QDs, similarly InP, GaAs belong to III-V QDs.[78-80]

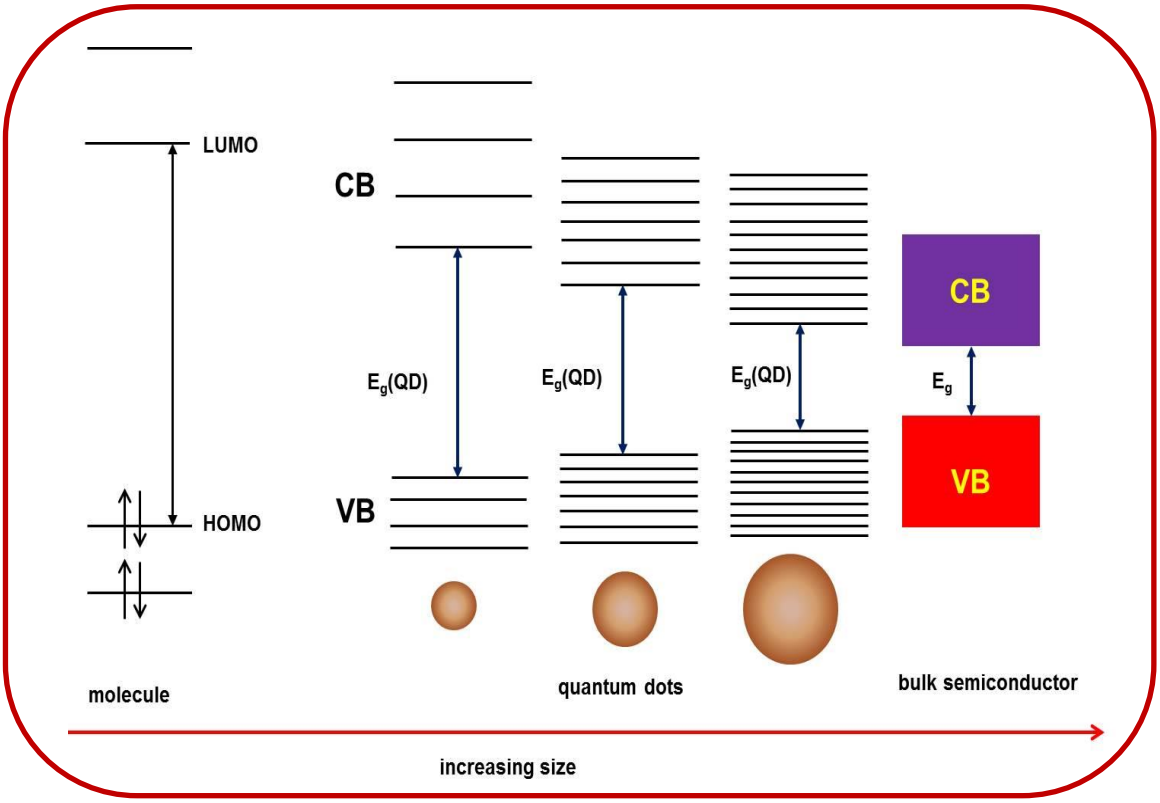

Scheme 1.8. Electronic energy levels of a molecule, quantum dots and bulk semiconductor.

There are many ways to confine an exciton in a semiconductor, which lead to many different methods for QDs synthesis. In general, quantum wires, wells and dots are formed by advanced epitaxial techniques using chemical methods or by ion implantation, or in nanodevices made by state of the art lithographic techniques.[81] A typical synthesis of colloidal QDs involves precursors, organic surfactants, and solvents.[82-84] Heating the solution at high temperature decomposes the precursors to form monomers. After then monomers nucleate and produce nanocrystals. The temperature during the QDs synthesis is a very critical factor, which determines the optimal condition for the growth of nanocrystals. It must

be high enough to allow rearrangement and annealing of atoms during the synthesis and low enough to promote crystal growth. QDs of a desired size can be synthesized at lower temperature with longer reaction time and at higher temperature with shorter reaction time. Out of the other synthesis methods colloidal synthesis is more suitable for better control of size, shape and monodispersity of the QDs.[67]

1.2.2. Surface stabilization and solubility:

The small size (nm) of the quantum dots also results in high surface to volume ratio. The surface atoms can also impact the optical properties of QDs. Atoms on the surface are not fully coordinated within the crystal lattice, thus disrupting the crystalline periodicity and leaves behind one or more dangling orbitals on each atom on the surface. These unpassivated/dangling orbitals form a band structure.[67,85,86] If these surface states are within the band gap of the QDs, they can trap the charge carriers at the surface and act as fast nonradiative de-excitation channels for photogenerated charge carriers. QDs with trap states display two emission bands, a narrow band edge emission from CB to VB and a broad emission at lower energy resulting due to recombination of electron from deep trap states and hole in the VB (Scheme 1.9).[67,85] Hence these surface states decrease the fluorescence quantum yield of the QDs and severely limit its application in various fields. The surface atoms, unless passivated, act like defects. To obtain highly luminescent QDs these defects need to be removed by passivating the surface dangling orbitals with surface stabilizing/capping agents.[67] The structures of some commonly used capping agents are given in the Chart 1.1. These surface stabilizing ligands are organic molecules containing N, S, O and P atoms, which can donate their electron pair to form metal-ligand dative bond which helps decreasing the nonradiative processes by removing the intra band-gap states. As chalcogenide ions (e.g. Se^{2-}) on the surface of the QDs binds poorly with most of the basic ligands and hence, actually responsible for deep trap emission.[67,85] These anionic sites on the surface of the QDs can be terminated by the addition of excess cations (e.g. Cd^{2+}) (Scheme 1.9).[67] This will yield a cation rich surface that can bind strongly with basic ligands and thereby reducing the deep trap emission (Scheme 1.9).

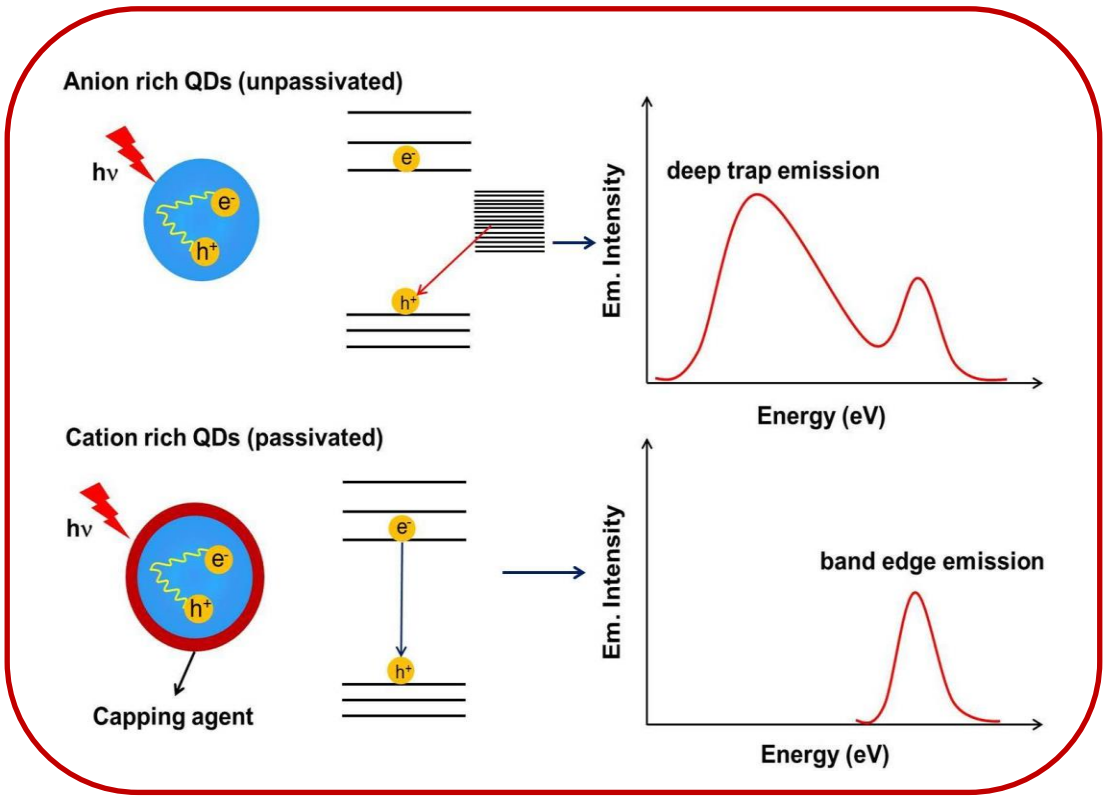

Scheme 1.9. Effect of surface trap states on QDs fluorescence.

The surface stabilizing agents are also responsible for QDs solubility. Long alkyl chains of trioctylphosphine oxide (TOPO), trioctylphosphine (TOP), and hexadecylamine (HDA) help QDs to solubilize in nonpolar solvents such as hexane, toluene, chloroform etc. (Chart 1.1). However, for biological applications QDs need to be soluble in water. For this purpose the hydrophobic capping agents on QDs surface is replaced by bifunctional molecules such as mercaptopropionic acid (MPA), aminoethanethiol (AET) hydrochloride etc.[87-89] Hydrophilic polymers and surfactants are also used to solubilize the QDs in polar solvents.[90-92] Nakashima and Kawai were the first successfully attempted to transfer the CdTe QDs into RTILs by extracting an aqueous solution of cationic thiol derivative capped CdTe QDs with 1-butyl-3-methylimidazolim bis(trifluorometahnesulfonyl) imide.[93] However, applicability of this method is only limited to hydrophobic RTILs. Recently, Santhosh et al. were able to solubilize CdTe QDs in various hydrophilic and hydrophobic RTILs by using task specific thiol capped imidazolium ionic liquid, 1-(1-undecanethiol)-3-methyl imidazolium bromide (SMIMBr), which acts as a capping agents for the QDs.[94] These QD-IL

hybrids (SMIM-capped) show superior optical properties than the conventional QDs and are potentially useful in many applications.

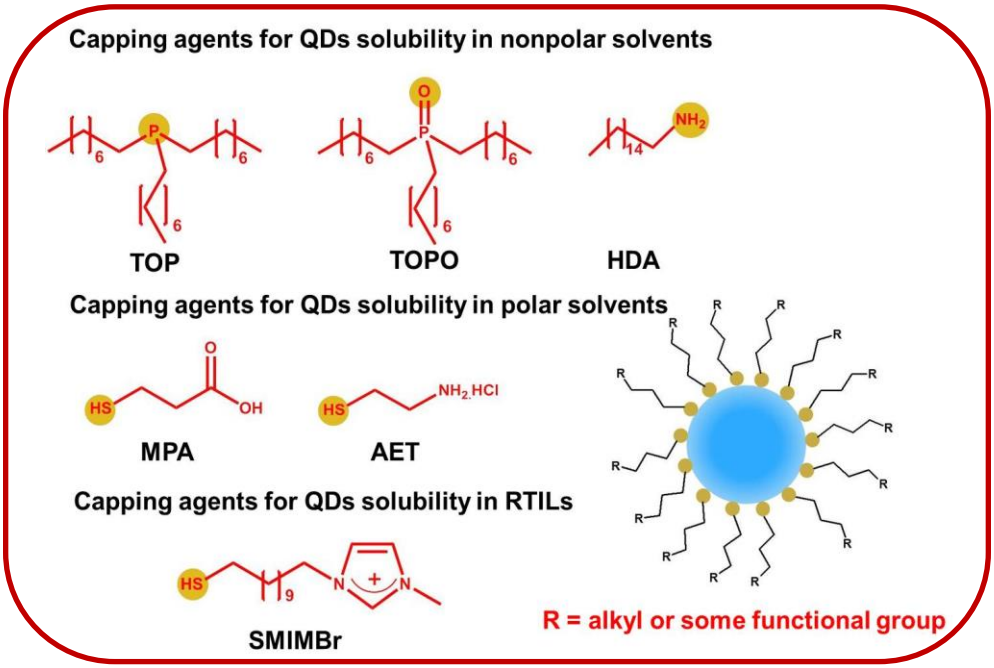

Chart 1.1. Structure of some capping agents used for surface stabilization of the QDs.

1.2.3. Core/shell quantum dots:

Although the organic surfactants serve good but it is very difficult to passivate both the cationic and anionic surface sites by the above mentioned surface capping agents. Hence, some surface trap states will always remain.[67] Again these QDs are not much stable under photooxidation which introduces further defects because of surface etching thereby decreasing the fluorescence quantum yield of the QDs.[67] An important strategy to improve QDs surface passivation is their overgrowth with a shell of a second semiconductor, resulting in core/shell QDs.[78,95,96] Inorganic epitaxial growth eliminates both cationic and anionic defects and also creates new QDs with novel properties.[78,95,96] In this manner fluorescence efficiency and stability against photooxidation for core/shell QDs has seen improvement compared to core only QDs.[67,78,95-97] Depending upon the band gaps and energy level alignment of the QDs, core/shell QDs are classified into type I, type II and reverse type I systems (Scheme 1.10.). In type I, band gap of shell material is larger than the core and hence

photogenerated electrons and holes are confined in the core. Therefore, surface defect states and environmental factors have less influence on the emission of these QDs. First reported type I system was CdSe/ZnS.[98] The ZnS shell significantly improves the stability and fluorescence quantum yield of the core CdSe QDs. Shell growth is accompanied by a small red shift of the excitonic peak in the absorption and fluorescence spectrum, which indicates partial leakage of the exciton into the shell material.[78,95] In type-II, either valence edge or conduction edge of the shell material is within the band gap of the core and based on the band alignment, either electrons or holes of the core interact with the shell material resulting in spatial separation of electrons and holes.[67,78] Type II systems (e.g. CdSe/ZnTe or CdTe/CdSe) are developed particularly for near infrared emission.[99] In reverse type I systems, a material with narrower band gap is overgrown onto the core with wider band gap and depending upon the shell thickness, the photogenerated electrons and holes will be confined into the shell material. Significant red shift of the band gap can be achieved with increase in shell thickness.[67,78] The most extensively studied systems of this type are CdS/HgS, CdS/CdSe, and ZnSe/CdSe.[100-102]

Core/shell systems are commonly synthesized in a two-step procedure.[78] In the first step core QDs of desired size are synthesized, followed by purification to remove excess starting materials and in the second step, shell material of few monolayers (typically 1-5) is grown over the core ODs. SILAR (successive ion layer adsorption and reaction) method is most extensively used for the growth of shell monolayers. In SILAR technique formation of one monolayer at a time is achieved by alternating the injections of cationic and anionic precursors of the shell material. In order to prevent self-nucleation of the shell material and uncontrolled ripening of the core NCs, the temperature T_2 for the shell growth is generally lower than temperature T_1 used for the preparation of core QDs.[78] Furthermore, the shell precursors are added slowly.

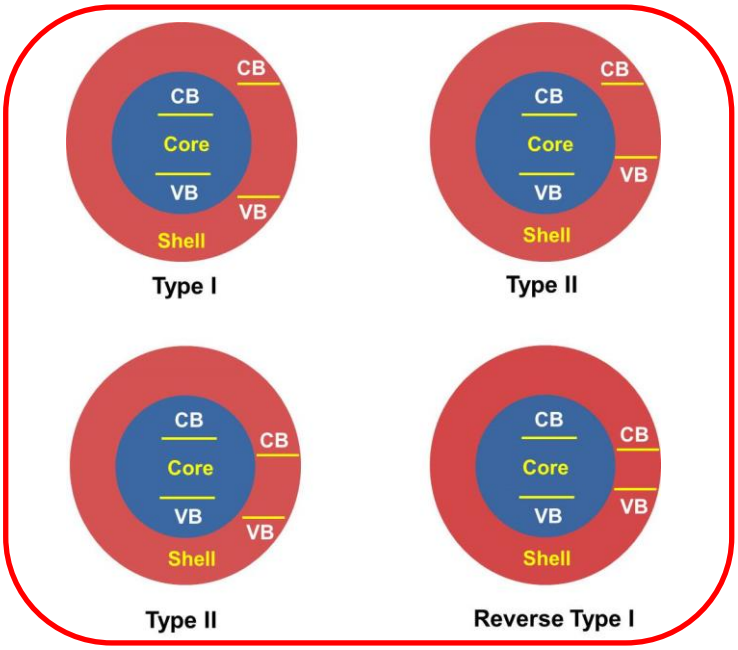

Scheme 1.10. Different types of core/shell QDs. VB and CB represents the valence band and conduction band.

1.2.4. Multiple exciton generation:

Multiple exciton generation (MEG) or carrier multiplication in QDs is an intriguing topic of research.[103-105] MEG is the phenomenon where a single photon excitation leads to the creation of multiple excitons (bound electron and hole pairs).[103,104] When a QD is excited by a photon with energy at least double the band gap, the resulting electron and hole may release their excess kinetic energy through the excitation of another electron and hole pair and thus forming a biexciton (Scheme 1.11).[104] This results in internal more than 100% quantum efficiency as biexciton is created in the QDs with a single photon. MEG is most efficient for smaller size QDs as the separation between energy levels increases and become greater than the phonon energy.[104] Therefore, the excess kinetic energy of electrons and holes can no longer be dissipated into lattice vibrations and is available for the creation of additional electron hole pairs as long as the photon energy is at least twice the band gap energy. MEG is potentially important for solar devices (photovoltaic and photoelectrochemical cells) to improve the conversion efficiency of solar radiant energy to electrical energy.[105] However, in this case Auger process where energy released due to

recombination of one electron hole pair is transferred to another electron or hole, which is either ejected from the core of the QDs to surface trap states or excited to higher electronic states, needs to be considered (Scheme 1.12). Auger processes are very fast (ps) and may eliminate the excess electron and hole pairs.[106] Hence, the extra electrons and holes must be separated, transported, and collected to yield enhanced photocurrent before their decay through Auger ionization/recombination.[106] Ultrafast pump probe spectroscopy is used to study the formation and recombination of multiple exciton states in QDs.[106,107]

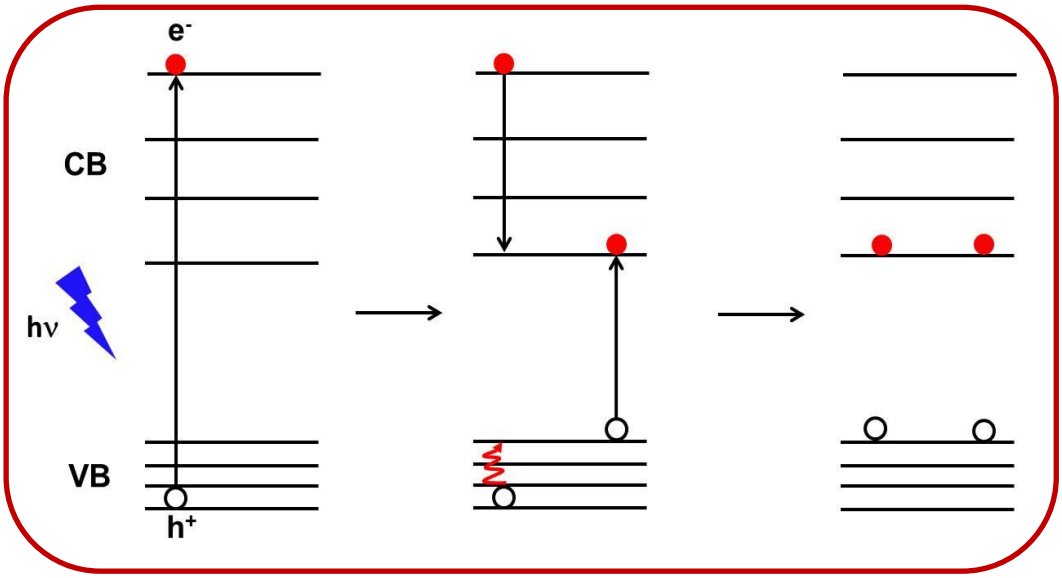

Scheme 1.11. Schematic of multiple exciton generation (MEG) in a QD. Here a single photon is creating two electron and hole pairs.

1.2.5. Fluorescence on and off blinking:

Fluorescence blinking is the random and reversible switching between fluorescent bright (on) and nonfluorescent dark state (off) of a fluorophore under continuous excitation conditions. During the off periods the fluorophore does not emit photons even though it is under continuous excitation. Fluorescence blinking is a single molecule property. As QDs have discrete electronic states, which is reminiscent of isolated atoms or molecules, a single QD also exhibits fluorescence blinking. Fluorescence blinking in QDs was first reported by Nirmal et al. in 1996.[108] The general consensus of fluorescence blinking in QDs is that it results due to trapping of charge carriers (electrons or holes), which produces

ionized core QDs (Scheme 1.12).[108-111] These ionized QDs are nonfluorescent due to very efficient Auger recombination which is several orders of magnitude greater than radiative relaxation rate.[112] QDs return to normal fluorescence when the core reneutralizes.[111] The duration of on and off events reflects the timescales on which QD charges and reneutralizes. Charge trapping from core QDs to surface trap states occur mostly via two ways. One is direct trapping of the hot carriers produced due to high energy excitation above the band gap.[109] These hot carriers can directly access the high energy trap states before their relaxation to band edge. Auger ionization is another mechanism via which trapping of charge carriers occurs.[108,109] Auger ionization occurs in the presence of multiple excitons within the QD.[108] In this case energy released due to recombination of one electron hole pair is transferred to another electron or hole, which is ejected from the core of the QDs to surface trap states. However, it is experimentally observed for QDs that the time scales of on and off events are not exponentially distributed as expected for single photoionization and neutralization rate constant.[113] Instead the distribution of the blinking time scales is highly nonexponential in nature and the time scale vary by several orders of magnitude.[109,114] The probability density of on and off time distribution follows a power law behavior. By using a static distribution of trap states, a wide range of neutralization rates is obtained which is a function of trap distance from QD core. This model successfully predicts power law behavior for off time distributions. This model however could not able to predict power law behavior for on time distribution. The fundamental reason is that even though electron is ejected to different trap states with different rate constants, the overall decay of the on state still can be described by a single rate constant which will be the sum of the individual ejection rate constants to different trap states. Hence the distribution of on times should follow exponential behavior. The failure of this model has motivated the scientists to consider other models that consider the role of dynamic processes such as fluctuating tunneling barrier between on and off state, energetic diffusion of the trap state or diffusion of the trap state and QD energy levels.[109-111,114-116] These models successfully predict power law behavior for both on and off time distribution. However, the details of the underlying mechanism of QDs blinking is still not completely understood and highly debated.[109]

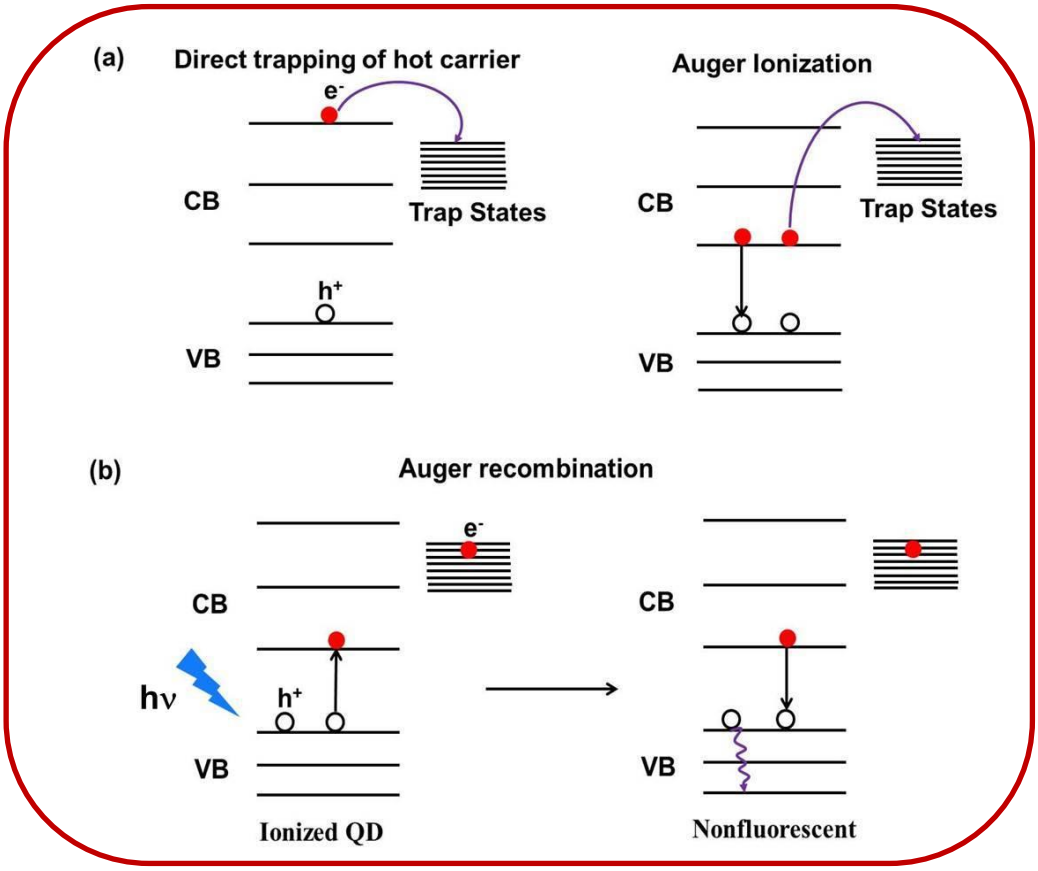

Scheme 1.12. Schematic description of (a) trapping of charge carrier from core to surface traps states and (b) Auger recombination process. In case of Auger recombination an electron nonradiatively recombine with a hole, producing an excited hole.

Although fluorescence blinking of QDs is fundamentally important to understand the mechanism and reaction rates of the charge transfer reaction from QDs to quencher molecules, it severely limits QDs applications in many areas. For example fields which require continuous excitation and emission, such as light emitting diodes, single particle tracking in biological environment and single photon sources. Hence, efforts were made to prepare a nonblinking QD. Since surface trap states are responsible for the blinking of QDs, surface passivation plays the key role in the preparation of nonblinking QDs. Near complete suppression of blinking is observed for CdSe QDs with the addition of antiblinking agent β-mercaptoethanol (BME), which binds to the surface of the QDs and passivates the trap states.[117] Another approach of preparing nonblinking QDs is to grow a thick shell (> 5nM) of another semiconductor material with larger band gap on the QDs to fully isolate the core

from the surface.[118,119] Recently, Bawendi and coworkers and Peng and coworkers independently reported nonblinking CdSe/CdS QDs with relatively thinner shell (~2 nm).[112,120]

1.2.6. Applications:

QDs offer a number of advantages over conventional organic fluorophore such as high photothermal stability, high molar extinction coefficient, long fluorescence lifetime, high fluorescence quantum yield etc.[76] These excellent properties of QDs enable them to use in various applications, for example in biological sensors, light emitting diodes, single particle tracking in biological environments, bioimaging, photodetector devices.[121-125] QDs have broad absorption and narrow emission profile.[67] Broad absorption allows excitation of multiple QDs at single excitation wavelength and narrow emission provides easy spectral separation. These properties make QD an efficient system for multicolor imaging of biological samples.[77] On the other hand low cost of production of these materials, size dependent optical and electronic properties, and possibility of multiple exciton generation (MEG) enable QDs to be used for the production of high performing and low cost QD based photovoltaic devices.[126-132]

1.3. Structure of protein molecules and their probing by fluorescence:

1.3.1. Structure of protein molecules:

The word protein is derived from the Greek word “protos” means “primary” or “first rank of importance”.[133] Protein forms the very basis of life.[134] As workhorses of the cell, proteins compose structural and motor elements in the cell, some proteins bind to and carry important molecules throughout the body.[135,136] Protein catalyzes virtually all biochemical reactions of a living system, when it serves as an enzyme. Proteins are polymers of amino acids.[134-136] All amino acids possess common structural feature, consisting of an alpha carbon atom linked to an amino group, a carboxyl group, a hydrogen atom, and a variable component called a side chain (Chart 1.2a) except proline. Two amino acid molecules can be covalently linked through a substituted amide linkage, termed as a peptide bond, to form a dipeptide (Chart 1.2b). In case of protein many amino acids are linked by such peptide bonds. So, a protein is a long polypeptide chain. An amino acid unit in a protein

is called a residue (the part left over after losing a hydrogen atom from its amino group and the hydroxyl moiety from its carboxyl group). There are four distinct aspects of a protein's structure.[134-136]

(a) Primary structure: Primary structure of protein is the linear sequence of amino acid residues in a polypeptide chain (Figure 1.1). Each protein has a specific sequence of amino acids defined by the sequence of a gene, which is encoded in the genetic code.[135,136] So, proteins differ from one another primarily by the sequence of amino acids. This unique amino acid sequence gives protein its distinct structure and function. Removing one amino acid or changing its position affects the protein's structure and functions.

(b) Secondary structure: Secondary structure of protein is the highly regular and recurring local structure in a polypeptide chain (Figure 1.1). The most common examples of secondary structure are α helix, β sheet and turns. These secondary structures are defined by the pattern of H-bonding between the peptide groups in a polypeptide backbone. α helix is the right handed coil or spiral arrangement of the polypeptide backbone around an imaginary axis. In case of β sheet polypeptide chains are arranged in a zigzag fashion and form a structure resembling a series of pleats. Turns are the region of protein where the polypeptide chain reverses its overall direction. In globular proteins, which have a compact folded structure, nearly one-third of the amino acid residues are in turns or loops. These are the elements which connect successive runs of α helix or β sheet. β turns are the most common, which connect the two segments of an antiparallel β sheet.

(c) Tertiary structure: Tertiary structure defines the overall three dimensional shape of a protein molecule (Figure 1.1). The secondary subunits (α helix and β sheets) of a polypeptide chain are folded into a compact globular structure. The polypeptide chain is folded in such a manner that the hydrophobic amino acids are buried in the interior of the protein structure and hydrophilic amino acids are exposed on the surface to interact with water molecules. Various interactions such as hydrophobic interaction, salt bridges, hydrogen bonding, ionic interaction, tight packing of side chains, disulfide bonds offer stability to the protein tertiary structure.

(d) Quaternary structure: Many proteins are composed of two or more polypeptide chains, called subunits. Quaternary structure is the combination of these subunits mainly by noncovalent interaction and in some cases by disulfide bonds (Figure 1.1).

A somewhat higher level of structural unit of a protein is a domain.[135] A structural domain of a protein is a compact self-stabilizing region folded independently from the rest of the polypeptide chain. A domain may consist of 40-400 amino acids for a large polypeptide backbone. A protein can exist in many conformations theoretically due to the free rotation around many single bonds in a polypeptide chain. Out of these conformations few are stable under biological condition. A stable conformation of protein is largely stabilized by weak interactions such as hydrophobic interaction, H-bonding and salt bridges etc.[135,136] It is the weak interactions which predominate as a stabilizing force in protein structure.

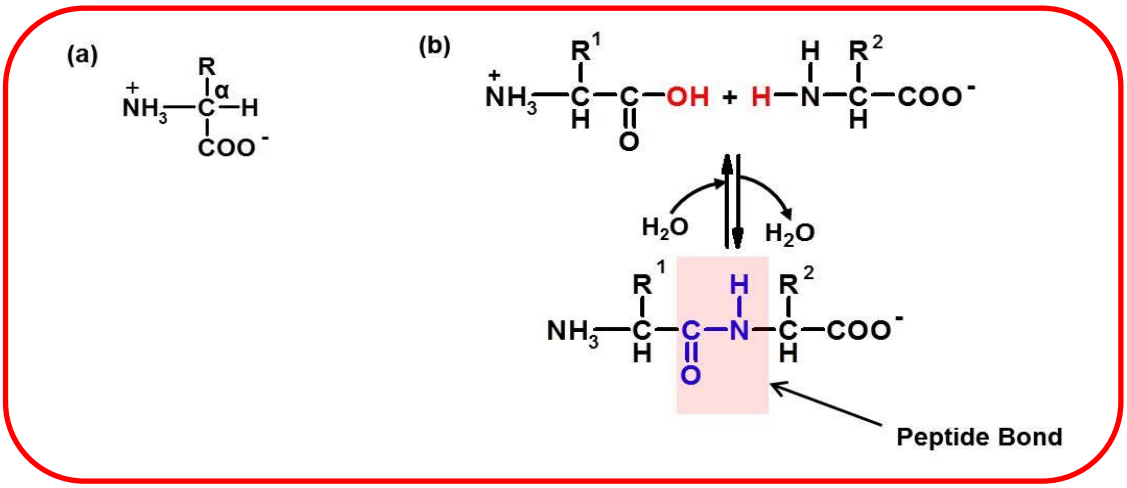

Chart 1.2. (a) General structure of an amino acid and (b) formation of a dipeptide by the combination of two amino acids.

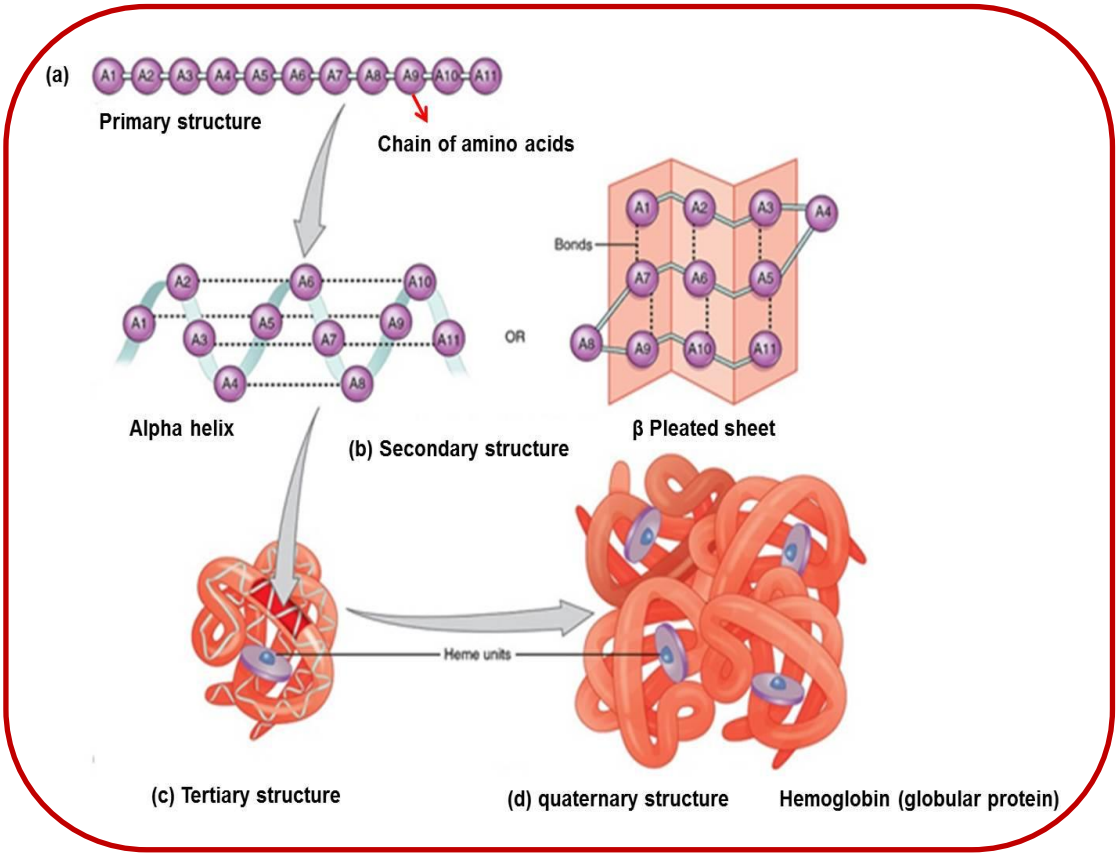

Figure 1.1. (a) Primary, (b) secondary, (c) tertiary and (d) quaternary structure of protein (source wikipedia). In this case the protein is hemoglobin, which contains heme units.

1.3.2. Probing of protein structure using fluorescence:

Fluorescence spectroscopy is one of the most popular and widely used techniques to investigate the structure and function of protein molecules.[4] Among the biopolymers, protein exhibits useful intrinsic fluorescence. Protein structure is probed by using both intrinsic and extrinsic fluorescence.[4]

(a) Intrinsic fluorescence: Protein's intrinsic fluorescence arises due to three amino acids, namely phenylalanine, tyrosine and tryptophan (Chart 1.3). Out of these three, tyrosine and tryptophan is used experimentally, as the fluorescence quantum yield of phenylalanine is very poor (0.03).[4] Tryptophan fluorescence is highly sensitive to its local environment.[4] On the other hand tyrosine fluorescence is rather insensitive to its local environment.[4] To selectively excite tryptophan, protein should be excited at 295 nm

as tyrosine does not have absorption at that wavelength. Buried tryptophan residues in the hydrophobic core displays a brighter 10-20 nm blue shifted emission spectrum compared to tryptophan residues at the surface, which experience polar environment.[4] Protein's conformational change, subunit association, substrate binding, denaturation to unfolded state changes the local environment of tryptophan residues and hence affect their fluorescence. This change in the intrinsic fluorescence can be used to monitor the structural changes occurring in the protein. Fluorescence anisotropies of both tryptophan and tyrosine depend on the overall rotational diffusion of the protein molecule and the extent of segmental motion during the excited state lifetime. Hence, intrinsic fluorescence of protein can lead to valuable information regarding protein structure and dynamics.

(b) Extrinsic fluorescence: Intrinsic fluorescence is only limited to tyrosine and tryptophan amino acid residues and is often interpretation of the data becomes complicated, when many tryptophan residues are present in different environment of proteins. Moreover short wavelength excitation source (280 or 295 nm) is not wise to study in cellular environment as it will create excessive scattering and can damage cell organelles and tissues. An alternative way to probe protein structure and dynamics is to use extrinsic fluorophore by employing external fluorophore with longer excitation and emission wavelength.[137] Some extrinsic fluorophores noncovalently label the protein due to their stronger binding affinity in the structural domains of the protein. 1-anilinonaphthalene-6-sulfonic acid (ANS) and 2-(p-toluidinyl) naphthalene-6-sulfonic acid (TNS) are the most common examples of such kind (Chart 1.3).[4,137,138] These kinds of fluorophores are weakly fluorescent in aqueous solution but become strongly fluorescent when bound to hydrophobic domains of a protein.[138] Alternatively the protein molecule of interest can be labelled covalently using an external fluorophore.[4] Most common example of these labelling fluorophores are dansyl chloride (DNS-Cl), 4-chloro-7-nitrobenz-2-oxa-1,3-diazole (NBD-Cl), fluorescein isothiocyanate (FITC) (Chart 1.3).[4,139,140] Alteration of protein structure affects the emission of these fluorophore. By monitoring the variation of fluorescence it is possible to probe the protein structure and dynamics.[4,29,59,141]

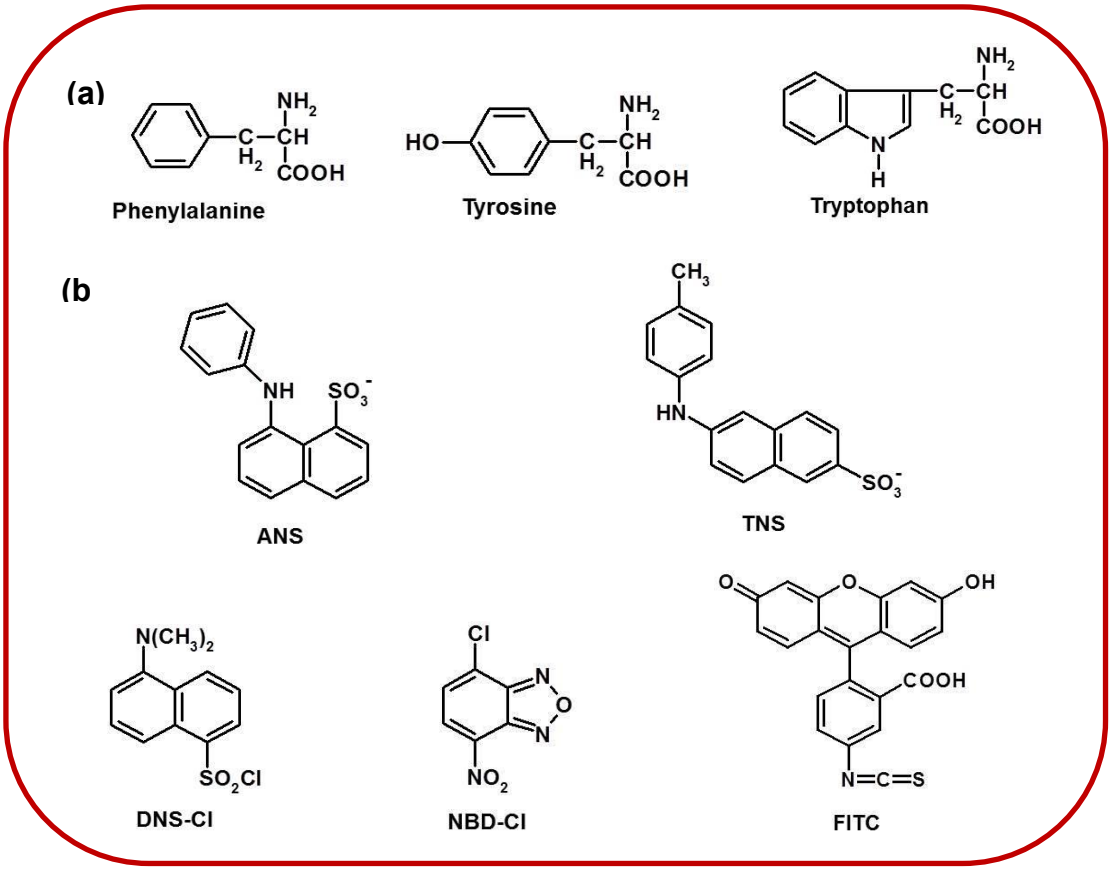

Chart 1.3. (a) Chemical formula of (a) three amino acids responsible for protein's intrinsic fluorescence and (b) the fluorophores used for extrinsic fluorescence.

1.4. Room temperature ionic liquids:

1.4.1. A brief introduction:

Over the past decade there has been an explosion of interest in room temperature ionic liquids, which stimulates new investigations on these medium.[142-151] Ionic liquids are low melting organic salts, entirely composed of ions. In academic literature the term "ionic liquids" indicates those substances which have melting point at 100^0C or lower.[152] Ionic liquids (ILs) are different from "molten salt", which represents salt melts at high temperature (803^0C for NaCl).[153] Molten salts such as NaCl at or above their melting points are highly corrosive and viscous with strong interaction between cations and anions. The low melting point of ILs is due to weak interaction between cations and anions.

Room temperature ionic liquids (RTILs) represent the class of ILs, which are liquid at ambient temperature (20-30^{0}C). The lowest melting point reported for a RTIL till date is -96^{0}C.[154] However, RTILs are not new and many of them are known for many years. In 1888, Gabriel and Weiner reported ethanolammonium nitrate (m.p. 52-55^{0}C).[155] The first true RTIL ethylammonium nitrate (m.p. 12^{0}C) was described in 1914 by Walden.[156] First generation RTILs were based on chloroaluminate anion, first reported in 1951[157] and studied in detail from 1970s onwards.[158-162] These RTILs were highly hygroscopic in nature and highly reactive towards water because of which inert environment was needed for their storage and handling. Hence, these RTILs did not receive much interest. In 1992, research in RTILs received a major boost with the discovery of air and moisture stable RTIL based on 1-ethyl-3-methylimidazolim cation and tetrafluoroborate anion, abbv. [emim][BF_4] by Wilkes et al.[163] This stimulated the research community to seriously think of RTILs as potential reaction medium and possible green alternatives to the traditional solvents, most of which are volatile organic solvents and extremely hazardous to the environment.[148,153,164,165] In the subsequent years air and moisture stable RTILs based on anions such as BF_4^-, PF_6^-, SbF_6^-, $(CF_3SO_2)_2N^-$ (known as Tf_2N^-), CH_3COO^- were developed, which belong to the second generation RTILs.[166,167] The commonly used cations of these RTILs are non-symmetrical (a) imidazolium, (b) pyrrolidinium, (c) pyridinium, (d) ammonium and (e) phosponium (Chart 1.4.). The major disadvantage of this second generation ILs is the toxicity and high cost (related to starting materials namely fluorinated component).[168] Also the presence of fluorine makes the disposal of these RTILs difficult.[169] These disadvantages of second generation RTILs led to exploration of alternative cheaper, non-fluorinated anions based RTILs.[170,171] In the recent years RTILs based on natural amino acids have been prepared and used extensively in biological applications.[172,173] There is now a growing interest in task specific RTILs, in which functional groups such as ester group, ether linkage, or chiral side chain are introduced in the alkyl group of the cation and anion.[94,174,175] These RTILs are optimized for specific applications.

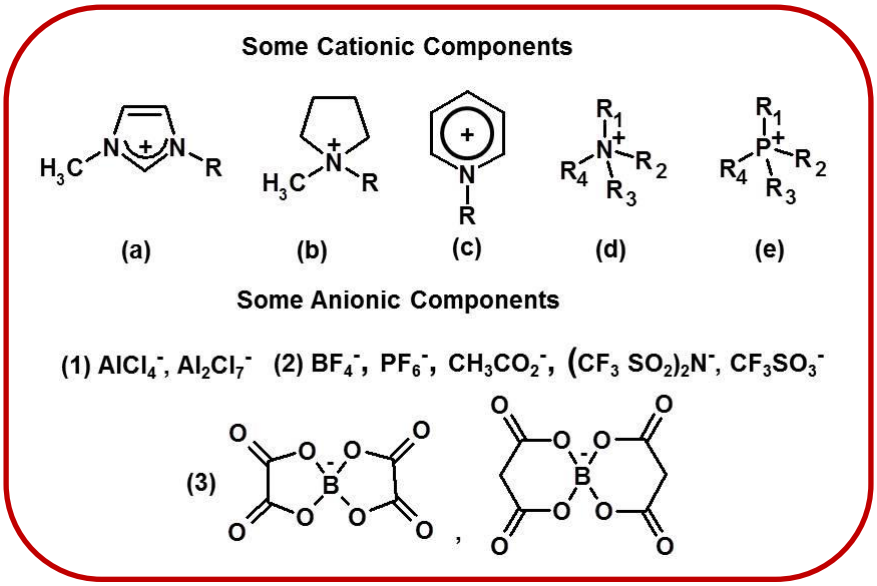

Chart 1.4. Structure of some cations and anions of the commonly used RTILs

1.4.2. Properties:

RTILs are very promising and attractive materials to research community due to their various unique and novel properties such as high thermal and chemical stability, negligible vapor pressure, non-flammable nature, wide liqudous range, moderate to high polarity, ability to dissolve large variety of inorganic and organic substances, high electrochemical window, and the advantage of recyclability.[142,148,165,176,177] The properties of RTIL strongly depend on its constituent ions. Hence, a RTIL with desired properties could be obtained by the proper selection of the two ionic components. This is why RTILs are also termed as "designer's solvent".[178] A large domain of physical and chemical properties could be available in RTILs by the iterative combination of the available cations and anions (10^{18} numbers of RTILs).[179]

Melting point: Melting points of most of the commonly used RTILs are far below than room temperature (25^0C). However, determination of exact melting point of RTILs is extremely difficult as they undergo substantial supercooling and glass formation.[180] The temperature of the phase transition can vary considerably depending on whether the sample is being heated or cooled.[180] Since the melting point of a compound depends on its structure, efforts were made to correlate the melting point of the RTILs with the nature of its ionic components.

Weak interaction between the ionic components is generally responsible for low melting point of RTILs. It has been observed for most of the RTILs that melting point decreases with increase in size, asymmetry and branching in the alky chain of the cation.[181] Although the effect of cation on the melting point is straightforward, particularly for imidazolium RTILs, the effect of anion is difficult to comprehend.[180] The delocalization of the charge density and inability of the anions to form hydrogen bonding with the hydrogen atoms of the cation is generally invoked to explain the lower melting point.[182] This is the main reason responsible for lower melting point of Tf_2N^- based RTILs, whereas more spherical anions BF_4^- and PF_6^- based RTILs, with good hydrogen bonding ability exhibit comparatively higher melting point.

Viscosity and density: RTILs are highly viscous solvents like oil in comparison to commonly used conventional organic solvents. Even the least viscous RTIL is around 30 times more viscous than water.[182] The viscosity of RTILs decreases with temperature and the trend follows non Arrhenius type of behavior.[183] Most of the cases temperature dependent viscosity data can be fitted to Vogel-Tammann-Fulcher Equation.[183,184] The presence of halide impurities and moisture seriously affect the viscosity of RTILs.[154,185] The viscosity increases with increasing alkyl chain length for imidazolium ionic liquids with Tf_2N^- and BF_4^- anions.[182] This is attributed to the increase in van der Waals interactions among cations and anions.[182] However, the effect of anion is higher on viscosity as compared to that of the cation. RTILs with Tf_2N^- anion exhibit lower viscosity compared to several other anions, while PF_6^- anion based RTILs shows higher viscosity.[181,186] High symmetry and good hydrogen bonding ability of spherical PF_6^- anion with the hydrogen of the cation offers higher viscosity in RTILs than Tf_2N^- anion.[181] However, the size of the anion and charge density also plays an important role in determining the viscosity of RTIL.[180] The higher viscosity of alcohol functionalized RTILs compared to their alkyl counterpart is solely due to hydrogen bonding.[187,188] The microviscosity of RTILs is different from their bulk viscosity as revealed by some photophysical experiments.[189] In this case the estimated microviscosity depends on the fluorescence probe employed.[189]

The density of RTILs is much higher than the most commonly used traditional organic solvents. The molar mass of the anion significantly affects the density of RTIL. The density of the RTILs decreases with increasing anionic volume.[171,181,190,191]

Polarity: Bulk polarity of any liquid is defined by the value of the static dielectric constant (ε). It has been observed that the ε value of some of the measured RTIL (ε = 9-13 at 25^0C)[192,193] is much lower than acetonitrile (ε = 35.9 at 25^0C)[194] and similar to pyridine (ε = 12.3 at 25^0C).[195] This indicates that the polarity of RTILs is much lower than acetonitrile. However, these ε values could not explain most of the experimental results in RTILs.[196] Since actual polarity is determined by the microscopic interactions (hydrogen bonding, couloumbic, electron pair donor acceptor interactions etc.) between solute and solvent molecules. The microscopic polarity is determined by E_T (30) or E_T^N values.[194,197] Several solvatochromic probes (Chart 1.5) have been used to determine the microscopic polarity parameter (E_T (30) or E_T^N) of a solvent using steady state absorption and emission techniques.[194,197-199] E_T (30) or E_T^N values for most of the commonly used RTILs have been determined.[197-199] These values indicate that RTILs are more polar than acetonitrile but less polar than methanol.[197] Actually RTILs are as polar as short chain alcohols e.g. butanol.[198,199] However, the purity of the RTILs severely affects the polarity.[197,198] This is the reason why the polarity of the same RTIL reported by different groups differ substantially as the purity of the RTIL is not same.

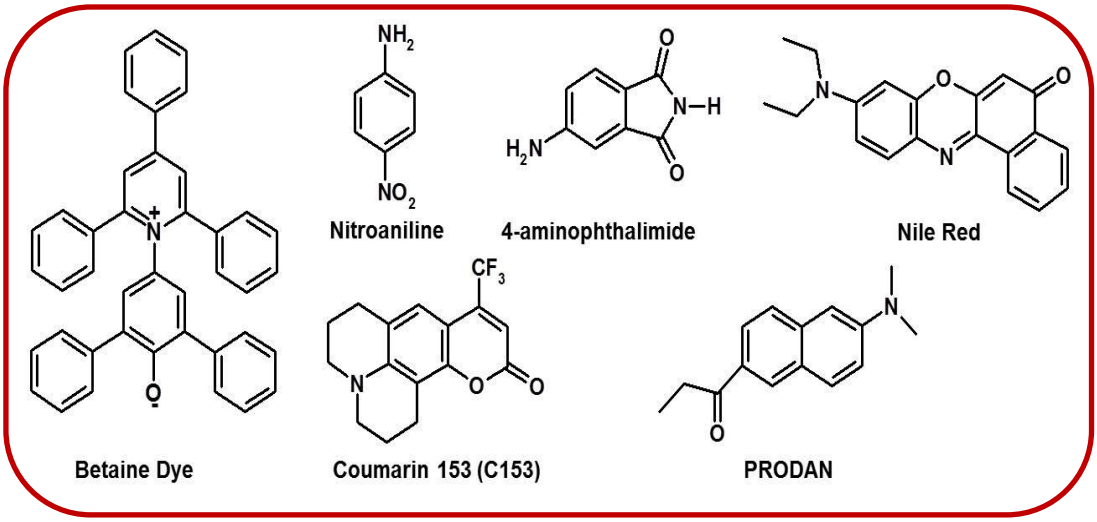

Chart 1.5. Chemical formula of some commonly used solvatochromic probe molecules used for the determination of polarity of RTILs.

Conductivity: RTILs are expected to have large conductivities as they are composed entirely of ions. However, the conductivity values of the RTILs are not so large and similar to organic solvent with added inorganic electrolytes.[200-202] For RTILs the conductivity decreases with decrease in planarity of the cationic component. This is why conductivity of 1-alkyl-3-

methylimidazolium is greater than N, N-dialkylpyrrolydinium and tetraalkylammonium.[202] For RTILs which have same cationic component but different anions, the conductivity values have been found to be similar.[180] Heat conductivities of RTILs are very high and hence they permit very rapid dispersal of heat of reaction.[180]

Thermal stability and volatility: RTILs exhibit higher thermal stability with decomposition temperature at or around 400^0C. However, appreciable thermal degradation is observed upon prolonged heating of RTIL at comparatively lower temperatures, for example 200^0C. With increasing hydrophilicity of the anionic components, decomposition temperature of the RTIL increases.[203] Thermal stability of the RTILs increases as halide < BF_4^- ~ Tf_2N^- < PF_6^-.[180,203] However, the cationic component of the RTIL does not have any significant contribution to the thermal stability of RTIL.[203]

RTILs have extremely low vapor pressure and are nonvolatile in nature. Hence, it was believed that RTILs can not be distilled. However, reports of Earle and coworkers show that some of the RTILs have significant vapor pressure and thus can be distilled under reduced pressure without any decomposition.[204] Existence of intact ion pair in the vapor state has been identified by mass spectroscopic method.[205]

Structural features and heterogeneity: Structural features of RTILs are very important in order to understand any process or chemical reaction in RTILs. Structural aspect of RTILs is widely investigated both in liquid and solid states using various experimental and theoretical studies.[206-215] Crystal structure of some of the RTILs has been determined by in situ crystallization at low temperature. Crystallographic data reveal extensive cation-anion hydrogen bonding network for imidazolium salt.[163,216] Such interaction is not clear yet for liquid salts. Some IR and NMR studies on a number of RTILs reveal the existence of H-bonding in liquid state too.[217-219]

Many experimental and theoretical studies in the past decade have revealed that RTILs are more structured in comparison to conventional organic solvents. This structural heterogeneity of RTILs is responsible for the peculiar properties of RTILs such as the ability to dissolve both polar and apolar compounds, complex solvation dynamics, anomalous viscosity trend observed upon increasing alkyl chain length etc.[220] This structural heterogeneity of the RTILs, which occurs over a spatial scale of few nm, arises due to

segregation of alkyl tails into the mesoscopic domains.[206,209,221-223] Some scatter experiments earlier indicate this structural heterogeneity.[214,215,224-226] Notable among them is the observation of the excitation wavelength dependent fluorescence behavior of dipolar system and reaction rate faster than diffusion.[215,224,225,227] Although these experiments did not provide structural details of RTILs but clearly indicates RTILs do not belong to the category of homogeneous medium. The local ordering in RTILs is also proposed by Hamaguchi and co-workers based on their Raman spectroscopic data of few RTILs.[228] This indirect evidence of local ordering in RTILs is also supported by a series of molecular dynamics simulations studies from independent groups.[209,229-231] These studies for the first time revealed nanoscale structural organization in RTILs as a consequence of the segregation of the alkyl chains. In 2007 small wide angle X-ray scattering (SWAXS) provided the first experimental evidence of this nanoscale structural heterogeneity of RTILs.[232] However, recently neutron scattering and computational studies question some of the conclusions of SWAXS study.[233,234] Hence, it appears that the structural detail of the RTILs is still not understood completely. Further experiments and simulations are required to explore the mesoscopic structural heterogeneity of RTILs.

Other properties: RTILs are classified as hydrophobic and hydrophilic depending on their miscibility with water. The anionic component plays a key role in determining solubility of the RTIL. For example PF_6^- and Tf_2N^- anion based RTILs are hydrophobic but BF_4^-, alkyl sulfate based RTILs are hydrophilic.[180] Alternatively hydrophobicity can be introduced in a RTIL by increasing alkyl chain length of the cation.[181,190] Addition of polar functional group such as OH, NH_2 in the alkyl chain increases the hydrophilicity of the RTILs and hence, its water miscibility. The refractive indices of the most commonly used RTILs are comparable to organic solvents.

1.4.3. Applications:

Some excellent properties of RTILs such as high thermal stability, non-volatile nature and ability to dissolve both polar and apolar molecules caught the attention of research community. This led to serious thoughts of using RTILs as a potential green replacement to conventional volatile organic compounds, which are used as solvents in organic synthesis. Since then RTILs are used extensively in organic synthesis, catalysis, mass spectrometry and

separation processes.[146,148,165,166,176,177,235] High proton conductivity, low reactivity, wide electrochemical window enabled RTILs to be used in electrochemical applications such as Li-ion batteries, fuel cells, double layer capacitors and actuators.[203,236-239] In material chemistry, RTILs are used as a potential candidate for the synthesis of different types of nanoparticles.[240-242] It has been found that transition metal nanoparticle synthesized in RTILs possess high stability and catalytic activity.[243] Synthesis of biocompatible RTILs have enabled them to be used as a solvent in biocatalysis, protein folding and unfolding studies and enzyme based reactions.[172,244] Several RTILs have been used for the production of biodiesel (fatty acid methyl esters), which is a renewable and environment friendly fuel.[245] RTILs can also be used as a stationary phase in gas chromatography.[246] The cation and anion of the RTILs can be functionalized to form a task specific RTILs for particular applications.[174,175] Recently imidazolium cation of the RTIL was functionalized with thiol group to cap semiconductor nanocrystalline materials (quantum dots) to form real quantum dot-ionic liquid hybrids.[94]

1.5. Motivation behind the thesis:

The work presented in this thesis has been carried out with two objectives; (i) to comprehend the photophysical behavior of the QDs that plays a key role in determining their applications in a wide variety of areas, and (ii) to obtain insight into the microenvironment of the complex media such as protein solution and ionic liquids by monitoring the diffusion of the fluorescent probes of different hydrophobicity in these media. The QDs and dye molecules chosen for this study are listed in Chart 1.6.

Due to the superior optical properties of the QDs than the conventional organic fluorophores, QDs appear at the first glance as ideal fluorophores for FCS applications. Despite this fact only a handful of FCS studies were reported on QDs photophysics.[247-254] Widely distributed time scale of blinking of QDs has limited their use in FCS experiments.[111,250] Hence, a proper mathematical model is required to understand the blinking dynamics of QDs. The amplitude of the correlation at time 0 [G(0)] in a FCS measurement is inversely proportional to the number of emitters present in the observation volume. Hence, a plot of the G(0) value vs excitation power can provide insights into the light induced changes in the QDs. It is observed that the G(0) value decreases with increasing excitation power and

this decrease is much larger for QDs compared to the organic fluorophore.[253] However, this light induced change in the QDs is not fully understood and it requires focused study considering that it plays a key role in determining the potential of these materials in various applications.

Light induced variation of the fluorescence properties (both increase and decrease of fluorescence intensity) is observed for QDs. Of the two, light induced enhancement of the QDs, termed as photoactivation, is more interesting. It is commonly believed that passivation of the surface trap states by light is responsible for photoactivation. However, the mechanism of surface passivation is not clear yet and a wide variety of mechanisms are reported.[255-262] As understanding of the mechanism of surface passivation is crucial to the utility of the QDs in diverse fields, we have chosen three CdTe QDs with different capping agents (Chart 1.6) and dispersed them in three different solvent media to conclusively establish the exact nature of surface passivation under illumination with light. We have also studied the effect of ZnS shell on the photoactivation of the CdTe QDs to further investigate the mechanism of surface passivation.

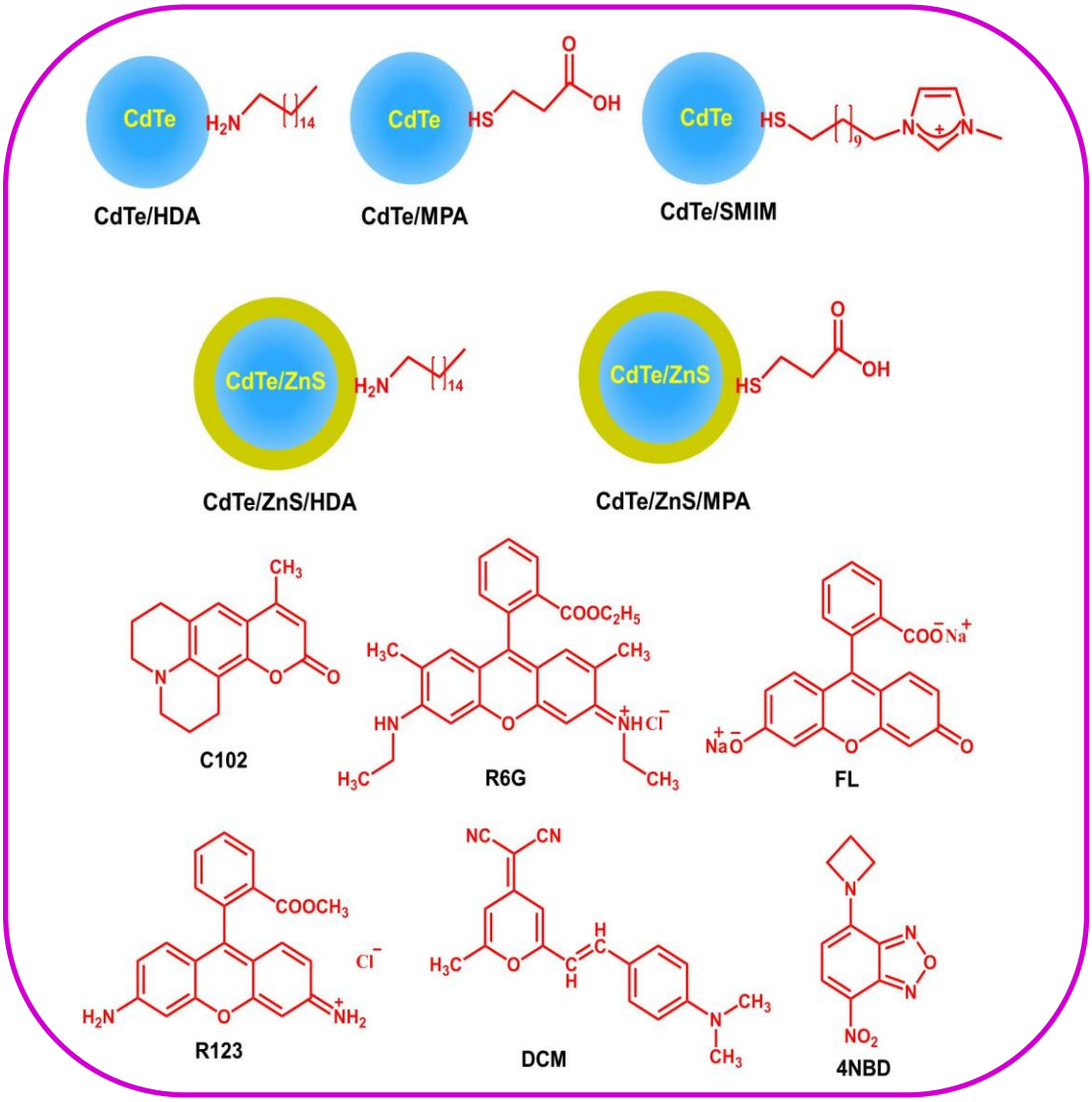

Chart 1.6. Chemical formula and abbreviations used for the QDs and probe molecules in the present study

Serum albumin is the most abundant protein in blood plasma of mammals. Serum albumin serves as depot proteins and transport proteins for a variety of compounds, like fatty acids, amino acids, bile salts, metals, hormones, drugs and pharmaceuticals.[263,264] So, the mobility of the molecules in the aqueous solution of serum albumin is of fundamental importance in drug delivery and for the design of drug molecules. We choose bovine serum albumin (BSA) protein to study the diffusion behavior of the small organic fluorophore as it is a widely studied protein and its structure and binding domains are well characterized.[265-267]

Since BSA has both hydrophilic and hydrophobic domains, the diffusion of the probe in BSA solution may vary depending on the binding site of the probes, as the nature and strength of interactions between the protein molecule and the probe will be different in hydrophilic and hydrophobic binding domains. To take into account this factor we select both electrically neutral (C102) and electrically charged (R6G, FL) dye molecule (Chart 1.6) to study the translational diffusion of the probes in BSA.

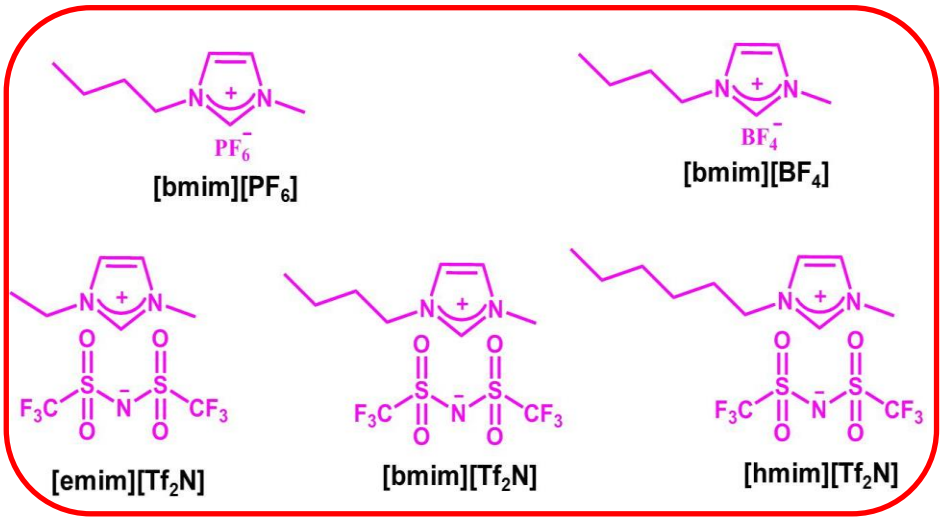

Chart 1.7. Chemical formula and abbreviations of the RTILs used in this work

As RTILs are emerging as a new class of solvents for various fundamental studies and applications, understanding its microscopic and structural dynamics is very important and remains as an intriguing topic of research. RTILs are more structured solvents than the common organic solvents in chemistry laboratory. This structural heterogeneity of RTILs occurs over a spatial scale of few nm.[206,222] The dimension of a dye molecule is ~1 nM and the diffusion of the molecules is highly sensitive to its surrounding environment. So, diffusion of the organic fluorophores can sense the local environment of RTILs. So, we studied the diffusion of three carefully chosen organic fluorophores R123 (cationic), 4NBD (neutral) and DCM (neutral) (Chart 1.6) to probe the structural heterogeneity of the five carefully selected RTILs (Chart 1.7). Fluorescence lifetime studies of these probe molecules also have been carried out to support the FCS data.

1.6. Thesis layout:

The thesis has been divided into eight chapters. ***Chapter 1*** starts with an overview of FCS technique and its various applications. The chapter introduces the QDs and discusses their various properties and applications. This is followed by a brief description of structures of the proteins and probing of their microenvironment by using fluorescence technique. The RTILs highlighting their key properties and applications are also discussed. Finally motivation of the thesis concludes this chapter. ***Chapter 2*** provides details of the materials, experimental procedure, instrumentation and various methodologies involved in the present study. ***Chapter 3*** presents modulation of photophysical properties of mercaptopropionic acid capped CdTe QDs upon exposure to light. ***Chapter 4*** deals with effect of capping agent and medium on light-induced variation of the luminescence properties of CdTe QDs. ***Chapter 5*** explains effect of ZnS shell on the photostability and photoactivation of the CdTe QDs. ***Chapter 6*** presents diffusion of organic dyes in BSA solution. ***Chapter 7*** discusses microheterogeneity of some imidazolium ionic liquids probed by fluorescence correlation spectroscopy and lifetime studies. ***Chapter 8*** summarizes the findings of the present investigations. The scope of the further studies based on the present work has also been outlined.

References:

(1) Magde, D.; Eison, E.; Webb, W. W. *Phys. Rev. Lett.* **1972**, *29*, 705.

(2) Magde, D.; L., E. E.; Webb, W. W. *Biopolymers* **1974**, *13*, 29.

(3) Thompson, N. L. *Topics in Fluorescence Spectroscopy, Volume 1: Techniques, edited by Joseph R. Lakowicz, Plenum Press, New York, 1991*.

(4) Lackowicz, J. R. *Principles of Fluorescence Spectroscopy, Third Edition, Springer, New York* **2006**.

(5) Krichevsky, O.; Bonnet, G. *Rep. Prog. Phys.* **2002**, *65*, 251.

(6) Schwille, P.; Haustein, E. *Fluorescence Correlation Spectroscopy: An introduction to its concepts and applications, Biophysical Textbooks online* **2004**, *1-33*.

(7) Perevoshchikova, I. V.; Kotova, E. A.; Antonenko, Y. N. *Biochemistry (Moscow)* **2011**, *76*, 497.

(8) Rigler, R.; Mets, U.; Widengren, J.; Kask, P. *Eur. Biophys. J.* **1993**, *22*, 169.

(9) Webb, W. W. *Fluorescence correlation spectroscopy: theory and applications, pp. 305–330, R Rigler, ES Elson (Ed.), Springer, New York, 2001*.

(10) Rigler, R.; Widengren, J. *Bioscience* **1990**, *3*, 180.

(11) Qian, H.; Elson, E. L. *Appl. Opt.* **1991**, *30*, 1185.

(12) Fatin-Rouge, N.; Wilkinson, K. J.; Buffle, J. *J. Phys. Chem. B* **2006**, *110*, 20133.

(13) Ghosh, S.; Mandal, U.; Adhikari, A.; Bhattacharyya, K. *Chem. Asian. J.* **2009**, *4*, 948.

(14) Wang, Z.; Shah, J. V.; Berns, M. W.; Cleveland, D. W. *Biophys. J.* **2006**, *91*, 343.

(15) Ribeiro, A. M.; Boukari, H.; Nossal, R.; Horkay, F. *Macromolecules* **2004**, *37*, 10212.

(16) Macháň, R.; Hof, M. *Biophys. Acta* **2010**, *1798*, 1377.

(17) Macháň, R.; Hof, M. *Int. J. Mol. Sci.* **2011**, *11*, 427.

(18) Haustein, E.; Schwille, P. *Annu. Rev. Biophys. Biomol. Struct.* **2007**, *36*, 151.

(19) Guigas, G.; Kalla, C.; Weiss, M. *Biophys. J.* **2007**, *93*, 316.

(20) Bernacchi, S.; Mueller, G.; Langowski, J.; Waldeck, W. *Biochem. Soc. Trans.* **2004**, *32*, 746.

(21) Schwille, P.; Korlach, J.; Webb, W. W. *Cytometry* **1999**, *36*, 176.

(22) Kim, S. A.; Schwille, P. *Curr. Op. Neurobiol.* **2003**, *13*, 583.

(23) Korlach, J.; Schwille, P.; Webb, W. W.; Feigenson, G. *Proc. Natl. Acad. Sci. USA* **1999**, *96*, 8461.

(24) Widengren, J.; Seidel, C. A. M. *Phys. Chem. Chem. Phys.* **2000**, *2*, 3435.

(25) Widengren, J.; Mets, U.; Rigler, R. *J. Phys. Chem.* **1995**, *99*, 13368.

(26) Korlach, J.; Baumgart, T.; Webb, W. W.; Feigenson, G. *Biochim. Biophys. Acta* **2005**, *1668*, 158.

(27) Patra, S.; Santhosh, K.; Pabbathi, A.; Samanta, A. *RSC Adv.* **2012**, *2*, 6079.

(28) Patra, S.; Samanta, A. *J. Phys. Chem. B* **2012**, *116*, 12275.

(29) Chattopadhyay, K.; Elson, E. L.; Frieden, C. *Proc. Natl. Acad. Sci. USA* **2005**, *102*, 2385.

(30) Kim, J.; Doose, S.; Neuweiler, H.; Sauer, M. *Nucleic Acids Res.* **2006**, *34*, 2516.

(31) Haustein E; P., S. *Methods* **2003**, *29*, 153.

(32) Gurunathan, K.; Levitus, M. *J. Phys. Chem. B* **2010**, *114*, 980.
(33) Mutze, J.; Ohrt, T.; Schwille, P. *Laser Photonics Rev.* **2011**, *5*, 52.
(34) Haustein, E.; Schwille, P. *Methods* **2003**, *29*, 153.
(35) Gratton, E.; Breusegem, S.; Barry, N.; Ruan, Q.; Eid, J. *Biophotonics-Optical Science and Engineering for the 21st Century, Kluwer Academic/Plenum Publishers* **2004**.
(36) Bismuto, E.; Gratton, E.; Lamb, D. C. *Biophys. J.* **2001**, *81*, 3510.
(37) Schwille, P.; Meyer-Almes, F. J.; Rigler, R. *Biophys. J.* **1997**, *72*, 1878.
(38) Starr, E.; Thompson, N. L. *J. Phys. Chem. B* **2002**, *106*, 2365.
(39) Berland, K. M.; So, P. T. C.; Chen, Y.; Mantulin, W. W.; Gratton, E. *Biophys. J.* **1996**, *71*, 410.
(40) Elson, E. L. *Traffic* **2001**, *2*, 789.
(41) Pack, C.-G.; Nishimura, G.; Tamura, M.; Aoki, K.; Taguchi, H.; Yoshida, M.; M., K. *Cytometry* **1999**, *36*, 247.
(42) Kinjo, M.; Rigler, R. *Nucleic Acids Res.* **1995**, *23*, 1795.
(43) Zettl, H.; Portnoy, Y.; Gottlieb, M.; Krausch, G. *J. Phys. Chem. B* **2005**, *109*, 13397.
(44) Wohland, T.; Friedrich, K.; Hovius, R.; Vogel, H. *Biochemistry*, *38*, 8671.
(45) Nomura, Y.; Fuchigami, H.; Kii, H.; Feng, Z. G.; Nakamura, T.; Kinjo, M. *Anal. Biochem.* **2006**, *350*, 196.
(46) Octobre, G.; Lemercier, C.; Khochbin, S.; Robert-Nicoud, M.; Souchier, C. *C. R. Biol.* **2005**, *328*, 1033.
(47) Borsch, M.; Turina, M.; Eggeling, C.; Fries, J. R.; Seidel, C. A. M.; Labahn, A.; Graber, P. *FEBS Lett.* **1998**, *437*, 251.
(48) Chattopadhyay, K.; Saffarian, S.; Elson, E. L.; Frieden, C. *Biophys. J.* **2005**, *88*, 1413.
(49) Valeur, B. *Molecular Fluorescence, Principles and Applications, WILEY-VCH Verlag GmbH, Weinheim (Federal Republic of Germany), 2002*.
(50) Novo, M.; Felekyan, S.; Seidel, C. A. M.; Al-Soufi, W. *J. Phys. Chem. B* **2007**, *111*, 3614.
(51) Ghosh, S.; Adhikari, A.; Mojumdar, S. S.; Bhattacharyya, K. *J. Phys. Chem. B* **2010**, *114*, 5736.
(52) Zustiak, S. P.; Nossal, R.; Sackett, D. L. *Biophys. J.* **2011**, *101*, 255.
(53) Werner, J. H.; Bakerb, S. N.; Baker, G. A. *Analyst* **2003**, *128*, 786.
(54) Guo, J.; Baker, G. A.; Hillesheim, P. C.; Dai, S.; Shaw, R. W.; Mahurin, M. *Phys. Chem. Chem. Phys.* **2011**, *13*, 12395.
(55) Sasmal, D. K.; Mandal, A. K.; Mondal, T.; Bhattacharyya, K. *J. phys. Chem. B* **2011**, *115*, 7781.
(56) Sarkar, A.; Ali, M.; Baker, G. A.; Tetin, S. Y.; Ruan, Q.; Pandey, S. *J. phys. Chem. B* **2009**, *113*, 3088.
(57) Widengren, J.; Schwille, P. *J. phys. Chem. A* **2000**, *104*, 6416.
(58) Haupts, U.; Maiti, S.; Schwille, P.; Webb, W. W. *Proc. Natl. Acad. Sci. USA* **1998**, *95*, 13573.
(59) Chattopadhyay, K.; Saffarian, S.; Elson, E. L.; Frieden, C. *Proc. Natl. Acad. Sci. USA* **2002**, *99*, 14171.
(60) Pabbathi, A.; Patra, S.; Samanta, A. *ChemPhysChem* **2013**, *14*, 2441.
(61) Chen, H.; Rhoades, E.; Butler, J. S.; Loh, S. N.; Webb, W. W. *Proc. Natl. Acad. Sci. USA* **2007**, *104*, 10459.

(62) Neuweiler, H.; Doose, S.; Sauer, M. *Proc. Natl. Acad. Sci. USA* **2005**, *102*, 16650.

(63) Mukhopadhyay, S.; Krishnan, R.; Lemke, E. A.; Lindquist, S.; Deniz, A. A. *Proc. Natl. Acad. Sci. USA* **2007**, *104*, 2649.

(64) Sasmal, D. K.; Mondal, T.; Mojumdar, S. S.; Choudhury, A.; Banerjee, R.; Bhattacharyya, K. *J. Phys. Chem. B* **2011**, *115*, 13075.

(65) Kim, H. D.; Nienhaus, G. U.; Ha, T.; Orr, J. W.; Williamson, J. R.; Chu, S. *Proc. Natl. Acad. Sci. USA* **2002**, *99*, 4284.

(66) Torres, T.; Levitus, M. *J. Phys. Chem. B* **2007**, *111*, 7392.

(67) Smith, A. M.; Nie, S. *Acc. Chem. Res.* **2010**, *43*, 190.

(68) Kippeny, T.; Swafford, L. A.; Rosenthal, S. J. *J. Chem. Edu.* **2002**, *79*, 1094.

(69) Brus, L. E. *J. Chem. Phys* **1984**, *80*, 4403.

(70) Reed, M. A.; Randall, J. N.; Aggarwal, R. J.; Matyi, R. J.; Moore, T. M.; Wetsel, A. E. *Phys. Rev. Lett.* **1988**, 535.

(71) Brus, L. E. *J. Chem. Phys* **1983**, *79*, 5566.

(72) Ekimov, A. I.; Efros, A. L.; Onushchenko, A. A. *Solid State Commun.* **1985**, *56*, 921.

(73) Rossetti, R.; Nakahara, S.; Brus, L. E. *J. Chem. Phys.* **1983**, *79*, 1086.

(74) Alivisatos, A. P. *Science* **1996**, *271*, 933.

(75) Bawendi, M. G.; Steigerwald, M. L.; Brus, L. E. *Annu. Rev. Phys. Chem.* **1990**, *41*, 477.

(76) Resch-Genger, U.; Grabolle, M.; Cavaliere-Jaricot, S.; Nitschke, R.; Nann, T. *Nat. Methods* **2008**, *5*, 763.

(77) Delehanty, J. B.; Bradburne, C. E.; Susumu, K.; Boeneman, K.; Mei, B. C.; Farrell, D.; Blanco-Canosa, J. B.; Dawson, P. E.; Mattoussi, H.; Medintz, I. L. *J. Am. Chem. Soc.* **2011**, *133*, 10482.

(78) Reiss, P.; Protiere, M.; Li, L. *Small* **2009**, *5*, 154.

(79) Chen, Z.; O'Brien, S. *ACS Nano* **2008**, *2*, 1219.

(80) Harris, D. K.; Bawendi, M. G. *J. Am. Chem. Soc.* **2012**, *134*, 20211.

(81) Bera, D.; Qian, L.; Tseng, T.-K.; Holloway, P. H. *Materials* **2010**, *3*, 2260.

(82) Yin, Y.; Alivisatos, A. P. *Nature* **2005**, *437*, 664.

(83) Murray, C. B.; Kagan, C. R.; Bawendi, M. G. *Annu. Rev. Mater. Sci.* **2000**, *30*, 545.

(84) Peng, X.; Wickham, J.; Alivisatos, A. P. *J. Am. Chem. Soc.* **1998**, *120*, 5343.

(85) Underwood, D. F.; Kippeny, T.; Rosenthal, S. J. *J. Phys. Chem. B* **2001**, *105*, 436.

(86) Pokrant, S.; Whaley, K. B. *Eur. Phys. J. D* **1999**, *6*, 255.

(87) Wang, J.; Han, S.; Ke, D.; Wang, R. *J. Nanomaterials* **2012**, doi:10.1155/2012/129041.

(88) Wuister, S. F.; Swart, I.; Driel, F. V.; Hickey, S. G.; Donega, D. D. M. *Nano Lett.* **2003**, *3*, 503.

(89) Kershaw, S. V.; Susha, A. S.; Rogach, A. L. *Chem. Soc. Rev.* **2013**, *42*, 3033.

(90) Liu, L.; Guo, X.; Li, Y.; Zhong, X. *Inorg. Chem.* **2010**, *49*, 3768.

(91) Kim, S.-W.; Kim, S.; Tracy, J. B.; Jasanoff, A.; Bawendi, M. G. *J. Am. Chem. Soc.* **2005**, *127*, 4556.

(92) Fan, H.; Leve, E. W.; Scullin, C.; Gabaldon, J.; Tallant, D.; Bunge, S.; Boyle, T.; Wilson, M. C.; Brinker, C. J. *Nano Lett.* **2005**, *5*, 645.

(93) Nakashima, T.; Kawai, T. *Chem. Commun.* **2005**, 1643.

(94) Santhosh, K.; Samanta, A. *J. Phys. Chem. C* **2012**, *116*, 20643.
(95) Dabbousi, B. O.; Rodriguez-Viejo, J.; Mikulec, F. V.; Heine, J. R.; Mattoussi, H.; Ober, R.; Jensen, K. F.; Bawendi, M. G. *J. Phys. Chem. B* **1997**, *101*, 9463.
(96) Peng, X.; Schlamp, M. C.; Kadavanich, A. V.; Alivisatos, A. P. *J. Am. Chem. Soc.* **1997**, *119*, 7019.
(97) Chaudhuri, R. G.; Paria, S. *Chem. Rev.* **2012**, *112*, 2373.
(98) Hines, M. A.; Guyot-Sionnest, P. *J. Phys. Chem.* **1996**, *100*, 468.
(99) Kim, S.; Fisher, B.; Eisler, H. J.; Bawendi, M. *J. Am. Chem. Soc.* **2003**, *125*, 11466.
(100) Mews, A.; Eychmüller, A.; Giersig, M.; Schooss, D.; Weller, H. *J. Phys. Chem. B* **1994**, *98*, 934.
(101) Battaglia, D.; Li, J. J.; Wang, Y. J.; Peng, X. G. *Angew. Chem. Int. Ed.* **2003**, *42*, 5035.
(102) Zhong, X. H.; Xie, R. G.; Zhang, Y.; Basche, T.; Knoll, W. *Chem. Mater.* **2005**, *17*, 4038.
(103) Binks, D. J. *Phys. Chem. Chem. Phys.* **2011**, *13*, 12693.
(104) Smith, C.; Binks, D. J. *Nanomaterials* **2014**, *4*, 19.
(105) Nozik, A. J.; Beard, M. C.; Luther, J. M.; Law, M.; Ellingson, R. J.; Johnson, J. C. *Chem. Rev.* **2010**, *110*, 6873.
(106) Klimov, V. I. *Annu. Rev. Phys. Chem.* **2007**, *58*, 635.
(107) Yang, Y.; Rodríguez-Córdoba, W.; Lian, T. *Nano Lett.* **2012**, *12*, 4235.
(108) Nirmal, M.; Dabbousi, B. O.; Bawendi, M. G.; Macklin, J. J.; Trautman, J. K. *Nature* **1996**, *383*, 802.
(109) Cordones, A. A.; Leone, S. R. *Chem. Soc. Rev.* **2013**, *42*, 3209.
(110) Xu, Z.; Cotlet, M. *Small* **2012**, *8*, 253.
(111) Peterson, J. J.; Nesbitt, D. J. *Nano Lett.* **2009**, *9*, 338.
(112) Qin, H.; Niu, Y.; Meng, R.; Lin, X.; Lai, R.; Fang, W.; Peng, X. *J. Am. Chem. Soc.* **2014**, *136*, 179.
(113) Kuno, M.; Fromm, D. P.; Hamann, H. F.; Gallagher, A.; Nesbitt, D. J. *J. Chem. Phys* **2000**, *112*, 3117.
(114) Tang, J.; Marcus, R. A. *J. Chem. Phys* **2005**, *123*, 054704 (1.
(115) Frantsuzov, P.; Kuno, M.; Janko, B.; Marcus, R. *Nature Physics* **2008**, *4*, 519.
(116) Pelton, M.; Smith, G.; Scherer, N. F.; Marcus, R. A. *Proc. Natl. Acad. Sci. USA* **2007**, *104*, 14249.
(117) Hohng, S.; Ha, T. *J. Am. Chem. Soc.* **2004**, *126*, 1324.
(118) Chen, Y.; Vela, J.; Htoon, H.; Casson, J. L.; Werder, D. J.; Bussian, D. A.; Klimov, V. I.; Hollingsworth, J. A. *J. Am. Chem. Soc.* **2008**, *130*, 5026.
(119) Mahler, B.; Spinicelli, P.; Buil, S.; Quelin, S.; Hermier, J. P.; Dubertret, B. *Nature Materials* **2008**, *7*, 659.
(120) Chen, O.; Zhao, J.; Chauhan, V. P.; Cui, J.; Wong, C.; Harris, D. K.; Wei, H.; Han, H. S.; Fukumura, D.; Jain, R. K.; Bawendi, M. G. *Nature Materials* **2013**, *12*, 445.
(121) Chen, M. L.; He, Y. J.; Chen, X. W.; Wang, J. H. *Bioconjugate Chem.* **2013**, *24*, 387.
(122) Larson, D. R.; Zipfel, W. R.; Williams, R. M.; Clark, S. W.; Bruchez, M. P.; Wise, F. W.; Webb, W. W. *Science* **2003**, *300*, 1434.
(123) Zhao, J.; Bardecker, J. A.; Munro, A. M.; Liu, M. S.; Niu, Y.; Ding, I. K.; Luo, J.; Chen, B.; Jen, A. K. Y.; Ginger, D. S. *Nano Lett.* **2006**, *6*, 463.

(124) Bakalova, R.; Zhelev, Z.; Ohba, H.; Baba, Y. J. *J. Am. Chem. Soc.* **2005**, *127*, 11328.

(125) Vaillancourt, J.; Vasinajindakaw, P.; Lu, X. *Optics and Photonics Lett.* **2011**, *4*, 57.

(126) Schaller, R. D.; Klimov, V. I. *Phys. Rev. Lett.* **2004**, *92*, 186601

(127) Nann, T.; Skinner, W. M. *ACS Nano* **2011**, *5*, 5291.

(128) Talapin, D. V.; Lee, J.-S.; Kovalenko, M. V.; Shevchenko, E. V. *Chem. Rev.* **2010**, *110*, 389.

(129) Kamat, P. V. *Acc. Chem. Res.* **2012**, *45*, 1906.

(130) Lohse, S. E.; Murphy, C. J. *J. Am. Chem. Soc.* **2012**, *134*, 15607.

(131) Etgar, L.; Zhang, W.; Gabriel, S.; Hickey, S. G.; Nazeeruddin, M. K.; Eychmüller, A.; Liu, B.; Grätzel, M. *Adv. Mater.* **2012**, *24*, 2202.

(132) Kamat, P. V. *J. Phys. Chem. Lett.* **2013**, *4*, 908.

(133) Lau, J. Y. *Protein structure database for structural genomics group, MS Thesis, The State University of New Jersey, pp. 293-315, 2005*.

(134) Berg, J. M.; Tymoczko, J. L.; Stryer, L. *Biochemistry, 5th ed. , W. H. Freeman and Company, 2002*.

(135) Nelson, D. L.; Cox, M. M. *Lehninger PRINCIPLES OF BIOCHEMISTRY* **2004**, *4th edn. W. H. Freeman and Company, New York, USA.*

(136) Voet, D.; Voet, J. G. *Biochemistry, 4th Edition* **2011**, *JOHN WILEY & SONS, INC, USA.*

(137) Brand, L.; Gohlke, J. R. *Annu. Rev. Biochemistry* **1972**, *41*, 843.

(138) Edelman, G. M.; McClure, W. O. *Acc. Chem. Res.* **1968**, *3*, 65.

(139) Weber, G. *Biochem. J.* **1951**, *51*, 155.

(140) Waggoner, A. *Methods Enzymol.* **1995**, *246*, 362.

(141) Cohen, B. E.; Pralle, A.; Yao, X.; Swaminath, G.; Gandhi, C. S.; Jan, Y. N.; Kobilka, B. K.; Isacoff, E. Y.; Jan, L. Y. *Proc. Natl. Acad. Sci. USA* **2005**, *102*, 965.

(142) Cevasco, G.; Chiappe, C. *Green Chem.* **2014**, *16*, 2375.

(143) Nagasawa, Y.; Miyasaka, H. *Phys. Chem. Chem. Phys.* **2014**, *16*, 13008.

(144) Kar, M.; Simons, T. J.; Forsyth, M.; MacFarlane, D. R. *Phys. Chem. Chem. Phys.* **2014**, *16*, 18658.

(145) Ho, T. D.; Zhang, C.; Hantao, L. W.; Anderson, J. L. *Anal. chem.* **2014**, *86*, 262.

(146) Duan, X.; Ma, J.; Lian, J.; Zheng, W. *Cryst. Eng. Comm.* **2014**, *16*, 2550.

(147) Fei, Z.; Dyson, P. J. *Chem. Commun.* **2013**, *49*, 2594.

(148) Hallett, J. P.; Welton, T. *Chem. Rev.* **2011**, *111*, 3508.

(149) Wang, H.; Gurau, G.; Rogers, R. D. *Chem. Soc. Rev.* **2012**, *41*, 1519.

(150) Rehman, A.; Zeng, X. *Acc. Chem. Res.* **2012**, *45*, 1667.

(151) Scholten, J. D.; Leal, B. C.; Dupont, J. *ACS Catal.* **2012**, *2*, 184.

(152) Seddon, K. R. *Nature Materials* **2003**, *2*, 363.

(153) Wasserscheid, P.; Keim, W. *Angew. Chem. Int. Ed.* **2000**, *39*, 3772.

(154) Seddon, K. R.; Stark, A.; Torres, M. J. *Pure Appl. Chem.* **2000**, *72*, 2275.

(155) Gabriel, S.; Weiner, J. *Ueber einige Abkömmlinge des Propylamins* **1888**, *21*, 2669.

(156) Walden, P. *Bull. Acad. Imper. Sci. (St. Petersbourg)* **1914**, *8*, 405.

(157) Hurley, F. H.; WIer, J., T. P. *J. Electrochem. Soc.* **1951**, *98*, 207.

(158) Chum, H. L.; Koch, V. R.; Miller, L. L.; Osteryoung, R. A. *J. Am. Chem. Soc.* **1975**, *97*, 3264.

(159) Carpio, R. A.; King, L. A.; Lindstrom, R. E.; Nardi, J. C.; Hussey, C. L. *J. Electrochem. Soc.* **1979**, *126*, 1644.
(160) Hussey, C. L.; King, L. A.; Carpio, R. A. *J. Electrochem. Soc.* **1979**, *126*, 1029.
(161) Wilkes, J. S.; Levisky, J. A.; Wilson, R. A.; Hussey, C. L. *Inorg. Chem.* **1982**, *21*, 1263.
(162) Boon, J. A.; Levisky, J. A.; Pflug, J. L.; Wilkes, J. S. *J. Org. Chem.* **1986**, *51*, 480.
(163) Wilkes, J. S.; Zaworotko, M. J. *Chem. Commun.* **1992**, 965.
(164) Endres, F.; Abedin, S. Z. E. *Phys. Chem. Chem. Phys.* **2006**, *8*, 2101.
(165) Welton, T. *Chem. Rev.* **1999**, *99*, 2071.
(166) Sheldon, R. *Chem. Commun.* **2001**, 2399.
(167) Chauvin, Y.; Mussmann, L.; Olivier, H. *Angew. Chem. Int. Ed.* **1995**, *34*, 2698.
(168) Gorke, J.; Srienc, F.; Kazlauskas, R. *Biotechnol. Bioprocess Eng.* **2010**, *15*, 40.
(169) Wasserscheid, P.; Welton, T. *WILEY-VCH Verlag GmbH & Co. KGaA, Weinheim, 2003*.
(170) Larsen, A. S.; Holbrey, J. D.; Tham, F. S.; Reed, C. A. *J. Am. Chem. Soc.* **2000**, *122*, 7264.
(171) Xu, W.; Wang, L. M.; Nieman, R. A.; Angell, C. A. *J. Phys. Chem. B* **2003**, *107*, 11749.
(172) Sankaranarayanan, K.; Sathyaraj, G.; Nair, B. U.; Dhathathreyan, A. *J. Phys. Chem. B* **2012**, *116*, 4175.
(173) Ohno, H.; Fukumoto, K. *Acc. Chem. Res.* **2007**, *40*, 1122.
(174) Davis, J. H. *Chem. Lett.* **2004**, *33*, 1072.
(175) Lee, S. *Chem. Commun.* **2006**, 1049.
(176) Seddon, K. R. *Ionic Liquids, Industrial Applications for Green Chemistry, American Chemical Society, Washington DC*, 2002.
(177) Dubreuil, J. F.; Bourahla, K.; Rahmouni, M.; Bazureau, J. P.; Hamelin, J. *Catal. Commun.* **2002**, *3*, 185.
(178) Freemantle, M. *Chem. Eng. News* **1998**, *76*, 32.
(179) Rogers, R. D.; Seddon, K. R. *Science* **2003**, *302*, 792.
(180) Chiappe, C.; Pieraccini, D. *J. Phys. Org. Chem.* **2005**, *18*, 275.
(181) Dzyuba, S. V.; Bartsch, R. A. *ChemPhysChem* **2005**, *3*, 161.
(182) Zhang, C.; Sun, N.; He, X.; Lu, X.; Zhang, X. *J. Phys. Chem. Ref. Data* **2006**, *35*, 1475.
(183) Weingartner, H. *Angew. Chem. Int. Ed.* **2008**, *47*, 654.
(184) Santhosh, K.; Banerjee, S.; Rangaraj, N.; Samanta, A. *J. phys. Chem. B* **2010**, *114*, 1967.
(185) Widegren, J. A.; Laesecke, A.; Magee, J. W. *Chem. Commun.* **2005**, 1610.
(186) Carda-Broch, S.; Berthold, A.; Armstrong, D. W. *Anal. Bioanal. Chem.* **2003**, *375*, 191.
(187) Holbrey, J. D.; Turner, M. B.; Reichert, W. M.; Rogers, R. D. *Green Chem.* **2003**, *5*, 731.
(188) Branco, L. C.; Rosa, J. N.; Ramos, J. J. M.; Afonso, C. A. M. *Chem. Eur. J.* **2002**, *8*, 3671.
(189) Paul, A.; Samanta, A. *J. Phys. Chem. B* **2008**, *112*, 16626.

(190) Huddleston, J. G.; Visser, A. E.; Reichert, W. M.; Willauer, H. D.; Broker, G. A.; Rogers, R. D. *Green Chem.* **2001**, *3*, 156.

(191) Pringle, J. M.; Golding, J.; Baranyai, K.; Forsyth, C. M.; Deacon, G. B.; Scott, J. L.; MacFarlane, D. R. *New J. Chem.* **2003**, *27*, 1504.

(192) Wakai, C.; Oleinikova, A.; Ott, M.; Weingartner, H. *J. Phys. Chem. B* **2005**, *109*, 17028.

(193) Daguenet, C.; Dyson, P. J.; Krossing, I.; Oleinikova, A.; Slattery, J.; Wakai, C.; Weingartner, H. *J. phys. Chem. B* **2006**, *110*, 12682.

(194) Reichardt, C. *Solvents and Solvent Effects in Organic Chemistry, Wiley-VCH, Weinheim, 3rd Edition*, 2003.

(195) Riddick, J.; Bunger, W. B. *Organic solvents, third edition (techniques of Chemistry, Volume 2), Willey-Interscience, New york, 1970*.

(196) Paul, A.; Samanta, A. *J. Phys. Chem. B* **2007**, *111*, 1957.

(197) Reichardt, C. *Green Chem.* **2005**, *7*, 339.

(198) Aki, S. N. V. K.; Brennecke, J. F.; Samanta, A. *Chem. Commun.* **2001**, 413.

(199) Karmakar, R.; Samanta, A. *J. Phys. Chem. A* **2002**, *106*, 6670.

(200) Bonhote, P.; Dias, A.; Papageorgiou, N.; Kalyanasundaram, K.; Gratzel, M. *Inorg. Chem.* **1996**, *35*, 1168.

(201) MacFarlane, D. R.; Meakin, P.; Sun, J.; Amini, N.; Forsyth, M. *J. Phys. Chem. B* **1999**, *103*, 4164.

(202) Buzzeo, M. C.; Evans, R. G.; Compton, R. G. *ChemPhysChem* **2004**, *5*, 1106.

(203) Ngo, H. L.; LeCompte, K.; Hargens, L.; McEwen, A. *Thermochim. Acta* **2000**, *357*, 97.

(204) Earle, M. J.; Esperanca, J. M. S. S.; Gilea, M. A.; Lopes, J. N. C.; Rebelo, L. P. N.; Magee, J. W. S., K. R.; Widegren, J. A. *Nature* **2006**, *439*, 831.

(205) Chambreau, S. D.; Vaghjiani, G. L.; Koh, C. J.; Golan, A.; Leone, S. R. *J. Phys. Chem. Lett.* **2012**, *3*, 2910.

(206) Russina, O.; Triolo, A.; Gontrani, L.; Caminiti, R. *J. Phys. Chem. Lett.* **2012**, *3*, 27.

(207) Fruchey, K.; Lawler, C. M.; Fayer, M. D. *J. phys. Chem. B* **2012**, *116*, 3054.

(208) Fruchey, K.; Fayer, M. D. *J. phys. Chem. B* **2010**, *114*, 2840.

(209) Canongia Lopes, J. N. A.; Costa Gomes, M. F.; Padua, A. A. H. *J. Phys. Chem. B* **2006**, *110*, 16816.

(210) Castner Jr, E. W.; Margulis, C. J.; Maroncelli, M.; Wishart, J. F. *Annu. Rev. Phys. Chem.* **2011**, *62*, 85.

(211) Li, S.; Banuelos, J. L.; Guo, J.; Anovitz, L.; Rother, G.; Shaw, R. W.; Hillesheim, P. C.; Dai, S.; Baker, G. A.; Cummings, P. T. *J. Phys. Chem. Lett.* **2012**, *3*, 125.

(212) Khara, D. C.; Samanta, A. *J. phys. Chem. B* **2012**, *116*, 13430.

(213) Hu, Z.; Margulis, C. J. *Acc. Chem. Res.* **2007**, *40*, 1097.

(214) Tokuda, H.; Hayamizu, K.; Ishi, K.; Susan, A. B. H.; Watanabe, M. *J. Phys. Chem. B* **2004**, *108*, 16593.

(215) Mandal, P. K.; Sarkar, M.; Samanta, A. *J. Phys. Chem. A* **2004**, *108*, 9048.

(216) Kolle, P.; Dronskowski, R. *Inorg. Chem.* **2004**, *43*, 2803.

(217) Jeon, Y.; Sung, J.; Seo, C.; Lim, H.; Cheong, H.; Kang, M.; Moon, B.; Ouchi, Y.; Kim, D. *J. Phys. Chem. B* **2008**, *112*, 4735.

(218) Mele, A.; Romano, G.; Giannone, M.; Ragg, E.; Fronza, G.; Raos, G.; Marcon, V. *Angew. Chem. Int. Ed.* **2006**, *45*, 1123.

(219) Mele, A.; Tran, C. D.; Lacerda, S. H. D. P. *Angew. Chem. Int. Ed.* **2003**, *42*, 4364.

(220) Padua, A. A. H.; Costa Gomes, M. F.; Canongia Lopes, J. N. A. *Acc. Chem. Res.* **2007**, *40*, 1087.

(221) Russina, O.; Triolo, A.; Gontrani, L.; Caminiti, R.; Xiao, D.; Hines Jr, L. G.; Bartsch, R. A.; Quitevis, E. L.; Plechkova, N.; Seddon, K. R. *J. Phys.: Condens. Matter* **2009**, *21*, 424121.

(222) Russina, O.; Triolo, A. *Faraday Discuss* **2012**, *154*, 97.

(223) Macchiagodena, M.; Gontrani, L.; Ramondo, F.; Triolo, A.; Caminiti, R. *J. Chem. Phys.* **2011**, *134*, 114521.

(224) Paul, A.; Mandal, P. K.; Samanta, A. *J. Phys. Chem. B* **2005**, *109*, 9148.

(225) Skrzypczak, A.; Neta, P. *J. Phys. Chem. A* **2003**, *107*, 7800.

(226) Tokuda, H.; Hayamizu, K.; Ishii, K.; Susan, M. A. B. H.; Watanabe, M. *J. Phys. Chem. B* **2005**, *109*, 6103.

(227) Paul, A.; Samanta, A. *J. Phys. Chem. B* **2007**, *111*, 1957.

(228) Iwata, K.; Okazima, H.; Saha, S.; Hamaguchi, H. *Acc. Chem. Res.* **2007**, *40*, 1174.

(229) Wang, Y.; Voth, G. A. *J. Am. Chem. Soc.* **2005**, *127*, 12192.

(230) Wang, Y.; Voth, G. A. *J. Phys. Chem. B* **2006**, *110*, 18601.

(231) Hu, Z.; Margulis, C. J. *J. Proc. Natl. Acad. Sci. U.S.A.* **2006**, *103*, 831.

(232) Triolo, A.; Russina, O.; Bleif, H. J.; Di Cola, E. *J. phys. Chem. B* **2007**, *111*, 4641.

(233) Hardacre, C.; Holbrey, J. D.; Mullan, C. L.; Youngs, T. G. A.; Bowron, D. T. *J. Chem. Phys.* **2010**, *133*, 074510.

(234) Annapureddy, H. V. R.; Kashyap, H. K.; De Biase, P. M.; Margulis, C. J. *J. Phys. Chem. B* **2010**, *114*, 16838.

(235) Armstrong, D. W.; Zhang, L. K.; He, L.; Gross, M. L. *Anal. Chem.* **2001** *73*, 3679.

(236) Armand, M.; Endres, F.; MacFarlane, D. R.; Ohno, H.; Scrosati, B. *Nat. Mater.* **2009**, *8*, 621.

(237) Ding, J.; Zhou, D.; Spinks, G.; Wallace, G.; Forsyth, S.; Forsyth, M.; MacFarlane, D. R. *Chem. Mater.* **2003**, *15*, 2392.

(238) Enomoto, T.; Nakamori, Y.; Matsumoto, K.; Hagiwara, R. *J. Phys. Chem. C* **2011**, *115*, 4324.

(239) Lewandowski, A.; Swiderska-Mocek, A. *J. Power Sources* **2009**, *194*, 601.

(240) Kuwabata, S.; Tsuda, T.; Torimoto, T. *J. Phys. Chem. Lett.* **2010**, *1*, 3177.

(241) Zhu, J.; Shen, Y.; Xie, A.; Qiu, L.; Zhang, Q.; Zhang, S. *J. phys. Chem. C* **2007**, *111*, 7629.

(242) Huang, W.; Chen, S.; Liu, Y.; Fu, H.; Wu, G. *Nanotechnology* **2011**, *22*, 025602

(243) Migowski, P.; Dupont, J. *Chem. Eur. J.* **2007**, *13* 32.

(244) Fujita, K.; Ohno, H. *Biopolymers* **2010**, *93*, 1093.

(245) Andreani, L.; Rocha, J. D. *Braz. J. Chem. Eng.* **2012**, *29*, 1.

(246) Anderson, J. L.; Armstrong, D. W. *Anal. Chem.* **2003**, *75*, 4851.

(247) Rochira, J. A.; Gudheti, M. V.; Gould, T. J.; Laughlin, R. R.; Nadeau, J. L.; Hess, S. T. *J. Phys. Chem. C* **2007**, *111*, 1695−1708.

(248) Ito, S.; Toitani, N.; Pan, L.; Tamai, N.; Miyasaka, H. *J. Phys.: Condens. Matter* **2007**, *19*, 486208.

(249) Yao, J.; Larson, D. R.; Vishwasrao, H. D.; Zipfel, W. R.; Webb, W. W. *Proc. Natl. Acad. Sci. USA* **2005**, *102*, 14284.

(250) Heuff, R. F.; Swift, J. L.; Cramb, D. T. *Phys. Chem. Chem. Phys.* **2007**, *9*, 1870.

(251) Heuff, R. F.; Marrocco, M.; Cramb, D. T. *J. Phys. Chem. C* **2007**, *111*, 18942.

(252) Peters, R.; Goh, J. B.; Dinglasan, J.; Thakur, A.; Shehata, S.; Anderson, D. J.; Fradin, C. *ECS Trans.* **2010**, *28*, 243.

(253) Doose, S.; Tsay, J. M.; Pinaud, F.; Weiss, S. *Anal. Chem.* **2005**, *77*, 2235.

(254) Murthy, A. V. R.; Patil, P.; Datta, S.; Patil, S. *J. Phys. Chem. C* **2013**, *117*, 13268.

(255) Carrillo-Carrion, C.; Cardenas, S.; Simonet, B. M.; Valcarcel, M. *Chem. Commun.* **2009**, , 5214−5226.

(256) Bao, H.; Gong, Y.; Li, Z.; Gao, M. *Chem. Mater.* **2004**, *16*, 3853.

(257) Wang, Y.; Tang, Z.; Correa-Duarte, M. A.; Pastoriza-Santos, I.; Giersig, M.; Kotov, N. A.; Liz-Marzan, L. M. *J. Phys. Chem. B* . **2004**, *108*, 15461.

(258) Cordero, S. R.; Carson, P. J.; Estabrook, R. A.; Strouse, G. F.; Buratto, S. K. *J. phys. Chem. B* **2000**, *104*, 12137.

(259) Biju, V.; Kanemoto, R.; Matsumoto, Y.; Ishii, S.; Nakanishi, S.; Itoh, T.; Baba, Y.; Ishikawa, M. *J. Phys.Chem. C* **2007**, *111*, 7924.

(260) Pechstedt, K.; Whittle, T.; Baumberg, J.; Melvin, T. *J. Phys. Chem. C* **2010**, *114*, 12069.

(261) Jones, M.; Nedeljkovic, J.; Ellingson, R. J.; Nozik, A. J.; Rumbles, G. *J. phys. Chem. B* **2003**, *107*, 11346.

(262) Oda, M.; Hasegawab, A.; Iwamib, N.; Nishiurab, K.; Andob, N.; Nishiyamab, A.; Horiuchib, H.; Tania, T. *Colloids Surf., B* **2007**, *56*, 241.

(263) Kamikubo, K.; Sakata, S.; Nakamura, S.; Komaki, T.; Miura, K. *J. Protein Chem.* **1990**, *9*, 461.

(264) Quinlan, G. J.; Martin, G. S.; Evans, T. W. *Hepatology* **2005**, *41*, 1211.

(265) Papadopoulou, A.; Green, R. J.; Frazier, R. A. *J. Agric. Food Chem.* **2005**, *53*, 158.

(266) Moriyama, Y.; Ohta, D.; Hadiya, K.; Mitsui, Y.; Takeda, K. *J. Protein Chem.* **1996**, *15*, 265.

(267) Sudlow, G.; Birkett, D. J.; Wade, D. N. *Mol. Pharmacol.* **1975**, *11*, 824.

CHAPTER 2

Materials, Instrumentation and Methods

This chapter provides details of the procurement sources, synthesis and purification of the different materials used in this study. The methods of sample preparation for spectral measurements and microscopic experiments have been described. The instrumentation details, especially the time-resolved confocal fluorescence microscope and time-correlated single photon counting based on picosecond set up have been discussed in detail. The methods of data analysis in FCS and fluorescence lifetime experiments have also been discussed. Various methodologies employed in the present study such as measurement of fluorescence quantum yield of the QDs, determination of the observation volume in an FCS measurement and calculation of the size and concentration of the QDs in solution have also been described.

2.1. Materials:

Laser grade coumarin 102 (C102) dye was purchased from Exciton Inc. and used without further purification. Coumarin 153 (C153) was procured from Eastman Kodak and used as received. Rhodamine 6G (R6G) and disodium hydrogen orthophosphate (Na_2HPO_4) (anhydrous) were obtained from Loba Chemie. Fluorescein (FL) and bovine serum albumin (BSA) (≥ 96%, fatty acid-free) were purchased from Sigma Aldrich and used as received. Sodium dihydrogen orthophosphate (NaH_2PO_4) and urea were purchased from the local suppliers. Sodium chloride (NaCl) and Potassium hydroxide (KOH) were purchased from Merck. Laser grade dye, 4-(Dicyanomethylene)-2-methyl-6-(4-dimethylaminostyryl)-4*H*-pyran (DCM), was purchased from Exciton Inc. and used as received. Rhodamine 123 (R123) was purchased from Aldrich and used as received. Azetidine and 4-chloro-7-nitrobenz-2-oxa-1,3-diazole (NBD-Cl) for the synthesis of 4-azetidinyl-7-nitrobenz-2-oxa-1,3-diazole (4NBD) were purchased from Sigma-Aldrich. [bmim][PF_6], [bmim][BF_4], [emim][Tf_2N], [bmim][Tf_2N], and [hmim][Tf_2N] were of "Advanced Materials Research" grade from Kanto Chemicals (Japan). These ionic liquids were rigorously dried under high vacuum for 48 h prior to use. Solvents such as ethanol (EtOH), acetonitrile (ACN), methanol (CH_3OH) and chloroform ($CHCl_3$) were purchased from Merck and distilled and dried prior to use following standard procedures. Cadmium acetate dihydrate [$(CH_3COO)_2Cd\cdot 2H_2O$] and tellurium (Te) powder for the synthesis of QDs were obtained from local suppliers.

Hexadecylamine (HDA), trioctylphosphine (TOP), 3-mercaptopropionic acid (MPA), octadecene (ODE), 1-Methylimidazole and 11-bromo-1-undecanethiol used for synthesis of task-specific ionic liquid 1-(1-undecanethiol)-3-methyl imidazolium bromide (SMIMBr) were also obtained from Sigma-Aldrich. Unless stated otherwise, all the experiments were carried out at 25°C. Milli-Q water was used in the present study. The purity of the compounds was checked by single spot in thin layer chromatography (TLC) and also by the nuclear magnetic resonance (NMR), UV-vis absorption and emission spectral data.

Various drying agents such as calcium chloride ($CaCl_2$), calcium hydride (CaH_2), phosphorous pentoxide (P_2O_5), iodine (I_2), and magnesium (Mg) turnings used at different stages of solvent purification, hydrochloric acid (HCl) for cleaning Mg turnings and molecular sieves for storage of dried solvents were purchased from local companies.

2.2. Synthesis of molecules and quantum dots:

2.2.1. Synthesis of 4NBD:

NBD was synthesized following a standard procedure,[1] in which 1 mmol of 4-chloro-7-nitrobenz-2-oxa-1,3-diazole (NBD-Cl) was dissolved in 3 mL of ethyl acetate. 1.2 mmol of azetidine was diluted in 2 mL of ethyl acetate and added dropwise to NBD-Cl solution at 0°C with stirring. After stirring for 30 min at this temperature, the reaction mixture was further stirred for another 2 hrs at room temperature. The product, a red precipitate, was filtered out and purified by column chromatography using a silica gel column. Hexane and ethylacetate were used as eluent for the purification of the compound. The purified compound was recrystallized from absolute ethanol.

2.2.2. Synthesis of SMIMBr:

Task-specific thiol functionalized imidazolium ionic liquid (IL), SMIMBr for the preparation of QD-IL hybrids was synthesized following a reported procedure.[2] 1-methylimidazole, which was distilled from KOH under reduced pressure prior to use, and 11-bromo-1-undecanethiol were taken in 1:1.5 mol ratio. The latter was slowly added to 1-methylimidazole under cooling conditions, and then the reaction was carried out at room temperature (298 K) for 24 hrs under N_2 atmosphere. Light yellow colored salt, SMIMBr,

obtained after the reaction was washed several times with ethylacetate to remove the unreacted starting materials and then dried under high vacuum for several hours.

2.2.3. Synthesis of QDs:

2.2.3.1. CdTe/HDA QDs:

CdTe/HDA QDs were prepared following a reported procedure.[2,3] Briefly, 5 g of HDA and 3 mL of TOP were taken in a two-necked, round-bottom (RB) flask and heated at 80°C for 15 min to bring the mixture to a liquid state. In the meantime, a separate solution was prepared in a reagent bottle containing 0.41 g of $(CH_3COO)_2Cd\cdot 2H_2O$ and 0.16 g of Te powder in 4 mL of TOP. The mixture was sonicated for 1 h to obtain an almost clear solution. This solution was then quickly injected into a RB flask containing HDA and TOP. The reaction was carried out at 180°C for several minutes so that the desired size of the CdTe core is reached. Because the luminescence of the QD depends on its size, the growth of the particle was monitored by its fluorescence at regular intervals of the reaction time. After completion of the reaction, excess starting materials were removed by washing the QDs with methanol followed by repeated precipitation and centrifugation. Then the QDs were dissolved in nonpolar solvents like $CHCl_3$.

2.2.3.2. CdTe/MPA QDs:

Water soluble CdTe/MPA QDs were prepared from CdTe/HDA by ligand exchange method as reported in the previously published literature.[3] 0.5 M methanolic solution of MPA-KOH (20 mol % excess KOH) was added dropwise to a stirring solution of CdTe/HDA QDs in $CHCl_3$ until the QDs flocculate out of the solution. The solution was then centrifuged to separate the precipitate, which was easily soluble in water as the exchange of HDA with MPA made the outer layer of the QDs polar. This transfer of the QDs from $CHCl_3$ to water was carried out under nitrogen environment. Stronger binding capability of the thiol with the surface Cd atoms helped the replacement of HDA by MPA.

2.2.3.3. QD-IL hybrid, CdTe/SMIM:

QD-ionic liquid hybrid CdTe/SMIM was synthesized according to the procedure reported by Santhosh et al.[2] A dilute solution (0.05 M in $CHCl_3$) of SMIMBr was added drop

wise to the $CHCl_3$ solution of CdTe/HDA until the QD was flocculated out of the solution. This solution was then centrifuged and dissolved in [bmim][PF_6].

2.2.3.4. CdTe/ZnS core/shell QDs:

Synthesis of core/shell QDs involve two steps.[4] Firstly, the core QDs were synthesized according to the procedure described earlier. Finally, the shell of few monolayers (typically 1-5) was grown over the core QDs through successive ion layer adsorption and reaction (SILAR) method.[5] In order to prevent self-nucleation of the shell material and uncontrolled Ostwald ripening of the core QDs, it is necessary to maintain a lower temperature for the shell growth compared to that used for the core QD synthesis. In the present study, ZnS shell is grown over CdTe QDs according to the following procedure. 8 mL 7.2 μM $CHCl_3$ solution of CdTe/HDA core QDs, 3 gm of HDA and 10 mL of ODE were taken in two-necked RB flask and kept in vacuum for 2 hours to remove chloroform and then heated to 80˚C for 1 hr to remove residual air. Then the mixture was kept at 160˚C to add the shell precursors. Zinc oleate precursor was prepared by mixing zinc oxide in required amount of oleic acid and 5 mL octadecene in a RB flask and heated at 240˚C in N_2 atmosphere until the solution became clear and then the solution was allowed to cool at 80^0C.[6] Sulphur precursor was prepared by sonicating sulphur powder in 3 mL TOP and 5 mL octadecene for 1 hr. These precursors were injected following SILAR technique[5] i.e. alternate addition of the shell precursors to the vigorously stirring mixture of the core CdTe QDs in the RB flask at 160˚C over a period of 5-10 minutes to form CdTe/ZnS core/shell QD. After the addition was complete, the mixture was monitored by eluting a fraction of the mixture at a certain time interval and comparing its luminescence. Herein, we synthesized 1-monolayer (ML) and 2 ML CdTe/ZnS QDs. On completion of the reaction, excess starting materials were removed by washing the core/shell QD with methanol and then the core/shell QD was dissolved in non-polar solvents like $CHCl_3$. Water soluble CdTe/ZnS/MPA QDs were prepared from CdTe/ZnS/HDA by ligand exchange method described earlier.

2.3. Purification of the conventional solvents:

Conventional solvents used at different stages of the experiments were purified by using standard procedures available in the literature.[7] After drying, molecular sieves were added to

protect the solvents from moisture.

Methanol and ethanol: Initially the solvents were dried over CaH_2 overnight. Further dehydration of the solvents was carried out using Mg-alkoxide. This was prepared by mixing 5 gm of clean dry Mg turnings and 0.5 gm of iodine in the RB flask, followed by 50-75 mL of alcohol and warming the mixture until all the Mg is converted into Mg-alkoxide. After then about 900 mL of alcohol was added slowly to this and refluxed for an hour and then distilled under moisture free atmospheric conditions.

Acetonitrile: Initially the solvent was refluxed for 3-4 hrs with anhydrous P_2O_5 and then distilled under dry conditions.

Chloroform: The solvent was stirred overnight with $CaCl_2$ and then distilled under moisture free conditions.

Ethyl acetate: After stirring with P_2O_5 for 3-4 hrs, the solvent was distilled out under dry atmosphere.

Water: Milli-Q water produced from Millipore, Synergy Pack was used for all the experiments.

2.4. Purification of the RTILs:

The RTILs obtained from Kanto Chemicals (Japan) were stored in a vacuum desiccator under nitrogen atmosphere. Prior to use, all the RTILs were dried under high vacuum (pressure 10^{-2} – 10^{-3} mbar), sometimes with heating at 50-60°C, for at least 8-10 hrs to minimize the water content.

2.5. Sample preparation:

2.5.1. Fluorescence spectral and temporal measurements:

For the steady state and time-resolved fluorescence measurements in conventional solvents and RTILs, the solutions were prepared such that the absorbance of the solution (1 cm pathlength) at the excitation wavelength was around 0.05-0.25, to avoid problems due to inner filter effects. Since RTILs are hygroscopic, care was taken to tightly seal the cuvettes with septum and parafilm.

2.5.2. Transmission electron microscopy (TEM) measurements:

The samples for TEM measurements were prepared by placing a drop of clear solution of the QDs (in H_2O and $CHCl_3$) on carbon-coated copper grids followed by removal of the solvent under high vacuum. The size of the QDs was determined using a Tecnai G2 FE1 F12 transmission electron microscope at an accelerating voltage of 200 kV.

2.5.3. Fluorescence correlation spectroscopy (FCS) measurements:

Samples were diluted for FCS measurements. After then the dilute sample was placed on a coverslip. To study the diffusion in BSA solution and RTILs the concentrations of the fluorophores were maintained at ~10-20 nM and ~35-40 nM, respectively. FCS measurements on QDs were carried out at different concentrations ranging from 20 nM to 400 nM.

2.6. Instrumentation:

NMR spectra were recorded using Bruker AVACE 400 MHz NMR spectrometer for the characterization of the compounds. Steady-state absorption and fluorescence spectra were recorded on a UV-vis spectrophotometer (Cary100, Varian) and a spectrofluorometer (FluoroLog-3, Jobin Yvon), respectively. The viscosities of the RTILs were measured by a LVDV-III Ultra Brookfield Cone and Plate viscometer (accuracy: 1% and repeatability: 0.2%). Tecnai G2 FE1 F12 transmission electron microscope at an accelerating voltage of 200 kV were used to examine the size and shape of the QDs. EDX spectra were captured in the transmission electron microscope mentioned above Equipped with an energy dispersive X-ray spectrometer. Photoirradiation of the QDs was carried out using a 8 W fluorescent tube lamp (FL8 D daylight, Toshiba) for different exposure time prior to recording the absorption and fluorescence spectra. Intensity of this exposure is 5 mW/cm^2. The details of the other instrumental set up employed in the present study are given in the following section.

2.6.1. Time-resolved confocal fluorescence microscope:

FCS measurements were carried out using a time-resolved confocal fluorescence microscope (MicroTime 200, PicoQuant). An inverted microscope (Olympus IX71) Equipped with a water immersion objective (UPlansApo NA 1.2, 60 X) served as the microscope body (Scheme 2.1). The samples were excited at 485 nm and 405 nm using pulsed diode lasers with full width half maximum of 176 ps (405 nm) and 144 ps (485 nm) respectively. The pulse repetition rate of the laser was 20 MHz. The output of this pulsed

diode laser was coupled to the main optical unit by a polarization maintaining single mode optical fiber. In the main optical unit the excitation light was guided through a dichroic mirror, which reflected the excitation light onto the entrance port of the microscope. The sample was placed on a cover-slip and the directed laser beam was focused onto the sample using the water immersion objective. Fluorescence was collected by the same objective, passed through a dichroic mirror, 430 nm long pass filter (for 405 nm) or 510 nm long pass (for 485 nm) to block the excitation light. After then the signal was spatially filtered by focusing onto a 50 µm diameter pinhole to cut the out-of-focus signals, re-collimated, and directed onto a (50/50) beam splitter prior to entering into two single photon avalanche photodiodes (SPADs). The fluorescence correlation traces were generated by cross-correlating signals from the two SPAD detectors. The data acquisition was performed with PicoHarp 300 TCSPC module in a time-tagged time-resolved (TTTR) mode.

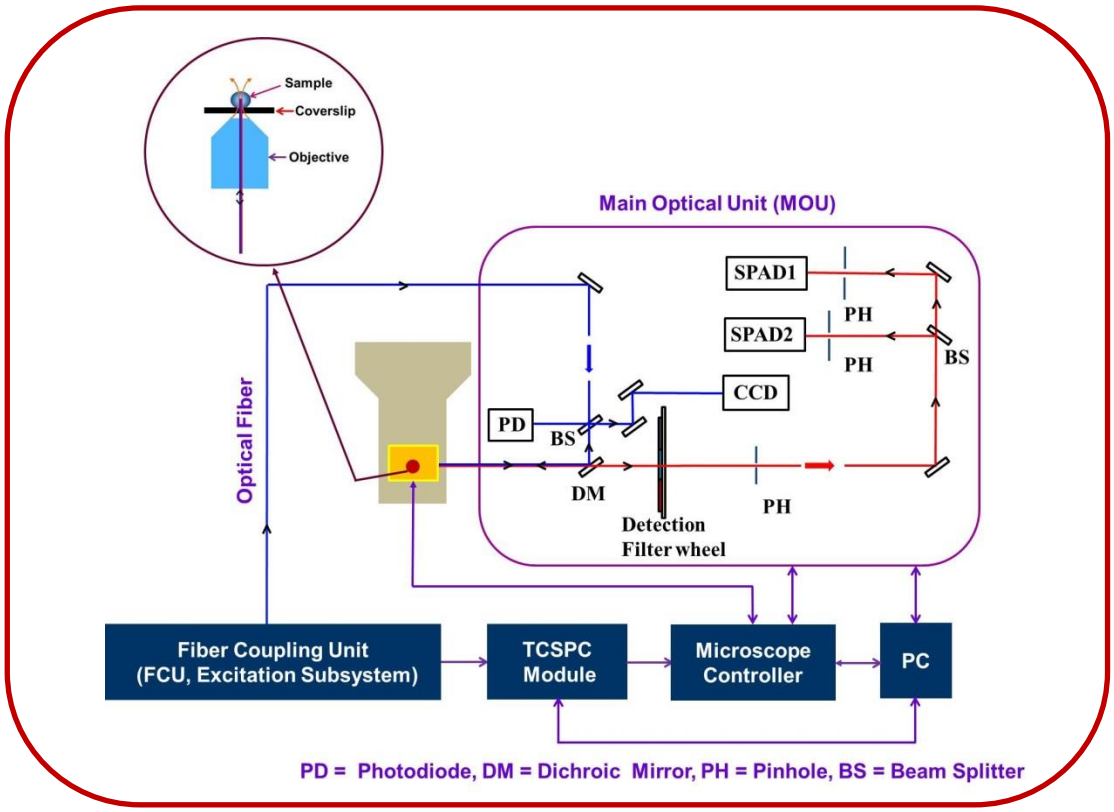

Scheme 2.1. Schematic diagram of the time-resolved confocal fluorescence microscope set up (adapted from PicoQuant MicroTime 200 user manual).

2.6.2. Time-correlated single photon counting setup:

Fluorescence lifetime measurements were carried out using a time-correlated single-photon counting (TCSPC) spectrometer (Horiba Jobin Yvon IBH). Nano LED (λ_{ex}= 439 nm, FWHM = 150 ps) was used as the excitation source and a MCP photomultiplier (Hammatsu R3809U-50) as the detector. The pulse repetition rate of the laser source was 1 MHz. The TCSPC experiment starts with the excitation pulse that simultaneously excites the samples and sends a signal to the electronics (Scheme 2.2). This excitation signal is received by a constant fraction discriminator (CFD), which accurately measures the arrival time of the pulse and then diverts the signal towards the time to amplitude convertor (TAC) to start the voltage ramp. This voltage ramp is a voltage that increases linearly with time on the nanosecond timescale. The second channel (CFD) which accurately measures the arrival time of the emitted photon sends a signal to stop the voltage ramp in TAC. This voltage in TAC is proportional to the time delay (Δt) between the excitation and emission signals. This voltage is amplified by a programmable gain amplifier (PGA) and later converted to a numerical value by the analog-to-digital converter (ADC). This numerical value is stored as a single event with the measured time delay. A histogram of the fluorescence intensity decay can be constructed by repeating this process numerous times with a pulsed-light source. The lamp profile was recorded by placing a dilute solution of Ludox in water as a scatterer (dilute solution of Ludox in water) in place of the sample. The analysis of the fluorescence decay curves is covered in the later section.

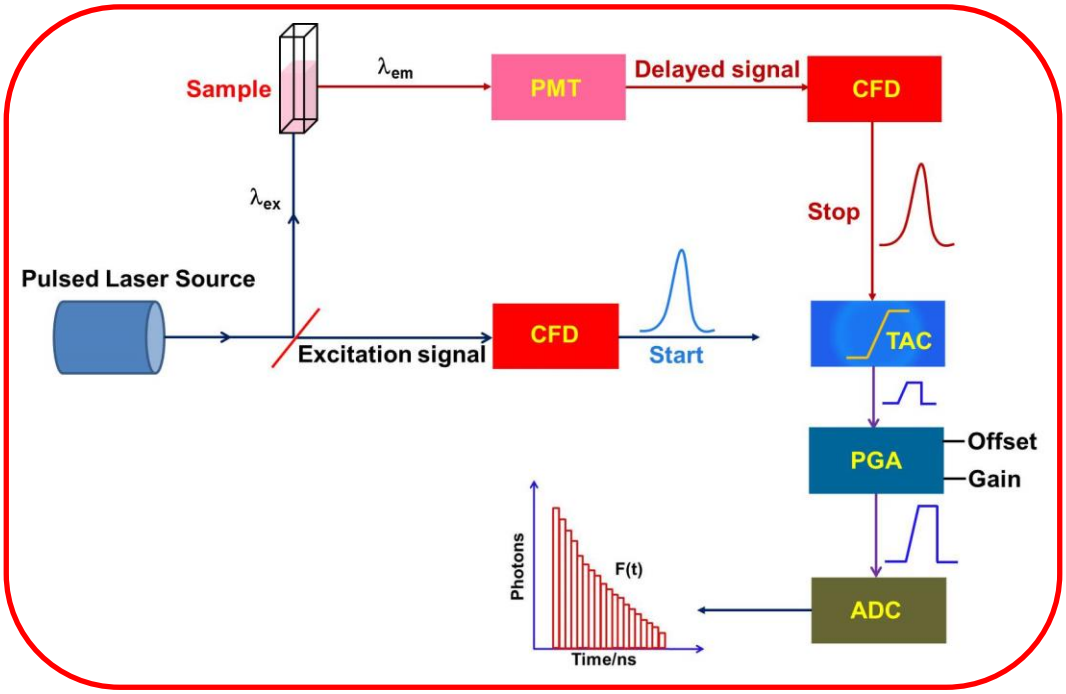

Scheme 2.2. Schematic diagram of the TCSPC setup

2.7. Measurement of Fluorescence Quantum Yield:

Fluorescence quantum yields (QYs) of the CdTe core and CdTe/ZnS core/shell QDs were determined by comparing the integrated emission of the QDs in $CHCl_3$ and H_2O to the emission of a solution of C153 in acetonitrile (QY=0.56)[8] of identical optical density at the excitation wavelength by using the following Equation:

$$QY\ (QD) = QY\ (C153) \times (I/I_R) \times (OD_R/OD) \times (n^2/n_R^2) \qquad (2.1)$$

R indicates here reference, I is the integrated fluorescence intensity, OD is optical density at the excitation wavelength and n is the refractive index of the solvent. OD was kept at less than 0.05.

2.8. Data Analysis:

2.8.1. FCS Measurements:

Data analysis of the individual correlation curves was performed by using the SymPhoTime software of PicoQuant. Following models were used to fit the correlation functions (defined in Equation 1.3). The quality of the fit was judged by the residuals and χ^2 values.

(1) 3-D diffusion with triplet state contribution:

$$G(\tau) = 1 - T + T\exp\left(-\frac{\tau}{\tau_{tr}}\right)\sum_{i=1}^{k}\rho_i\left(1+\frac{\tau}{\tau_i}\right)^{-1}\left(1+\frac{\tau}{\tau_i\kappa^2}\right)^{-\frac{1}{2}} \tag{2.2}$$

Where, ρ_i is given by,

$$\sum_{i=1}^{k}\rho_i = \frac{1}{\langle N\rangle(1-T)} \tag{2.3}$$

Which implies,

$$\rho_i = \frac{\alpha_i}{\langle N\rangle(1-T)} \tag{2.4}$$

In the above expressions, the diffusion time, τ_i, denotes the average time a dye molecule resides in the confocal volume, τ_{tr} is the lifetime of the triplet state of the molecule, τ is the delay or lag time, N is the average number of fluorescent molecules in the observation volume, T is the fraction of the molecules in the triplet state, α_i is the fraction of the molecules having diffusion time, τ_i. Here $i = 1$ and 2 corresponds to a 1-component a 2-component diffusion model respectively. κ is the structure parameter of the observation volume and is given by $\kappa = r_0/z_0$, where, z_0 and r_0 are the longitudinal and transverse radii, respectively, of the observation volume (Scheme 1.3). τ_i is related to r_0 by the following Equation

$$\tau_i = \frac{r_0^2}{4D_t} \tag{2.5}$$

Here, D_t is the diffusion coefficient of the fluorescent probes.

(2) Simple 3-D diffusion model:

$$G(\tau)=\frac{1}{N}\sum_{i=1}^{n}\frac{\alpha_i}{\left(1+\frac{\tau}{\tau_i}\right)\left(1+\frac{\tau}{\kappa^2\tau_i}\right)^{\frac{1}{2}}} \qquad (2.6)$$

$i=1$ and 2 correspond to 1- and 2-component diffusion model, respectively.

(3) 1-component 3-D diffusion model with a stretched exponential term:

$$G(\tau)=\left[1+\frac{T}{1-T}\exp\left(-\frac{\tau}{\tau_t}\right)^{\beta}\right]\frac{1}{N}\left(1+\frac{\tau}{\tau_D}\right)^{-1}\left(1+\frac{\tau}{\kappa^2\tau_D}\right)^{-\frac{1}{2}} \qquad (2.7)$$

Where, τ_D is the diffusion time of the QDs. N is the average number of molecules undergoing reversible transition between on and off state in the observation volume. T is fraction of the off state. τ_t is the dark state relaxation time, β is the stretching exponent with value between 0 and 1, and this is related to the distribution of τ_t.

2.8.2. TCSPC measurements:

Fluorescence decay curves were analyzed by nonlinear least-squares iteration procedure using IBH DAS6 (Version 2.2) decay analysis software. The quality of the fit was assessed by the χ^2 values and the distribution of the residuals.

2.9. Determination of the observation volume in the FCS measurements:

FCS can measure absolute diffusion coefficients and concentration values only when the exact size and shape of the observation volume is known. The diffusion time (τ_D) depends on the transverse radius (r_0) of the observation volume (Equation 1.15). The size and elongation of the observation volume is determined by calibration measurement with a known diffusion coefficient. In the present study, calibration was performed using aqueous solution of rhodamine 6G and rhodamine 123 with known diffusion coefficients of 426 and 460 $\mu m^2/s$ respectively.[9,10] The estimated excitation volume was found to be ~0.8 fL for 485 nm excitation and ~0.4 fL for 405 nm excitation.

2.10. Estimation of size and concentration of the CdTe QDs in solution:

The concentrations of the QDs in the solution were calculated following the method suggested by Yu et al.[11] First, the diameter (D, nm) of the CdTe QDs was estimated from the following Equation:

$$D_{CdTe} = \left(9.8127 \times 10^{-7}\right)\lambda^3 - \left(1.7147 \times 10^{-3}\right)\lambda^2 + \left(1.0064\right)\lambda - 194.84 \qquad (2.8)$$

Where, λ (nm) is the wavelength corresponding to the first excitonic absorption peak. The calculated D values correlated well with the experimental values obtained from the TEM measurements. The D value was used to find out the molar extinction coefficients (ε) of CdTe QDs using the following relation

$$\varepsilon_{CdTe} = 10043\left(D\right)^{2.12} \qquad (2.9)$$

The concentration (C) of the QDs in solution was then estimated using the relation,

$$C = \frac{A}{\varepsilon l} \qquad (2.10)$$

Where, A is the optical density and *l* is the optical path length of the solution.

2.11. Calculation of the amount of the shell precursors required for the preparation of core/shell QDs:

The amounts of shell precursors required to grow a shell of desired thickness were calculated according to a published report.[4] In order to grow a shell of certain thickness one needs to know the concentration of the core QDs. The concentration of the core QD was calculated by first estimating the molar extinction coefficient from the measured size of the QD using the empirical formula of Peng and co-workers,[11] and then using the measured optical density of the solution. With the knowledge of the QD's size and molar quantity, the required amount of shell precursors to obtain a shell thickness of x monolayers (CD) on the surface of the core QDs AB can be calculated, using the bulk crystal parameters of the shell materials as follows

$$V_{CD}\,(ML_x) = 4/3 \times \pi \times ((r_{AB} + x \times d)^3 - r_{AB}^3) \qquad (2.11)$$

$$n_{CD}(ML_x) = \rho_{CD} \times V_{CD}(ML_x) \times 10^{-27} / m_{CD} \quad (2.12)$$

$$n_{CD} = n_{AB} \times n_{CD}(ML_x) \quad (2.13)$$

V_{CD} (ML_x) is the volume of the shell containing x monolayers (nm^3), r_{AB} is the radius of the core (nm) and d is the thickness of one monolayer of the shell (nm). n_{CD} (ML_x) is the number of CD monomer units per nanocrystal contained in x monolayers of the shell (dimensionless), ρ_{CD} is the density of the bulk shell material (kg m^{-3}), m_{CD} is the mass of a shell monomer unit (kg), n_{CD} is the molar quantity of precursor CD needed for the growth of x monolayers (mmol), and n_{AB} is the molar quantity of core QDs used for the synthesis of the core shell system. The term monomer indicates smallest subunit of the shell material consisting of one cation and one anion.

2.12. Standard error limits:

Standard error limits involved in the experimental results were

λ_{max} (abs./flu.)	± 1 nm
Φ_f	± 10%
τ_f	± 5%
Viscosity	± 2%
QD size (D / nm)	± 5 – 10%

The error limits of other quantities related to FCS measurements are given in the subsequent chapters while reporting the experimental results.

References:

(1) Saha, S.; Samanta, A. *J. Phys. Chem. A* **1998**, *102*, 7903.
(2) Santhosh, K.; Samanta, A. *J. Phys. Chem. C* **2012**, *116*, 20643.
(3) Wuister, S. F.; Swart, I.; Driel, F. V.; Hickey, S. G.; Donega, D. D. M. *Nano Lett* **2003**, *3*, 503.
(4) Reiss, P.; Protiere, M.; Li, L. *Small* **2009**, *5*, 154.
(5) Li, J. J.; Wang, Y. A.; Guo, W. Z.; Keay, J. C.; Mishima, T. D.; Johnson, M. B.; Peng, X. G. *J. Am. Chem. Soc.* **2003**, *125*, 12567.
(6) Hewa-Kasakarage, N. N.; El-Khoury, P. Z.; Tarnovsky, A. N.; Kirsanova, M.; Nemitz, I.; Nemchinov, A.; Zamkov, M. *ACS Nano* **2010**, *4*, 1837.
(7) Perrin, D. D.; Armerego, W. L. F.; Perrin, D. R. *Purification of Laboratoty Cheimicals; Pergamon Press: New York, 1980.*
(8) Jones-II, G.; Jackson, W. R.; Choi, C.-Y.; Bergmark, W. R. *J. Phys. Chem.* **1985**, *89*, 294.
(9) Petrasek, Z.; Schwille, P. *Biophys. J.* **2008**, *94*, 1437.
(10) Kapusta, P. *Absolute Diffusion Coefficients: Compilation of Reference Data for FCS Calibration, July 2010, Rev 1*.
(11) Yu, W. W.; Qu, L. H.; Guo, W. Z.; Peng, X. G. *Chem. Mater.* **2003**, *15*, 2854.

CHAPTER 3

Modulation of Photophysical Properties of Mercaptopropionic Acid Capped CdTe Quantum Dots upon Exposure to Light

Light-induced modulation of the fluorescence behavior of mercaptopropionic acid (MPA) capped CdTe quantum dots (QDs) in aqueous solution is studied by a combination of fluorescence correlation spectroscopy (FCS) and steady state and time-resolved fluorescence techniques. These investigations reveal a dramatic variation in the fluorescence properties of the QDs under exposure to light. In the FCS measurement, a large decrease in amplitude and change in shape of the correlation curves are observed with increasing excitation power. The change in the shape of the correlation curves, particularly at short lag time, e.g., a faster relaxation at high excitation power, is attributed to the increasing contribution of the off state of the QDs. Interestingly, despite this increasing contribution of the off state, which reduces the effective number of emitters in the observation volume and hence should increase the amplitude of the correlation curve, the latter actually decreases at high excitation power. This apparent contradiction is resolved by considering light-induced transformation of the dark QDs to bright QDs due to surface passivation of the QDs with increasing excitation power. Enhancement of the steady state fluorescence intensity under light irradiation, both in aerated and deaerated environments, supports the mechanism of passivation of the surface trap states by photoadsorption of water molecules. Fluorescence lifetime data is also shown to be consistent with this light-induced surface passivation mechanism.

3.1. Introduction:

Semiconductor quantum dots (QDs) have been receiving increasing attention in recent years because of their interesting size-dependent optical and electronic properties,[1−4] which is due to quantum confinement of both electron and hole (produced because of electronic excitation) in all three dimensions.[1,4−7] Emission covering the entire visible and infrared region can be obtained simply by tuning the size of the QDs.[1,8] As the QDs exhibit broad absorption and narrow emission profile in comparison to organic fluorophores,[9] it is possible to excite multiple QDs at a single excitation wavelength.[10] Furthermore, the narrow emission profile of the QDs provides easy spectral separation,[9] thus making them an efficient system for multicolor imaging of biological samples.[10] QDs also exhibit a higher photostability and superior optical properties compared to conventional organic fluorophores.[9] All these

excellent properties make QDs ideal candidates for applications ranging from biological imaging to lasing to optoelectronics.[3,10−17] Given the huge potential scientific and technological impact of QDs in various applications, the fluorescence response of QDs has remained an intriguing topic of research since its discovery.

The small size of QDs results in a high surface-to-volume ratio of the substances,[1,8] and it has long been believed that the surface of the QD plays an important role in determining its luminescence properties.[5,18−25] Uncoordinated atoms on the surface disrupt the crystalline periodicity and leave behind one or more dangling orbitals on each atom.[1,23] These dangling orbitals form the mid band gap states and reduce the luminescence efficiency of the QDs by providing additional nonradiative deactivation pathways.[1,8,26,27] Surface passivation is a crucial parameter for the preparation of QDs with high fluorescence quantum yield and photostability.[1,8,23,28,29] One of the major obstacles to the progress of the development of highly luminescent and stable QDs is the poorly understood QD surface chemistry and the relation of the surface chemistry to QD photophysical properties[30−32] It is reported that the fluorescence efficiency of the QDs is enhanced under irradiation with light.[22,32−41] This enhancement of emission on exposure to light, which is termed photoactivation, is attributed to photoinduced passivation of the surface trap states. However, no general consensus on the mechanism of photoactivation has yet been reached because of the complicated photophysics and photochemistry of QDs. Suggested mechanisms include elimination of the topological surface defects (i.e., smoothing of the surface during the process of photocorrosion),[26,32,34,42−44] passivation of the surface trap states by photoadsorbed molecules,[22,32,35,38] photoinduced rearrangement of the surface stabilizing agents,[32,33,36,44−47] photoneutralization of the local charged centers inside and outside the QDs, etc.[48] Solvents also have been found to play an important role in the photoactivation of QDs.[32,35,38,48] Photoluminescence enhancement of QDs often strongly depends on the amount of water vapor present in the atmosphere.[35,38,48] This is ascribed to photoadsorption of the water molecules on the QD surface leading to the passivation of the nonradiative surface trap states.[32,35,38,48,49] Polarity of the solvent also affects the photoactivation.[22,32,36] It is observed that addition of methanol to trioctylphosphine oxide (TOPO)-hexane or TOPO-toluene solution shows an accelerated increase of the fluorescence efficiency compared to TOPO-toluene only or TOPO-hexane only QD solutions.[36] Hence, a clear understanding of the

photoactivation mechanism is absolutely essential to understand the role of surface states and surface reaction on the luminescence yields and photostability of QDs. We have studied light-induced changes in the fluorescence behavior of MPA-coated CdTe QDs in water by a combination of FCS, steady-state, and time-resolved spectroscopic techniques. CdTe QDs are chosen as the subject matter of this investigation because the effect of light irradiation on the QD optical properties is not as widely investigated as that on CdSe QDs.

It is known that FCS is a highly sensitive and powerful technique in which the fluorescence fluctuations arising from a small observation volume (on the order of a femtoliter) is correlated to obtain the temporal evolution of the system about its equilibrium state.[50] This technique has been successfully applied to study the fluorescence blinking dynamics and the kinetics of bimolecular reactions, binding of ligands to a protein, protein-protein interaction, DNA hybridization, and conformational fluctuation and translational diffusion of the fluorescent probes in polymer, lipid vesicles, micelles, ionic liquids etc.[51−61] Considering that QDs are superior fluorescent probes compared to organic fluorophores, the FCS technique has been used for the characterization of QDs; specifically, it has been used to determine their hydrodynamic radius, concentration, monodispersity, and aggregation tendency.[12,37,62−68] Interestingly, only a handful of FCS studies on QDs photophysics have been made despite the potential of this technique to determine the blinking kinetics at faster time scales.[51,52,69−74] Widely distributed kinetics of fluorescence blinking[75] of QDs limited its study using the FCS technique.[70,71,73] The blinking kinetics of QDs complicates the analysis of the FCS data as it distorts the shape of the correlation curve, especially at shorter correlation times,[73] thus making it difficult to model QD blinking dynamics. Doose et al. attempted to simulate the anomalous shape of the correlation curve by employing Monte Carlo calculations of the diffusing and blinking dots.[73] However, no unique set of blinking parameters for a given data set could be found. As the amplitude of the correlation curve, G(0), provides information on the number of emitters in the observation volume, a comparison of the G(0) value as a function of the laser power is expected to provide a comprehensive understanding of the light-induced changes in QDs. Larson et al. observed a decrease in the G(0) value with increasing excitation power by two photon excitation FCS and attributed this to the broadening of the observation volume on excitation saturation.[12] Doose et al. compared the photophysical and colloidal properties of some biocompatible QDs

using FCS.[73] They examined the G(0) values at different excitation power and compared them with those obtained for the fluorescence beads and rhodamine 6G. The decrease of the G(0) value for the QDs is found to be much higher than that of the beads and rhodamine 6G and is attributed to excitation saturation and change in the blinking statistics at high excitation power, which increases the concentration of the emitters in the observation volume. However, they could not model the blinking statistics of the QDs as a function of the excitation power. Miyasaka and coworkers could fit the blinking dynamics of water-soluble CdTe QDs by introducing a stretched exponential term in the correlation function.[52] This stretched exponential term takes care of the widely distributed kinetics of the blinking of QDs. These authors also observed a decrease in the G(0) value and a faster decay of the autocorrelation with increasing excitation power. They agreed to the point that excitation saturation alone could not explain the changes in the shape and amplitude of the correlation curves and ascribed the observation to a faster relaxation from the dark state at higher excitation power. These authors, however, did not compare the fraction of the dark state as a function of the excitation power, which would have provided more information on the changes in the shape of the correlation curves. Dong et al. attributed the decrease of G(0) value with irradiation times to the photoactivation of the QDs.[37] According to them, photoactivation occurred because of laser-induced aggregation of the QDs and consequent modification of the QD surface structure, which turns the permanently dark QDs to bright QDs.[37] It is therefore evident that no single mechanism can explain light-induced variation of the luminescence efficiency of the QDs and determination of the mechanism of photoactivation requires a thorough and detailed investigation. This explains the motivation for the present study. We have also carried out steady state and time-resolved conventional emission studies to supplement the results of the FCS measurements and also to obtain a clear understanding of the mechanism of this light-induced change in the luminescence properties of the QDs. To the best of our knowledge, this is the first study in which the origin of decreasing amplitude of the correlation curve with increasing excitation power is explained clearly. We have also successfully monitored the evolution of the blinking parameters as a function of the excitation power to provide support for the mechanism involved in the photoactivation process.

3.2. FCS study of CdTe/MPA QDs in aqueous solution:

Figure 3.1 shows the FCS curves of the 55 nM CdTe QDs in water (size of the QD estimated from TEM measurement is 4.7 nm and emission peak is at 635 nm) and G(0) values at different excitation power. The correlation curves could be best fitted (as determined by the residuals) to a stretched exponential with a 1-component diffusion model (Equation 2.7). The quality of the fits to other models is provided in Figure 3.2. This stretched exponential fit is in accordance with the distributed kinetics of fluorescence blinking of the QDs, as reported in the literature.[52,70,75] It is important to note that the amplitude of the correlation curve decreases sharply with increasing excitation power (Figure 3.1). The G(0) value decreases from 0.98 ± 0.13 at 6 μW to 0.30 ± 0.12 at 186 μW. A further increase in power, however, slightly increases the G(0) value (0.45 ± 0.12 at 392 μW). This decrease in G(0) value with increasing excitation power for CdTe/MPA is much larger than that for R123 in water (Figure 3.3). Figure 3.4 shows the normalized correlation curves and the dependence of the diffusion time on increasing excitation power. The shape of the correlation curves is strongly dependent on the excitation power especially at short correlation times.[73] Figure 3.5 shows the dependence of the off-state fraction (T) and the blinking time (τ_t) on increasing excitation power. T increases and τ_t decreases with increasing excitation power and attains a saturation value at around 186 μW.

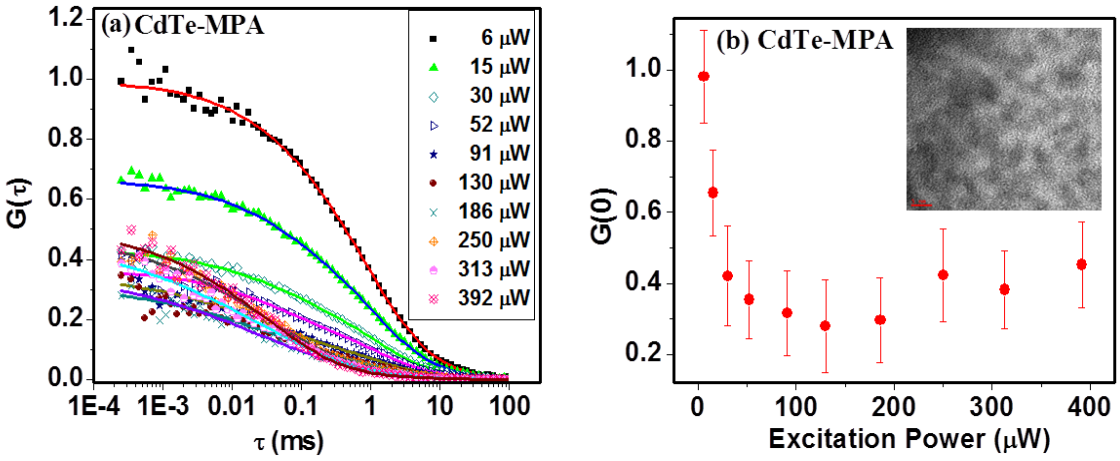

Figure 3.1. (a) Correlation curves of the 55 nM CdTe/MPA QDs in aqueous media at different excitation power. Points are the data and lines represent fit to Equation 2.7 and (b) change of the G(0) value with excitation power (inset shows the TEM images of the QDs). Excitation wavelength is 485 nm.

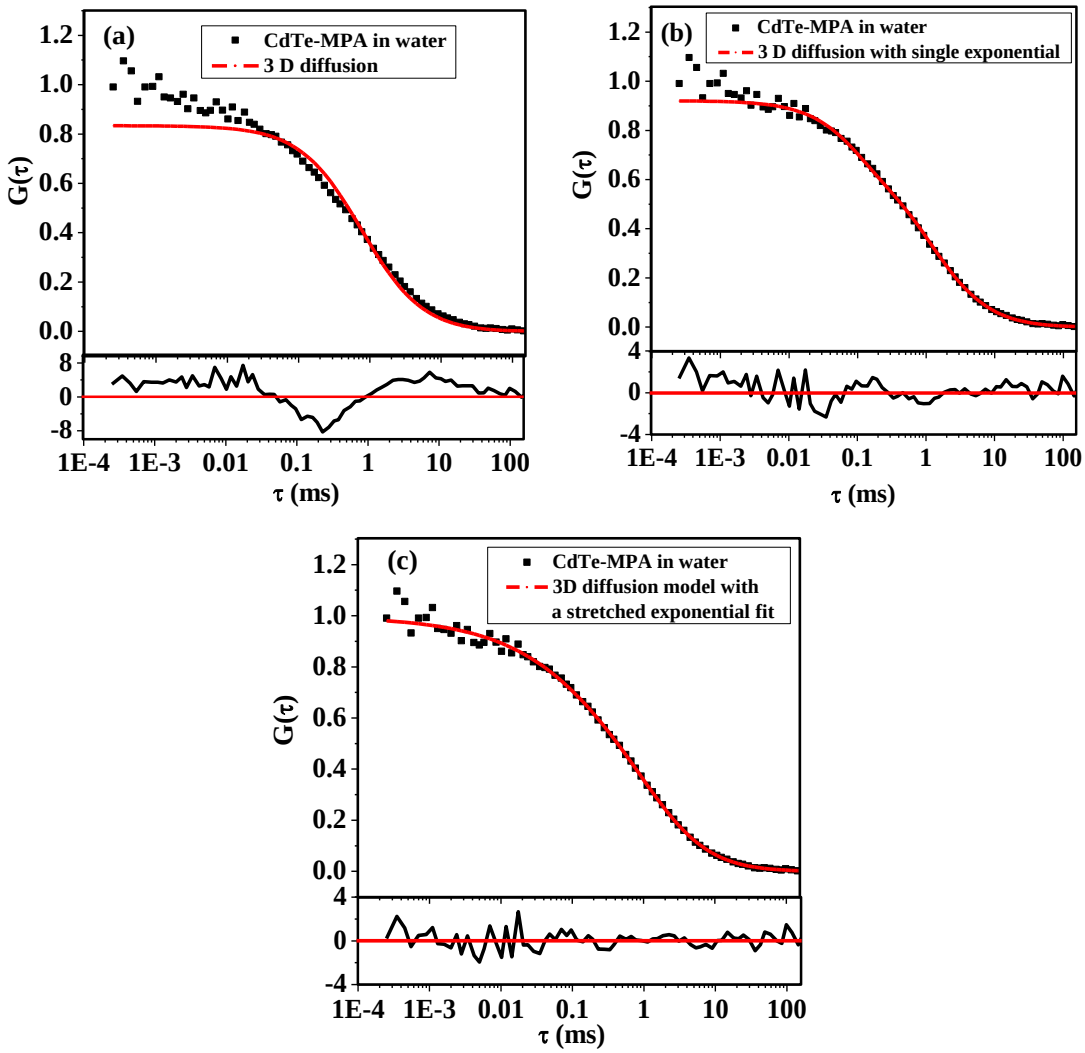

Figure 3.2. Fit of the correlation curves of a 55 nM aqueous solution of CdTe-MPA at 6 μW excitation power into (a) simple 3 D diffusion model, (b) 3 D diffusion model with single exponential term and (c) 3D diffusion model with a stretched exponential term. Here black points are the data and red line represents the fit. The residuals depicting the quality of the fits are shown in the lower part of each panel.

These results suggest that the blinking kinetics becomes faster and dominant with increasing excitation power. At high excitation power blinking kinetics dominates the entire correlation curve. This is why the correlation curves are shifted to shorter correlation time with increasing excitation power. As the amplitude of the correlation curve depends on the number of fluorescent molecules in the observation volume, $G(0) = 1/N(1-T)$,[50] where, N is the average number of molecules in the observation volume undergoing reversible transition

between fluorescent on and off state, an increase in T implies a decrease in the number of fluorescent molecules N(1−T) in the confocal volume. Hence, the amplitude of the correlation curves should increase with increasing excitation power. However, a completely opposite observation is made in the experiment. A decrease in the G(0) value is commonly rationalized considering the broadening of the observation volume due to excitation saturation that increases N.[12,70,73]

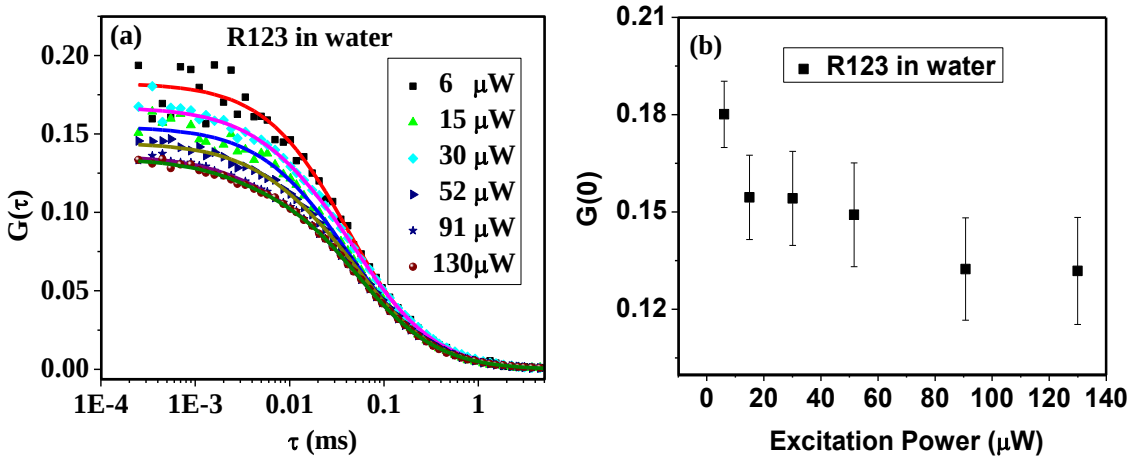

Figure 3.3. Plot of (a) correlation curves of R123 at different excitation power, (b) G(0) value versus excitation power.

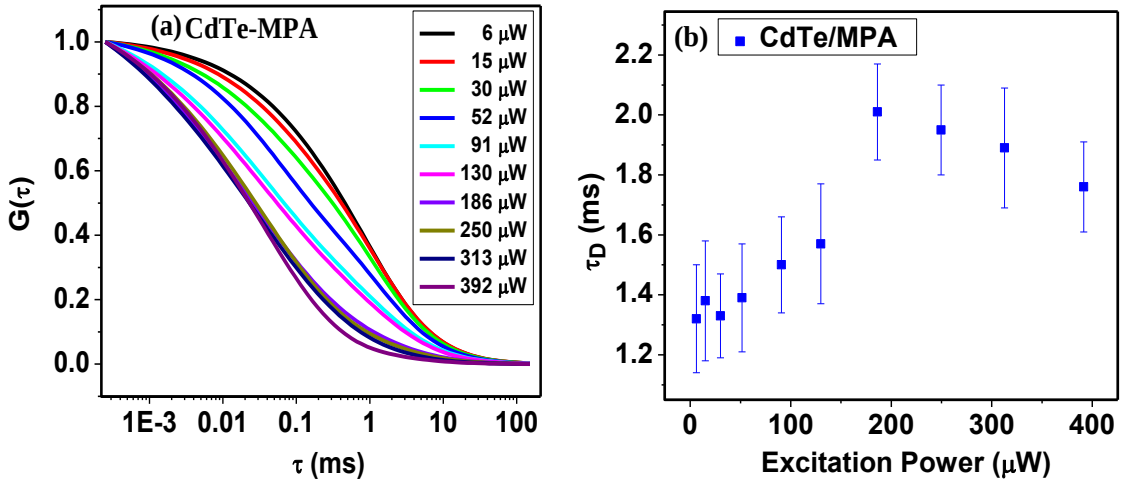

Figure 3.4. (a) Normalized fitted correlation curves of the 55 nM CdTe/MPA QDs in aqueous media for different excitation power. (b) A plot of the measured diffusion time of the QDs against excitation power.

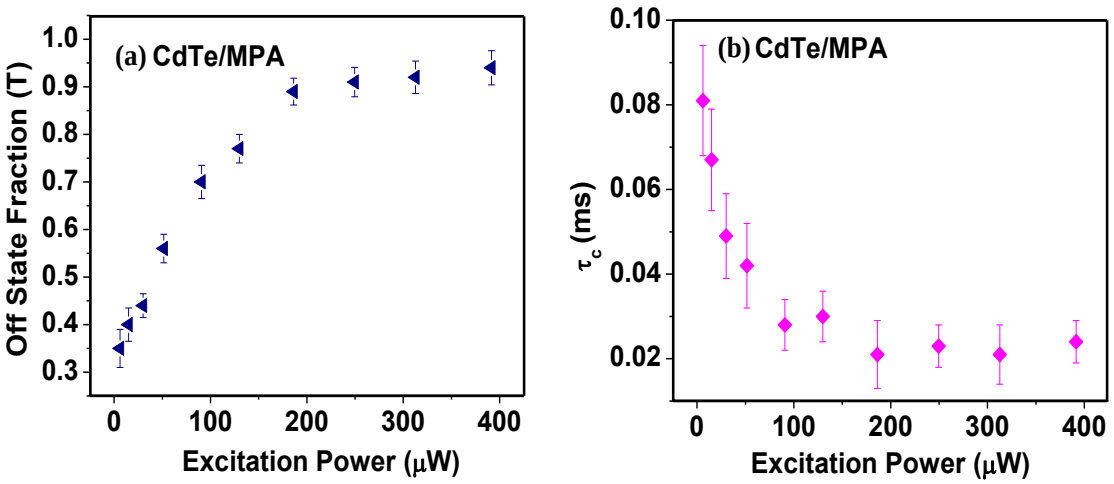

Figure 3.5. Variation of the estimated (a) off-state fraction (T) and (b) blinking time (τ_t), obtained from the fit to Equation (2.6), on the excitation power.

However, the changes in diffusion time in the low excitation power regime (Figure 3.4) is almost negligible, and in this regime the decrease of the G(0) value is huge. A decrease in the G(0) value after 100μW excitation power can be rationalized as due to excitation saturation. However, the decrease of the G(0) value in the low excitation regime is certainly not due to excitation saturation and hence some other processes must be involved. Because the decrease of the G(0) value is much larger in the case of QDs compared to R123, an increase of background intensity with increasing excitation power is not responsible for this observation (Figure 3.3). As stated in the Introduction, Doose et al. assigned a decrease in the amplitude of the correlation curve to excitation saturation and blinking[73] but could not model the excitation power-dependent blinking of the QDs. We have successfully modeled the excitation power-dependent blinking kinetics by fitting the data to a stretched exponential model and found out that this decrease in the G(0) value is not due to blinking (as it increases the fraction of the off-state) (Figure 3.5). Under these circumstances, this decrease of the G(0) value can be explained only if N increases by exposure to light. This suggests light-induced brightening of the otherwise dark particles (which does not fluoresce), and this process is enhanced with an increase in excitation power, a process commonly termed photoactivation.[35] In this context, it is to be noted that Dong et al. attributed a decrease of the G(0) value under laser irradiation of different times to photoactivation of the quantum dots[37] resulting from facile aggregation of the QDs that led to a shift of the correlation curves to

longer correlation times.[37] However, in our study we did not observe any increase in the diffusion time in the lower excitation power region where the decrease of G(0) value is huge (Figures 3.1 and 3.4). Hence, even though photoactivation is responsible for the decrease of the G(0) value upon increasing excitation power, it is clearly not due to laser-induced aggregation. The increase in the G(0) value from 0.30 ± 0.12 (at 186 μW) to 0.45 ± 0.12 (at 392 μW) (Figure 3.1) is clearly due to photobleaching, which decreases the number of fluorescent molecules in the observation volume. This fact is also supported by the decrease in the diffusion time from 2.01 ± 0.16 ms (at 186 μW) to 1.76 ± 0.15 ms (at 392 μW) (Figure 3.4) due to a decrease in the residence time of the QDs because of photobleaching.

An important point to note here is that for low excitation power, the number of QDs in the observation volume (10^{-15} L) estimated from the FCS measurement (N) is much lower than the actual number of QDs (N_{actual}) present in this volume. For example, for a concentration of 55 nM, the actual number of QDs in the observation volume is 33. However, the number of QDs calculated from the measured G(0) value of 0.98 ± 0.13 and an off-state fraction of 0.35 is only 1.56 ± 0.25, indicating that a large fraction of the QDs remain in their dark state (absorb light but do not emit). The experiments carried out for various QD concentrations, the results of which are collected in Table 3.1, show a very similar behavior. That the concentration mismatch in the case of the QDs is indeed due to the dark fraction is further substantiated by the fact that for the molecular system, R123, no such mismatch is observed (Figure 3.6). With increasing excitation power, as the dark fractions are turned into bright ones, the G(0) value decreases despite an increase in the off-state fraction under this condition. At even higher excitation power, when almost all the QDs are turned bright and participate in the on-off transition, the saturation of the G(0) value is observed.

Table 3.1. Some FCS parameters at different concentrations of the QDs in aqueous solution for an excitation power of 6 μW.

Parameters	30 nM	55 nM	64 nM	270 nM
G(0)	3.0770 ± 0.3100	0.9800 ± 0.1300	0.8293 ± 0.0800	0.1462 ± 0.0100
N(1-T)	0.3250 ± 0.030	1.020 ± 0.150	1.201 ± 0.080	6.840 ± 0.440
T	0.42 ± 0.04	0.35 ± 0.04	0.34 ± 0.05	0.32 ± 0.04
N	0.56 ± 0.05	1.56 ± 0.25	1.83 ± 0.13	10.04 ± 0.69
$^{\dagger}N_{actual}$	18 ± 1	33 ± 2	38 ± 2	162 ± 6
*Dark Fraction	0.970 ± 0.002	0.950 ± 0.002	0.950 ± 0.002	0.940 ± 0.004

†Estimated from the concentration of QDs for an observation volume of 10^{-15} L. *N/N_{actual} gives the bright fraction of the QDs. Dark fraction = (1 - bright fraction).

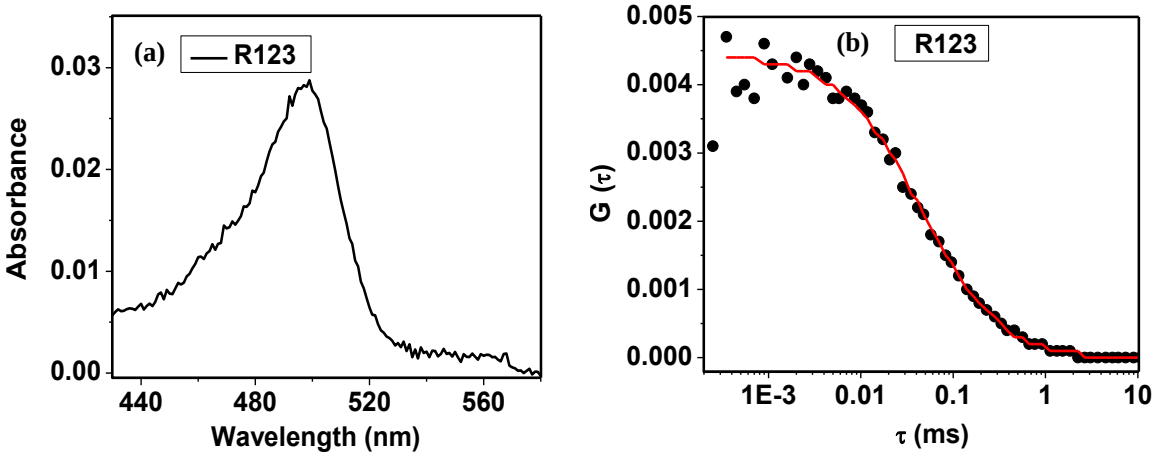

Figure 3.6. (a) Absorption spectrum of an aqueous solution of R123. Concentration of R123 obtained from absorption measurement is 379 nM. (b) Correlation curve of R123 at 379 nM concentration. Black spheres are the data and red line represents the simple 3-D diffusion fit to the data points. Exactly same G(0) value obtained in the FCS experiment as expected from the absorption measurement.

3.3. Steady state behavior of the QDs at different illumination times:

To identify the process(es) responsible for the change in luminescence behavior of the QDs, the experiments have also been performed under steady-state conditions for different irradiation periods using deoxygenated solutions of QDs (prepared by nitrogen bubbling of the solution). The effect of exposure to light on the UV−vis absorption spectrum

also was studied. A noticeable decrease of the absorbance throughout the entire absorption band is observed with increasing exposure time (Figure 3.7). As the absorption peak position is not well-resolved, it is difficult to figure out from the data whether light irradiation leads to any shift of the absorption maximum. Figure 3.7 depicts the effect of illumination of an aqueous solution of the QDs for different exposure times on the integrated emission intensity (I_{em}) and wavelength corresponding to the emission peak (λ_{max}^{em}). The illumination leads to a nearly 3-fold enhancement of I_{em} up to a certain time (350 min under experimental conditions) beyond which the emission intensity decreases rapidly. During this irradiation process, λ_{max}^{em} decreases slightly at the early stages, but it decreases sharply after a certain time (which coincides with the time when the I_{em} value starts dropping). To examine any possible role of oxygen on these results, the aqueous solution of the QDs in the cuvette was purged with nitrogen and the experiments were repeated in an oxygen-free environment. These results are also shown in Figure 3.7. As can be seen, also in deaerated condition the initial luminescence enhancement on exposure to light is observed, but the subsequent rapid reduction of I_{em} that is observed in aerated condition is not present. In the N_2-purged solution, the λ_{max}^{em} value, unlike that in the other case, also remains more or less constant. These findings clearly exhibit the distinct role of oxygen in the rapid reduction of I_{em} and the blue shift of λ_{max}^{em} observed following post-maximization of the luminescence intensity. The results also clearly show two competing processes; one enhances the luminescence intensity (the photoactivation of the QDs), and the other diminishes the luminescence of the system. The former is the dominant process at the early stages, and the latter dominates at longer times. It is also evident that the photoactivation process is not sensitive to oxygen, but the latter is. Oxygen-induced photocorrosion of the QDs is well-known,[22,32] and we attribute the rapid drop of luminescence of the system coupled with a blue shift of the emission maximum to photooxidation of the QDs. In this context, it is to be noted that while the overall trend of photoinduced variation of luminescence intensity is found to be very similar for QDs of different sizes, the time required for the maximization of the luminescence intensity or the subsequent rate of drop of the intensity due to photooxidation of the QDs varies from sample to sample.

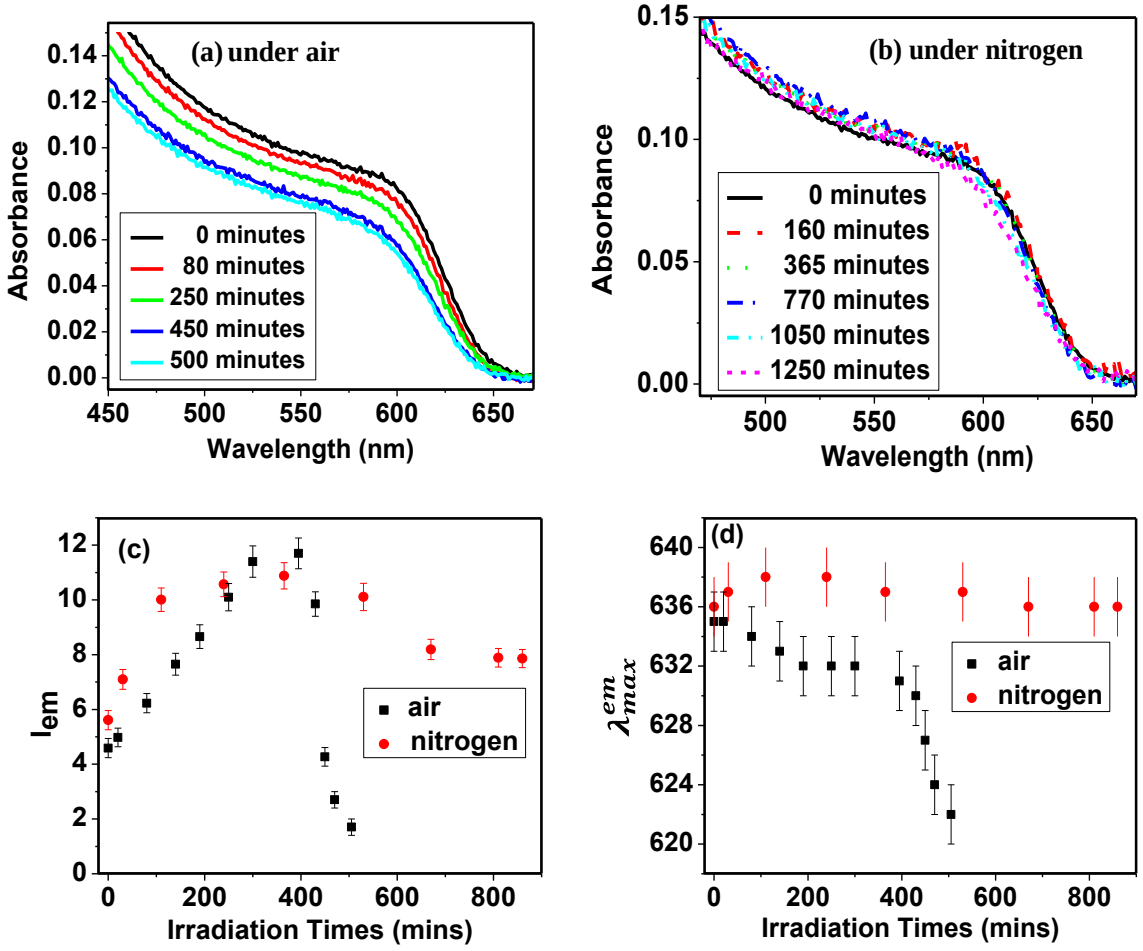

Figure 3.7. Absorption spectra of an aqueous solution of CdTe/MPA QDs at different exposure times to light in (a) air and (b) nitrogen environment. Corresponding variation of the (c) integrated fluorescence intensity (I_{em}) and (d) emission peak wavelength (λ^{em}_{max}) of the CdTe/MPA QDs as a function of irradiation times.

Insight into the mechanism of photoactivation or luminescence enhancement of the QDs can be obtained from some control experiments. Following its photoactivation in aerated or nitrogen environment, if the QD solution is kept in the dark, the luminescence intensity drops again (Figure 3.8). The decrease in luminescence and its recovery on light exposure under the experimental conditions suggests photoadsorption of water molecules on the QD surface as a possible mechanism of the photoactivation of QDs, as reported for CdSe QDs.[32,35,38,48] The photoadsorption of the water molecules passivates the surface charge carrier trap states and enhances the luminescence of the QDs. However, the fact that

luminescence intensity of the QDs does not return completely to its original state, suggests some irreversible change in the surface structure of the QDs. It is difficult to conclude at this stage about the exact nature of the change of the QD surface, but it is possible that some of the chemisorbed water molecules do not leave the QD surface when kept in the dark.

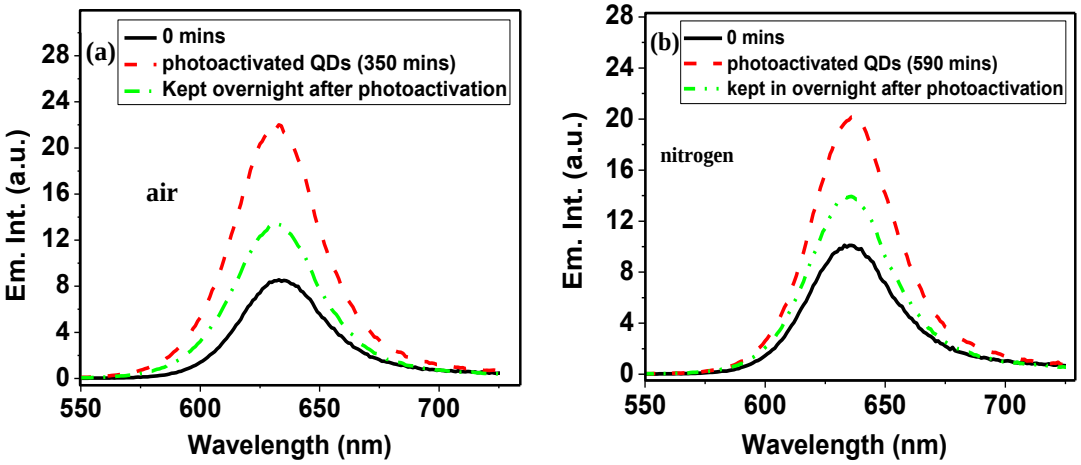

Figure 3.8: Emission spectra of the photo-activated QDs and after keeping the photo-activated QDs in dark for overnight in (a) air and (b) N_2 environment. Luminescence does not come to its original state (t=0).

3.4. Fluorescence lifetime study of CdTe/MPA at different irradiation times:

The mechanism of photoinduced fluorescence enhancement is further substantiated by the fluorescence lifetime data of an aqueous solution of QDs measured after different irradiation times. Figure 3.9 shows the dependence of the fluorescence decay curves of the QDs on the illumination times. The decay curves could be best fit (as determined from the residuals and χ^2 values) to a three-exponential function. This multi-exponential decay of the fluorescence time-profiles of the QDs is due to the existence of a number of discrete relaxation pathways from the excited states with characteristic lifetime components and is consistent with the literature.[5,19,76] The individual lifetime values and the corresponding amplitudes are listed in Table 3.2. As can be seen, the fluorescence lifetime data parallels the steady state data. The average fluorescence lifetime of the QDs increases on photoexposure up to a certain time, beyond which a decrease of fluorescence lifetime is observed. Another point to note here is that the relative weightage of the 0.60 ± 0.02 and 7.12 ± 0.30 ns components vary significantly, while that of the longest lifetime component (48.07 ± 1.45 ns) remains more or less unaltered during light irradiation from 0 to 330 mins. The amplitude

associated with the 0.60 ± 0.02 ns component decreases, while that of 7.12 ± 0.30 ns component increases upon irradiation. After 330 minutes of irradiation, the weightage of the 7.12 ± 0.30 ns component decreases and that of the fastest component increases (Table 3.2).

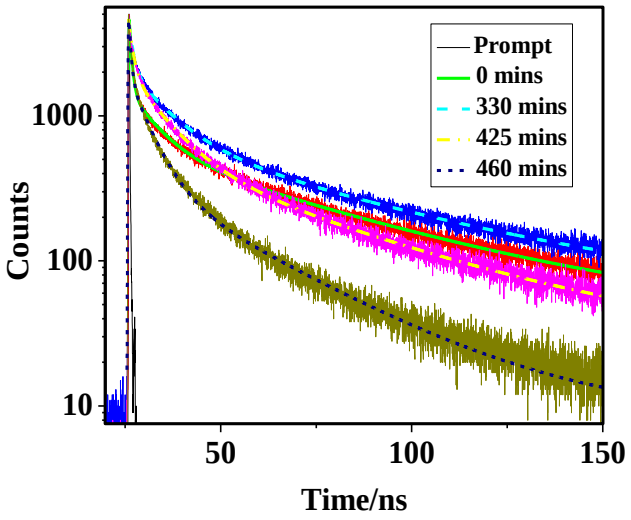

Figure 3.9: Fluorescence decay profiles of CdTe/MPA QDs in aqueous media at different irradiation times. The lines are the fit to the decay traces. In all the cases, the traces are fit to a three exponential model $I(t) = a_1 \exp(-t/\tau_1) + a_2 \exp(-t/\tau_2) + a_3 \exp(-t/\tau_3)$. Excitation wavelength is 439 nm and the emission is monitored at the peak wavelength.

The observation can be rationalized after considering the origin of the each lifetime component of the QDs. The 0.60 ± 0.02 ns component arises from intrinsic electron-hole recombination at the core with little contribution from the surface states.[19] The long lifetime component is often attributed to the involvement of the surface states where overlap of the wave functions of electron and hole is poor.[5,19] In some other instances, the long lifetime component is attributed to the involvement of the spin-forbidden optically passive states present in the band edge (dark exciton states).[36,77] The 7.12 ± 0.30 ns emission component can be considered arising from the involvement of the shallow trap states just below the band edge states and the 48.07 ± 1.45 ns component to the spin-forbidden state in the band edge. As exposure to light passivates the surface trap states and decreases the nonradiative deactivation pathways, it is understandable why the lifetimes are increased on irradiation. In order to explain the change of the amplitudes on photoexposure, one need to consider that all QDs are not bright, some are dark (having very poor surface that provides a broad distribution of the deep trap states that quenches the luminescence). Irradiation of light not

only suppresses the nonradiative pathways of the bright QDs but also converts some dark fraction into bright QDs (as evident from the FCS data) by stabilizing the shallow trap states of the dark QDs.[36,22] Photoadsorption of water molecules stabilizes these trap states containing charge carriers (electron or hole) and increases the probability of the charge carrier to repopulate the emitting band edge state instead of undergoing nonradiative relaxation to deep trap states from where nonradiative processes dominate.[38] When photooxidation of the QDs dominates over the photoactivation process, new surface defects are introduced, which provide additional nonradiative pathways and thus decrease the emission lifetime of the components.[22, 32] As more surface trap states are now generated due to photooxidation of QDs, this decreases the lifetime as well as amplitude of the 7.12 ± 0.30 ns (t=0). So, at later stages of photoirradition the fluorescence is mainly due to the involvement of electron and hole recombination in the core as the surface becomes poor and contributes less to the total luminescence. So the lifetime studies under light irradiation corroborate the findings obtained in the FCS and steady state experiments.

Table 3.2: Time-resolved fluorescence parameters of CdTe-MPA QDs in aqueous solution after different illumination times.

Irradiation times (mins)	τ_1 (ns)	α_1	τ_2 (ns)	α_2	τ_3 (ns)	α_3	$\langle\tau\rangle$ (ns)*
0	7.12 ± 0.30	0.17	48.07 ± 1.45	0.10	0.60 ± 0.02	0.73	6.46 ± 0.21
50	7.40 ± 0.35	0.18	48.30 ± 1.40	0.10	0.71 ± 0.02	0.72	6.67 ± 0.22
110	8.09 ± 0.40	0.21	50.00 ± 1.50	0.11	0.84 ± 0.02	0.68	7.77 ± 0.26
170	8.70 ± 0.30	0.22	51.60 ± 1.35	0.11	0.93 ± 0.02	0.67	8.21 ± 0.23
220	9.38 ± 0.35	0.23	52.02 ± 1.40	0.12	1.08 ± 0.02	0.65	9.10 ± 0.26
280	9.32 ± 0.40	0.25	52.00 ± 1.45	0.12	1.05 ± 0.02	0.63	9.23 ± 0.29
330	9.67 ± 0.30	0.27	52.20 ± 1.35	0.12	1.15 ± 0.02	0.61	9.58 ± 0.26
425	8.02 ± 0.35	0.29	42.10 ± 1.30	0.10	0.80 ± 0.02	0.61	7.02 ± 0.24
460	5.30 ± 0.25	0.23	29.00 ± 1.10	0.05	0.48 ± 0.02	0.71	3.01 ± 0.13
480	4.37 ± 0.20	0.18	24.50 ± 1.10	0.03	0.40 ± 0.02	0.79	1.840 ± 0.085
500	3.83 ± 0.25	0.18	21.76 ± 1.20	0.03	0.34 ± 0.01	0.79	1.670 ± 0.089
535	3.87 ± 0.20	0.17	22.07 ± 1.10	0.03	0.31 ± 0.01	0.80	1.51 ± 0.075

*$\langle\tau\rangle$ is defined as, $\langle\tau\rangle = (\alpha_1\tau_1+\alpha_2\tau_2+\alpha_3\tau_3)/\alpha_1+\alpha_2+\alpha_3$

3.5. Conclusions:

Significant changes of the fluorescence behavior of an aqueous solution of CdTe/MPA QDs under exposure to light have been studied by using a combination of FCS, steady state and time-resolved fluorescence techniques. A faster relaxation of the correlation at higher excitation power, especially at shorter correlation time, is attributed to increasing contribution of the off-state of the QDs. A decrease in the G(0) value with increasing excitation power, despite an increasing fraction of the molecules in their off-state, is mainly attributed to light-induced brightening of the dark QDs to bright QDs because of surface passivation at higher excitation power. The simultaneous of the occurrence of two competing processes, photoactivation leading to fluorescence enhancement and photo-degradation resulting in quenching of the luminescence of the QDs, has been substantiated by the steady state and time-resolved emission measurements. It is suggested that surface passivation by photoadsorption of water molecules leads to photoactivation of the QDs and dissolved oxygen-induced photooxidation of the surfaces is responsible for subsequent drop of the luminescence intensity of the system.

References:

(1) Smith, A. M.; Nie, S. *Acc. Chem. Res.* **2010**, *43*, 190.

(2) Murray, C. B.; Norris, D. J.; Bawendi, M. G. *J. Am. Chem. Soc.* **1993**, *115*, 8706.

(3) Alivisatos, A. P. *Science* **1996**, *271*, 933.

(4) Brus, L. E. *J. Chem. Phys.* **1983**, *79*, 5566.

(5) Bawendi, M. G.; Carroll, P. J.; Wilson, W. L.; Brus, L. E. *J. Chem. Phys.* **1992**, *96*, 946.

(6) Norris, D. J.; Bawendi, M. G. *J. Chem. Phys.* **1995**, *103*, 5260.

(7) Frederick, M. T.; Amin, V. A.; Cass, L. C.; Weiss, E. A. *Nano Lett.* **2011**, *11*, 5455.

(8) Reiss, P.; Protiere, M.; Li, L. *Small* **2009**, *5*, 154.

(9) Resch-Genger, U.; Grabolle, M.; Cavaliere-Jaricot, S.; Nitschke , R.; Nann, T. *NATURE METHODS* **2008**, *5*, 763.

(10) Delehanty, J. B.; Bradburne, C. E.; Susumu, K.; Boeneman, K.; Mei, B. C.; Farrell, D.; Blanco-Canosa, J. B.; Dawson, P. E.; Mattoussi, H.; L., M. I. *J. Am. Chem. Soc.* **2011**, *133*, 10482.

(11) Chen, M. L.; He, Y. J.; Chen, X. W.; Wang, J. H. *Bioconjugate Chem.* **2013**, *24*, 387.

(12) Larson, D. R.; Zipfel, W. R.; Williams, R. M.; Clark, S. W.; Bruchez, M. P.; Wise, F. W.; Webb, W. W. *Science* **2003**, *300*, 1434.

(13) Michalet, X.; Pinaud, F. F.; Bentolila, L. A.; Tsay, J. M.; Doose, S.; Li, J. J.; Sundaresan, G.; Wu, A. M.; Gambhir, S. S.; Weiss, S. *Science* **2005**, *307*, 538.

(14) Lim, Y. T.; Kim, S.; Nakayama, A.; Stott, N. E.; Bawendi, M. G.; Frangioni, J. V. *Mol. Imaging* **2003**, *2*, 50.

(15) Zhao, J.; Bardecker, J. A.; Munro, A. M.; Liu, M. S.; Niu, Y.; Ding, I. K.; Luo, J.; Chen, B.; Jen, A. K. Y.; Ginger, D. S. *Nano Lett.* **2006**, *6*, 463.

(16) Robel, I.; Subramanian, V.; Kuno, M.; Kamat, P. V. *J. Am. Chem. Soc.* **2006**, *128*, 2385.

(17) Kamat, P. V. *J. Phys. Chem. Lett.* **2013**, *4*, 908.

(18) Qu, L.; Peng, X. *J. Am. Chem. Soc.* **2002**, *124*, 2049.

(19) Wang, X.; Qu, L.; Zhang, J.; Peng, X.; Xiao, M. *Nano Lett.* **2003**, *3*, 1103.

(20) Borchert, H.; Talapin, D. V.; Gaponik, N.; McGinley, C.; Adam, S.; Lobo, A.; Möller, T.; Weller, H. *J. Phys. Chem. B* **2003**, *107*, 9662.

(21) Kuno, M.; Lee, J. K.; Dabbousi, B. O.; Mikulec, F. V.; Bawendi, M. G. *J. Chem. Phys.* **1997**, *106*, 9869.

(22) Biju, V.; Kanemoto, R.; Matsumoto, Y.; Ishii, S.; Nakanishi, S.; Itoh, T.; Baba, Y.; Ishikawa, M. *J. Phys. Chem. C* **2007**, *111*, 7924.

(23) Peng, X.; Schlamp, M. C.; Kadavanich, A. V.; Alivisatos, A. P. *J. Am. Chem. Soc.* **1997**, *119*, 7019.

(24) Spanhel, L.; Haase, M.; Weller, H.; Henglein, A. *J. Am. Chem. Soc.* **1987**, *109*, 5649.

(25) Jones, M.; Lo, S. S.; Scholes, G. D. *J. Phys. Chem. C* **2009**, *113*, 18632.

(26) Jasieniak, J.; Mulvaney, P. *J. Am. Chem. Soc.* **2007**, *129*, 2841.

(27) Kilina, S.; Ivanov, S.; Tretiak, S. *J. Am. Chem. Soc.* **2009**, *131*, 7717.

(28) Kalyuzhny, G.; Murray, R. W. *J. Phys. Chem.* **2005**, *109*, 7012.

(29) Talapin, D. V.; Rogach, A. L.; Kornowski, A.; Haase, M.; Weller, H. *Nano Lett.* **2001**, *1*, 207.

(30) Knowles, K. E.; Frederick, M. T.; Tice, D. B.; Morris-Cohen, A. J.; Weiss, E. A. *J. Phys. Chem. Lett.* **2012**, *3*, 18.

(31) Frederick, M. T.; Amin, V. A.; Weiss, E. A. *J. Phys. Chem. Lett.* **2013**, *4*, 634.

(32) Carrillo-Carrion, C.; Cardenas, S.; Simonet, B. M.; Valcarcel, M. *Chem. Commun.* **2009**, 5214.

(33) Bao, H.; Gong, Y.; Li, Z.; Gao, M. *Chem. Mater.* **2004**, *16*, 3853.

(34) Wang, Y.; Tang, Z.; Correa-Duarte, M. A.; Pastoriza-Santos, I.; Giersig, M.; Kotov, N. A.; Liz-Marzan, L. M. *J. Phys. Chem. B* **2004**, *108*, 15461.

(35) Cordero, S. R.; Carson, P. J.; Estabrook, R. A.; Strouse, G. F.; Buratto, S. K. *J. Phys. Chem. B* **2000**, *104*, 12137.

(36) Jones, M.; Nedeljkovic, J.; Ellingson, R. J.; Nozik, A. J.; Rumbles, G. *J. Phys. Chem. B* **2003**, *107*, 11346.

(37) Dong, C.; Qian, H.; Fang, N.; Ren, J. *J. Phys. Chem. C* **2007**, *111*, 7918.

(38) Pechstedt, K.; Whittle, T.; Baumberg, J.; Melvin, T. *J. Phys. Chem. C* **2010**, *114*, 12069.

(39) Impellizzeri, S.; McCaughan, B.; Callan, J. F.; Raymo, F. M. *J. Am. Chem. Soc.* **2012**, *134*, 2276.

(40) Osborne, M. A.; F., L. S. *ACS Nano* **2011**, *5*, 8295.

(41) Nazzal, A. Y.; Qu, L.; Peng, X.; Xiao, M. *Nano Lett.* **2003**, *3*, 819.

(42) Gaponik, N.; Talapin, D. V.; Rogach, A. L.; Hoppe, K.; Shevchenko, E. V.; Kornowski, A.; Eychmüller, A.; Weller, H. *J. Phys. Chem. B* **2002**, *106*, 7177.

(43) Wang, Y.; Tang, Z.; Correa-Duarte, M. A.; Liz-Marzán, L. M.; Kotov, N. A. *J. Am. Chem. Soc.* **2003**, *125*, 2830.

(44) Sato, K.; Kojima, S.; Hattori, S.; Chiba, T.; Ueda-Sarson, K.; Torimoto, T.; Tachibana, Y.; Kuwabata, S. *Nanotechnology* **2007**, *18*, 465702 (1.

(45) Hess, B. C.; Okhrimenko, I. G.; Davis, R. C.; Stevens, B. C.; Schulzke, Q. A.; Wright, K. C.; Bass, C. D.; Evans, C. D.; Summers, S. L. *Phys. Rev. Lett.* **2001**, *86*, 3132.

(46) Shavel, A.; Gaponik, N.; Eychmuller, A. *J. Phys. Chem. B* **2004**, *108*, 5905.

(47) Kloefper, J. A.; Bradforth, S. E.; Nadeau, J. L. *J. Phys. Chem. B* **2005**, *109*, 9996.

(48) Oda, M.; Hasegawab, A.; Iwamib, N.; Nishiurab, K.; Andob , N.; Nishiyamab, A.; Horiuchib, H.; Tania, T. *Colloids Surf. B* **2007**, *56*, 241.

(49) Mandal, A.; Nakayama, J.; Tamai, N.; Biju, V.; Isikawa, M. *J. Phys. Chem. B* **2007**, *111*, 12765.

(50) Lackowicz, J. R. *Springer: New York* **2006**, *Chapter 24*.

(51) Rochira, J. A.; Gudheti, M. V.; Gould, T. J.; Laughlin, R. R.; Nadeau, J. L.; Hess, S. T. *J. Phys. Chem. C* **2007**, *111*, 1695.

(52) Ito, S.; Toitani, N.; Pan, L.; Tamai, N.; Miyasaka, H. *J. Phys.: Condens. Matter* **2007**, *19*, 486208 (1.

(53) Zawadzki, P.; Slosarek, G.; Boryski, J.; Wojtaszek, P. *Biol. Chem.* **2010**, *391*, 43.

(54) Li, X.; Zhu, R.; Yu, A.; Zhao, X. S. *J. Phys. Chem. B* **2011**, *115*, 6265.

(55) Schuler, J.; Frank, J.; Trier, U.; Schafer-Korting, M.; Saenger, W. *Biochemistry* **1999**, *38*, 8402.

(56) Fron, E.; Auweraer, M.; Moeyaert, B.; Michiels, J.; Mizuno, H.; Hofkens, J.; Adam, V. *J. Phys. Chem. B* **2013**, *117*, 2300.

(57) Mojumdar, S. S.; Ghosh, S.; Mondal, T.; Bhattacharyya, K. *Langmuir* **2012**, *28*, 10230.

(58) Patra, S.; Samanta, A. *J. Phys. Chem. B* **2012**, *116*, 12275.

(59) Mojumdar, S. S.; Chowdhury, R.; Chattoraj, S.; Bhattacharyya, K. *J. Phys. Chem. B* **2012**, *116*, 12189.

(60) Cherdhirankorn, T.; Harmandaris, V.; Juhari, A.; Voudouris, P.; G., F.; Kremer, K.; Koynov, K. *Macromolecules* **2009**, *42*, 4858.

(61) Zettl, H.; Portnoy, Y.; Gottlieb, M.; Krausch, G. *J. phys. Chem. B* **2005**, *109*, 13397.

(62) Liedl, T.; Keller Dr., S.; Simmel Dr., F. C.; Rädler Prof., J. O.; J., P. D. W. *Small* **2005**, *1*, 997.

(63) Chakraborty, S. K.; Fitzpatrick, J. A. J.; Phillippi, J. A.; Andreko, S.; Waggoner, A. S.; Bruchez, M. P.; Ballou, B. *Nano Lett.* **2007**, *7*, 2618.

(64) Dong, C.; Irudayaraj, J. *J. phys. Chem. B* **2012**, *116*, 12125.

(65) Nakane, Y.; Sasaki, A.; Kinjo, M.; Jin, T. *Anal. Methods* **2012**, *4*, 1903.

(66) Bussian, D. A.; Malko, A. V.; Htoon, H.; Chen, Y.; Hollingsworth, J. A.; Klimov, V. I. *J. phys. Chem. C* **2009**, *113*, 2241.

(67) Dong, C.; Huang, X.; Ren, J. *Ann. N.Y. Acad. Sci.* **2008**, *1130*, 253.

(68) Tsay, J. M.; Doose, S.; Weiss, S. *J. Am. Chem. Soc.* **2006**, *128*, 1639.

(69) Yao, J.; Larson, D. R.; Vishwasrao, H. D.; Zipfel, W. R.; Webb, W. W. *Proc. Natl. Acad. Sci. U. S. A.* **2005**, *102*, 14284.

(70) Heuff, R. F.; Swift, J. L.; Cramb, D. T. *Phys. Chem. Chem. Phys.* **2007**, *9*, 1870.

(71) Heuff, R. F.; Marrocco, M.; Cramb, D. T. *J. Phys. Chem. C* **2007**, *111*, 18942.

(72) Petersa, R.; Goh, J. B.; J., D.; Thakur, A.; Shehata, S.; Anderson, D. J.; Fradin, C. *ECS Transactions* **2010**, *28*, 243.

(73) Doose, S.; Tsay, J. M.; Pinaud, F.; Weiss, S. *Anal. Chem.* **2005**, *77*, 2235.

(74) Murhty, A. V. R.; Patil, P.; Datta, S.; Patil, S. *J. Phys. Chem. C* **2013**, *117*, 13268.

(75) Peterson, J.; Nesbitt, D. J. *Nano Lett.* **2009**, *9*, 338.

(76) Santhosh, K.; Patra, S.; Soumya, S.; Khara, D. C.; Samanta, A. *ChemPhysChem* **2011**, *12*, 2735.

(77) Efros, A. L.; Rosen, M.; Kuno, M.; Nirmal, M.; Norris, D. J.; Bawendi, M. G. *Phys. Rev. B* **1996**, *54*, 4843.

CHAPTER 4

Effect of Capping Agent and Medium on Light-Induced Variation of the Luminescence Properties of CdTe Quantum Dots

The influence of ligand and solvent on light-induced modulation of the emission behavior of the quantum dots (QDs) has been studied for CdTe QDs capped with hexadecylamine (HDA), mercaptopropionic acid (MPA), and 1-(1-undecanethiol)-3-methyl imidazolium bromide (SMIM) in $CHCl_3$, H_2O, and [bmim][PF_6] ionic liquid, respectively, using steady state and time-resolved fluorescence and fluorescence correlation spectroscopy techniques. While an aqueous solution of CdTe/MPA QDs exhibits fluorescence enhancement and a small blue shift of the emission peak (λ_{max}^{em}) in the early stages of the light irradiation, such enhancement could not be observed in the case of $CHCl_3$ solution of CdTe/HDA and [bmim][PF_6] solution of CdTe/SMIM. Instead, exposure to light leads to a rapid reduction in luminescence intensity and large blue shift of λ_{max}^{em} in the case of $CHCl_3$ solution of CdTe/HDA and a very slow decrease of luminescence intensity with negligible shift of λ_{max}^{em} in the case of an ionic liquid solution of CdTe/SMIM. The time-resolved fluorescence behavior of the QDs is found to be consistent with the steady state results. Fluorescence correlation spectroscopy measurements on the other hand reveal a large decrease of the amplitude of correlation at time zero [G(0)] for the aqueous solution of CdTe/MPA and negligible change in the G(0) value for the ionic liquid solution of CdTe/SMIM with increasing excitation power. The mechanism of these light-induced changes of the luminescence behavior of the QDs is investigated.

4.1. Introduction:

Semiconductor quantum dots (QDs) have attracted great attention in recent years because of their interesting size-dependent optical and electronic properties due to 3-dimensional confinement of the photogenerated electron and hole pair.[1-5] High molar extinction coefficient, thermal and photostability,[6,7] and emission quantum yield, long emission lifetime,[8,9] narrow emission profile, possibility of multiple exciton generation, etc.,[10,11] make the QDs superior to the conventional organic fluorophores[12] and explain why these substances have been found to be so useful in a wide variety of applications ranging from lasing and photovoltaics to biological imaging.[13-16]

The small dimension of the QDs (typically a few nanometers) results in a large surface/volume ratio. The uncoordinated atoms on the surface, when not passivated by any stabilizing ligand, form surface trap states which lie between the valence and the conduction bands.[2,17] These surface trap states can capture the charge carrier (electron or hole) and decrease the fluorescence efficiency of the QDs.[17] One of the major limitations in the development and utilization of the QDs in many applications is their poorly understood surface chemistry and surface related processes that modulate their emission behavior.[5,18-21] As an understanding of the factors that influence the fluorescence behavior of the QDs helps in utilization of these substances in various applications, it continues to remain as an important area of research ever since the discovery of these substances.

A common but not well understood phenomenon associated with the QDs is the variation of their luminescence intensity on exposure to light of low to moderate intensity. Both increase and decrease of luminescence intensity are reported.[8,19,22-30] Of the two, fluorescence enhancement on light irradiation, commonly termed as photoactivation,[19,23,24] is more interesting. A number of mechanisms have been proposed to account for photoactivation of the QDs.[19,23-27,31] These include surface modification by light-induced heat generation,[19] passivation of the surface trap states by photoadsorbed molecules, which include polar solvent molecules as well,[19,23,25,27,31] photo-induced rearrangement of the capping agents leading to surface passivation, smoothening of the surface on photooxidation or photocorrosion etc.[19,31] Photoadsorption of water molecules is known to passivate the surface and contribute to the photoactivation of the QDs.[19,23,25,27,32-35] Large fluorescence enhancement of the QDs in the presence of wet O_2/N_2 gases, but not in dry condition[25,27] established the role of water in the photoactivation process. Carrilio-Carrion et al. proposed a combination of both photooxidation and photoadsorption of water molecules as possible mechanism of photoactivation of the QDs in aqueous solution.[19] Considering the enormous importance of photoactivation, which influences the optical properties of the QDs and hence their applications, a thorough understanding of the mechanism of the process is necessary.

During the course of a recent study using fluorescence correlation spectroscopy (FCS) technique[36-38] on an aqueous solution of MPA-capped CdTe QDs, we observed a large decrease of the value of amplitude of correlation at time zero [G(0)], a quantity proportional to the inverse of the number of emitters in the confocal volume, with increasing excitation

power despite an increase in the contribution of the off-state fraction of the molecules.[23] This surprising observation was explained considering transformation of the QDs from their dark (non-emitting) state to a bright state with increasing excitation power.[23] Photoadsorption of water molecules was thought to be the key mechanism involved in the surface passivation and transformation of the dark QDs to their bright state on the basis of our experimental findings and literature reports.[19,23,25,27,32,34,35]

Considering that surface chemistry of the QDs largely depends on the nature of the capping agent and medium of dispersion, to establish conclusively that surface passivation by the photoadsorbed H_2O molecules is responsible for fluorescence enhancement of the QDs under light exposure, this work is undertaken wherein we have chosen three CdTe QDs with different capping agents and studied them in three different solvent media (Chart-1.6). We have used ionic liquid as one of the media, and for this purpose we have employed 1-(1-undecanethiol)-3-methyl imidazolium salt capped CdTe QDs, abbreviated here as CdTe/SMIM, which exhibits superior optical properties compared to the CdTe QDs in conventional solvents.[39] We have used steady state absorption and emission, time-resolved emission and FCS techniques to study these QDs in respective solvents to conclusively establish the critical role of the water molecules in the photoactivation of the CdTe QDs.

4.2. Steady state absorption and emission spectra and size of the QDs:

Figure 4.1 shows the steady state absorption and emission spectra of the QDs. The first exciton band maximum of CdTe/HDA in $CHCl_3$, CdTe/MPA in H_2O and CdTe/SMIM in [bmim][PF_6] are observed at 557, 552 and 510 nm respectively. The sizes of the QDs, estimated from these first absorption peak positions using a standard protocol,[40] are 3.3, 3.3 and 2.5 nm, respectively. The sizes of the CdTe/HDA and CdTe/MPA QDs obtained from the TEM images (Figure 4.2.) are 3.4 and 3.5 nm, respectively. These values match closely with the sizes estimated from the absorption spectral data.[40] Attempts to measure the size of CdTe/SMIM using TEM technique were not successful as clear image of CdTe/SMIM could not be obtained due to the difficulty involved in removal of the nonvolatile ionic liquid, [bmim][PF_6]. The molar extinction coefficients (ε) of the QDs at the first exciton band maximum calculated from the size following a reported procedure[40] are 1.34×10^5 M^{-1} cm^{-1}, 1.43×10^5 M^{-1} cm^{-1} and 7.01×10^4 $M^{-1}cm^{-1}$ for CdTe/HDA in $CHCl_3$, CdTe/MPA in

H_2O and CdTe/SMIM in [bmim][PF_6], respectively. Absorption cross sections (σ) of CdTe/HDA in $CHCl_3$, CdTe/MPA in H_2O and CdTe/SMIM in [bmim][PF_6], calculated from the molar extinction coefficients (ε) using equation,[36] $\sigma = 3.82 \times 10^{-21}\varepsilon$, are 5.46×10^{-16} cm^2, 5.46×10^{-16} cm^2 and 2.68×10^{-16} cm^2, respectively. Emission spectra of CdTe/HDA in $CHCl_3$, CdTe/MPA in H_2O and CdTe/SMIM in [bmim][PF_6] (Figure 4.1**)** indicate emission peaks (λ_{max}^{em}) at 602, 592 and 556 nm, respectively. These values are consistent with the estimated sizes of the QDs.

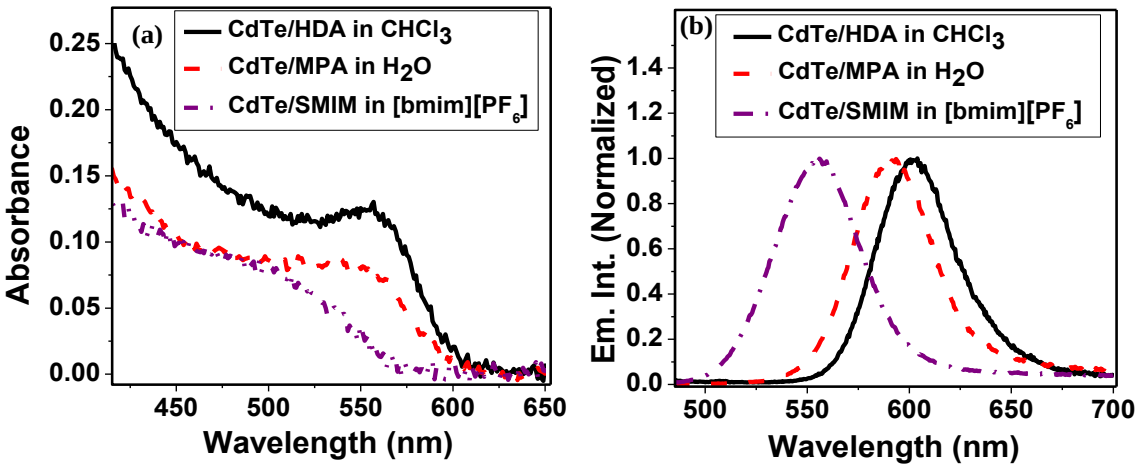

Figure 4.1. (a) Absorption and (b) emission spectra (λ_{ex} = 440 nm) of CdTe/HDA, CdTe/MPA and CdTe/SMIM in $CHCl_3$, H_2O and [bmim][PF_6], respectively.

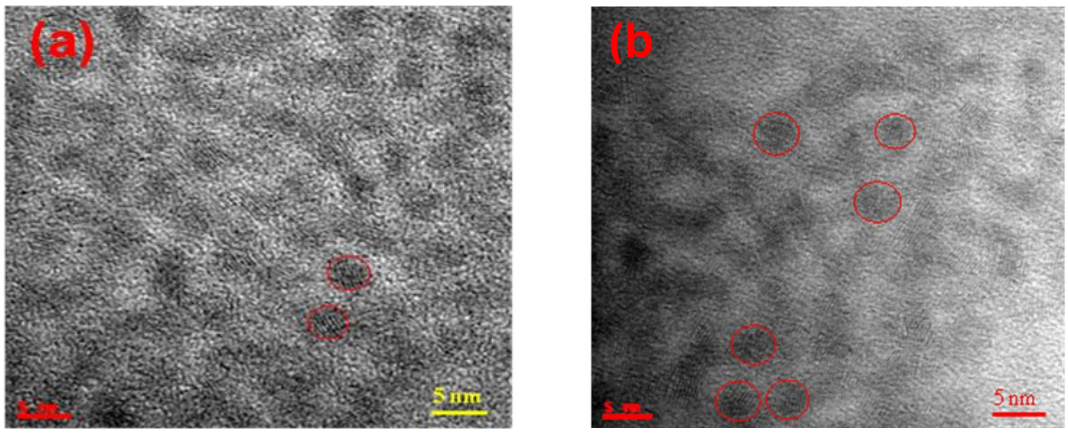

Figure 4.2. TEM images of (a) CdTe/HDA and (b) CdTe/MPA

4.3. Steady state fluorescence behavior as a function of light exposure time:

The effect of exposure to light on the emission spectra of the QDs is depicted in Figure 4.3. It can be seen that CdTe/HDA studied in $CHCl_3$ is the most sensitive QD, whose luminescence intensity drops drastically within an hour. On the other hand, CdTe/SMIM in [bmim][PF_6] is found to be far more stable, whose luminescence decreases much more slowly under similar exposure condition. It is only in the case of CdTe/MPA in H_2O that we observe an enhancement of luminescence. In addition, the emission peak position also changes on photo-irradiation. Both these changes are highlighted in Figure 4.4. As can be seen, the rapid drop of emission intensity of CdTe/HDA QDs in $CHCl_3$, which indicates almost complete photo-bleaching in ~60 mins, is accompanied by a large blue shift of λ_{max}^{em} from 603 to 568 nm in 60 minutes. In the case of aqueous solution of CdTe/MPA, nearly 3-fold enhancement of the fluorescence is observed with a shift of the emission peak from 592 to 585 nm in ~220 mins. Further illumination however leads to a decrease in emission intensity along with a large blue shift of the λ_{max}^{em} value from 585 nm (at 220 mins) to 569 nm (at 720 mins). On the other hand, the ionic liquid solution of CdTe/SMIM is found to be much more stable compared to the other two QDs. In this case, the emission intensity decreases very slowly with negligible shift of its emission maximum.

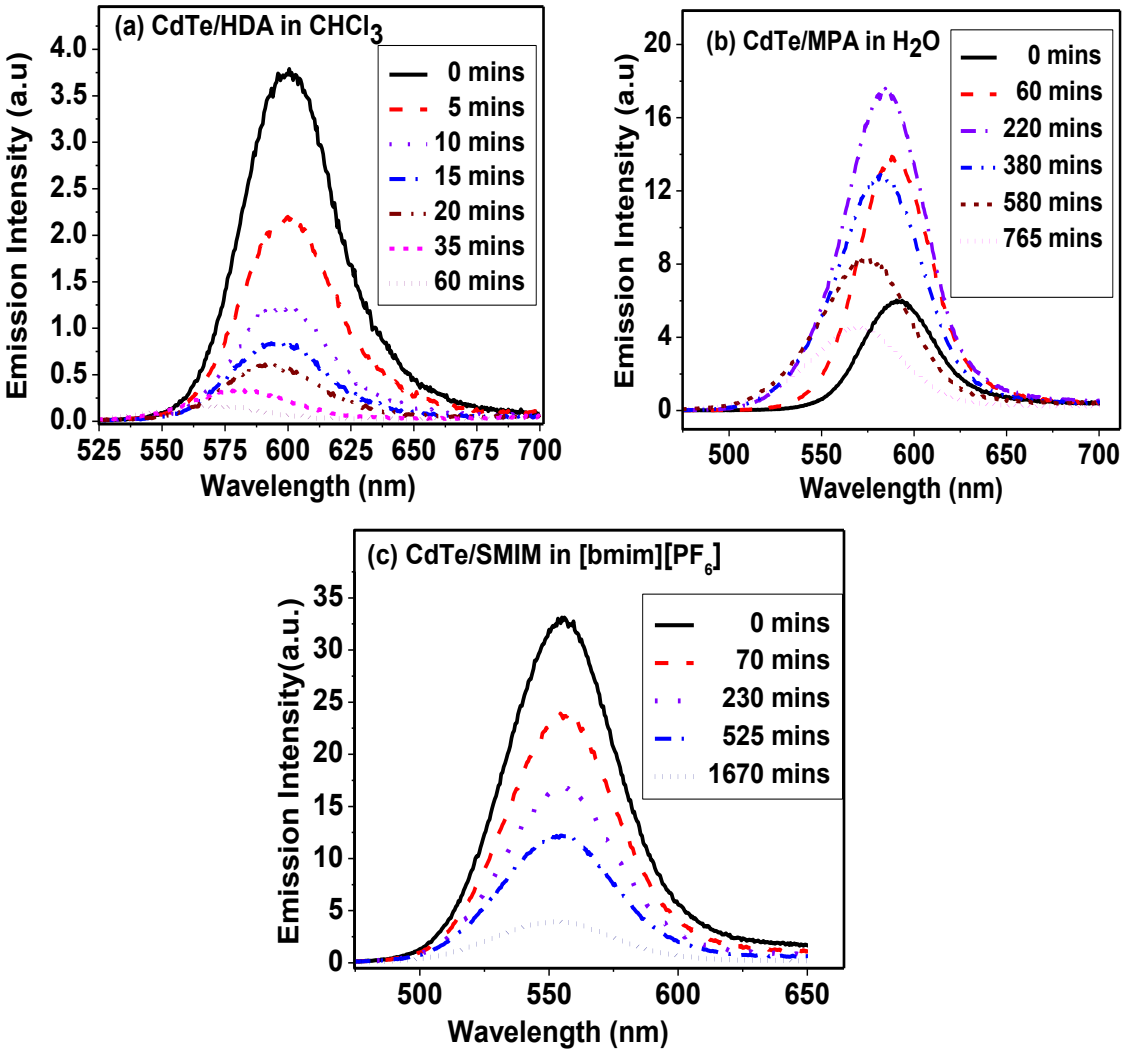

Figure 4.3. Steady state emission spectra (λ_{ex} = 440 nm) of (a) CdTe/HDA in $CHCl_3$, (b) CdTe/MPA in H_2O and (c) CdTe/SMIM in [bmim][PF_6] after different periods of exposure.

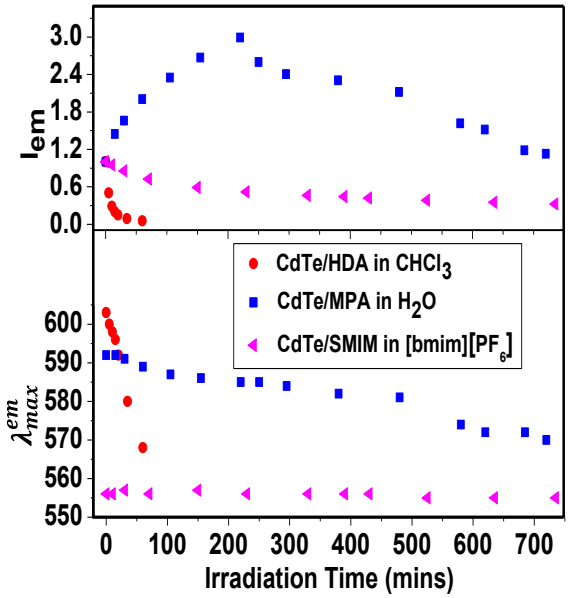

Figure 4.4. Plot of variation of the integrated fluorescence intensity I_{em} (top panel, normalized at t = 0) and emission peak wavelength λ_{max}^{em} (nm) (bottom panel) of the QDs with irradiation time.

In order to understand the origin of light-induced fluorescence enhancement of CdTe/MPA in aqueous environment, or more specifically, to find out whether dissolved oxygen (O_2) has anything to do with the effect, we have carried out irradiation experiments in N_2 environment as well (Figure 4.5). The fluorescence enhancement observed under deoxygenated condition (5-fold) is higher than that observed in the presence of air (~3-fold). The shift of λ_{max}^{em} observed (595 to 591 nm) even after prolonged exposure to light (14 hrs) in N_2 atmosphere is also much smaller (Figure 4.5).

The rapid reduction of luminescence intensity of CdTe/HDA QDs in $CHCl_3$ accompanied by a large blue shift of λ_{max}^{em} is due to photooxidation of the QD, which not only results in etching/photocorrosion of the surface, but also introduces defect states and facilitates nonradiative deactivation of the excited state. A much higher solubility of O_2 in $CHCl_3$ (9.8 mM)[41] compared to < 0.2 mM in [bmim][PF_6][42] and 0.28 mM in H_2O[43] explains why the photooxidation process is so efficient for CdTe/HDA in $CHCl_3$. Weak interaction (hard-soft) between the amine moiety and the surface Cd atoms compared to the thiol-Cd interaction (soft-soft) can also contribute to the photo-bleaching of the CdTe/HDA QDs.

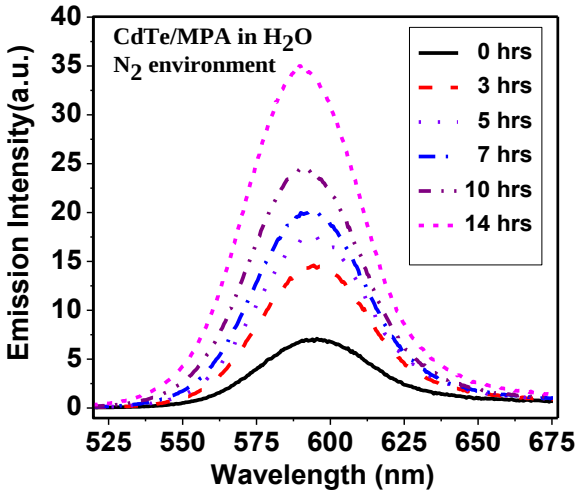

Figure 4.5. Emission spectra of CdTe/MPA (in H_2O) recorded at different periods of light irradiation in N_2 environment. λ_{ex} = 440 nm.

Low solubility of O_2 and also its slow diffusion in viscous [bmim][PF_6] gives a greater photostability to CdTe/SMIM in [bmim][PF_6] from corrosion and explain negligible shift of λ_{max}^{em}. However, even though surface etching is insignificant in [bmim][PF_6], the emission intensity of CdTe/SMIM decreases slowly on exposure to light. This is most likely due to photo-conversion of the surface protective thiol moiety to disulfide (a process known to occur in the absence of O_2[22]) and removal of the capping agent from the QDs. The exposed surface sites of the QDs serve as the trap states for the charge carriers and contribute to the drop of luminescence intensity of CdTe/SMIM QDs in [bmim][PF_6].[19]

The nature of variation of the emission intensity, which increases rapidly in the early stages of irradiation, but decreases slowly later, of the aqueous solution of CdTe/MPA, is clearly an indication of two competing processes. A process, which enhances the luminescence intensity at the early stages, and another process, which decreases emission intensity, dominates at a later time. The later process, which is also accompanied by a large blue shift of the λ_{max}^{em} value, is clearly due to slow photooxidation of the QDs by oxygen. As far as the process of luminescence enhancement or photoactivation is concerned, we can rule out any possible role of O_2 in the photoactivation of the QDs, as proposed in many literatures[19,24,28] as fluorescence enhancement is also observed in N_2 purged aqueous solution of CdTe/MPA (Figure 4.5). A drop of fluorescence intensity of the photoactivated QDs observed when kept in dark in both aerated and deaerated environment and its recovery again

under light (Figure 4.6) hints towards the photoadsorption of the water molecules as most likely mechanism of photoactivation, which we observed in our earlier study.[23] Photo-induced adsorption of water molecules leads to the passivation of the surface trap states and a decrease of the nonradiative events occurs at the early stages of irradiation.[23]

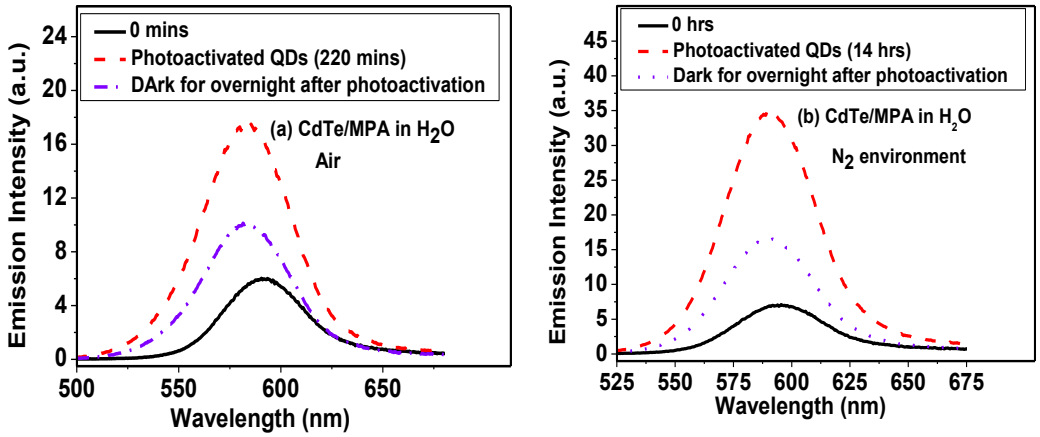

Figure 4.6. Emission spectra of the photoactivated CdTe/MPA QDs and after keeping the photoactivated QDs in dark for overnight in (a) air and (b) N_2 environment.

4.4. Fluorescence lifetime as a function of the duration of light exposure:

Figure 4.7 depicts the influence of light irradiation on the fluorescence decay profiles of the QDs. The measured decay curves are found best represented by triexponential function of the form, $I(t) = a_1 \exp(-x/\tau_1) + a_2 \exp(-x/\tau_2) + a_3 \exp(-x/\tau_3)$, where τ_1, τ_2, τ_3 are the lifetime components and a_1, a_2, a_3 are the corresponding amplitudes. The lifetime components, associated amplitudes and average lifetime $<\tau>$, estimated using $<\tau> = (a_1\tau_1 + a_2\tau_2 + a_3\tau_3)/ (a_1 + a_2 + a_3)$, are collected in Table 4.1. It can be seen, the $<\tau>$ value of CdTe/HDA (in $CHCl_3$) decreases drastically on irradiation from 2.74 ± 0.14 to 0.74 ns in just 20 mins. On the other hand, $<\tau>$ value of CdTe/SMIM in [bmim][PF_6] decreases very slowly and to observe a significant change of lifetime one needs to expose the solution to light for a much longer time. Another point to note here is that the amplitude associated with the fastest lifetime component increases and that of the two slow components decreases for both CdTe/HDA and CdTe/SMIM on exposure with light. In the case of aqueous solution of CdTe/MPA, the $<\tau>$ value increases upon light irradiation until a certain time (220 mins) and then decreases slowly. At the initial stages of irradiation (≤ 220 mins), the amplitude associated with the

shortest component decreases, and that of the longer components increases. This trend is exactly opposite to what is observed for CdTe/HDA & CdTe/SMIM. At longer irradiation time (beyond 220 mins), however, like in other two cases the amplitude of the shortest component increases and that of the long components decreases. This trend is consistent with our earlier study.[23]

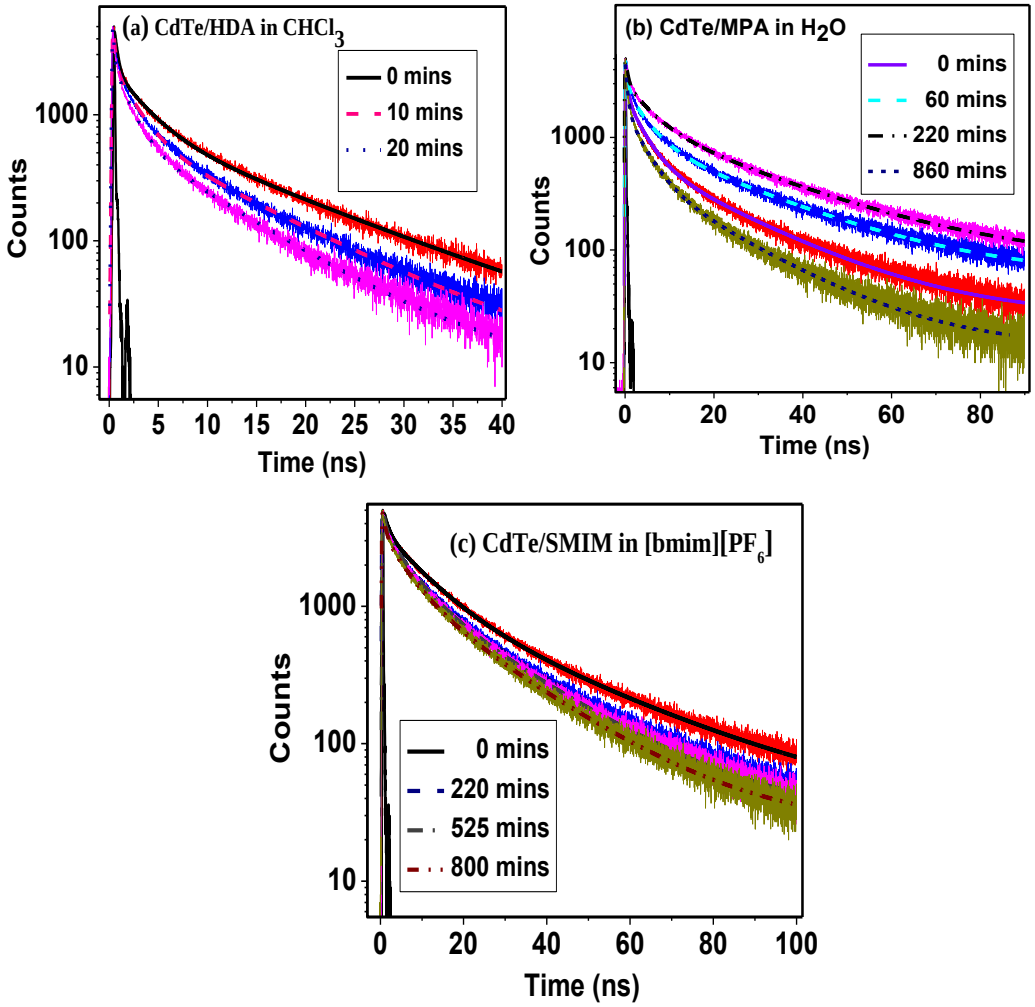

Figure 4.7. Fluorescence decay (λ_{ex} = 439 nm) profiles of (a) CdTe/HDA in $CHCl_3$, (b) CdTe/MPA in H_2O and (c) CdTe/SMIM in [bmim][PF_6] after different periods of illumination. The instrument response function is shown as black solid line. Emission is monitored at the peak wavelength.

The variation of the <τ> values, the individual lifetime components and their amplitudes is consistent with the steady state behavior of the systems and in agreement with the explanation offered for the variation. It is known that the shortest lifetime component arises due to intrinsic electron and hole recombination at the core of the QD.[8,44] The two long lifetime components involve the surface states and spin forbidden optically passive state present in the band edge (dark exciton state).[8,31,44-47] As surface passivation is not possible for CdTe/HDA and CdTe/SMIM due to the absence of H_2O molecules, the values of the individual lifetime components and amplitude associated with the surface-related lifetime components decrease on irradiation with light due to formation of more defect states on the surface (Table 4.1).

In the case of CdTe/MPA, photoadsorption of H_2O molecules passivates the surface trap states thereby decreasing the probability of nonradiative events at the initial stages of irradiation and increasing the <τ> value and individual lifetime components. As this surface passivation also converts a dark QD to a bright one by stabilizing the shallow trap states containing charge carriers, the process increases the lifetime of these trap states and enhance the probability of repopulation of the emitting band edge state (Scheme 4.1).[23] This increases the contribution of the surface-related long lifetime components of this QD at the early stages of irradiation. Upon prolonged exposure to light (> 220 mins), when photo-corrosion dominates over the photoactivation process, the lifetime data vary similar to that observed for the other two QDs, CdTe/HDA and CdTe/SMIM.

Table 4.1. Fluorescence decay parameters of CdTe/HDA, CdTe/MPA and CdTe/SMIM in $CHCl_3$, H_2O and [bmim][PF_6], respectively at different irradiation times

QDs	Medium	Irradiation Time (mins)	τ_1 (ns)	α_1	τ_2 (ns)	α_2	τ_3 (ns)	α_3	$<\tau>$ (ns)
CdTe/HDA	$CHCl_3$	0	2.95	0.24	14.05	0.13	0.30	0.67	2.74
		5	2.47	0.22	12.05	0.10	0.20	0.68	1.88
		10	2.16	0.21	10.95	0.08	0.17	0.71	1.45
		20	1.56	0.15	8.78	0.05	0.08	0.80	0.74
CdTe/MPA	H_2O	0	3.80	0.25	20.67	0.10	0.37	0.65	3.25
		60	4.43	0.28	24.70	0.15	0.43	0.57	5.19
		220	5.34	0.29	26.41	0.22	0.51	0.49	7.62
		480	4.75	0.30	20.74	0.18	0.43	0.52	5.38
		765	3.75	0.23	18.89	0.12	0.21	0.65	3.27
		860	3.12	0.23	16.40	0.08	0.26	0.69	2.21
CdTe/SMIM	[bmim][PF_6]	0	9.57	0.44	31.76	0.22	1.15	0.34	11.45
		220	6.50	0.36	22.50	0.26	0.72	0.38	8.46
		525	6.21	0.36	21.69	0.25	0.65	0.39	7.91
		800	5.88	0.35	20.52	0.25	0.68	0.40	7.46

Scheme 4.1: Passivation of the trap states of QDs by photoadsorption H_2O molecules. This schematic description of the decay route is originally proposed by Bawendi et al.[51] and later adapted by Jones et al.[31] and Pechstedt et al.[27]

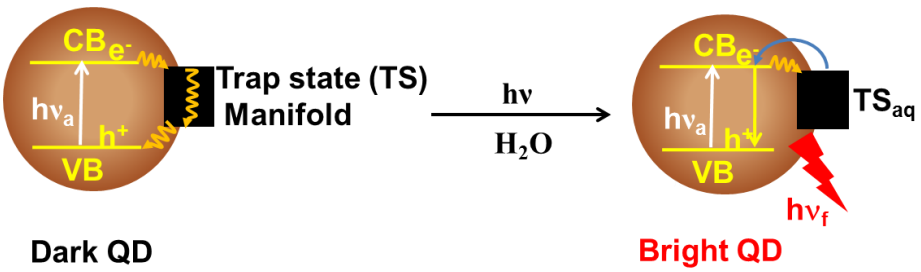

4.5. FCS study of the QDs:

The FCS measurements have been carried out with CdTe/MPA and CdTe/SMIM in aqueous medium and ionic liquid, respectively. These measurements could not be performed on CdTe/HDA in $CHCl_3$ due to high photo-instability of the QD and volatility of $CHCl_3$. Figure 4.8 depicts time-dependence of the fluorescence correlation for CdTe/MPA and CdTe/SMIM at different excitation powers. The best fits to the data points using Equation 2.7, which take into account fluorescence blinking of the QDs (stretched exponential model of distributed kinetics) [48-52] and 1-component diffusion, are also shown.

The important point to note here is the dependence of the G(0) value on the excitation power. A steady and appreciable decrease of the G(0) value is observed for CdTe/MPA QD. In the case of CdTe/SMIM, the variation is not so pronounced; a small increase followed by a small decrease of the G(0) value with increasing excitation power is observed. This is highlighted in panel (c) of Figure 4.8.

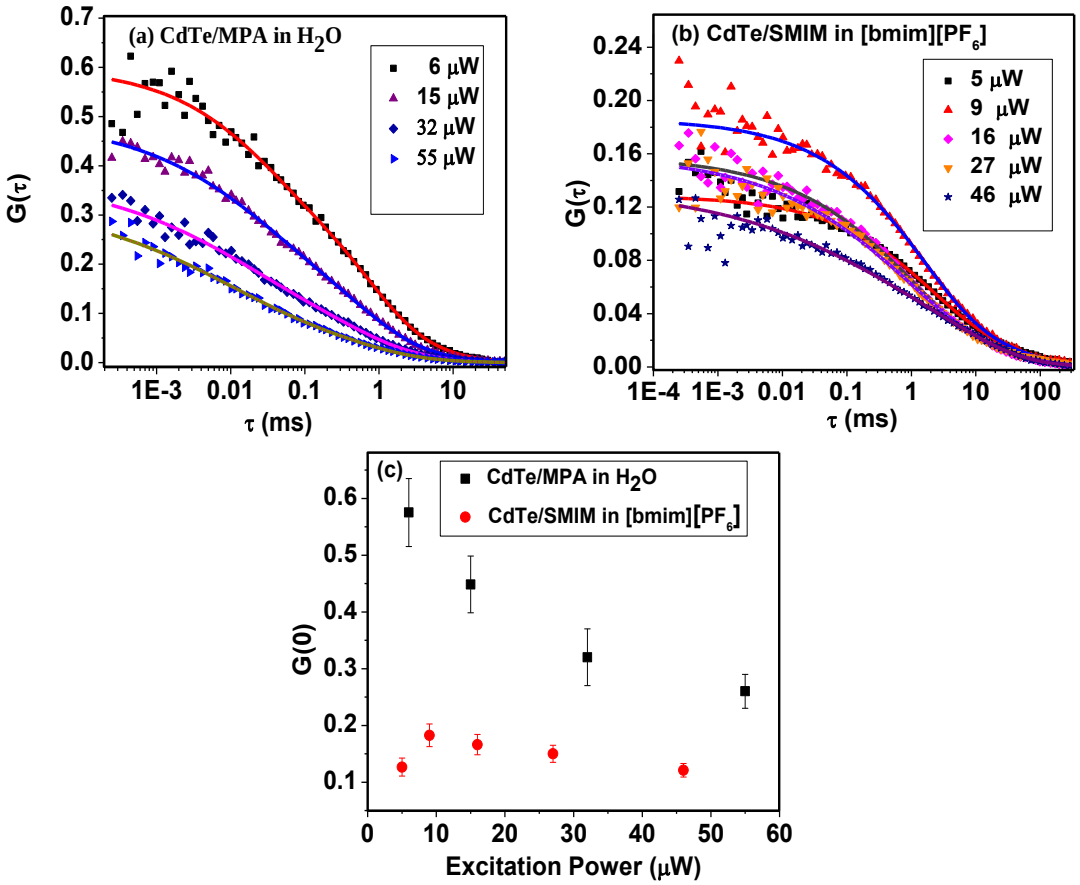

Figure 4.8. Correlation curves of (a) CdTe/MPA in H_2O and (b) CdTe/SMIM in [bmim][PF_6] recorded at various excitation power. Here the symbols are the original data and the line represents the fit to the data according to Equation 2.7. (c) Corresponding variation of G(0) value with increasing excitation power for CdTe/MPA in H_2O (black square) and CdTe/SMIM in [bmim][PF_6] (red sphere). λ_{ex} = 485 nm

Several factors, such as background noise, photophysical process, optical trapping, photoactivation and broadening of the observation volume due to excitation saturation can affect the G(0) value in an FCS experiment.[15,23,53-57] We have considered all the possibilities carefully before arriving at a definite conclusion. That a broadening of the observation volume and optical trapping are not responsible for the changes in the G(0) value observed is evident from the fact that the diffusion time show very little change with increasing excitation power (Figure 4.9). That background noise at high laser power is not responsible for the large decrease of the G(0) observed for CdTe/MPA in aqueous medium is evident from the fact that a very little decrease of the G(0) value is observed for R123 in aqueous

medium with increasing excitation power.[23] That blinking of the QD is not responsible for the large change of the G(0) value of the CdTe/MPA QD in H_2O is evident from the fact that a faster blinking (τ_t) at higher excitation power of both the QDs (Figure 4.10) is compensated by the increase of the off-state fraction (T) under this condition (Figure 4.10).

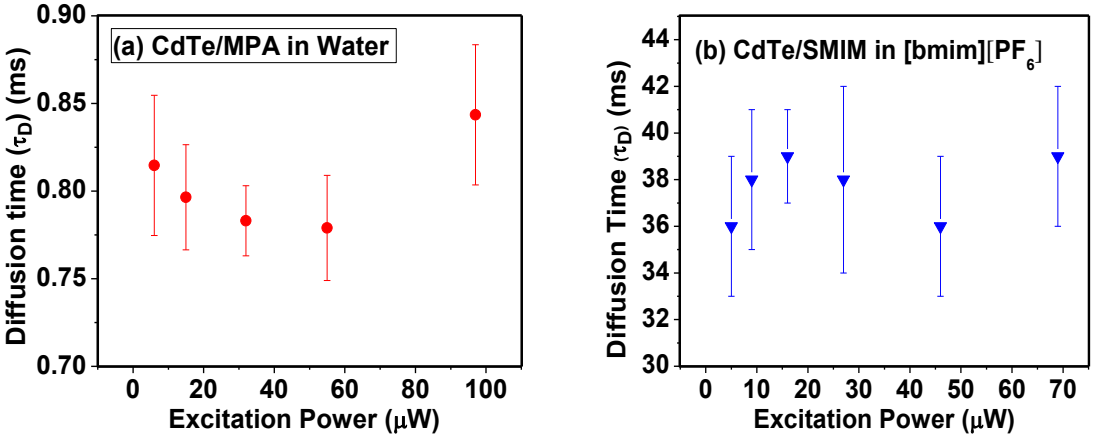

Figure 4.9. Plot of diffusion time (τ_D) vs excitation power for (a) CdTe/MPA in H_2O and (b) CdTe/SMIM in [bmim][PF_6].

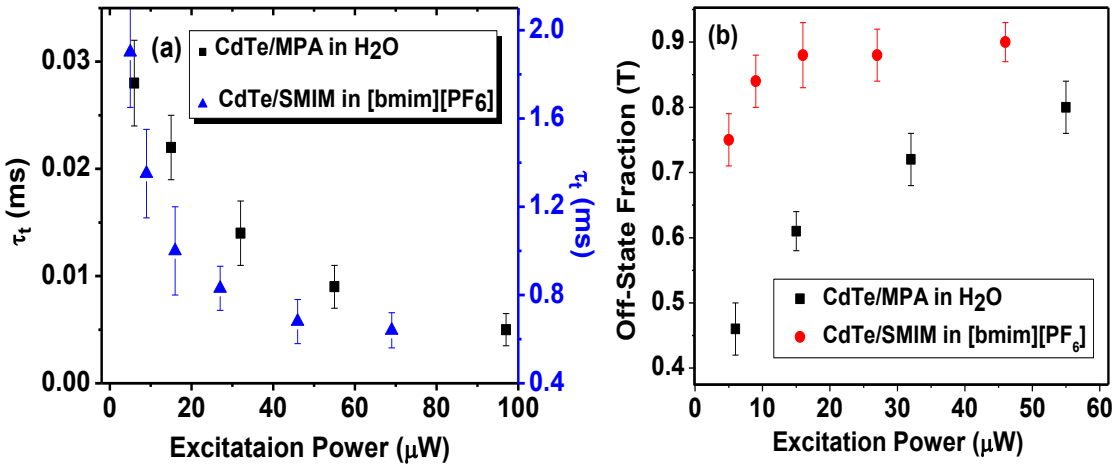

Figure 4.10. Variation of (a) blinking time (τ_t) and (b) off-state fraction of the QDs with increasing excitation power.

One important point to note here is that the number of particles (N) in the observation volume estimated from the G(0) value and off-state fraction (T) is much less than the actual number of particles (N_{actual}) calculated from the concentration of the QDs (Table

4.2). As a large fraction of the QDs are present in their dark state at low excitation power, the G(0) value is high under this condition. With increasing excitation power as these dark QDs get converted into their bright state due to surface passivation of the CdTe/MPA QDs by H_2O, a large decrease of the G(0) value is observed with increasing excitation power despite an increase of the value of T. For CdTe/SMIM in [bmim][PF_6], the decrease of the G(0) value with excitation power is much smaller compared to CdTe/MPA in H_2O. This small decrease in the G(0) value is most likely due to light scattering at high excitation power by the ionic liquid observed for CdTe/SMIM with increasing excitation power can be understood from the fact that with increasing excitation power the background counts due to scattering from IL also increases and counteract the increase of G(0) value due to increase in T value. At low excitation power the background noise is less and increase in T value dominates so, a small increase in the G(0) value is observed. Later the G (0) value decreases slowly but gradually with increasing excitation power because background scattering due to [bmim][PF_6] becoming larger and dominates the effect of increasing T value.

Table 4.2. Some parameters relating to the FCS studies on CdTe/MPA and CdTe/SMIM QDs in H_2O and [bmim][PF_6] respectively at lowest excitation power.

Parameters	CdTe/MPA in H_2O	CdTe/SMIM in [bmim][PF_6]
C (nM)	56 ± 3	400 ± 10
G(0)	0.575 ± 0.060	0.127 ± 0.016
N(1-T)	1.74 ± 0.20	7.87 ± 0.90
T	0.46 ± 0.04	0.75 ± 0.04
N	3.2 ± 0.6	31.5 ± 7.0
N_{actual}†	33.6 ± 2	240 ± 6
Dark fraction*	0.91 ± 0.02	0.87 ± 0.03

†Estimated from the concentration of QDs for an observation volume of 10^{-15} L. *N/N_{actual} gives the bright fraction of the QDs. Dark fraction = (1 - bright fraction).

It is thus evident from this combined steady state and time-resolved fluorescence and FCS study that two photoprocesses primarily contribute to the light induced variation of the emission behavior of the CdTe QDs. In aqueous environment, photoadsorption of H_2O

molecules by the QD leads to its photoactivation, which dominates the early part of irradiation. The other process, photooxidation of the QD, which introduces surface defects, contributes to the corrosion of the surface and results in a decrease of the emission intensity, is observable at the later stages of irradiation. For the QDs studied in non-aqueous environment, no photoactivation could be observed (thereby suggesting clearly the important role of H_2O in the process); only the effect of the photooxidation is observable. Thus the present findings are best represented by Scheme 2.

Scheme 2: Mechanism of modulation of fluorescence properties of the QDs under light irradiation

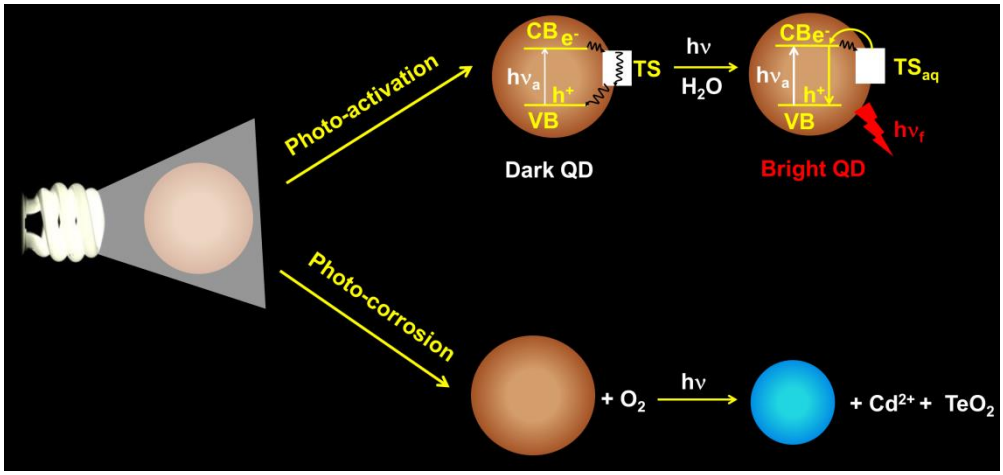

4.6. Conclusion:

The mechanism of light-induced variation of the emission behavior of CdTe QDs comprising different capping agents dispersed in three different environments is investigated. Significant emission enhancement only for CdTe/MPA in both aerated and deaerated aqueous environment under light irradiation and a large decrease of the G(0) value at higher excitation power only in the aqueous environment unambiguously establish the critical role of the H_2O molecules in the passivation of the surface trap states. In addition to H_2O-assisted photoactivation, photooxidation of the QDs is also shown to contribute to the light-induced modulation of their luminescence behavior.

References:

(1) Alivisatos, A. P. *Science* **1996**, *271*, 933.
(2) Smith, A. M.; Nie, S. *Acc. Chem. Res.* **2010**, *43*, 190.
(3) Brus, L. E. *J. Chem. Phys.* **1983**, *79*, 5566.
(4) Murray, C. B.; Norris, D. J.; Bawendi, M. G. *J. Am. Chem. Soc.* **1993**, *115*, 8706.
(5) Frederick, M. T.; Amin, V. A.; Cass, L. C.; Weiss, E. A. *Nano Lett.* **2011**, *11*, 5455.
(6) Ihly, R.; Tolentino, J.; Liu, Y.; Gibbs, M.; Law, M. *ACS Nano* **2011**, *5*, 8175.
(7) Tan, Y.; Jin, S.; Hamers, R. J. *ACS Appl. Mater. Interfaces, 2013, 5 (24), pp 12975–12983* **2013**, *5* 12975.
(8) Wang, X.; Qu, L.; Zhang, J.; Peng, X.; Xiao, M. *Nano Lett.* **2003**, *3*, 1103.
(9) Efros, A. L.; Rosen, M. *Annu. Rev. Mater. Sci.* **2000**, *30*, 475.
(10) Deuk, K. H.; Kobayashi, Y.; Tamai, N. *J. Phys. Chem. Lett.* **2014**, *5*, 99.
(11) Beard, M. C. *J. Phys. Chem. Lett.* **2011**, *2*, 1282.
(12) Resch-Genger, U.; Grabolle, M.; Cavaliere-Jaricot, S.; Nitschke , R.; Nann, T. *Nature Methods* **2008**, *5*, 763.
(13) Zhao, J.; Bardecker, J. A.; Munro, A. M.; Liu, M. S.; Niu, Y.; Ding, I. K.; Luo, J.; Chen, B.; Jen, A. K. Y.; Ginger, D. S. *Nano Lett.* **2006**, *6*, 463.
(14) Kamat, P. V. *J. Phys. Chem. Lett.* **2013**, *4*, 908.
(15) Larson, D. R.; Zipfel, W. R.; Williams, R. M.; Clark, S. W.; Bruchez, M. P.; Wise, F. W.; Webb, W. W. *Science* **2003**, *300*, 1434.
(16) Delehanty, J. B.; Bradburne, C. E.; Susumu, K.; Boeneman, K.; Mei, B. C.; Farrell, D.; Blanco-Canosa, J. B.; Dawson, P. E.; Mattoussi, H.; L., M. I. *J. Am. Chem. Soc.* **2011**, *133*, 10482.
(17) Reiss, P.; Protiere, M.; Li, L. *Small* **2009**, *5*, 154.
(18) Knowles, K. E.; Frederick, M. T.; Tice, D. B.; Morris-Cohen, A. J.; Weiss, E. A. *J. Phys. Chem. Lett.* **2012**, *3*, 18.
(19) Carrillo-Carrion, C.; Cardenas, S.; Simonet, B. M.; Valcarcel, M. *Chem. Commun.* **2009**, 5214.
(20) Hines, D. A.; Kamat, P. V. *ACS Appl. Mater. Interfaces* **2014**, *6*, 3041.
(21) Frederick, M. T.; Amin, V. A.; Weiss, E. A. *J. Phys. Chem. Lett.* **2013**, *4*, 634.
(22) Bao, H.; Gong, Y.; Li, Z.; Gao, M. *Chem. Mater.* **2004**, *16*, 3853.
(23) Patra, S.; Samanta, A. *J. Phys. Chem. C* **2013**, *117*, 23313.
(24) Wang, Y.; Tang, Z.; Correa-Duarte, M. A.; Pastoriza-Santos, I.; Giersig, M.; Kotov, N. A.; Liz-Marzan, L. M. *J. Phys. Chem. B* **2004**, *108*, 15461.
(25) Cordero, S. R.; Carson, P. J.; Estabrook, R. A.; Strouse, G. F.; Buratto, S. K. *J. Phys. Chem. B* **2000**, *104*, 12137.
(26) Biju, V.; Kanemoto, R.; Matsumoto, Y.; Ishii, S.; Nakanishi, S.; Itoh, T.; Baba, Y.; Ishikawa, M. *J. Phys. Chem. C* **2007**, *111*, 7924.
(27) Pechstedt, K.; Whittle, T.; Baumberg, J.; Melvin, T. *J. Phys. Chem. C* **2010**, *114*, 12069.
(28) Kloefper, J. A.; Bradforth, S. E.; Nadeau, J. L. *J. Phys. Chem. B* **2005**, *109*, 9996.

(29) Impellizzeri, S.; McCaughan, B.; Callan, J. F.; Raymo, F. M. *J. Am. Chem. Soc.* **2012**, *134*, 2276.

(30) Sato, K.; Kojima, S.; Hattori, S.; Chiba, T.; Ueda-Sarson, K.; Torimoto, T.; Tachibana, Y.; Kuwabata, S. *Nanotechnology* **2007**, *18*, 465702 (1.

(31) Jones, M.; Nedeljkovic, J.; Ellingson, R. J.; Nozik, A. J.; Rumbles, G. *J. Phys. Chem. B* **2003**, *107*, 11346.

(32) Oda, M.; Hasegawab, A.; Iwamib, N.; Nishiurab, K.; Andob , N.; Nishiyamab, A.; Horiuchib, H.; Tania, T. *Colloids Surf. B* **2007**, *56*, 241.

(33) Ladizhansky, V.; Hodes, G.; Vega, S. *J. phys. Chem. B* **2000**, *104*, 1939.

(34) Gomez, D. E.; Embden, J. V.; Mulvaney, P.; Fernee, M. J.; Dunlop, H. R. *ACS Nano* **2009**, *3*, 2281.

(35) Mandal, A.; Nakayama, J.; Tamai, N.; Biju, V.; Isikawa, M. *J. Phys. Chem. B* **2007**, *111*, 12765.

(36) Lackowicz, J. R. *Springer: New York* **2006**, *Chapter 24*.

(37) Beranová, L.; Humpolíčková, J.; Hof, M. *Chemicke Listy* **2009**, *103*, 125.

(38) Haustein, E.; Schwille, P. *Annu. Rev. Biophys. Biomol. Struct.* **2007**, *36*, 151.

(39) Santhosh, K.; Samanta, A. *J. phys. Chem. C* **2012**, *116*, 20643.

(40) Yu, W. W.; Qu, L.; Guo, W.; Peng, X. *Chem. Mater.* **2003**, *15*, 2854.

(41) Monroe, B. M. *Photochem. Photobiol.* **1982**, *35*, 863.

(42) Alvaro, M.; Ferrer, B.; Garcia, H.; Narayana, M. *Chem. Phys. Lett.* **2002**, *362*, 435.

(43) Battino, R.; Rettich, T. R.; Tominaga, T. *J. Phys. Chem. Ref. Data* **1983**, *12*, 163.

(44) Santhosh, K.; Patra, S.; Soumya, S.; Khara, D. C.; Samanta, A. *ChemPhysChem* **2011**, *12*, 2735.

(45) Efros, A. L.; Rosen, M.; Kuno, M.; Nirmal, M.; Norris, D. J.; Bawendi, M. G. *Phys. Rev. B* **1996**, *54*, 4843.

(46) Nirmal, M.; Murray, C. B.; Bawendi, M. G. *Phys. Rev. B* **1994**, *50*, 2293.

(47) Bawendi, M. G.; Carroll, P. J.; Wilson, W. L.; Brus, L. E. *J. Chem. Phys.* **1992**, *96*, 946.

(48) Heuff, R. F.; Swift, J. L.; Cramb, D. T. *Phys. Chem. Chem. Phys.* **2007**, *9*, 1870.

(49) Heuff, R. F.; Marrocco, M.; Cramb, D. T. *J. Phys. Chem. C* **2007**, *111*, 18942.

(50) Peterson, J.; Nesbitt, D. J. *Nano Lett.* **2009**, *9*, 338.

(51) Ito, S.; Toitani, N.; Pan, L.; Tamai, N.; Miyasaka, H. *J. Phys.: Condens. Matter* **2007**, *19*, 486208.

(52) Yao, J.; Larson, D. R.; Vishwasrao, H. D.; Zipfel, W. R.; Webb, W. W. *Proc. Natl. Acad. Sci. U. S. A.* **2005**, *102*, 14284.

(53) Widengren, J.; Mets, U.; Rigler, R. *J. Phys. Chem.* **1995**, *99*, 13368.

(54) Doose, S.; Tsay, J. M.; Pinaud, F.; Weiss, S. *Anal. Chem.* **2005**, *77*, 2235.

(55) Dong, C.; Qian, H.; Fang, N.; Ren, J. *J. Phys. Chem. C* **2007**, *111*, 7918.

(56) Gregor, I.; Patra, D.; Enderlein, J. *ChemPhysChem* **2005**, *6*, 164.

(57) Hess, S. T.; Webb, W. W. *Biophys. J.* **2002**, *83*, 2300.

Effect of ZnS Shell on the Photostability and Photoactivation of the CdTe Quantum Dots

Photostability and photoactivation of the quantum dots (QDs) are the two important parameters which determine their applications in diverse fields. ZnS shell is grown over CdTe QDs to study its effect on the photoactivation and photostability of the CdTe QDs. Huge enhancement of the fluorescence intensity is observed for the core/shell CdTe/ZnS QDs with a shell thickness of one monolayer (1 ML) and two monolayers (2 ML), compared to the core-only QDs in both $CHCl_3$ and H_2O medium. Fluorescence lifetime of the CdTe/ZnS QDs is found to be much longer than that of the CdTe QDs indicating suppression of the nonradiative pathways by effective passivation of the surface dangling orbitals by the ZnS shell. Exceptional photostability of the mercaptopropionic acid (MPA) capped core/shell CdTe/ZnS (2ML) QD in water is also demonstrated by light-exposure of the QDs over a long period of time. Almost 3-fold enhancement in the fluorescence intensity is observed for CdTe/MPA core QDs in aqueous solution upon light irradiation. On the otherhand the increase in fluorescence intensity for CdTe/ZnS (2ML)/MPA QDs is very small upon light exposure. FCS measurement reveals large decrease in the amplitude of the correlation at time zero [G(0)] for the aqueous solution of CdTe/MPA, whereas a negligible change in the G(0) value is observed for CdTe/ZnS (2ML)/MPA QDs.

5.1. Introduction:

QDs are emerging as a potential agent in various applications because of their several advantages over traditional organic fluorophores such as size tunable optical and electronic properties, narrow emission spectra, broad absorption spectra, high fluorescence quantum yield, long fluorescence lifetime, large absorption cross section and possibility of multiple exciton generation.[1-15] However, the lack of proper understanding of some of the photophysical properties of the QDs restrict their utility in many applications.[16,17] One such process is fluorescence enhancement of the QDs under illumination, commonly termed as photoactivation.[16] Photoactivation of the QDs has been observed under various conditions even inside a cell.[16,18] Despite extensive efforts towards improving the understanding of the photochemistry of the QDs, the mechanism of photoactivation has remained controversial.[16] It is commonly agreed that light induced passivation of the surface trap states, which act as nonradiative centers in QDs, contributes to the photoactivation of the QDs. However, no

consensus on the mechanism of this light induced passivation of the surface trap states has been achieved yet. A wide variety of models has been proposed to explain the photoactivation of the QDs. These include passivation of the surface trap states by photoadsorbed molecules, which include polar solvent molecules as well,[16,19-29] removal of topological surface defects due to photooxidation (i.e. smoothing of the surface during the process of photocorrosion),[16,26,30-32] photoinduced rearrangement of the surface stabilizing agents,[16,21] surface reconstruction by the light induced heat generation, formation of shell structure around the core QDs due to photodegradation of the surface stabilizing agent (thioglycolic acid) etc.[16,33,34] Formation of metal oxide layer on the surface of a QD due to photooxidation and photoadsorption of water molecules on the QDs surface are also proposed as a mechanism of photoactivation.[16,27,35] Carrilio-Carrion et al. proposed a model involving both photooxidation and photoadsorption of water molecules to account for surface passivation of the QDs in aqueous solution upon exposure to light.[16] As photoactivation restricts the applications of the QDs in many disciplines, a clear understanding of the mechanism of the photoactivation is crucial for the design of the QDs which show minimum photoactivation as well as enhanced stability under light exposure.

In a recent article, we investigated the photoactivation of the CdTe QDs by employing three different capping agents dispersed in three different solvents using both conventional ensemble fluorescence and FCS technique.[23] We conclusively proved passivation of the surface trap states of the QDs by photoadsorption of water molecules on the QDs surface as the prominent mechanism of photoactivation on the basis of the fact that light induced fluorescence enhancement could be observed only in aqueous medium. So, passivation of the surface trap states holds the key to the development of the QDs exhibiting minimum photoactivation and high stability. A very efficient method of surface passivation of the QDs is their overgrowth with a shell of higher band gap second semiconductor materials, resulting in type 1 core/shell QDs.[36,37] Unlike organically passivated QDs, inorganic epitaxial growth of another semiconductor material eliminates both cationic and anionic defects on the surface and also creates new QDs with novel properties.[2,36-41] These type I core/shell QDs not only provide better passivation of the surface trap states of the core QDs but also the larger band gap of the shell materials confines the charge carrier mostly on the core QDs.[2,36,38,42] As the shell physically separates the core from the surface and thus

reduces the influence of the local environmental factors such as presence of oxygen and water molecules on the emission properties of the QDs. Hence, type I core/shell QDs are expected to exhibit better stability against photoactivation and photocorrosion. However, photoactivation and photocorrosion have been reported for type I CdSe/CdS and CdSe/ZnS core/shell QDs.[16,30,43,44] This observation was attributed to incomplete shell formation on the core. Thus providing regions where core QD is exposed to the surrounding environment or shell layer around the core is not a closed epitaxial layer but rather a layer with grain boundaries, which are the places where shell islands, which started to grow at different locations on the core QDs, meet.[16,30] At these exposed places or grain boundaries oxygen and water molecules can diffuse to the core QDs and as a result photoactivation and photocorrosion can occur.[16,30]

In the present case we have studied the optical properties of CdTe/ZnS core/shell QDs synthesized by SILAR (successive ion layer adsorption and reaction) method and compared with the CdTe core QDs. SILAR is a very popular and efficient technique for the preparation for high quality core/shell QDs.[43] This technique is based on the formation of one monolayer at a time by alternating the injections of cationic and anionic precursors of the shell material. We have also investigated the photoinduced variation of the emission behavior of the QDs in aqueous solution using steady state emission and FCS technique, considering the fact that photostability of the QDs in aqueous solution is very important for their utility in biological applications. The main reason we have selected CdTe/ZnS core shell QDs based on the fact that light induced variation on the optical properties CdTe/ZnS QDs is not studied yet in details like core/shell QDs based on CdSe core.

5.2. **Structural characterization of the QDs:**

The sizes of the hexadecyl amine (HDA) capped CdTe core, CdTe/ZnS(2ML) core/shell QDs, determined from their TEM images (Figure 5.1), are 3.9 ± 0.3 nm and 5.3 ± 0.4 nm, respectively. The TEM-measured sizes of the core and core/shell QDs correlate well with the sizes estimated from the first exciton band absorption peak of the core QDs[45] and assumed shell thickness of around 0.35 nm for each monolayer. Increase in size of the QDs is observed when coated with ZnS shell.

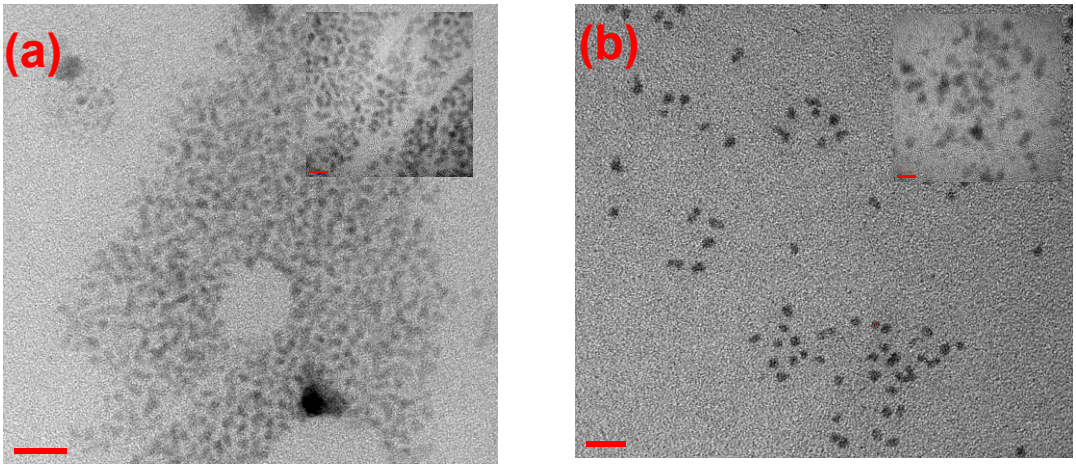

Figure 5.1: TEM images of (a) CdTe/HDA and (b) CdTe/ZnS(2ML)/HDA QDs. Inset shows the image at 10 nm Scale.

We also carried out energy dispersive X-ray (EDX) spectroscopic measurement on CdTe/ZnS(2ML)/HDA QDs. The EDX spectrum, shown in Figure 5.2, confirms the presence of ZnS layer around the core CdTe.

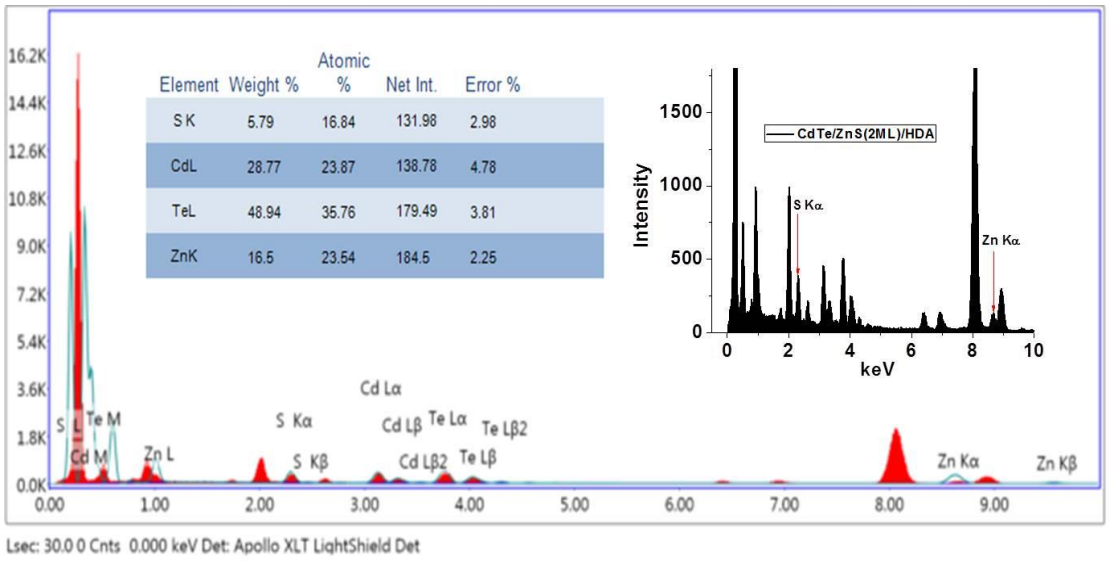

Figure 5.2. EDX spectrum of CdTe/ZnS(2ML)/HDA (S K_α peak at 2.3 keV and Zn K_α peak at 8.9 keV).

5.3. Steady state fluorescence behavior:

Absorption spectra of the QDs are shown in Figure 5.3. HDA-capped QDs are soluble in $CHCl_3$. To solubilize the QDs in H_2O medium HDA is replaced by mercaptopropionic acid (MPA).[46] The carboxylate group of MPA makes the QDs polar to dissolve in polar water medium. As the absorption peak position (λ_{max}^{abs}) is not well resolved,* it is difficult to Figure out from the data the extent of red shift of the first exciton band maximum upon shell formation.

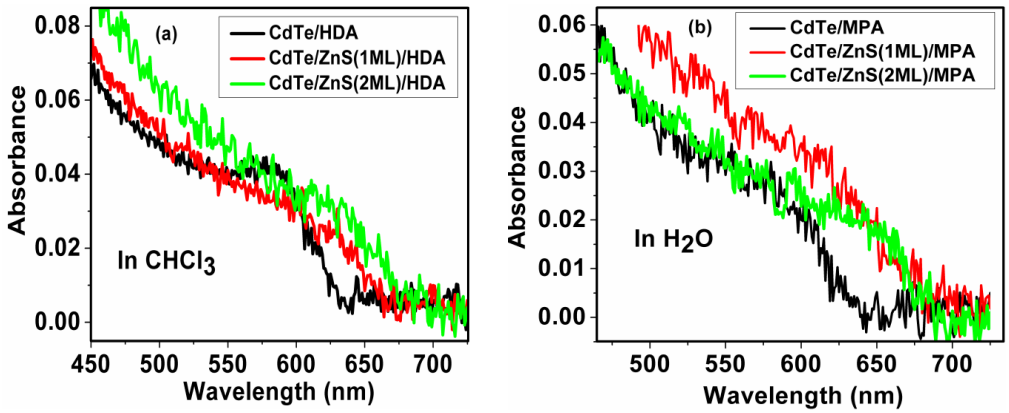

Figure 5.3: Absorption spectra of (a) CdTe/HDA and CdTe/ZnS(1ML&2ML)/HDA QDs in $CHCl_3$ and (b) CdTe/MPA and CdTe/ZnS(1ML&2ML)/MPA QDs in H_2O.

Figure 5.4 displays the emission spectra of the QDs in $CHCl_3$ and H_2O. Huge enhancement of fluorescence intensity is observed in case of CdTe/ZnS QDs with increasing shell thickness than the core CdTe QDs. We have calculated the emission quantum yield (QY) of the QDs. Emission QY and peak wavelength (λ_{max}^{em}) of the QDs are collected in table 5.1. The QY increases from 2.7% in CdTe/HDA core to 12.4% in 1ML and 20.0% in 2ML-CdTe/ZnS/HDA core/shell QDs in $CHCl_3$. The enhancement of emission QY is even higher in case of CdTe/ZnS/MPA QDs in aqueous medium with increasing shell thickness compared

* Rough estimation of the first exciton band maximum (λ_{max}^{abs}) of the core QD is possible (Figure 5.3. a). A 30 nm shift of the λ_{max}^{abs} only changes the D value (determined from λ_{max}^{abs}) by ± 0.2 nm.

to the core CdTe/MPA QDs (Table 5.1). Emission QY increases from 3.7% in CdTe/MPA to 27% In CdTe/ZnS(1ML)/MPA and 35% in CdTe/ZnS(2ML)/MPA QDs.

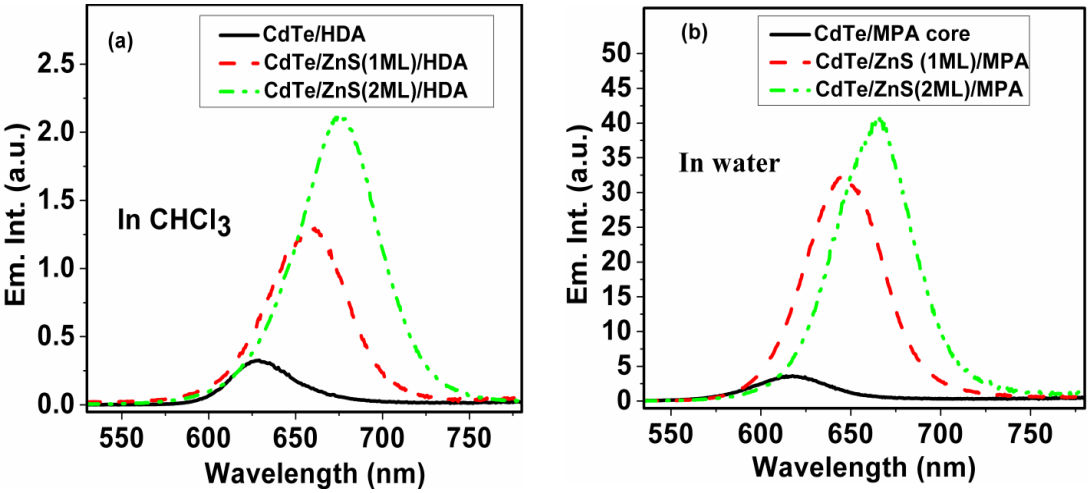

Figure 5.4: Emission spectra of (a) CdTe/HDA and CdTe/ZnS(1ML&2ML)/HDA QDs in $CHCl_3$and (b) CdTe/MPA and CdTe/ZnS(1ML&2ML)/MPA QDs in H_2O.

The large enhancement in the emission QY of CdTe/ZnS QDs is due to effective passivation of the surface dangling orbitals (defects) by epitaxial growth of the ZnS shell around core. Along with the enhancement of the QY a red shift of the λ_{max}^{em} is also observed for the core/shell CdTe/ZnS QDs with increasing shell thickness (Table 5.1). λ_{max}^{em} shifts from 630 nm in case of CdTe/HDA QDs to 660 nm & 676 nm for CdTe/ZnS (1ML)/HDA and CdTe/ZnS (2ML)/HDA QDs respectively. Exchanging HDA ligand with MPA leads to a blue shift in the λ_{max}^{em} of the QDs (Table 5.1). This observation is consistent with the literature report, that replacement of amine ligand with MPA or aminoethanethiol (AET) induces a redistribution of electron density and increase in the confinement energy of the QDs due to stronger thiol-Cd interaction compared to amine-Cd interaction.[46] For MPA-capped QDs, λ_{max}^{em} shifts from 618 nm in core CdTe/MPA to 645 nm in CdTe/ZnS(1ML)/MPA to 665 nm in CdTe/ZnS(2ML)/MPA. This red shift in the λ_{max}^{em} peak in core/shell QDs is well known[38,42] and is attributed to partial leakage of the exciton from core to shell.

Table 5.1: Emission properties of the QDs in $CHCl_3$ and H_2O.

QDs	Medium	λ_{max}^{em} (nm)	QY(%)
CdTe/HDA	$CHCl_3$	630	2.7
CdTe/ZnS(1ML)/HDA	$CHCl_3$	660	12.4
CdTe/ZnS(2ML)/HDA	$CHCl_3$	676	20.0
CdTe/MPA	H_2O	618	3.7
CdTe/ZnS(1ML)/MPA	H_2O	645	27.0
CdTe/ZnS(2ML)/MPA	H_2O	665	35.0

5.4. Fluorescence lifetime study:

Fluorescence decay profiles of the QDs are shown in Figure 5.5. Triexponential fit of the fluorescence decay profiles is found to be superior compared to mono- or bi-exponential fit for CdTe/HDA, CdTe/ZnS(1ML&2ML)/HDA in $CHCl_3$ and CdTe/MPA QDs in H_2O. On the other hand, for the CdTe/ZnS(1ML&2ML)/MPA QDs, fluorescence decay profile can be properly fit to a biexponential function. This suggests that the surface states are passivated efficiently in aqueous medium compared to the chloroform medium. Table 5.2 listed the fluorescence decay parameters of the QDs. Large enhancement of fluorescence lifetime is observed for the QDs in both solvents when ZnS shell is overgrown around CdTe core QDs. For HDA-capped QDs in $CHCl_3$ the average fluorescence lifetime ($<\tau>$) increases significantly from 1.62 ns (in core CdTe QDs) to 6.41 ns & 9.54 ns in CdTe/ZnS(1ML) and CdTe/ZnS (2ML) core/shell QDs respectively. In aqueous medium, $<\tau>$ increases from 4.44 ns to 14.20 ns in CdTe/ZnS(1ML)/MPA and 16.77 ns in CdTe/ZnS(2ML)/MPA QDs. These results clearly suggest a much more effective passivation of CdTe surface dangling orbitals or defects by the overgrowth of ZnS shell. The extent of passivation is larger for MPA-capped CdTe/ZnS QDs than the HDA-capped CdTe/ZnS QDs.

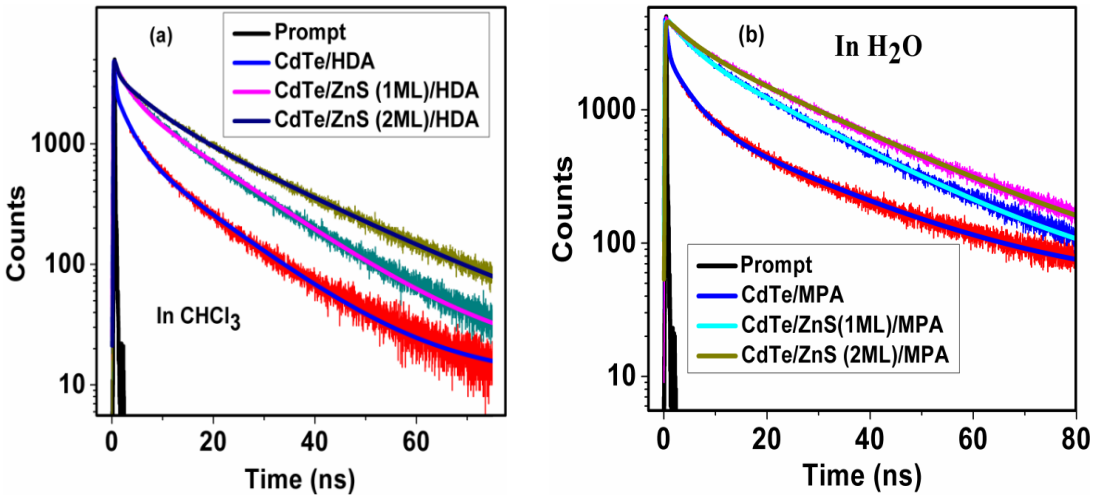

Figure 5.5. Fluorescence decay profile of (a) HDA-capped CdTe core and CdTe/ZnS 1ML & 2 ML QDs in $CHCl_3$ and (b) CdTe/MPA core and CdTe/ZnS/MPA 1ML & 2ML core/shell QDs in water. In each case lines represent the best fit to the decay traces. Lamp profile is shown as black solid line. λ_{exc} = 439 nm.

Table 5.2. Time resolved fluorescence parameters of the QDs in $CHCl_3$ and H_2O

Quantum Dots	Medium	τ_1 (ns)	α_1	τ_2 (ns)	α_2	τ_3 (ns)	α_3	$\langle\tau\rangle$ (ns)*
CdTe/HDA	$CHCl_3$	2.80	0.25	13.75	0.13	0.21	0.62	2.62
CdTe/ZnS(1ML)/HDA	$CHCl_3$	4.85	0.28	16.46	0.30	0.27	0.42	6.41
CdTe/ZnS(2ML)/HDA	$CHCl_3$	6.04	0.26	21.00	0.37	0.54	0.37	9.54
CdTe/MPA	H_2O	4.22	0.26	23.73	0.13	0.38	0.61	4.41
CdTe/ZnS(1ML)/MPA	H_2O	4.45	0.41	20.96	0.59			14.20
CdTe/ZnS(2ML)/MPA	H_2O	5.72	0.31	21.74	0.69			16.77

*$\langle\tau\rangle$ is defined as, $\langle\tau\rangle = (\alpha_1\tau_1+\alpha_2\tau_2+\alpha_3\tau_3)/\alpha_1+\alpha_2+\alpha_3$ for triexponential fit and $\langle\tau\rangle = (\alpha_1\tau_1+\alpha_2\tau_2)/\alpha_1+\alpha_2$ for biexponential fit. Here α_1, α_2, and α_3 are the corresponding amplitudes of the lifetime components.

5.5. Effect of illumination on the fluorescence of QDs:

Herein, we study the effect of light on the fluorescence properties of CdTe/MPA core and CdTe/ZnS(2ML)/MPA core/shell QDs in aqueous medium. QDs were irradiated under light over a long period of time and the emission spectra were recorded at different time intervals to monitor the effect of light. Figure 5.6 depicts the effect of illumination on the

fluorescence behavior of the QDs. In case of CdTe/MPA, emission intensity increases under light irradiation, reaches its highest value after 27 hours, and then starts decreasing. The emission is almost completely quenched after 50 hrs of light irradiation. However, in case of CdTe/ZnS (2ML), very little change of the emission intensity is observed even after 88 hours of illumination. Figure 5.7 shows the normalized emission spectra of the QDs at various illumination times to highlight the spectral shift. Huge blue shift of the emission peak (a decrease of λ_{max}^{em} from 618 nm to 586 nm in 50 hrs) is observed for CdTe/MPA under irradiation of light. On the other hand, no such shift is observed in case of CdTe/ZnS(2ML)/MPA QDs even after prolonged exposure to light (88 hrs).

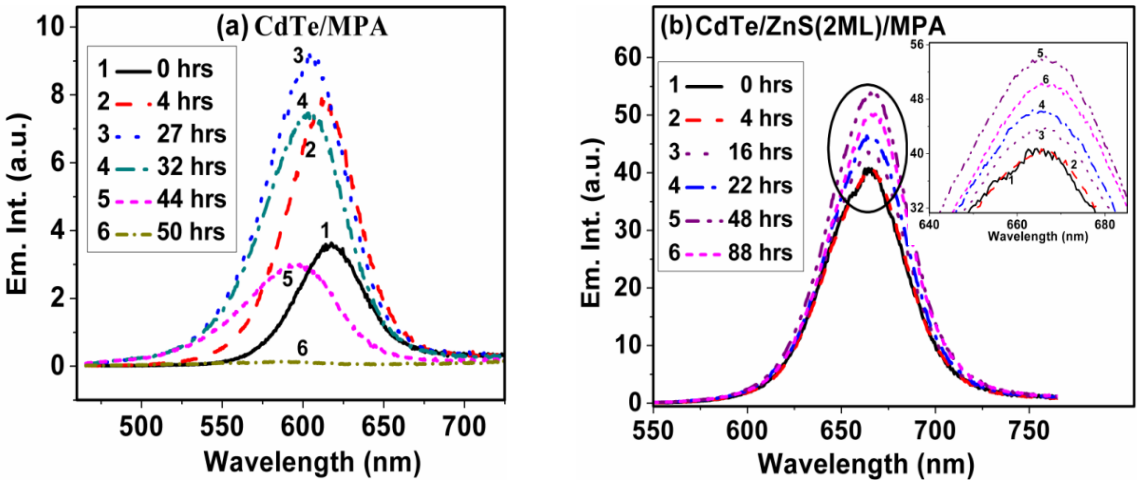

Figure 5.6. Steady state emission spectra (λ_{ex} = 440 nm) of (a) CdTe/MPA and, (b) CdTe/ZnS(2ML)/MPA in H_2O after different periods of light irradiation (inset shows the magnified regions of the spectra indicated by an ellipse).

The enhancement of emission intensity observed for CdTe/MPA is due to photoactivation of the QDs, which in our earlier study we have shown occurs only in aqueous medium and is due to passivation of the surface trap states of the QDs by photoadsorbed H_2O molecules.[23] However, aqueous solution of CdTe/ZnS(2ML)/MPA exhibits very little enhancement in the emission intensity upon light irradiation (Figure 5.6. b). This clearly indicates that the ZnS shell around the core very effectively passivates the surface trap states

and protects the core from external perturbation such as light. No shift in λ_{max}^{em} is observed for CdTe/ZnS(2ML)/MPA upon light exposure (Figure 5.7). Blue shift of the λ_{max}^{em} accompanied by a decrease in emission intensity of CdTe/MPA upon light exposure is due to surface photooxidation leading to etching of the surface fragments (photocorrosion) of the QDs.[16,23] ZnS shell thus protects the core in CdTe/ZnS QDs from photooxidation and offers stability under light. Scheme 5.1 shows the photoactivation and photocorrosion of the QDs.

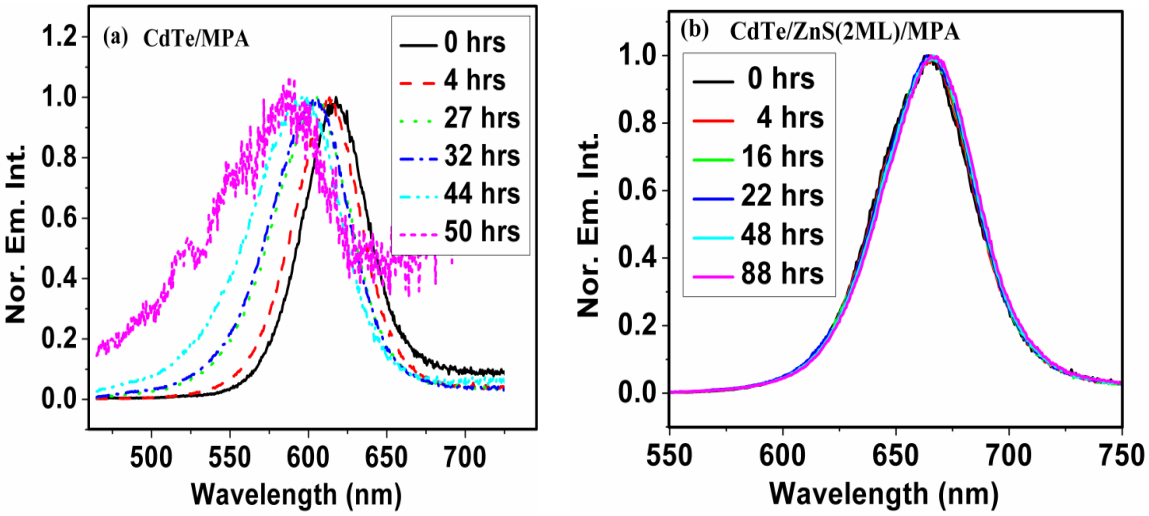

Figure 5.7. Normalized emission spectra of (a) CdTe/MPA & (b) CdTe/ZnS(2ML)/MPA in aqueous medium at different light irradiation times.

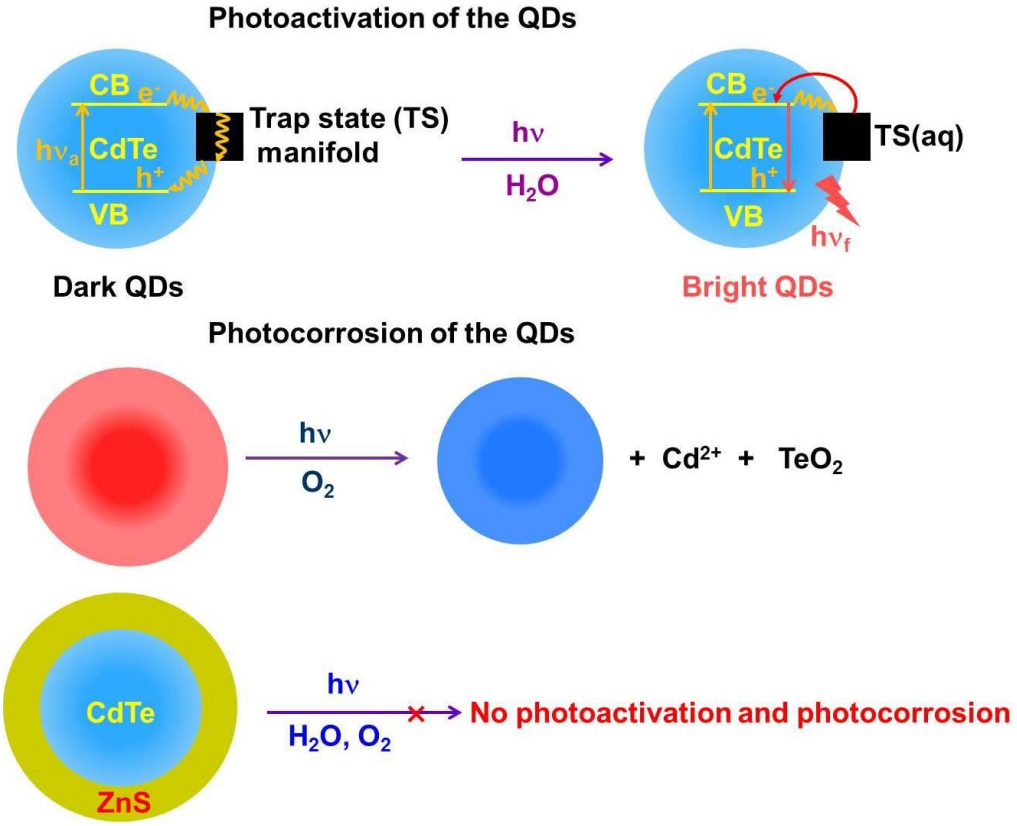

Scheme 5.1. Mechanism of photoactivation and photocorrosion of the QDs. In case of CdTe/ZnS shell protects the core from photoactivation and photocorrosion.

5.6. FCS study of the QDs:

FCS measurements are also carried out on CdTe/MPA and CdTe/ZnS(2ML)/MPA in aqueous medium to further investigate the photoactivation/photocorrosion of the QDs and to support the finding of the results stated in the earlier sections. The amplitude of correlation at time 0, [G(0)], in an FCS measurement is inversely proportional to the number of emitters present in the observation volume.[47,48] Hence, any variation of the G(0) value with excitation power is a reflection of light induced changes in the number of emitting QDs. Correlation curves of the QDs are recorded at different excitation power. Figure 5.8 shows the correlation curves of the QDs and the changes of the G(0) value as a function of the excitation power. The correlation curves could be best fitted (as determined by the residuals) to a stretched

exponential with a 1- component diffusion model (Equation 2.7) considering the distributed kinetics of fluorescence blinking of the QDs as reported in literature.[17,49-51] For CdTe/MPA QDs appreciable decrease of the G(0) value from 0.87 at 6.1 μW to 0.14 at 52.8 μW is observed with increasing excitation power. On the other hand for CdTe/ZnS(2ML)/MPA decrease of the G(0) value is much smaller (from 0.43 at 6.1 μW to 0.26 at 53.1 μW) than that observed in CdTe/MPA QDs with increasing excitation power. Figure 5.9 shows the plot of normalized correlation curves and diffusion time of the QDs with increasing excitation power. Changes in the shape of the correlation curves particularly at short lag times (τ) are observed with increasing excitation power (Figure 5.9). Variation of the off-state fraction (T) and blinking time (τ_t) with increasing excitation power are shown in Figure 5.10. With increasing excitation power, T increases and τ_t decreases for both the QDs.

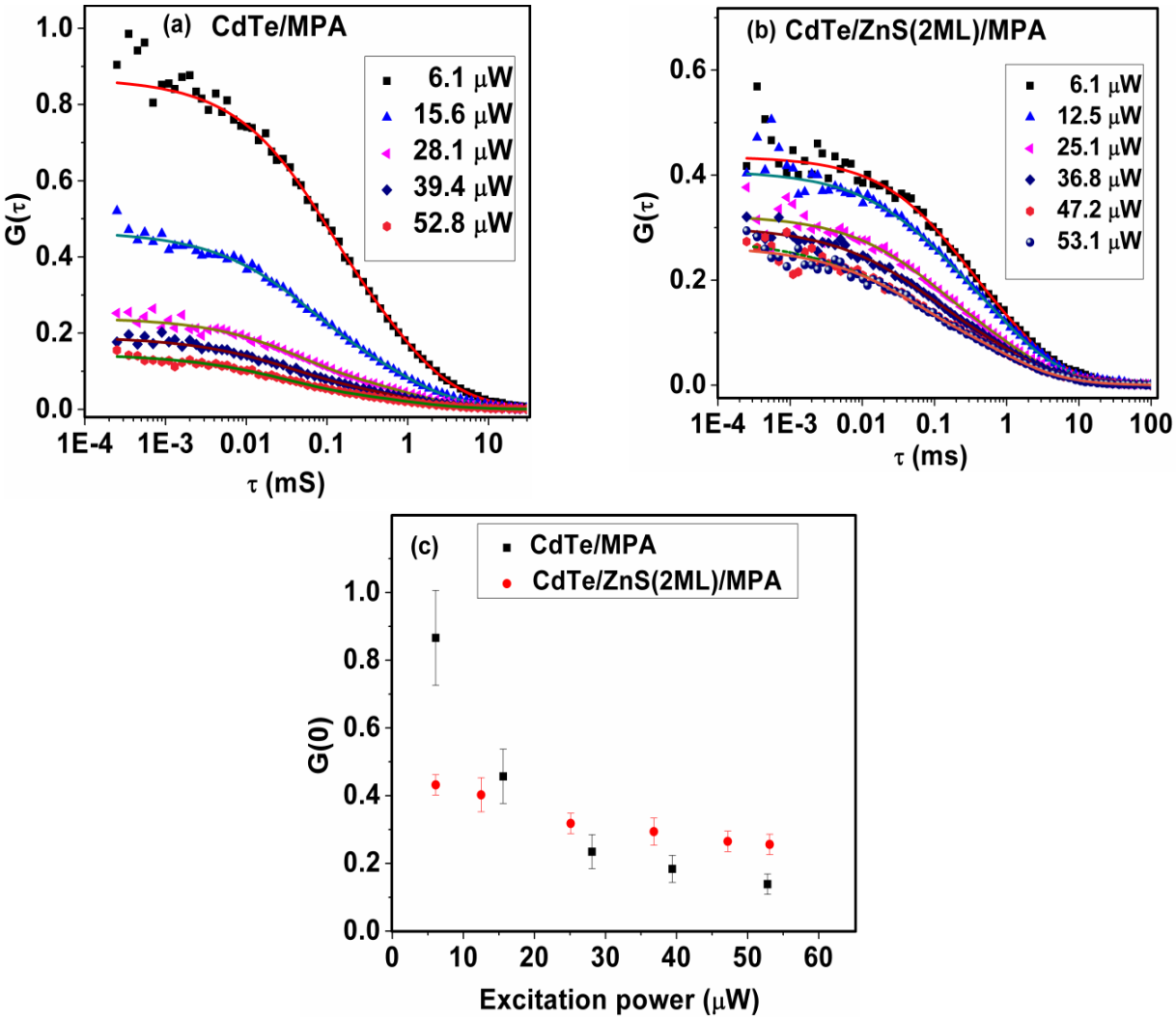

Figure 5.8. Correlation curves of (a) 74 nM CdTe/MPA and (b) 20 nM CdTe/ZnS(2ML)/MPA in H_2O, recorded at various excitation power. Here the symbols are the original data and the line represents the fit to the data according to Equation 2.7. (c) Corresponding variation of G(0) value with increasing excitation power for CdTe/MPA (Red sphere) and CdTe/ZnS(2ML)/MPA (black square). λ_{ex} = 485 nm.

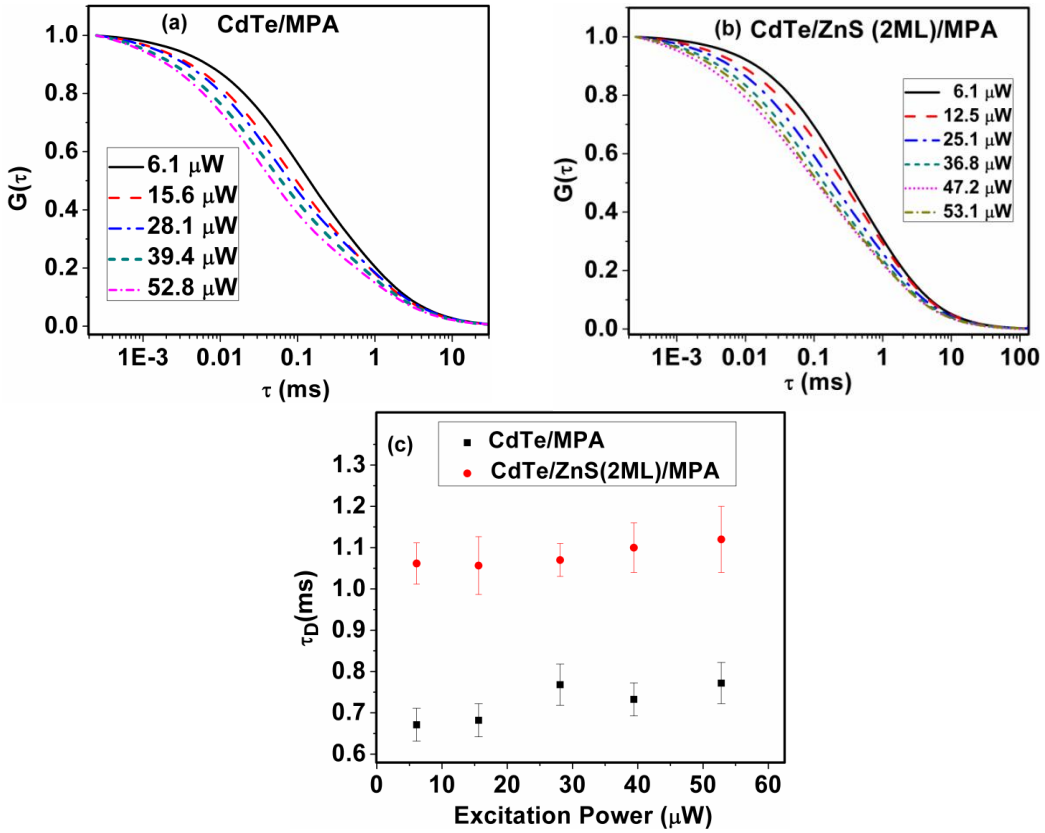

Figure 5.9. Normalized fitted correlation curves of (a) 74 nM CdTe/MPA core and (b) 20 nM CdTe/ZnS(2ML)/MPA core/shell QDs in H_2O. (b) A plot of measured diffusion time (τ_D) of CdTe/MPA (black square) and CdTe/ZnS(2ML)/MPA (red sphere) QDs vs excitation power.

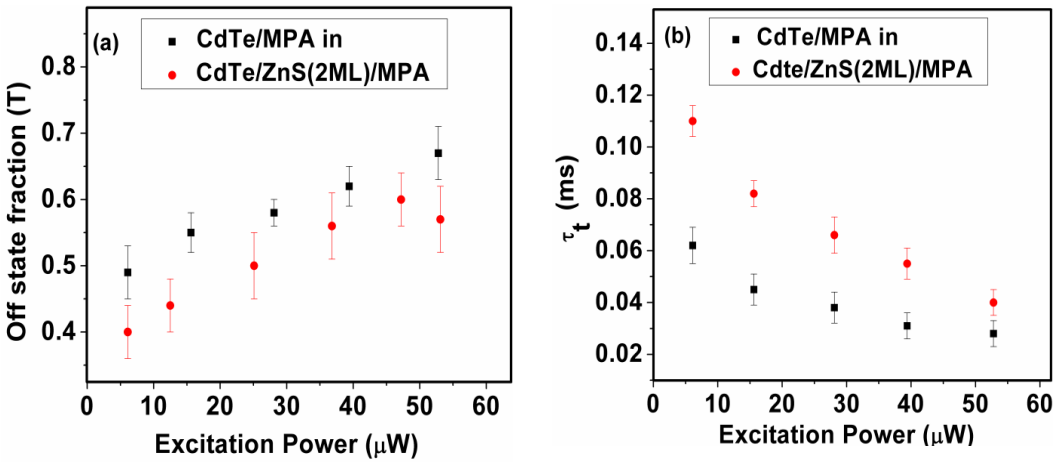

Figure 5.10. Plot of (a) off state fraction (T) and (b) blinking time (τ_t) vs excitation power for CdTe/MPA (black square) and CdTe/ZnS(2ML)/MPA (red sphere) QDs in H_2O.

One important point to note is that G(0) is related to the average number of molecules (N) in the observation volume undergoing reversible transition between fluorescence on- and off-state, as G(0) = 1/N(1-T). An increase in the value of T implies a decrease in the number of fluorescent molecules, N(1-T), in the observation volume. Consequently, the G(0) value should increase with excitation power. However, a large decrease of the G(0) value is observed for CdTe/MPA QDs. For CdTe/ZnS QDs, this decrease is however, very small compared to the core QDs. In our earlier reports, considering all possibilities we came to the conclusion that photoactivation contributes to the decrease in G(0) value with increasing excitation power.[23,24] This conclusion is substantiated by the present observation of an appreciable decrease in G(0) value with increasing excitation power only for CdTe/MPA QDs in H_2O which also exhibits an appreciable increase in fluorescence intensity upon light irradiation. For CdTe/ZnS(2ML)/MPA QDs, the increase in fluorescence intensity upon light irradiation (photoactivation) is very small and the decrease in G(0) value is also much smaller than that of CdTe/MPA QDs. Hence photoactivation of the QDs and decrease in the G(0) value with increasing excitation power in case of QDs in the FCS measurement is intimately related.

Another important aspect here is that for CdTe/MPA the number of particles (N) in the observation volume estimated from the G(0) value and off-state fraction (T) is much less than the actual number of particles (N_{actual}) calculated from the concentration of the QDs (Table 5.3). This suggests that a large fraction of CdTe/MPA QDs (95%) are in their dark state. Photoadsorption of H_2O molecules passivates the surface trap state and convert the dark QDs to bright ones and increases the number of emitters in the observation volume and also, a decrease in the G(0) value of the QDs with increasing excitation power.[23] The difference between N_{actual} and N is much smaller for CdTe/ZnS(2ML)/MPA compared to CdTe/MPA (Table 5.3) indicating better passivation of the surface states of CdTe core by the overgrowth of ZnS shell. N_{actual} is expected to be 12 in the observation volume for 20 nM CdTe/ZnS(2ML)/MPA QDs but the measured N value from FCS experiment is 3.85. This difference is largely due to the dark fraction of CdTe/ZnS(2ML)/MPA QDs (interfacial trap states capturing the charge carriers and promoting nonradiative deactivation).[52] Lattice parameter of ZnS (5.41Å) is significantly smaller than the lattice parameter of CdTe (6.482 Å).[36] This mismatch in lattice parameter (19.8%) creates strain in core/shell QDs.[41] Epitaxial

growth of ZnS shell around core CdTe QDs results in tensile strain in ZnS shell and compressional strain in CdTe core.[41] To obtain relief from this strain there occurs lattice dislocations at the interface between core and shell.[41,52] These lattice defects at the interfaces of core and shell introduces electronic states within the band gap, which acts as trap state for the charge carriers.[52] These dark QDs do not convert into bright ones as these are protected by the ZnS shell from the surrounding environment.

Table 5.3. Some FCS parameters for CdTe/MPA and CdTe/ZnS(2ML)/MPA QDs in H_2O at lowest excitation power.

Parameters	CdTe/MPA in H_2O	CdTe/ZnS(2ML)/MPA in H2O
C (nM)	74	20
G(0)	0.87 ± 0.14	0.43 ± 0.03
N(1-T)	1.74 ± 0.20	2.33 ± 0.16
T	0.49 ± 0.04	0.40 ± 0.03
N	2.25 ± 0.31	3.85 ± 0.30
N_{actual}†	44.4	12
Dark fraction*	0.95 ± 0.01	0.68 ± 0.02

† Estimated from the concentration of QDs for an observation volume of 10^{-15} L. *N/N_{actual} gives the bright fraction of the QDs. Dark fraction = (1 - bright fraction).

5.7. Conclusions:

Effect of ZnS shell on the fluorescence behavior of the CdTe QDs has been investigated. Significant improvement of the fluorescence properties is observed for CdTe/ZnS QDs compared to CdTe QDs in both $CHCl_3$ and H_2O, indicates effective passivation of the surface dangling orbitals of CdTe QDs by the overgrowth of the ZnS shell. Photoactivation and photocorrosion is only observed in CdTe/MPA QDs but not in CdTe/ZnS(2ML)/MPA QDs in aqueous medium. The results suggest that ZnS shell effectively protects the CdTe core QDs from external perturbations. FCS study substantiates this fact as a large decrease in G(0) value with increasing excitation power is only observed for CdTe/MPA QDs but not in CdTe/ZnS(2ML)/MPA QDs.

References:

(1) Alivisatos, A. P. *Science* **1996**, *271*, 933.
(2) Smith, A. M.; Nie, S. *Acc. Chem. Res.* **2010**, *43*, 190.
(3) Brus, L. E. *J. Chem. Phys.* **1983**, *79*, 5566.
(4) Brus, L. E. *J. Chem. Phys.* **1984**, *80*, 4403.
(5) Efros, A. L.; Rosen, M. *Annu. Rev. Mater. Sci.* **2000**, *30*, 475.
(6) Kippeny, T.; Swafford, L. A.; Rosenthal, S. J. *J. Chem. Edu.* **2002**, *79*.
(7) Bawendi, M. G.; Steigerwald, M. L.; Brus, L. E. *Annu. Rev. Phys. Chem.* **1990**, *41*, 477.
(8) Binks, D. J. *Phys. Chem. Chem. Phys.* **2011**, *13*, 12693.
(9) Ekimov, A. I.; Efros, A. L.; Onushchenko, A. A. *Solid State Commun.* **1985**, *56*, 921.
(10) Delehanty, J. B.; Bradburne, C. E.; Susumu, K.; Boeneman, K.; Mei, B. C.; Farrell, D.; Blanco-Canosa, J. B.; Dawson, P. E.; Mattoussi, H.; Medintz, I. L. *J. Am. Chem. Soc.* **2011**, *133*, 10482.
(11) Beard, M. C. *J. Phys. Chem. Lett.* **2011**, *2*,, 1282.
(12) Resch-Genger, U.; Grabolle, M.; Cavaliere-Jaricot, S.; Nitschke, R.; Nann, T. *Nature Methods* **2008**, *5*., 763.
(13) Kamat, P. V. *J. Phys. Chem. Lett.* **2013**, *4*, 908.
(14) Klimov, V. I. *Annu. Rev. Phys. Chem.* **2007**, *58*, 635.
(15) M., B. J.; Moronne, M.; Gin, P.; Weiss, S.; Alivisatos, A. P. *Science* **1998**, *281*, 2013.
(16) Carrillo-Carrion, C.; Cardenas, S.; Simonet, B. M.; Valcarcel, M. *Chem. Commun.* **2009**, 5214.
(17) Cordones, A. A.; Leone, S. R. *Chem. Soc. Rev.* **2013**, *42*, 3209.
(18) Zhang, Y.; He, J.; Wang, P.-N.; Chen, J.-Y.; Lu, Z.-J.; Lu, D.-R.; Guo, J.; Wang, C.-C.; Yang, W.-L. *J. Am. Chem. Soc.* **2006**, *128*, 13396.
(19) Cordero, S. R.; Carson, P. J.; Estabrook, R. A.; Strouse, G. F.; Buratto, S. K. *J. Phys. Chem. B* **2000**, *104*, 12137.
(20) Pechstedt, K.; Whittle, T.; Baumberg, J.; Melvin, T. *J. Phys. Chem. C* **2010**, *114*, 12069.
(21) Jones, M.; Nedeljkovic, J.; Ellingson, R. J.; Nozik, A. J.; Rumbles, G. *J. Phys. Chem. B* **2003**, *107*, 11346.
(22) Cooper, D. R.; Suffern, D.; Carlini, L.; Clarke, S. J.; Parbhoo, R.; Bradforth, S. E.; Nadeau, J. L. *Phys. Chem. Chem. Phys.* **2009**, *11*, 4298.
(23) Patra, S.; Samanta, A. *J. Phys. Chem. C* **2014**, *118*, 18187.
(24) Patra, S.; Samanta, A. *J. Phys. Chem. C* **2013**, *117*, 23313.
(25) Gooding, A. K.; Gomez, D. E.; Mulvaney, P. *ACS Nano* **2008**, *2*, 669.
(26) Biju, V.; Kanemoto, R.; Matsumoto, Y.; Ishii, S.; Nakanishi, S.; Itoh, T.; Baba, Y.; Ishikawa, M. *J. Phys. Chem. C* **2007**, *111*, 7924.
(27) Kloepfer, J. A.; Bradforth, S. E.; Nadeau, J. L. *J. Phys. Chem. B* **2005**, *109*, 9996.
(28) Osborne, M. A.; Lee, S. F. *ACS Nano* **2011**, *5*, 8295.

(29) Duncan, T. V.; Polanco, M. A. M.; Kim, Y.; Park, S.-J. *J. Phys. Chem. C* **2009**, *113*, 7561.

(30) Wang, Y.; Tang, Z.; Correa-Duarte, M. A.; Pastoriza-Santos, I.; Giersig, M.; Kotov, N. A.; Liz-Marzan, L. M. *J. Phys. Chem. B* **2004**, *108*, 15461.

(31) Gaponik, N.; Talapin, D. V.; Rogach, A. L.; Hoppe, K.; Shevchenko, E. V.; Kornowski, A.; Eychmuller, A.; Weller, H. *J. Phys. Chem. B* **2002**, *106*, 7177.

(32) Wang, Y.; Tang, Z.; Correa-Duarte, M. A.; Liz-Marzan, L. M.; Kotov, N. A. *J. Am. Chem. Soc.* **2003**, *125*, 2830.

(33) Manna, L.; Scher, E. C.; Li, L.-S.; Alivisatos, A. P. *J. Am. Chem. Soc.* **2002**, *124*, 7136.

(34) Bao, H.; Gong, Y.; Li, Z.; Gao, M. *Chem. Mater.* **2004**, *16*, 3853.

(35) Underwood, D. F.; Kippeny, T.; Rosenthal, S. J. *J. Phys. Chem. B* **2001**, *105*, 436.

(36) Reiss, P.; Protiere, M.; Li, L. *Small* **2009**, *5*, 154.

(37) Reiss, P.; Bleuse, J.; Pron, A. *Nano Lett.* **2002**, *2*, 781.

(38) Dabbousi, B. O.; Rodriguez-Viejo, J.; Mikulec, F. V.; Heine, J. R.; Mattoussi, H.; Ober, R.; Jensen, K. F.; Bawendi, M. G. *J. Phys. Chem. B* **1997**, *101*, 9463.

(39) Hines, M. A.; Guyot-Sionnest, P. *J. Phys. Chem.* **1996**, *100*, 468.

(40) Talapin, D. V.; Rogach, A. L.; Kornowski, A.; Haase, M.; Weller, H. *Nano Lett.* **2001**, *1*, 207.

(41) Smith, A. M.; Mohs, A. M.; Nie, S. *Nat. Nanotechnol.* **2009**, *4*, 56.

(42) Peng, X.; Schlamp, M. C.; Kadavanich, A. V.; Alivisatos, A. P. *J. Am. Chem. Soc.* **1997**, *119*, 7019.

(43) Li, J. J.; Wang, Y. A.; Guo, W.; Keay, J. C.; Mishima, T.; Johnson, M. B.; Peng, X. *J. Am. Chem. Soc.* **2003**, *125*, 12567.

(44) van Sark, W. G. J. H. M.; Frederix, P. L. T. M.; Van den Heuvel, D. J.; Gerritsen, H. C. *J. Phys. Chem. B* **2001**, *105*, 8281.

(45) Yu, W. W.; Qu, L.; Guo, W.; Peng, X. *Chem. Mater.* **2003**, *15*, 2854.

(46) Wuister, S. F.; Swart, I.; Driel, F. V.; Hickey, S. G.; Donega, C. D. M. *Nano Lett.* **2003**, *3*, 503.

(47) Lackowicz, J. R. *Principles of Fluorescence Spectroscopy., Springer: New York, 2006; Chapter 24.*

(48) Schwille, P.; Haustein, E. *Fluorescence Correlation Spectroscopy: An introduction to its concepts and applications, Biophysical Textbooks online 2004, 1-33*.

(49) Ito, S.; Toitani, N.; Pan, L.; Tamai, N.; Miyasaka, H. *J. Phys.: Condens. Matter* **2007**, *19*, 486208.

(50) Peterson, J.; Nesbitt, D. J. *Nano Lett.* **2009**, *9*, 338.

(51) Heuff, R. F.; Swift, J. L.; Cramb, D. T. *Phys. Chem. Chem. Phys.* **2007**, *9*, 1870.

(52) Chen, X.; Lou, Y.; Samia, A. C.; Burda, C. *Nano Lett.* **2003**, *3*, 799.

CHAPTER 6

Diffusion of Organic Dyes in Bovine Serum Albumin Solution Studied by Fluorescence Correlation Spectroscopy

The understanding of the transport of drugs and naturally occurring molecules in living cells and tissues requires a thorough knowledge of the diffusion behavior of the molecular systems in these media. In this work, we studied the translational diffusion of three fluorescent molecules, electrically neutral coumarin 102 (C102), cationic rhodamine 6G (R6G) and anionic fluorescein (FL) in phosphate-buffered (pH 7) aqueous solutions of bovine serum albumin (BSA) protein in the absence and presence of common salt and urea using fluorescence correlation spectroscopy (FCS) by monitoring the fluorescence intensity fluctuations in a small confocal observation volume. The diffusion due to both free and BSA-bound molecules is observed in the case of the C102-BSA system. While no exchange between the bound and free states of the molecule is observed in this case, a rapid exchange between the two states is observed in the case of electrically charged hydrophilic dyes R6G and FL. This molecular picture, which is the first of its kind, is a reflection of a weaker binding of R6G and FL compared to C102 with the protein molecule. The binding sites of the probe molecules in BSA were identified based on the urea-induced change of diffusion of the probes in BSA.

6.1. Introduction:

Serum albumins, which are the most abundantly found proteins in blood plasma, serve as depot protein and transport protein for a variety of compounds like fatty acids, amino acids, bile salts, metals, hormones, drugs and pharmaceuticals.[1-7] The nature of binding between small molecular probes and the albumins is an important topic of investigation for many reasons.[8-13] Unlike human serum albumin (HSA), the crystal structure of bovine serum albumin (BSA), which has a molecular mass of 66,200 Da with 583 amino acids in a single polypeptide chain,[14] is unknown. A model structure of BSA, which can be obtained from its amino acid sequence and crystal structure of related homologous protein, HSA, indicates that it is made up of three homologous domains (I, II, and III) divided into nine loops (L1–L9) by 17 disulphide bridges. Each domain in turn is the product of two sub-domains A and B.[15] BSA has two tryptophan (Trp) residues that possess intrinsic fluorescence. Trp-212 locates

within a hydrophobic binding pocket in subdomain IIA, and Trp-134 on the surface of the albumin molecule in domain I.[16] The principal ligand binding sites of BSA are located in the subdomain IIA and IIIA,[17,18] which are termed binding sites I and II (Figure 6.1).[17,18]

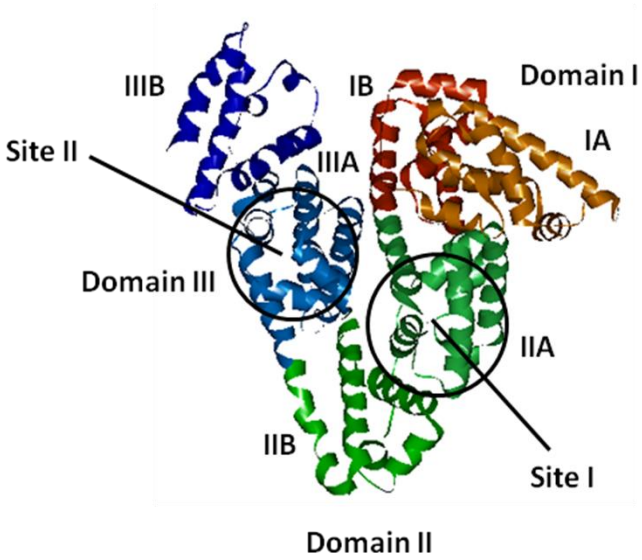

Figure 6.1. A pictorial representation of the BSA model structure obtained from homology modelling indicating the domains and the binding sites.

In the present work, we explore the utility of FCS in studying the diffusion processes in phosphate-buffered (pH 7.0) BSA solution. FCS is a method in which spontaneous intensity fluctuation arising from a very small confocal volume (approx. 1 fL), defined by the tightly focused laser beam and a confocal pinhole, are correlated to quantify the temporal evolution of the system about its equilibrium state. Even though the basics of FCS were developed in the early 1970s,[19,20] it became a popular technique after the development of confocal optics and highly sensitive detectors in the 1990s.[21] Fluctuation of fluorescence arises due to diffusion of the fluorescent molecules in and out of the observation volume and changes in quantum yield due to different processes.[21] Analysis of the correlation function provides the information on the dynamic processes responsible for the fluctuation. The correlation function is fitted to a model, which contains the information about the possible dynamics processes that may contribute to the fluctuation. Fitting of the data to these models give dynamic parameters ranging from reaction times to diffusion coefficients. In the present study, we are particularly interested in the latter, which are related to the

hydrodynamic radii of the diffusing molecules, thus offering a sensitive method for size determination.

FCS has been previously used to study the diffusion of fluorescent probes in many organized assemblies, which include vesicles and membranes,[22-24] colloidal particles,[25] ionic liquids,[26-29] agarose gel,[30,31] polymer matrix,[32,33] micelles,[34-37] microemulsions[38] and to study protein aggregation,[39,40] and conformational changes of the protein.[41-46] As BSA is a carrier protein, the mobility of the molecules in BSA solution is of fundamental importance in drug delivery and for the design of drug molecules. Considering the fact that a protein solution consists of both hydrophilic and hydrophobic domains, the diffusion of a probe may be location dependent with fast diffusion near the surface and slow diffusion in the core region. Andrade and coworkers studied the translational and rotational motion of BSA under physiological and acidic pH by FCS and time-resolved anisotropy measurements.[47] Using anionic meso-tetrakis (p-sulfonatophenyl) porphyrin sodium salt (TSPP) as a probe molecule, they found a higher diffusion coefficient of TSPP in BSA at acidic pH. They attributed the result to structural change of the protein at acidic pH and wobbling motion of the porphyrin at the binding site. Reyes and coworkers studied the effect of temperature and salt on the diffusion coefficient of BSA using photon correlation spectroscopic technique.[48] They found a decrease in the diffusion coefficient of BSA with ionic strength, which was rationalized in terms of conformational change of protein and protein aggregation at high ionic strength. Bhattacharyya and co-workers recently studied the interaction of C153 and R6G with immobilized human serum albumin (HSA) and determined the association sites of the probes in HSA by studying the effect of guanidinium hydrochloride on the binding kinetics of the probes with HSA.[44] Salts such as Na_2SO_4, NaCl, NaI, NaSCN at high concentrations have significant effects on the conformational stability of biomacromolecules.[49,50] Salt induced association or dissociation of many biological macromolecules depends upon their "salting out" and "salting in" properties. The influence of an ion on the solubility and stability of protein follows the classical Hofmeister series.[51] The anions appear to have a larger effect than the cations, and are usually ordered $CO_3^{2-}>SO_4^{2-}>S_2O_3^{2-}>H_2PO_4^{-}>F^{-}>Cl^{-}>Br^{-}>I^{-}>ClO_4^{-}>SCN^{-}$.[52] Early Members of the series promote "*salting out"*, whereas the later members contribute to "*salting in"*. Earlier members provide stability to the protein structure, while the latter ones destabilize it. These salts can also affect the transport properties of BSA.

Considering the fact that NaCl is found in nearly all biological systems, we have investigated its effect on the diffusion properties of the dyes in BSA solution.

While the interaction between BSA and various fluorophores has been studied previously using conventional steady state and time-resolved techniques primarily to obtain information relating to the binding interaction, the present study focuses on the translational diffusion of electrically neutral and charged dye molecules (Chart 1.6) in aqueous solutions of BSA at neutral condition by FCS technique, an information that cannot be obtained by the conventional techniques. As is shown below, the results presented here provide deep insight into the nature of interaction of the molecular systems with BSA and on their diffusion behavior.

6.2. Diffusion in bulk solvent:

Figure 6.2 shows the autocorrelation curves of the three dye molecules. The translational diffusion coefficients (D_t) estimated from these data are 640 and 420 $\mu m^2/s$ for C102 and FL respectively. These D_t values are in good agreement with the reported values shown in Table 6.1.[37,53,54] The hydrodynamic radii of these dyes estimated from the Stokes Einstein Equation are 0.34 ± 0.03, 0.51 ± 0.01, and 0.51 ± 0.01 nm for C102, FL and R6G, respectively.

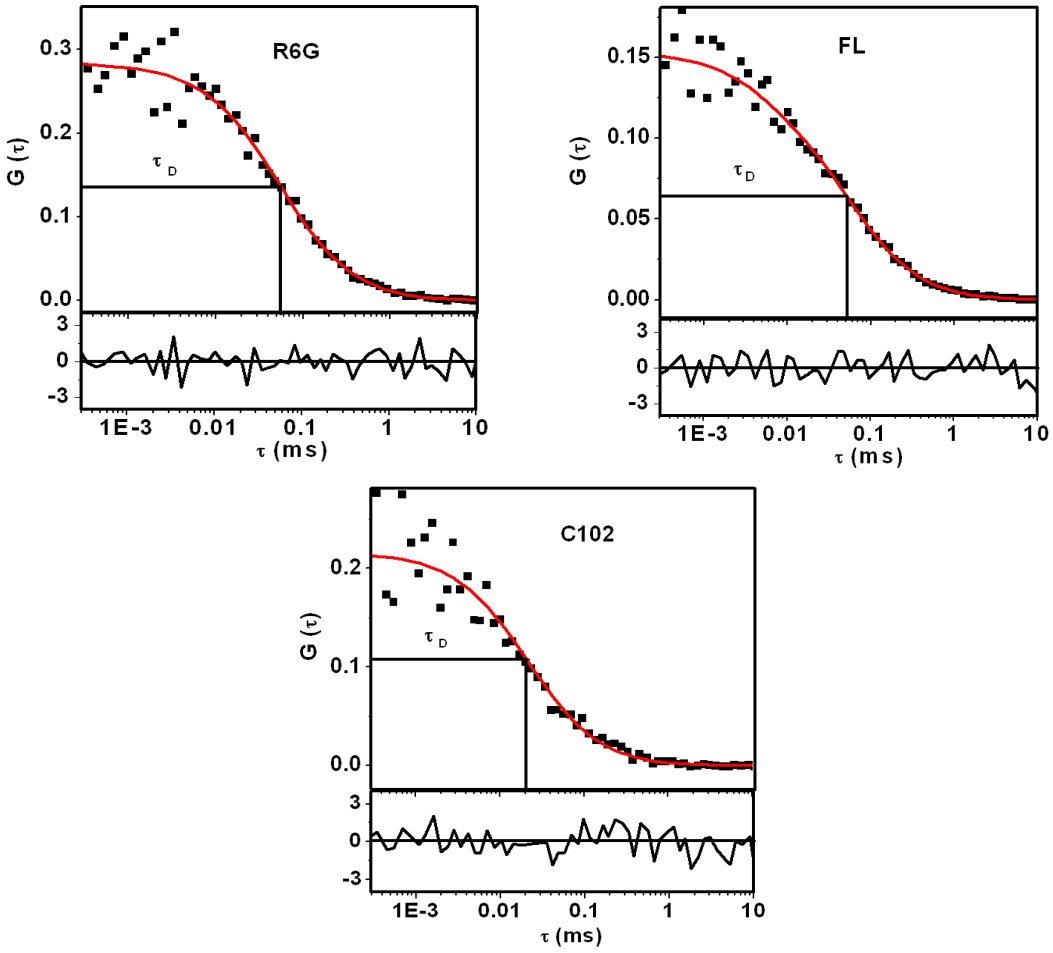

Figure 6.2. Fluorescence correlation data points and best fits to those for R6G, FL and C102 in phosphate-buffered solution (pH = 7). λ_{ex} for FL, R6G is 485 nm and 405 nm for C102. Residuals are shown at the bottom of each plot.

Table 6.1. Diffusion coefficients of the dyes in aqueous solution

Medium	D_t ($\mu m^2/s$)		
	C102	R6G	FL
Phosphate-buffered (pH=7.0)	640 ± 60 (600)†	440 ± 15 (426)‡	420 ± 10 (425)*

The quantities in the bracket are the literature values of D_t from reference [37]†, [53]‡ and [54]*.

6.3. Diffusion in BSA solution:

6.3.1. C102

Figure 6.3 shows the normalized correlation curves for C102 as a function of the concentration of BSA. These curves represent the fits to the experimental data to a 2-component diffusion model (Equation 2.2). Apart from the best quality of the fit, the rationale for this treatment is also based on strong binding between C102 and BSA (The binding constant, K is ~ 10^5 M^{-1})[9]. One can expect to observe the bound and free forms of C102 to contribute to the diffusion process, which is indeed found to be the case. The two diffusion components (~ 550 and 60 $\mu m^2/s$) obtained from the curves for various [BSA] match closely with the previously reported D_t values for free C102[37] and BSA[55]. The analysis reveals that the shift of the curves towards the longer time scale is due to gradual increase in the weightage of the BSA-bound C102. It is also observed that for [BSA] > 8 μM, the contributions from free C102 becomes almost negligible and the correlation curves show 1-component diffusion due to the bound C102 only. The binding constant (K) is estimated from the plot of the fraction of the bound molecules (α_b) vs [BSA] (Figure 6.4) using Equation 6.1

$$\alpha_b = \frac{K[BSA]}{1 + K[BSA]} \tag{6.1}$$

which is obtained from the equilibrium relation

$$K = \frac{\alpha_b}{\alpha_f [BSA]} \tag{6.2}$$

α_f is the fraction of the free C102 molecules. It should be noted in this context that as [BSA] used in this experiment (μM range) was much larger than [Probe] (nM range), the initial concentration of BSA, $[BSA]_0$ is used for [BSA] in the estimation of the K value for this and other two probes. The estimated value of the binding constant between C102 and BSA is (6.0 ± 0.6)×10^5 M^{-1}. This binding constant is of the same order of magnitude as that obtained from a conventional technique[9].

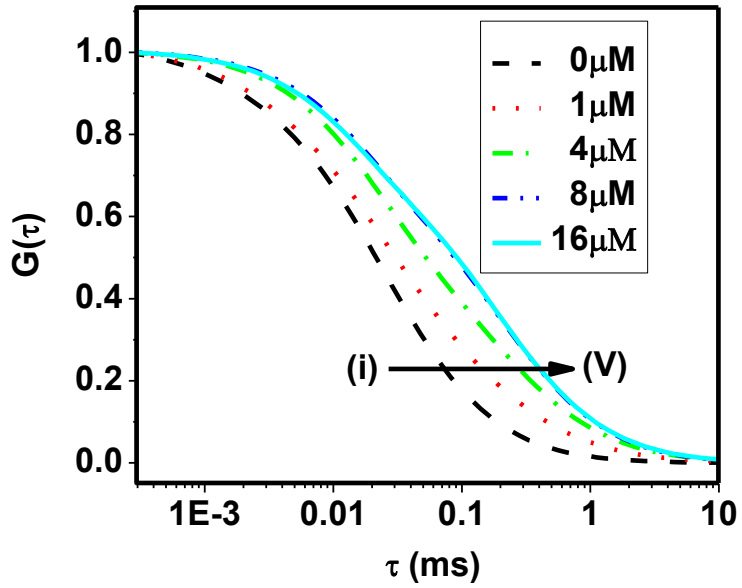

Figure 6.3. Normalized correlation curves of C102 for [BSA] of (i) 0 (ii) 1.0 (iii) 4.0 (iv) 8.0 (v) 16.0 μM. The curves shown are the best fits to Equation 2.2.

.

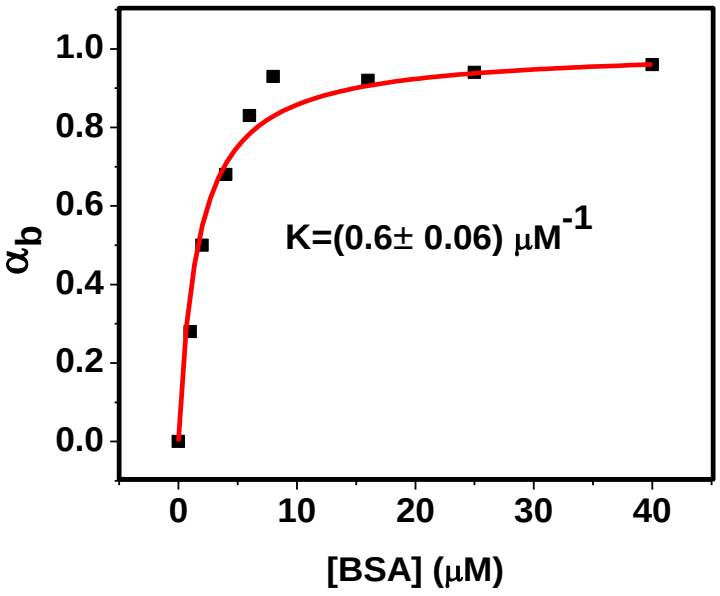

Figure 6.4. Plot of the bound fraction (α_b) of C102 vs [BSA]. The line indicates the fit to the data according to Equation 6.1.

6.3.2. R6G and FL

Unlike C102, the fluorescence correlation data could not be fit to a two-diffusion model for hydrophilic probes, R6G and FL. Considering the hydrophilic nature of these systems and their relatively weak association with BSA,[56] one expects exchange of the fluorescent probes between the free and bound state to be faster than the diffusion time through the observation volume. Hence, one obtains an average diffusion coefficient in these measurements with contributions from both the free and bound molecules. The treatment of the correlation data that takes into consideration the exchange dynamics of the system is as follows:[57]

Association of a fluorescent guest (A) with a nonfluorescent host (H) yielding a fluorescent complex (AH) can be represented as

$$A + H \underset{k_-}{\overset{k_+}{\rightleftharpoons}} AH \tag{6.3}$$

Where, k_+ and k_- are the association and dissociation rate constants, respectively. If D_A and D_{AH} represent the diffusion coefficients of the free and bound molecules, respectively, the average diffusion coefficient of the system, $\overline{D}_t$ is given by

$$\overline{D}_t = x_A D_A + x_{AH} D_{AH} \tag{6.4}$$

Where, x_A and x_{AH} are the mole fractions of the respective components. Under this condition, using Equation (2.5) and (6.4), one can express the average diffusion time, $\overline{\tau}_i$ as

$$\overline{\tau}_i = \frac{\tau_A\left(1 + K_1[H]_0\right)}{1 + \frac{\tau_A}{\tau_{AH}} K_1[H]_0} \tag{6.5}$$

Where, K_1 is the binding constant of the system and is given by, $K_1 = k_+/k_-$.

With increasing $[H]_0$ value the observed diffusion time, $\overline{\tau}_i$, shifts from τ_A to τ_{AH}. Figure 6.5 shows the normalized correlation curves for FL as a function of the concentration of BSA. The K_1 value is determined from the plot of $\overline{\tau}_i$ vs $[H]_0$ (Figure6.6). Thus the estimated K_1 value for FL ($1.50 \pm 0.04 \times 10^5$) M^{-1} is 5 times higher than that obtained from equilibrium

dialysis method (2.8×10^4 M^{-1}).[56] However, a higher binding constant of ~10^6 M^{-1} is also reported in the literature.[58,59]

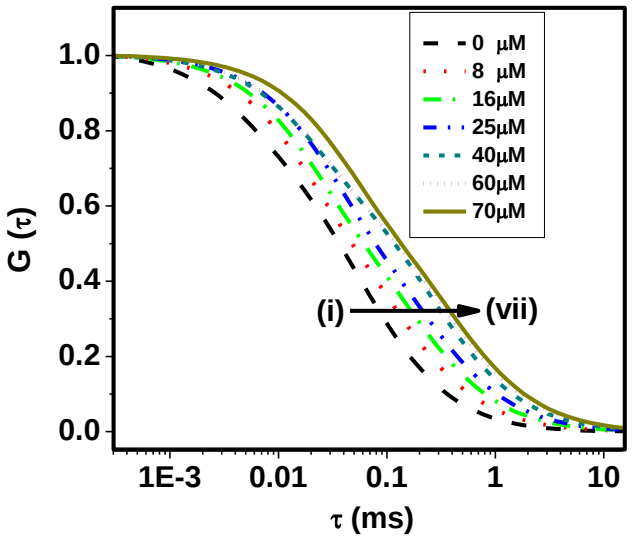

Figure 6.5. Normalized best fit correlation curves of FL for [BSA] of (i) 0 (ii) 8 (iii) 16 (iv) 25 (v) 40 (vi) 60 and (vii) 70 μM.

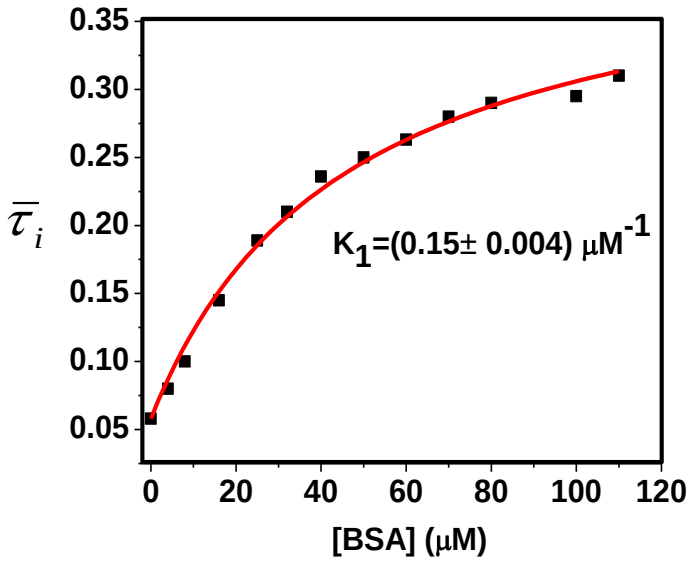

Figure 6.6. Plot of the mean diffusion times ($\overline{\tau}_i$) of FL vs [BSA]. The line represents the fit to the data according to Equation (6.5) from which K_1 is estimated.

6.4. Effect of NaCl on diffusion:

NaCl can have a significant effect on the diffusion behavior of the dyes in BSA as it affects the protein stability by altering the electrostatic interaction between the charged amino acid residues.[60,61] The correlation curves for the systems in aqueous solution of BSA (8 μM, pH 7) in the presence of various concentrations of NaCl are shown in Figure 6.7 and the estimated values of the diffusion coefficients for the systems are collected in Table 6.2. Among all of the probes studied, C102 shows little effect upon addition of NaCl. The D_t value of C102 changes from 65 to 50 $\mu m^2/s$ upon treatment with 1.5 M NaCl. For R6G, a steady decrease in the diffusion coefficient is observed with increase in concentration of NaCl.[62]

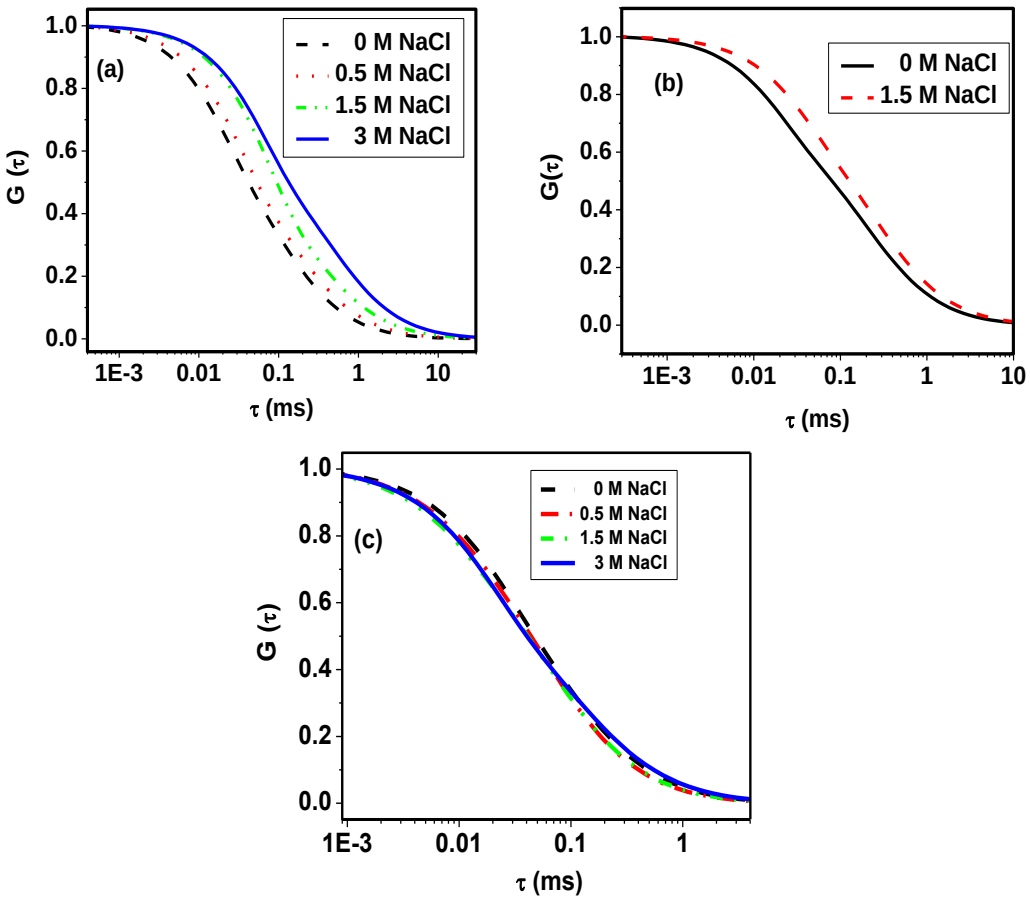

Figure 6.7. Effect of NaCl on the correlation curves (normalized) of (a) R6G (b) C102 and (c) FL in the presence of a constant amount of (8 μM) of BSA.

Table 6.2. Diffusion coefficients of the dye molecules in BSA solution (8 μM) for different concentrations of NaCl

Medium	D_t ($\mu m^2/s$)		
	C102	R6G	FL
BSA (8 μM)	65 ± 10	280 ± 40	270 ± 35
BSA (8 μM) + 0.5 M NaCl		170 ± 15	390 ± 15
BSA (8 μM) + 1.5 M NaCl	50 ± 5	90 ± 10	310 ± 15
BSA (8 μM) + 3.0 M NaCl		45 ± 5	220 ± 10

This observation can be rationalized as follows. Damodaran and Kinsella while studying the binding of 2-nonanone with BSA, observed a decrease in the free ligand concentration in the solution upon addition of NaCl.[49,50] This implies that with increasing NaCl concentration more dye molecules are transferred from the bulk to the protein phase and thus contribute to the decrease in the diffusion coefficient. It is not difficult to understand why the effect of NaCl is more pronounced in the case of R6G compared to C102. As the binding is relatively weaker in case of R6G, more free molecules are present in the aqueous phase, their passage to protein phase mainly leads to the significant change in the diffusion coefficient. Whereas in the case of C102, due to strong binding most molecules are in bound state and hence little decrease in the diffusion coefficient is observed. It is difficult to suggest whether this small decrease is due to the structural change of BSA or not because there is small decrease in the diffusion coefficient of C102 in phosphate buffered solution at pH 7.0 upon addition of 1.5 M NaCl. (Table 6.3).

Table 6.3. Diffusion coefficients of the probes in buffer in absence and presence of NaCl and urea.

Fluorophores	D_t ($\mu m^2/s$)			
	In buffer	4 M urea	1.5 M NaCl	3 M NaCl
FL	420 ± 10	400 ± 15	390 ± 25	370 ± 20
R6G	440 ± 15	415 ± 15	390 ± 30	350 ± 15
C102	640 ± 60	520 ± 30	550 ± 15	

The case of FL is found to be not so straightforward as the diffusion coefficient passes through a maximum with increase in the concentration of NaCl. Even though this implies that more than one factor, something that strengthens binding and something else that weakens it, contributes to this complex behavior, we are currently not in a position to comment on what these factors are. We have verified by performing several measurements that the trend is reproducible. We plan to address this point in more detail at a later stage.

6.5. Effect of urea on diffusion:

The effect of urea on the correlation curves of the dyes in aqueous solution (pH 7) of BSA (8 μM) are shown in Figure 6.8 and the estimated diffusion coefficients of the probes are listed in Table 6.4. Except R6G, the diffusion coefficients increase in all cases upon addition of urea.[63] This increase is found most pronounced in the case of C102. The D_t value in this case increases by a factor of ~ 4 in presence of 4 M urea. As urea is a strong denaturing agent, it disrupts the native structure of the protein and affects the binding sites[64] by exposing them to bulk water. As binding is the strongest in the case of C102, the effect of urea is most prominent in this case. In case of FL, for lower concentration of BSA (8 μM), when a large number of molecules are in the aqueous solution in the free state, urea induced denaturation of protein does not have much impact on the diffusion of FL. But at higher BSA concentration, this change is more appreciable upon denaturation. Nearly 2-fold enhancement in diffusion is observed in 60 μM BSA solution upon treatment with urea. This behavior is consistent with the fact that FL binds to the hydrophilic sites of BSA. Diffusion coefficient of R6G does not show any change in the presence of urea even at higher concentration of BSA when most of the R6G molecules are in bound state. This is perhaps a reflection of the fact that positively charged R6G molecules remain bound to the negatively charged amino acid residues (at pH 7) of the denatured protein. However, as denatured BSA has a larger hydrodynamic radius (4.3 nm) compared to native BSA (3.6 nm),[65] one expects a 1.2-fold decrease of the D_t value of R6G upon addition of 4 M urea. Since this is not the case, it is evident that additional factor is involved, which nullifies the effect of increasing hydrodynamic radius of denatured BSA on the D_t value. This factor is simply the change in binding strength between R6G and BSA on denaturation. Recently Bhattacharyya and co-workers shown a 1.2-fold decrease in the binding constant between R6G and HSA upon addition of 5 M guanidinium hydrochloride.[44] Hence, it is not surprising to find a situation

where the two factors counter-balance each other resulting in very little or negligible change in the D_t value of R6G in BSA.

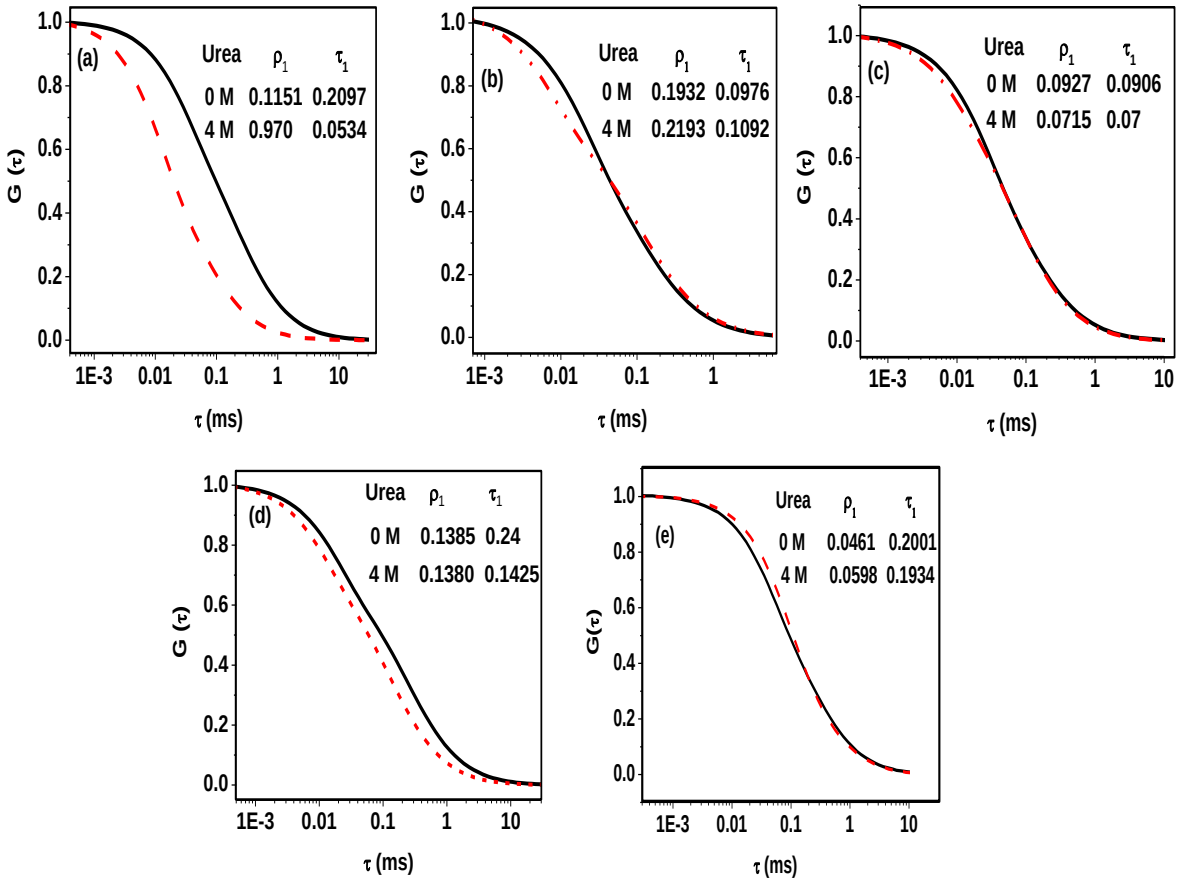

Figure 6.8. Effect of urea (4 M) on the normalized correlation curves of (a) C102, (b) R6G and (c) FL in the presence of 8 μM BSA. Traces in (d) and (e) highlight the effect of same amount of urea (4 M) on the correlation curves of FL and R6G in the presence of a larger quantity of BSA (60 μM), respectively. The curves with solid and dashed line represent 0 and 4 M urea conditions, respectively.

Table 6.4. Diffusion coefficients (D_t, in $\mu m^2/s$) of the dyes in 8 μM BSA and 60 μM BSA in absence and in presence of urea.

Fluorophores	D_t in 8 μM BSA		D_t in 60 μM BSA	
	0 M urea	4 M urea	0 M urea	4 M urea
C102	65 ± 10	250 ± 25		
R6G	280 ± 40	250 ± 35	100 ± 10	105 ± 20
FL	270 ± 35	295 ± 45	90 ± 5	155 ± 20

The effect of urea on the diffusion of the fluorescent molecules allows identification of the binding sites of the probes in BSA, as the diffusion of the hydrophilic probes is not much affected by urea, but that of the hydrophobic probe is highly affected, implies that the hydrophobic domains are unfolded on addition of urea without affecting the structure of hydrophilic domains. Bhattacharyya and co-workers also observed a similar behaviour recently in HSA on addition of guanidinium hydrochloride which is also a denaturing agent.[44] One can perhaps obtain more definite information on the location of the probe molecules from the recent work of Leggio C. et al, who observed a multistep unfolding process of HSA induced by urea.[65] They proposed two intermediates during the denaturation process. In the presence of 3 M urea domain I begins to open up, while domain II and III remain closed. At 4.35 M urea, domain II becomes unfolded. Domain III opens up only at high urea concentration (C > 8 M). In an earlier work, the binding site of C102 in HSA was assigned to the subdomain IIA by a molecular docking study.[9] Taking into consideration of these literature reports and careful consideration of our data we can conclude that C102 binds to the hydrophobic region IIA of BSA, which is almost completely denatured in presence of 4 M urea showing a large increase in diffusion coefficient. R6G is expected to be associated with domain IIIA, which retains its structure even in presence of 4 M urea. As FL shows small enhancement upon denaturation by urea, this probe is not entirely associated with domain III and may also be located in between subdomains IIA and IIIA.

6.6. Conclusion

The diffusion behavior of electrically neutral and charged dye molecules in protein solution has been investigated using FCS technique. The measured diffusion coefficients provide insight into the nature and strength of the interaction between the guest and host revealing the heterogeneity of the binding sites of the protein and fast exchange between the bound and free states of the molecules. The common salt and urea induced changes of the diffusion behaviour allow identification of the association sites of the probes with the protein molecule.

References and notes:

(1) Carter, D. C.; Ho, J. X. *Adv. Protein Chem.* **1994**, *45*, 153.
(2) Sengupta, B.; Sengupta, P. K. *Biochem. Bioph. Res. Co.* **2002**, *299*, 400.
(3) Makino, S.; Reynolds, J. A.; Tanford, C. *J. Biol. Chem.* **1973**, *248*, 4926.
(4) Zhang, Y.; Wilcox, D. E. *J. Biol. Inorg. Chem.* **2002**, *7*, 327.
(5) Choi, J. K.; Ho, J.; Curry, S.; Qin, D.; Bittman, R.; Hamilton, J. A. *J. Lipid Res.* **2002**, *43*, 1000.
(6) Kamikubo, K.; Sakata, S.; Nakamura, S.; Komaki, T.; Miura, K. *J. Protein Chem.* **1990**, *9*, 461.
(7) Feng, X. Z.; Liu, Z.; Yang, L. J.; Wang, C.; Bai, C. L. *Talanta* **1998**, *47*, 1223.
(8) Chatterjee, S.; Srivastav, T. S. *J. Porphyr. Phthalocya.* **2000**, *4*, 147.
(9) Bhattacharya, B.; Nakka, S.; Guruprasad, L.; Samanta, A. *J.Phys.Chem.B* **2009**, *113*, 2143.
(10) Pal, S. K.; Mandal, D.; Sukul, D.; Sen, S.; Bhattacharyya, K. *J.Phys.Chem.B* **2001**, *105*, 1438.
(11) Samanta, A.; Paul, B. K.; Gucchait, N. *Biophys. Chem* **2011**, *156*, 128.
(12) Hu, Y. J.; Liu, Y.; Wang, J. B. *J. Pharmaceut. Biomed.* **2004**, *36*, 915.
(13) wang, Y. Q.; Zang, H. M.; Zang, G. C. *J. Pharmaceut. Biomed.* **2007**, *43*, 1869.
(14) Foster, J. F. *Albumin Structure, Function and Uses; Pergamon Press, Oxford, UK*, **1977**.
(15) Papadopoulou, A.; Green, R. J.; Frazier, R. A. *J. Agr. Food Chem.* **2005**, *53*, 158.
(16) Moriyama, Y.; Ohta, D.; Hadiya, K.; Mitsui, Y.; Takeda, K. *J. Protein Chem.* **1996**, *15*, 265.
(17) Sudlow, G.; Birkett, D. J.; Wade, D. N. *Mol. Pharmacol.* **1975**, *11*, 824.
(18) Sudlow, G.; Birkett, D. J.; Wade, D. N. *Mol. Pharmacol.* **1976**, *12*, 1052.
(19) Magde, D.; Webb, W. W.; Elson, E. *Phys. Rev. Lett* **1972**, *29*, 705.
(20) Magde, D.; Elson, E. L.; Webb, W. W. *Biopolymers* **1974**, *13*, 29.
(21) Lackowicz, J. R. *Principle of Fluorescence Spectroscopy* **2006**, *Springer: New York*, Chap 24.
(22) Korlach, J.; Scwille, P.; Webb, W. W.; Feigenson, G. W. *Proc. Natl. Acad. Sci. USA* **1999**, *96*, 8461.
(23) Benda, A.; Benes, M.; Marecek, V.; Lhotsky, A.; Hermens, W. T.; Hof, M. *Langmuir* **2003**, *19*, 4120.
(24) Humpolickova, J.; Gielen, E.; Benda, A.; Fagulova, J.; Vercammen, J.; VandeVen, M.; Hof, M.; Ameloot, M.; Engelborghs, Y. *Biophysics. J.* **2006**, *91*, L 23.
(25) Muller, C. B.; Loman, A.; Richtering, W.; Enderlein, J. *J. Phys. Chem. B* **2008**, *112*, 8236.
(26) Werner, J. H.; Baker, S. N.; Baker, G. A. *Analyst* **2003**, *128*, 786.
(27) Sarkar, A.; Ali, M.; Baker, G. A.; Tetin, S. Y.; Ruan, Q.; Pandey, S. *J. Phys. Chem. B* **2009**, *113*, 3088.
(28) Guo, J.; Baker, G. A.; Hillesheim, P.; Dai, S.; Shaw, R. W.; Mahurin, S. M. *Phys. Chem. Chem. Phys.* **2011**, *13*, 12395.
(29) Sasmal, D.; Mandal, A. K.; Mondal, T.; Bhattacharya, K. *J. Phys. Chem. B* **2011**, *115*, 7781.

(30) Fatin-Rouge, N.; Wilkinson, K. J.; Buffle, J. *J. Phys. Chem. B* **2006**, *110*, 20133.
(31) Fatin-Rouge, N.; Starchev, K.; Buffle, J. *Biophys. J.* **2004**, *86*, 2710.
(32) Michelman-Ribeiro, A.; Boukari, H.; Nossal, R.; Horkay, F. *Macromolecules* **2004**, *37*, 10212.
(33) Cherdhirankorn, T.; Best, A.; Koynov, K.; Peneva, K.; Muellen, K.; Fytas, G. *J. Phys. Chem. B* **2009**, *113*, 3355.
(34) Erhardt, R.; Zhang, M.; Boker, A.; Zettl, H.; Abetz, C.; Frederik, P.; Krausch, G.; Abetz, V.; Muller, A. H. E. *J. Am. Chem. Soc.* **2003**, *125*, 3260.
(35) Nörenberg, R.; Klingler, J.; Horn, D. *Angew. Chem. Int. Ed.* **1999**, *38*, 1626.
(36) Zettl, H.; Portnoy, Y.; Gottlieb, M.; Krausch, G. *J. Phys. Chem. B* **2005**, *109*, 13397.
(37) Ghosh, S.; Mandal, U.; Adhikari, A.; Bhattacharyya, K. *Chem. Asian. J.* **2009**, *4*, 948.
(38) Burnett, G. R.; Rees, G. D.; Steytler, D. C.; Robinson, B. H. *Colloids Surf. A* **2004**, *250*, 171.
(39) Sahoo, B.; Balaji, J.; Nag, S.; Kaushalya, S. K.; Maiti, S. *J. Chem. Phys.* **2008**, *129*, 075103.
(40) Ghosh, R.; Sharma, S.; K., C. *Biochemistry* **2009**, *48*, 1135.
(41) Chattopadhyay, K.; Saffarian, S.; Elson, E. L.; Frieden, C. *Proc. Natl. Acad. Sci. USA* **2002**, *99*, 14171.
(42) Sherman, E.; Itkin, A.; Kuttner, Y. Y.; Rhoades, E.; Amir, D.; Haas, E.; Haran, G. *Biophys. J.* **2009**, *94*, 4819.
(43) Haupts, U.; Maiti, S.; Schwille, P.; Webb, W. W. *Proc. Natl. Acad. Sci. USA* **1998**, *95*, 13573.
(44) Das, D. K.; Mondal, T.; Mandal, A. K.; Bhattacharyya, K. *Chem. Asian. J.* **2011**, *6*, 3097.
(45) Das, D. K.; Das, A. K.; Mandal, A. K.; Mondal, T.; Bhattacharyya, K. *ChemPhysChem* **2011**, DOI:10.1002/cphc.201100421.
(46) Sasmal, D. K.; Mondal, T.; Mojumdar, S. S.; Choudhury, A.; Banerjee, R.; Bhattacharyya, K. *J.Phys.Chem.B* **2011**, *115*, 13075.
(47) Andrade, S. M.; Costa, S. M. B.; Borst, J. W.; Hoek, A. V.; Viser, A. J. W. G. *J. Fluoresc.* **2008**, *18*, 601.
(48) Reyes, L.; Bert, J.; Fornazero, J.; Cohen, R.; Heinrich, L. *Colloids and Surfaces B: Biointerfaces* **2002**, *25*, 99.
(49) Damodaran, S.; Kinsella, J. E. *J. Biol. Chem.* **1981**, *256*, 3394.
(50) Damodaran, S.; Kinsella, J. E. *J. Biol. Chem.* **1980**, *255*, 8503.
(51) Hofmeister, F. *Arch. Exp. Pathol. Pharmacol.* **1888**, *24*, 247.
(52) Zhang, Y.; Cremer, P. S. *Current Opinion in Chemical Biology* **2006**, *10*, 658.
(53) Petrasek, Z.; Schwille, P. *Biophys. J.* **2008**, *94*, 1437.
(54) Kapusta, P. *Technical Note,PicoQuant GmbH* **July 2010**, Rev1.
(55) Gaigalas, A. K.; Hubbard, J. B.; McCurley, M.; Woo, S. *J. Phys. Chem.* **1992**, *96*, 2355.
(56) Andersson, L. O.; Rehnstorm, A.; Eaker, D. L. *Eur. J. Biochem.* **1971**, *20*, 371.

(57) Al-Soufi, W.; Reija, B.; Novo, M.; Felekyan, S.; Kühnemuth, R.; Siedel, C. A. M. *J. Am. Chem. Soc.* **2005**, *127*, 8775.

(58) Barbero, N.; Barni, E.; Barolo, C.; Quagliotto, P.; Viscardi, G.; Napione, L.; Pavan, S.; Bussolino, F. *Dyes and Pigments* **2009**, *80*, 307.

(59) *An important point to note here is that while measuring the diffusion behavior, BSA at higher concentrations (μM) contributes to the fluorescence signal and hence, can influence the correlation curves. To avoid any error arising from this effect, the experiments have been conducted with low excitation power (3.6 μW for 485 and 3.7 μW for 405 nm). The counts of BSA alone are negligible compared to the probes in BSA.*

(60) Damodaran, S. *Int. J. Biol. Macromol.* **1989**, *11*, 2.

(61) Yamasaki, M.; Yano, H.; Aoki, K. *Int. J. Biol. Macromol.* **1991**, *13*, 322.

(62) *That these changes are indeed due to NaCl-induced structural changes of BSA (and not due to any other effect arising out of salt addition), is evident from the results of control experiments performed on the probe molecules in aqueous buffered solution in the presence of NaCl without using any BSA.*

(63) *That this increase is not because of urea-induced change of the refractive index of the medium and consequent change of the confocal volume, is verified by examining the effect of urea on the diffusion of the probes in the absence of BSA.*

(64) Shikama, K. *J. Biochem.* **1968**, *64*, 55.

(65) Leggio, C.; Galantini, L.; Konarev, P. V.; Pavel, N. V. *J.Phys.Chem.B* **2009**, *113*, 12590.

CHAPTER 7

Probing of the Microheterogeneity of Some Imidazolium Ionic Liquids

The microscopic structure and dynamics of the room temperature ionic liquids (RTILs) that are responsible for some of the peculiar properties of this class of solvents continue to intrigue the researchers and stimulate new investigations. Herein, we use fluorescence correlation spectroscopy (FCS) technique to study the diffusion of some probe molecules in RTILs, the results of which when combined with those obtained from fluorescence lifetime studies, provide insights into the microscopic structural details of this class of novel solvents. Experiments performed with three charged and neutral probe molecules in five carefully selected 1-alkyl-3-methyl imidazolium ionic liquids reveal that unlike in conventional solvents these probes exhibit a bimodal diffusion behavior in RTILs thus indicating the presence of two distinct environments. It is found that the contribution of the slow component of the diffusion increases with increasing alkyl chain length of the cation. These results are not only supported by the biexponential decay behavior of the fluorescence intensity of the systems, but the individual values of the lifetime components and their weightage allow determination of the nature of the two major environments. In essence, the results point to the potential of the two combined techniques in unraveling some of the complex features of the ionic liquids.

7.1. Introduction:

Room temperature ionic liquids (RTILs) possess some extraordinary properties, such as low vapor pressure, liquidous over a wide range of temperature, high conductivity, high thermal stability, high electrochemical window, moderate to high polarity, nonflammable nature, which make them useful media for a large number of organic and inorganic reactions, catalysis, separation and energy related applications, such as fuel cell, photovoltaics, super capacitors, and batteries.[1-8] It is thus not difficult to understand why these substances have attracted such huge attention in recent years. The fact that it is possible to develop ionic liquids with desirable properties or tune their properties gradually by appropriate selection of the constituent ions makes them ‘designer solvent’ for fundamental studies and applications.

Many experimental and theoretical studies in recent years have indicated that the RTILs are more structured liquid when compared to the conventional solvents.[9-34] This

structural heterogeneity of the RTILs, which appears to be responsible for many of the peculiar properties of these substances, is understood to occur over a spatial scale of few nanometers and arises from the segregation of the alkyl tails into the mesoscopic domains.[13,14,16,17,21-26] The early indication on this heterogeneity came through some scattered experiments based on various techniques.[9-12] Notable among those are the observation of the excitation wavelength dependence of the fluorescence behavior of dipolar systems and reaction rates faster than the diffusion.[9-11,19] These experiments did not provide any structural details of these liquids, but indicated that the RTILs are not homogeneous media at the microscopic level. Hamaguchi and co-workers proposed a local ordering in these materials to interpret the Raman spectroscopy data of a few RTILs.[18,34] The spatial heterogeneity in RTILs was subsequently supported by the molecular dynamics (MD) simulation studies by different groups.[13-17] These studies revealed for the first time that the nanoscale organization in RTILs is the consequence of the segregation of the alkyl chains. The first experimental evidence of the spatial heterogeneity of the RTILs and its scale came from small wide angle X-ray scattering (SWAXS) experiments.[21-27] However, recent neutron scattering and computational studies question some of the conclusions of the SWAXS study.[35,36] Thus it appears that the structure of the RTILs is yet to be fully understood and it requires further experiments and simulation to unravel some of the details of the local structure and dynamics. Russina et al presents the current understanding of the mesoscopic structural heterogeneity of the RTILs in two very recent articles.[25,26]

Fluorescence correlation spectroscopy (FCS) is a highly sensitive and powerful technique for the study of diffusion of molecular systems in a medium. In this technique, one measures the fluctuations of the fluorescence intensity in a highly dilute solution arising from a small excitation volume (approx. 1fl) defined by the focused laser beam and pinhole.[37] These fluctuations are correlated to generate the correlation function. The decay of this correlation function with time contains information on the dynamic molecular processes responsible for the fluorescence fluctuation e.g. translational diffusion, conformation fluctuation, reaction kinetics, etc.[37] This technique has been used to study blinking dynamics, bimolecular reaction, conformational fluctuation and translational diffusion in organized assembly like polymer, lipid, membranes etc.[38-41] A few FCS studies in neat RTILs and in solutions have been carried out to understand the diffusion behavior of molecular systems in

these media.[42-45] Werner et al were the first to study the diffusion behavior of some probe molecules using FCS measurements in a RTIL.[42] Apart from demonstrating the usefulness of the technique in probing the frictional resistance experienced by the molecules, the extent of solvent association of the probe molecules in RTIL was estimated.[42] Bhattacharyya and coworkers observed an unusually broad distribution of the diffusion coefficients of some fluorescent probe molecules in RTILs, which they attributed to the microheterogeneity of ionic liquids.[43] In a more recent FCS study, Guo et al. observed biphasic diffusion dynamics of rhodamine 6G in a series of pyrrolidinium ionic liquids comprising different alkyl chain length.[44] They observed an increase in the relative contribution of the slow diffusion component with increasing alkyl chain length and this finding was ascribed to the increase in the size of aggregated domains formed by the alkyl tails of the cationic group. These are very interesting findings, which however, require further investigations as the experiments have so far been conducted only on a very few select ionic liquids employing a few fluorescent probes. This is why we undertake this present study in which we employ three carefully chosen fluorescent dyes, R123 (cationic), DCM (neutral) and 4NBD (neutral) to probe the microscopic structure and dynamics in five carefully selected 1-alkyl-3-methyl imidazolum ionic liquids. Moreover, we carry out parallel fluorescence lifetimes studies of these three environment sensitive probe molecules[46-49] to supplement the results of the FCS measurements, to understand the structural origin of this bimodal diffusion behavior and to obtain a more compelling evidence of the structural heterogeneity of the ionic liquids. A total of five ionic liquids have been chosen for this study. The first two ionic liquids contain a common 1-butyl-3-methyl imidazolium cation, represented here as [$bmim^+$] and two different anions, BF_4^- and PF_6^-. The three other ionic liquids comprise a common bis (trifluoromethanesulphonyl) imide [Tf_2N] anion and 1-alkyl-3-methylimidazolium [C_nmim] cations with an alkyl chain length, n = 2, 4 and 6. Structures of the RTILs and probe molecules are given in Chart 1.6 and 1.7, respectively.

7.2. Diffusion in acetonitrile (ACN)-ethanol (EtOH) mixture:

In order to obtain an estimate of the size of the probes in RTILs, the diffusion of the probe molecules is first studied in a ACN-EtOH mixture (mole fraction, x_{ACN} = 0.8) considering the fact that these liquids are more polar than ACN but less polar than MeOH.[50-53] The van der Waals radii (R_v) of R123, DCM and 4NBD, calculated from the van der Waals

increments for atoms or groups, are 0.41, 0.40 and 0.34 nm, respectively.[54] Thus R123 and DCM are almost equal in size and 4NBD is smaller than the other two probes. Correlation curves of the probes in ACN-EtOH mixture (x_{ACN} = 0.8) are shown in Figure 7.1 and the diffusion coefficients (D_t) of the probes estimated from the data are listed in Table 7.1. The hydrodynamic radii of the probes are calculated from the Stokes-Einstein equation,

$$D_t = \frac{kT}{6\pi\eta R} \tag{7.1}$$

where, k is the Boltzmann constant, T is temperature, η is viscosity of the medium and R is the hydrodynamic radius of the solute molecule. The calculated hydrodynamic radii (Table 7.1) of R123 and DCM are found to be almost the same (0.53 and 0.52 nm respectively) in ACN-EtOH mixture (x_{ACN} = 0.8), while that for 4NBD is significantly smaller (0.37 nm). A comparison of the van der Waals and hydrodynamic radii of the molecules suggests a greater degree of solvent association of R123 and DCM compared to 4NBD.

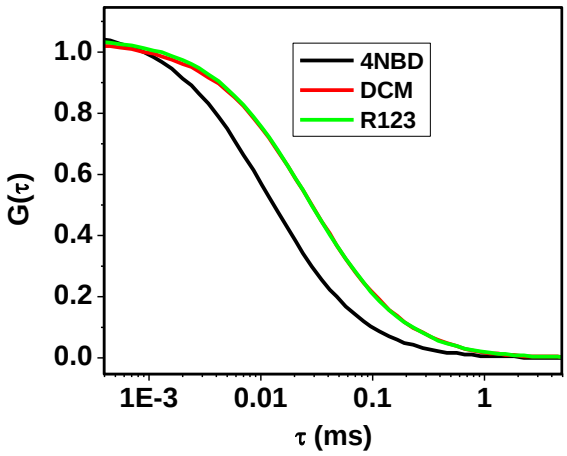

Figure 7.1. Normalized correlation curves for the diffusion of the probes in ACN-EtOH mixture (x_{ACN} = 0.8). The curves shown here are the fits to a single-component diffusion model. The curves for R123 and DCM overlap almost throughout the entire region.

Table 7.1: Diffusion coefficients (D_t in $\mu m^2 s^{-1}$) of the probes in ACN-EtOH mixture (x_{ACN} = 0.8) along their van der Waals radius (R_v) and hydrodynamic radius (R).

Probe	D_t	R_v (nm)	R (nm)
4NBD	1410 ± 150	0.34	0.37
DCM	950 ± 80	0.40	0.52
R123	930 ± 70	0.41	0.53

7.3. Diffusion and lifetime study of the probes in [bmim][BF_4] and [bmim][PF_6]:

Figure 7.2 shows the correlation curves of the probes in [bmim][PF_6] and [bmim][BF_4]. These curves were fitted to a 2-component diffusion model (Equation 2.6) as the fits to a single-component diffusion model was found to be unsatisfactory (as judged by the residuals and χ^2 values). It is thus evident that all the probes exhibit a bimodal diffusion behavior in both the ionic liquids. The diffusion coefficients for the probes in these ionic liquids, estimated from an average of 50 data sets, are collected in Table 7.2. The results reveal the following. The fast and slow diffusion coefficients of the molecules differ by a factor of 4 to 8. The relative contribution of the individual components does not change significantly for 4NBD and DCM, but decreases from 76% to 62% for the slow component of R123 as one moves from [bmim][PF_6] to [bmim][BF_4]. Another point to note here is that the diffusion of the ionic probe, R123 is slower than that of the neutral probes 4NBD and DCM in both ionic liquids.

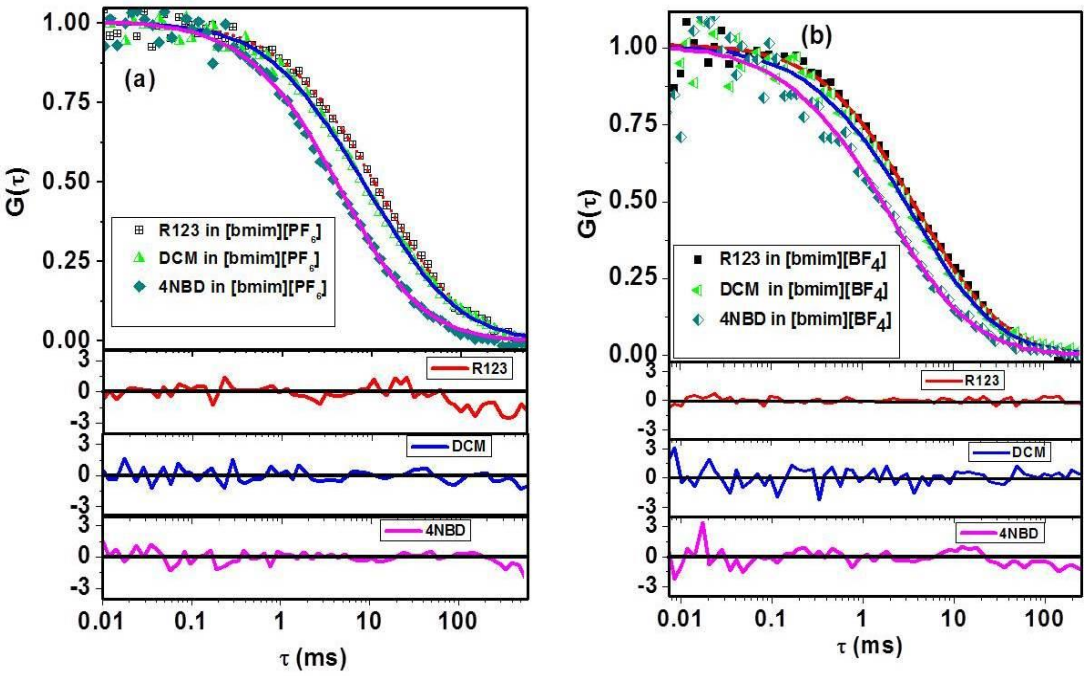

Figure 7.2. Normalized fluorescence correlation curves of the probes in (a) [bmim][PF_6] and (b) [bmim][BF_4]. The points are the experimental data and the lines represent best fits to the data considering a two-component diffusion model. The residuals depicting the quality of the fits are shown at the bottom of each panel in the same color.

Table 7.2. Diffusion parameters of the probes in [bmim][PF_6] and [bmim][BF_4].

Probe	RTILs[†]	D_1 ($\mu m^2/s$)	α_1	D_2 ($\mu m^2/s$)	<D> ($\mu m^2/s$)
4NBD	[bmim][PF_6]	3.4 ± 0.6	0.73	18.0 ± 3.0	7.3 ± 1.3
	[bmim][BF_4]	8 ± 2	0.69	40 ± 10	18.0 ± 4.5
DCM	[bmim][PF_6]	1.30 ± 0.04	0.63	9.6 ± 3.0	4.4 ± 1.1
	[bmim][BF_4]	3.5 ± 1.0	0.68	28.4 ± 5.0	11.5 ± 2.1
R123	[bmim][PF_6]	1.20 ± 0.03	0.76	8.4 ± 3.0	2.94 ± 0.9
	[bmim][BF_4]	3.2 ± 1.0	0.62	20 ± 5	9.6 ± 2.5

[†]The viscosities of [bmim][PF_6] and [bmim][BF_4] are 260 cP and 90 cP, respectively, at 25^0C.[55]

Considering the fact that these systems exhibit a single-component diffusion in conventional solvents, the bimodal diffusion behavior of the probes in ionic liquids can perhaps be attributed to the presence of two distinct environments of the RTILs, as indicated in several theoretical and experimental studies in recent years.[9-33] In this context, it is

pertinent to note that Guo et al. also observed a similar bimodal diffusion behavior of rhodamine 6G in a series of pyrrolidinium ionic liquids in a recent work.[44] Bhattacharyya and co-workers while studying the diffusion behavior of some fluorescent molecules observed an unusually broad distribution of diffusion coefficient in ionic liquids when compared with that in conventional solvent.[43] Considering these reports we assign the bimodal diffusion of the molecules to molecular motion in two different regions; domains formed by the alkyl tails and the ionic constituents of the ionic liquids. As the domains formed by the segregation of the alkyl tails of the ionic liquids are of the order of a few nanometers,[18,21,34] and are much smaller than the confocal dimension, while passing through the confocal volume a molecule can pass through both hydrophobic and hydrophilic environments. However, under this situation, one expects a single-component diffusion with the diffusion coefficient equal to the average of the diffusion coefficients in two environments. The observation of two distinct diffusion components (as is the present case) suggests that molecules do not change between two different solvent environments while passing through the observation volume. This is possible when each type of domains is interconnected. A continuity in the domain structure, which is indicated in molecular dynamics simulation studies, allows molecular diffusion only within a given type of environment during the passage through the confocal volume. It is to be noted that Guo et al. offered a similar interpretation to account for their findings.[44] As the size of the aggregated domains of the imidazolium ionic liquids does not change significantly on changing only the anionic component from $[PF_6]^-$ to $[BF_4]^-$,[22] it is understandable why the relative contribution of the diffusion components does not change significantly for 4NBD and DCM. On the other hand, a small decrease in the contribution of the slow component of R123 from [bmim][PF_6] to [bmim][BF_4] is probably due to a stronger association of this probe with the solvent molecules in [bmim][PF_6] than in [bmim][BF_4].

In order to substantiate the structural origin of these bimodal diffusion behavior and obtain further insight into this aspect, the fluorescence decay behavior of the probe molecules has been studied in [bmim][PF_6] and [bmim][BF_4]. Representative fluorescence decay profiles of the probes are shown in Figure 7.3 and the lifetime data are presented in Table 7.3. A biexponential fit to the decay profiles were found to be superior to the single exponential ones except for R123 in [bmim][PF_6]. In all cases, the weightage of the long lifetime

component is found to be higher and no significant change in the relative contributions of the decay components observed in both ionic liquids.

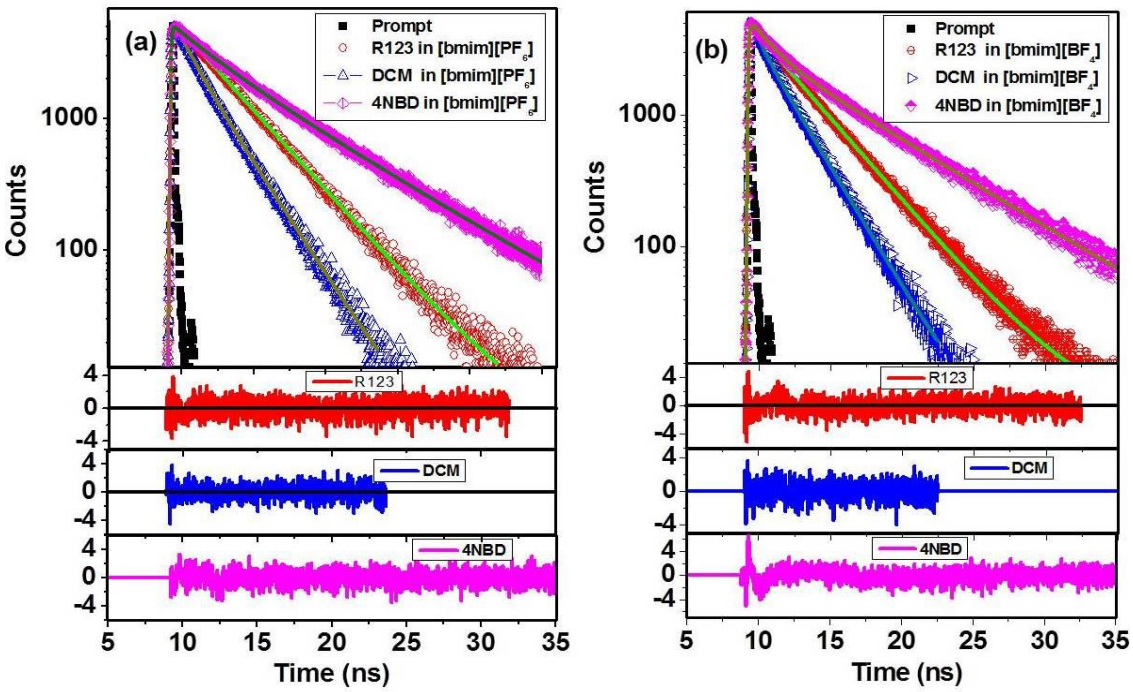

Figure 7.3. Fluorescence decay profile of the probes (a) [bmim][PF_6] and (b) [bmim][BF_4]. The points are the experimental data and the lines represent the best fits to the data. The black points (filled square) represent the lamp profile. Except in the case of R123 in [bmim][PF_6], all data points are fitted to a biexponential function, $I(t)= a_1\exp(-t/\tau_1) + a_2\exp(-t/\tau_2)$, where a_1 and a_2 are the pre-exponential factors, τ_1 and τ_2 are the lifetime components. Excitation wavelength was 439 nm and the emission was monitored at 550 nm for R123, 610 nm for 4NBD and 620 nm for DCM. The residuals depicting the quality of the fits are shown in the lower part of each figure.

Table 7.3. Time-resolved fluorescence parameters[†] of the probe molecules in [bmim][PF_6] and [bmim][BF_4].

RTIL	Probe	τ_1 (a_1)	τ_2 (a_2)	$\langle\tau\rangle$[‡]
	R123	--	3.6	3.6
[bmim][PF_6]	DCM	1.1 (0.31)	2.6 (0.69)	2.1
	4NBD	1.3 (0.37)	6.2 (0.63)	4.4
	R123	0.6 (0.18)	3.5 (0.82)	3.0
[bmim][BF_4]	DCM	0.6 (0.27)	2.4 (0.73)	2.0
	4NBD	1.4 (0.40)	6.5 (0.60)	4.5

[†]The lifetimes, τ, are in ns; [†]$\langle\tau\rangle$ is defined as, $\langle\tau\rangle = a_1\tau_1+a_2\tau_2/a_1+a_2$

Both 4NBD and DCM are molecular systems, whose fluorescence properties are sensitive to the environment due to the highly polar nature of the emitting state of the molecules.[46,47] Considering the environment sensitive properties of these molecules and the fact that these probes exhibit monoexponential decay in the conventional solvents,[46,47,49] we attribute the biexponential decay behavior of the systems to the heterogeneity in ionic liquids. As these molecular systems possess a short fluorescence lifetime in polar environments, the fast decay component of DCM and 4NBD can be assigned to molecules from a polar region and the long lifetime component to molecules from a less polar or nonpolar region. Having assigned the two lifetime components to molecules from the two distinct environments of the ionic liquids, we can use the weightage of the two lifetime components to determine the distribution of the molecules into these regions. As the weightage of the long decay component is more than that of the short component, we conclude that DCM and 4NBD are predominantly distributed in the nonpolar domains formed by the segregation of the alkyl tails. Hence, the slow component of the diffusion, whose contribution is also higher, arises from diffusion in the nonpolar region of the ionic liquids. Considering the literature on the rhodamine dyes,[48,49] we can attribute the long lifetime component of R123 to molecules from a polar environment and the fast decay component in [bmim][BF_4] to those from a nonpolar region. As the weightage of the long lifetime component is higher for R123, it is evident that this molecule resides predominantly in the polar environments of [bmim][BF_4]. On the basis

of the above picture, the origin of slow diffusion of R123 compared to the two other probes in these ionic liquids can be understood. As R123 is mainly located in the polar environment, it experiences a strong dragging force due to both hydrogen bonding and electrostatic interaction with the ionic constituents of the ionic liquids. On the other hand, neutral probes, DCM and 4NBD, which reside mainly in the nonpolar region, do not experience any specific or electrostatic interaction with the ionic constituents of the ionic liquids. Thus the lifetime data complements the diffusion data and confirms the structural origin of the microenvironments and the location of the probe molecules in specific regions of the ionic liquids.

7.4. Diffusion and lifetime study of the probes in ionic liquids of varying chain length:

The diffusion behavior of the molecules in a series of $[C_nmim][Tf_2N]$ ionic liquids with n = 2, 4 and 6 has been studied to understand the effect of the chain length. Figure 7.4 shows the correlation curves of the probes in these ionic liquids. Like in earlier cases, the molecules show two-component diffusion dynamics in these ionic liquids as well. The estimated diffusion coefficients and their relative contributions are listed in Table 7.4. Like in $[bmim][PF_6]$ and $[bmim][BF_4]$, the diffusion of R123 is found to be slower compared to the neutral probes. In all cases, it is found that the fraction associated with the slow component increases with increasing chain length of the alkyl group.

The bimodal diffusion behavior of the probes in ionic liquids, as described in the previous section, can be interpreted due to the existence of two kinds of solvent environments. Even though a slow diffusion of R123 compared to 4NBD is expected based on the hydrodynamic radii of the systems, the slowness of the diffusion of R123 compared to DCM, whose hydrodynamic radius is very similar to that of DCM, can only be explained taking into account the positively charged nature of R123 and its association with the solvent in the polar ionic region. An increase in the fraction of the slow component with increasing chain length is consistent with the results of MD simulation studies, and small wide angle X-ray scattering (SWAXS) experiments, both indicating an increase in the size of the nonpolar domain formed by the aggregation of the alkyl tail with increasing chain length.[13,14,16,17,21,22,25-27] Perhaps the most surprising result of the present experiments is the observation of a bimodal diffusion behavior of the probes even in small alkyl chain length

containing ionic liquid, [emim][Tf_2N]. This is because the MD simulation studies proposed nansoscale organization in ionic liquids with n≥4.[13,14,16,17] However, recent SWAXS study suggests the existence of the nanoscale structure in [$C_n$mim][Tf_2N] for n=3 as well.[22] Atkin and Warr also observed low Q peak for alkyl ammonium nitrates for n=2 and 3.[23]

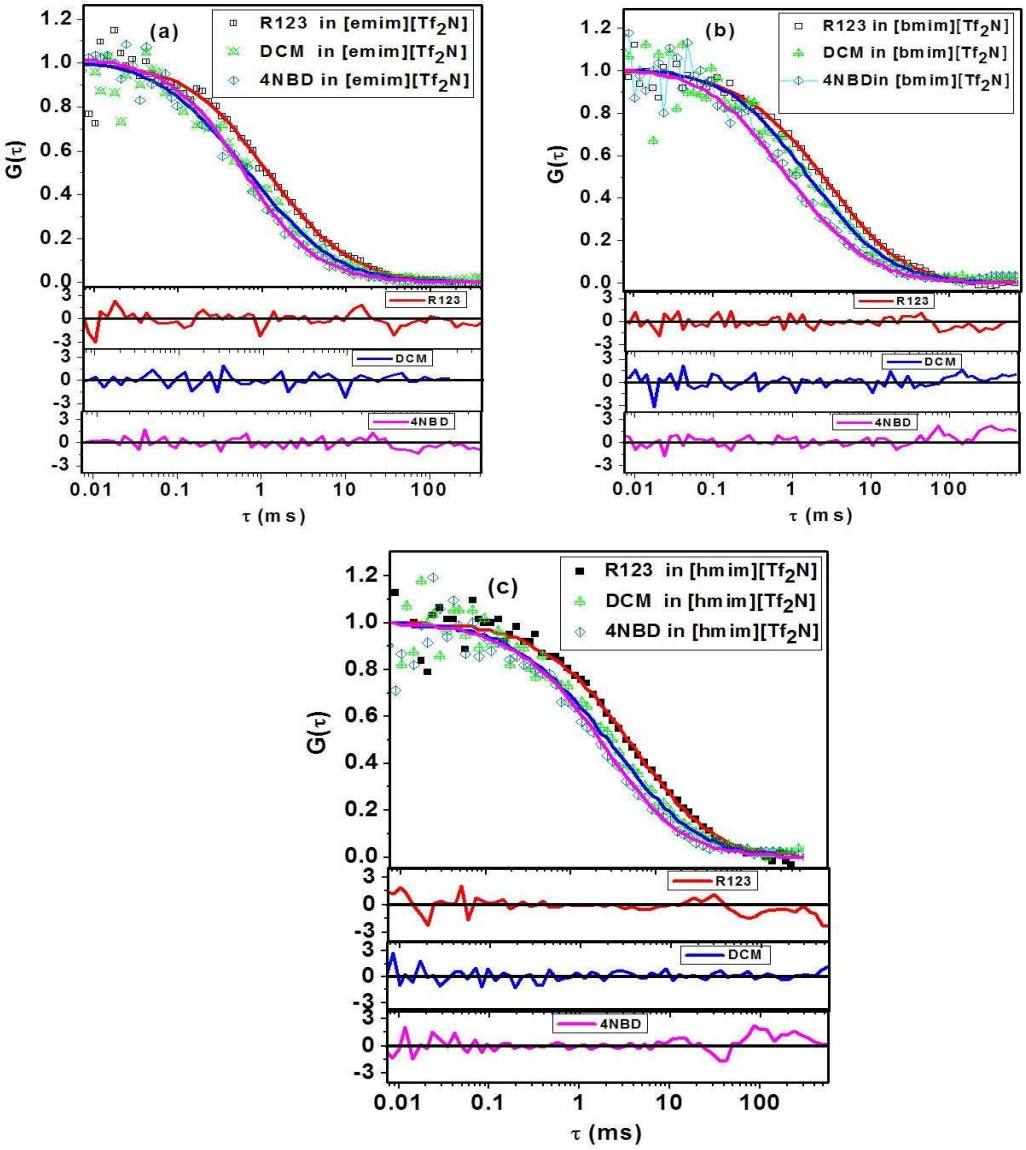

Figure 7.4. Normalized fluorescence correlation curves for the diffusion of the probes (a) [emim][Tf_2N], (b) [bmim][Tf_2N] and (c) [hmim][Tf_2N]. The points are the experimental data and the lines represent best fits to the data considering a two-component diffusion model. The residuals depicting the quality of the fits are shown at the bottom of each figure in the same color.

Table 7.4. Results of the two component diffusion model fits for R123, DCM, and 4NBD in [emim][Tf_2N], [bmim][Tf_2N] and [hmim][Tf_2N].

Probe	RTILs[†]	D_1 ($\mu m^2/s$)	α_1	D_2 ($\mu m^2/s$)	<D> ($\mu m^2/s$)
R123	[emim][Tf_2N]	7.8 ± 2.0	0.39	28 ± 8	20.1 ± 5.7
	[bmim][Tf_2N]	4.5 ± 1.0	0.65	32.6 ± 5.0	14.4 ± 2.4
	[hmim][Tf_2N]	3 ± 0.6	0.68	19 ± 5	8.1 ± 2.0
DCM	[emim][Tf_2N]	13 ± 2	0.43	50.2 ± 10	34.2 ± 6.6
	[bmim][Tf_2N]	5.6 ± 1.0	0.54	38± 4	20.5 ± 2.4
	[hmim][Tf_2N]	3 ± 0.6	0.68	31.5 ± 8.0	11.8 ± 3.0
4NBD	[emim][Tf_2N]	12 ± 3	0.29	49.2 ± 15	38.4 ± 11.5
	[bmim][Tf_2N]	9.3 ± 2.0	0.47	44 ± 10	29.3 ± 6.2
	[hmim][Tf_2N]	4.5 ± 1.5	0.53	20 ± 4	12.1 ± 3.0

[†]The viscosities of [emim][Tf_2N], [bmim][Tf_2N] and [hmim][Tf_2N] are 32 cP, 50 cP and 67 cP, respectively, at 25^0C.[20,56]

In order to confirm these findings, we have studied the fluorescence lifetimes of the molecules in these ionic liquids. The fluorescence decay profiles of all the probes in these ionic liquids have been found to be biexponential with the two lifetime components typical for the respective probes in polar and nonpolar environments. Figure 7.5 shows the fluorescence decay profiles of the molecules along with the biexponential fits to the data. The fluorescence lifetime data of the systems are collected in Table 7.5. As can be seen, the short and long lifetime components of each molecule do not vary appreciably with the change of the ionic liquids. However, some variation of the weightage of the two components can be observed. For DCM, the percentage associated with the long lifetime component that represents molecules in the nonpolar region exceeds 70% in all cases indicating the preference of this molecule to the nonpolar region of the ionic liquid. For NBD, whose long lifetime component also represents the molecules residing in the nonpolar region increases from 51% in [emim][Tf_2N] to 61% in [hmim][Tf_2N] indicating the passage of more molecules to the nonpolar region with increase in the alkyl chain length. This observation is consistent with the increase in the size of the nonpolar domain for higher members of the series.[21,22] As far as R123 is concerned, the fraction associated with the long lifetime component represents the molecules in the polar environments. This fraction changes from 0.53 in [emim][Tf_2N] to 0.65 in [hmim][Tf_2N]. This observation can be explained based on

the increased hydrophobicity of the nonpolar environment with increasing chain length. As charged molecule R123 prefers to reside in a hydrophilic environment, an increased hydrophobicity of the nonpolar environment enhances the population of the R123 in the polar environment. Thus, the lifetime study corroborates the presence of two different kinds of environment in these ionic liquids.

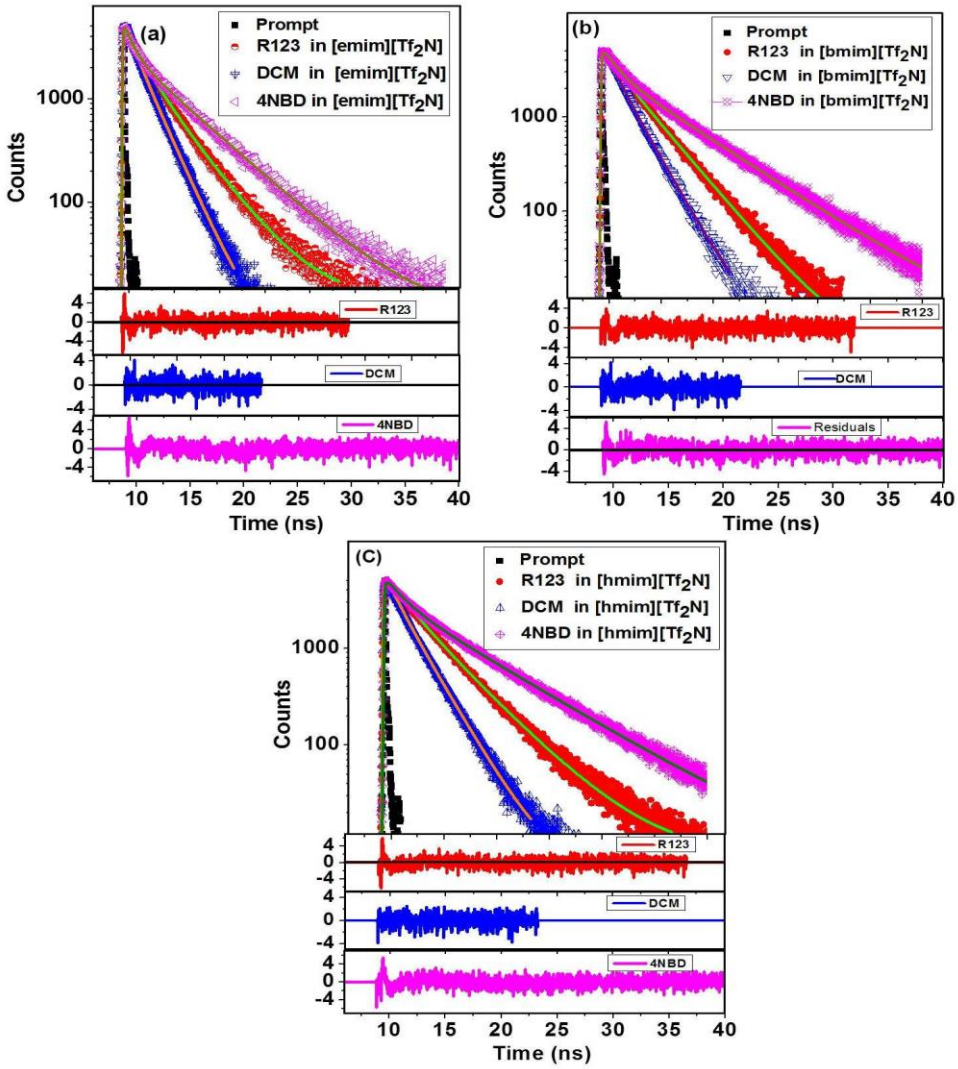

Figure 7.5. Time-resolved fluorescence behavior of the probes in (a) [emim][Tf_2N], (b) [bmim][Tf_2N] and (c) [hmim][Tf_2N]. The points are the experimental data and the lines represent the best biexponential fits to these data points. Excitation wavelength was 439 nm and the emission was monitored at 550 nm for R123, 610 nm for 4NBD and 620 nm for DCM. The residuals depicting the quality of the fits are shown in the lower part of each figure.

Table 7.5. Time-resolved fluorescence parameters[†] of the probes in [emim][Tf_2N], [bmim][Tf_2N] and [hmim][Tf_2N].

RTIL	Probe	τ_1 (a_1)	τ_2 (a_2)	$\langle\tau\rangle$[‡]
	R123	1.7 (0.47)	3.6 (0.53)	2.8
[emim][Tf_2N]	DCM	1.0 (0.21)	2.4 (0.79)	2.1
	4NBD	1.0 (0.49)	5.6 (0.51)	3.3
	R123	2.3 (0.39)	3.6 (0.61)	3.1
[bmim][Tf_2N]	DCM	1.0 (0.26)	2.2 (0.74)	1.9
	4NBD	1.3 (0.42)	6.1 (0.58)	4.1
	R123	2.4 (0.35)	4.12 (0.65)	3.5
[hmim][Tf_2N]	DCM	1.2 (0.26)	2.4 (0.74)	2.1
	4NBD	1.7 (0.39)	6.8 (0.61)	4.8

[†]The lifetimes, τ, are in ns; [‡]$\langle\tau\rangle$ is defined as, $\langle\tau\rangle = (a_1\tau_1+a_2\tau_2)/(a_1+a_2)$

7.5. Conclusion:

We have studied the translational diffusion of some environment sensitive probe molecules in several ionic liquids using fluorescence correlation spectroscopy techniques. Biphasic diffusion dynamics observed for the probes in these media is attributed to the microheterogeneous nature of these media resulting from the segregation of the alkyl chain of the constituents. The presence of polar and nonpolar regions in these ionic liquids is further substantiated by studies on the time-resolved fluorescence decay profiles of the system, which indicate biexponential decay behavior with lifetimes typical of the probes in polar and nonpolar environment. It is shown that a combination of the fluorescence correlation and lifetime techniques can provide useful information on the nature of the micro-environment of the complex media such as the ionic liquids.

References:

(1) Rogers, R. D.; Seddon, K. R. *Science* **2003**, *302*, 792.

(2) Dupont, J.; de Suja, R. F.; Suarez, P. A. Z. *Chem. Rev.* **2002**, *102*, 3667.

(3) Wasserscheid, P.; Keim, W. *Angew. Chem. Int. Ed.* **2000**, *39*, 3772.

(4) Ranu, B. C.; Jana, R. *Eur. J. Org. Chem* **2006**, 3767.

(5) Wang, P.; Wenger, B.; Humphry-Baker, R.; Moser, J.-E.; Teuscher, J.; Kantlehner, W.; Mezger, J.; Stoyanov, E. V.; Zakeeruddin, S. M.; Gratzel, M. *J. Am. Chem. Soc.* **2005**, *127*, 6850.

(6) Kuang, D.; Wang, P.; Ito, S.; Zakeeruddin, S. M.; Gratzel, M. *J. Am. Chem. Soc.* **2006**, *128*, 7732.

(7) Hallett, J. P.; Welton, T. *Chem. Rev.* **2011**, *111*, 3508.

(8) Sun, X.; Luo, H.; Dai, S. *Chem. Rev.* **2012**, *112*, 2100.

(9) Mandal, P. K.; Sarkar, M.; Samanta, A. *J. Phys. Chem. A* **2004**, *108*, 9048.

(10) Paul, A.; Mandal, P. K.; Samanta, A. *J. Phys. Chem. B* **2005**, *109*, 9148.

(11) Skrzypczak, A.; Neta, P. *J. Phys. Chem. A* **2003**, *107*, 7800.

(12) Tokuda, H.; Hayamizu, K.; Ishii, K.; Susan, M. A. B. H.; Watanabe, M. *J. Phys. Chem. B* **2005**, *109*, 6103.

(13) Wang, Y.; Voth, G. A. *J. Am. Chem. Soc.* **2005**, *127*, 12192.

(14) Wang, Y.; Voth, G. A. *J. Phys. Chem. B* **2006**, *110*, 18601.

(15) Hu, Z.; Margulis, C. J. *Proc. Natl. Acad. Sci. U.S.A.* **2006**, *103*, 831.

(16) Lopes, J. N. C.; Padua, A. A. H. *J. Phys. Chem. B* **2006**, *110*, 3330.

(17) Lopes, J. N. C.; Costa Gomes, M. F.; Padua, A. A. H. *J. Phys. Chem. B* **2006**, *110*, 16816.

(18) Iwata, K.; Okajima, H.; Saha, S.; Hamaguchi, H. *Acc. Chem. Res.* **2007**, *40*, 1174.

(19) Paul, A.; Samanta, A. *J. Phys. Chem. B* **2007**, *111*, 1957.

(20) Paul, A.; Samanta, A. *J. Phys. Chem. B* **2008**, *112*, 16626.

(21) Triolo, A.; Russina, O.; Bleif, H.-J.; Di Cola, E. *J. Phys. Chem. B* **2007**, *111*, 4641.

(22) Russina, O.; Triolo, A.; Gontrani, L.; Caminiti, R.; Xiao, D.; Hines Jr, L. G.; Bartsch, R. A.; Quitevis, E. L.; Plechkova, N.; Seddon, K. R. *J. Phys.: Condens. Matter* **2009**, *21*, 424121.

(23) Atkin, R.; Warr, G. G. *J. Phys. Chem. B* **2008**, *112*, 4164.

(24) Hayes, R.; Imberti, S.; Warr, G. G.; Atkin, R. *Phys. Chem. Chem. Phys* **2011**, *13*, 3237.

(25) Russina, O.; Triolo, A.; Gontrani, L.; Caminiti, R. *J. Phys. Chem. Lett.* **2012**, *3*, 27.

(26) Russina, O.; Triolo, A. *Faraday Discuss.* **2012**, *154*, 97.

(27) Macchiagodena, M.; Gontrani, L.; Ramondo, F.; Triolo, A.; Caminiti, R. *J. Chem. Phys.* **2011**, *134*, 11521.

(28) Funston, A. M.; Fadeeva, T. A.; Wishart, J. F.; Castner Jr, E. W. *J. Phys. Chem. B* **2007**, *111*, 4963.

(29) Fruchey, K.; Fayer, M. D. *J. Phys. Chem. B* **2010**, *114*, 2840.

(30) Arzhantsev, S.; Jin, H.; Baker, G. A.; Maroncelli, M. *J. phys. Chem. B* **2007**, *111*, 4978.

(31) Fruchey, K.; Lawler, C. M.; Fayer, M. D. *J. Phys. Chem. B* **2012**, *116*, 3054.

(32) Jin, H.; Li, X.; Maroncelli, M. *J. Phys. Chem. B* **2007**, *111*, 13473.

(33) Adhikari, A.; Sahu, K.; Dey, S.; Ghosh, S.; Mandal, U.; Bhattacharyya, K. *J. Phys. Chem. B* **2007**, *111*, 12809.

(34) Yoshida, K.; Iwata, K.; Nishiyama, Y.; Kimura, Y.; Hamaguchi, H. *J. Chem. Phys.* **2012**, *136*, 104504.

(35) Hardacre, C.; Holbrey, J. D.; Mullan, C. L.; Youngs, T. G. A.; Bowron, D. T. *J. Chem. Phys.* **2010**, *133*, 74510.

(36) Annapureddy, H. V. R.; Kashyap, H. K.; De Biase, P. M.; Margulis, C. J. *J. Phys. Chem. B* **2010**, *114*, 16838.

(37) Lackowicz, J. R. *Principles of Fluorescence Spectroscopy* **2006**, *Springer: New York, Chap 24*.

(38) Al-Soufi, W.; Reija, B.; Novo, M.; Felekyan, S.; Kuhnemuth, R.; Seidel, C. A. M. *J. Am. Chem. Soc.* **2005**, *127*, 8775.

(39) Rochira, J. A.; Gudheti, M. V.; Gould, T. J.; Laughlin, R. R.; Nadeau, J. L.; Hess, S. T. *J. Phys. Chem. C* **2007**, *111*, 1695.

(40) Haupts, U.; Maiti, S.; Schwille, P.; Webb, W. W. *Proc. Natl. Acad. Sci. U.S.A.* **1998**, *95*, 13573.

(41) Chattopdhyay, K.; Saffarian, S.; Elson, E. L.; Frieden, C. *Biophys. J.* **2005**, *88*, 1413.

(42) Werner, J. H.; Baker, S. N.; Baker, G. A. *Analyst* **2003**, *128*, 786.

(43) Sasmal, D. K.; Mandal, A. K.; Mondal, T.; Bhattacharyya, K. *J. Phys. Chem. B* **2011**, *115*, 7781.

(44) Guo, J.; Baker, G. A.; Hillesheim, P. C.; Dai, S.; Shaw, R. W.; Mahurin, S. M. *Phys. Chem. Chem. Phys* **2011**, *13*, 12395.

(45) Sarkar, A.; Ali, M.; Baker, G. A.; Tetin, S. Y.; Ruan, Q.; Pandey, S. *J. Phys. Chem. B* **2009**, *113*, 3088.

(46) Saha, S.; Samanta, A. *J. Phys. Chem. A* **1998**, *102*, 7903.

(47) Mialocq, J. C.; Meyer, M. *Laser Chem.* **1990**, *10*, 277.

(48) Lopez Arbeloa, L.; Lopez Arbeloa, F.; Tapia Estevej, M. J.; Lopez Arbeloa, I. *J. Phys. Chem.* **1991**, *95*, 2203.

(49) Chowdhury, S. A.; Lim, M. *Bull. Korean Chem. Soc.* **2011**, *32*, 583.

(50) Aki, S. N. V. K.; Brennecke, J. F.; Samanta, A. *Chem. Commun.* **2001**, 413.

(51) Karmakar, R.; Samanta, A. *J. Phys. Chem. A* **2002**, *106*, 6670.

(52) Karmakar, R.; Samanta, A. *J. Phys. Chem. A* **2003**, *107*, 7340.

(53) Weingartner, H. *Angew. Chem. Int. Ed.* **2008**, *47*, 654.

(54) Edward, J. T. *J. Chem. Edu.* **1970**, *47*, 261.

(55) Santhosh, K.; Banerjee, S.; Rangaraj, N.; Samanta, A. *J. Phys. Chem. B* **2010**, *114*, 1967.

(56) Widegren, J. A.; Magee, J. W. *J. Chem. Eng. Data* **2007**, *52*, 2331.

CHAPTER 8

Concluding Remarks

This chapter summarizes the results of the investigations presented in this thesis. The scope of further studies based on the findings of the present work is also outlined.

8.1. Overview:

The work embodied in this thesis has been undertaken to explore the photophysical behavior of the quantum dots (QDs) and to understand the diffusion behavior of some fluorescent dyes in complex environments such as protein solution and ionic liquids to obtain insights into these microheterogeneous media. These studies have been carried out using fluorescence correlation spectroscopy technique.

We Chose CdTe QDs with different capping agents (Chart 1.6) and dispersed them in different solvents to understand the influence of surface related processes on the photophysics of the QDs. CdTe/ZnS core/shell QDs were also studied for the same purpose. As a study of the diffusion of organic fluorophores can effectively report the local environment of complex media such as protein solutions and room temperature ionic liquids (RTILs), we studied the diffusion behavior of the fluorescent probes in protein solution and RTILs. Apart from the FCS technique, several other instrumental techniques such as NMR and IR spectroscopy for compound characterization, TEM for determination of morphology, a cone and plate viscometer for measurements of RTIL's viscosity, UV-vis spectrophotometer, steady-state and time-resolved fluorescence techniques for spectral and kinetic information were employed for carrying out the work presented here. The findings of the present work are summarized below.

The evolution of the fluorescence properties of an aqueous solution of mercaptopropionic acid (MPA)-capped CdTe QDs under light exposure has been investigated. A faster relaxation of correlation at higher excitation power, especially at shorter correlation time in the FCS measurement, is attributed to increasing contribution of the off-state of the QDs. A decrease in the amplitude of the correlation at time zero [G(0)] with increasing excitation power, despite an increasing fraction of the molecules in their off-state, is attributed to light-induced brightening of the dark QDs due to surface passivation at higher excitation power. The simultaneous occurrence of the two competing processes,

photoactivation leading to fluorescence enhancement and photodegradation resulting in quenching of the luminescence of the QDs, has been substantiated by the steady state and time-resolved emission measurements. It is suggested that surface passivation by photoadsorbed water molecules leads to photoactivation of the QDs and dissolved oxygen-induced photooxidation of the surfaces is responsible for subsequent drop of the luminescence intensity of the system.

The influence of ligand and solvent on light-induced modulation of the emission behavior of the QDs has been studied for CdTe QDs capped with hexadecylamine (HDA), mercaptopropionic acid (MPA) and 1-(1-undecanethiol)-3-methyl imidazolium bromide (SMIM) in $CHCl_3$, H_2O and [bmim][PF_6] ionic liquid, respectively. Significant emission enhancement is observed only for CdTe/MPA in both aerated and de-aerated aqueous environment under light irradiation. A large decrease of the G(0) value at higher excitation power in the FCS measurements is also observed only in the aqueous environment. These results unambiguously establish the critical role of the H_2O molecules in the passivation of the surface trap states of the QDs. In addition to H_2O-assisted photoactivation, photooxidation of the QDs is also shown to contribute to the light-induced modulation of their luminescence behavior.

Photostability and photoactivation of the QDs are the two important parameters which determine their applications in diverse fields. In order to study the effect of shell on the photoactivation and photostability of the CdTe QDs ZnS shell is grown over CdTe QDs. Significant improvement in the fluorescence properties is observed for CdTe/ZnS QDs compared to CdTe QDs in both $CHCl_3$ and aqueous environment. This indicates effective passivation of surface dangling orbitals of the CdTe QDs by the overgrowth of the ZnS shell. Photoactivation and photocorrosion in aqueous medium are observed only in CdTe/MPA QDs, but not in CdTe/ZnS(2ML)/MPA QDs. This clearly indicates that ZnS shell effectively protects the CdTe core QDs from external perturbations. FCS study further substantiates this fact as a large decrease in G(0) value with increasing excitation power is observed only for CdTe/MPA QDs. This study clearly indicates that photoactivation of the QDs and decrease in the G(0) value observed with increase in intensity of the exciting source are intimately related.

The diffusion behavior of three fluorescent system, electrically neutral coumarin 102 (C102), cationic rhodamine 6G (R6G), and anionic fluorescein (FL) in pH 7 phosphate buffered solutions of bovine serum albumin (BSA) protein in the absence and presence of NaCl and urea, has been investigated using FCS technique. The measured diffusion coefficients provide insight into the nature and strength of the interaction between the guest and host revealing the heterogeneity of the binding sites of the protein. The diffusion due to both free and BSA-bound molecule is observed in the case of C102-BSA system. This observation coupled with the fact that no exchange between free and bound probe is observed in the confocal volume, indicates stronger binding of C102 with BSA. On the other hand, fast exchange between the bound and free states of the molecules is observed for electrically charged hydrophilic dyes, R6G and FL, reflecting weaker binding of these dyes with BSA. The common salt and urea induced changes of the diffusion behavior allow identification of the association sites of the probes with the protein molecule.

The microscopic structure and dynamics of the RTILs that are responsible for some of the peculiar properties of this class of solvents continue to intrigue the researchers and stimulate new investigations. In the present study we have studied the translational diffusion of some environment sensitive probe molecules in several ionic liquids using FCS technique. Biphasic diffusion dynamics observed for the probes in these media is attributed to the microheterogeneous nature of these media resulting from the segregation of the alkyl chain of the constituents. The presence of polar and nonpolar regions in these ionic liquids is further substantiated by studies on the time-resolved fluorescence decay profiles of the system, which indicate biexponential decay behavior with lifetimes typical of the probes in polar and nonpolar environment. It is shown that a combination of the fluorescence correlation and lifetime techniques can provide useful information on the nature of the micro-environment of the complex media such as the ionic liquids.

8.2. Future Scope:

We have conclusively established that passivation of the surface trap states of the QDs by photoadsorbed H_2O molecules is responsible for photoactivation of the QDs. Photoactivation dominates during the early stages of irradiation whereas, at longer irradiation times surface photooxidation (known as photocorrosion) takes over. Both photoactivation

and photocorrosion of the QDs severely restrict the utility of the QDs in various applications. We have shown that for MPA-capped core/shell CdTe/ZnS(2ML) QDs in aqueous medium remain stable even after prolonged exposure to light. However, fluorescence quantum yield (QY) of these QDs (35%), is much lower than that of CdSe/CdS (QY ~ 90%) core/shell QDs. The low fluorescence QY of the CdTe-core based type-I core/shell QDs compared to the CdSe/CdS QDs is due to the presence of trap states at the interface between core and shell. Most of the shell materials resulting type-I band alignment with the CdTe core exhibit huge lattice mismatch, which creates strain in the core/shell QDs based on CdTe core, thus generating interfacial trap states. This interfacial strain can be reduced by using an intermediate shell material sandwiched between core and outer shell. In such kind of core/shell/shell structured QDs the intermediate layer acts as a lattice adapter between core and outer shell materials having a huge lattice mismatch. A second approach is to spread the lattice strain between two mismatched materials across a large number of atoms. Core/gradient alloy-shell/shell such as CdSe/$Cd_{1-x}Zn_xSe$/ZnSe is a perfect example of such kind of structure where lattice strain can be spread over many atoms by gradually increasing x from 0 at the center to 1 at the surface. These core/shell/shell and core/gradient alloy shell/shell QDs has been studied for CdSe based core system. However, as such studies are yet to be undertaken on the CdTe core based system, one can explore this aspect.

Binding strength as well as the binding sites of the probe in BSA was determined following the diffusion behavior of the fluorescent probes in solutions of the protein in the absence and presence of urea and NaCl. Hydrophilic dyes R6G and FL exhibit fast exchange dynamics between the free and protein-bound probe. However, this exchange kinetics could not be determined from FCS measurements as the probe molecules exhibit similar brightness in the bound and free states. It is possible to study this fast exchange dynamics (association and dissociation constant of the probe molecule with protein) by using a dye molecule, which binds weakly with protein and whose brightness changes significantly upon binding. It will be then interesting to see how the structural changes in protein molecule affect this exchange kinetics on addition of denaturing agents such as urea. Understanding the interplay between protein structure and exchange dynamics is very important in drug delivery and for the design of the drug molecules.

Microheterogeneous nature of the RTILs is revealed from the FCS and fluorescence lifetime study. This microheterogeneity of the RTILs that arises due to the segregation of the alkyl tails into mesoscopic domains, is known to occur over a scale of few nanometers (nm) and. It will be interesting to study the diffusion of the fluorescent dyes in RTILs with increasing polarity of the side chains. The mesoscopic structure of the RTILs can be disrupted due to repulsion of the polar side chains. In addition to FCS, measurements based on other techniques such as small and wide angle X-ray scattering (SWAX), Raman scattering, neutron scattering, optical Kerr effect can also be carried out to obtain a clear picture on the structural details of RTILs. One of the major obstacles in the FCS study on RTILs is the large background scattering due to the RTILs, which interferes with the fluorescence signal of the probe molecules. However, this problem can be dealt with by using a combination of stimulated emission depletion and FCS (STED-FCS) technique. STED-FCS will significantly lower the observation volume and thus will minimize the background signal. This will also allow one to use a higher concentration of the fluorophore in the measurements. We hope that FCS-STED approach will provide more detailed insights on the microscopic structural details of the RTILs in recent future.